




Serie R  
No 323

ISSN 0909-587X  
ISBN 87-7740-164-6

 Afdelingen for Bærende Konstruktioner  
Department of Structural Engineering  
Danmarks Tekniske Universitet • Technical University of Denmark

**Ultra High-Strength Steel Fibre  
Reinforced Concrete**

Part I

Basic Strength Properties of Compressive Matrix

Claus Vestergaard Nielsen

Serie R

No 323

1995

# Ultra High-Strength Steel Fibre Reinforced Concrete

## Part I

Basic Strength Properties of Compressit Matrix  
With Review on Properties of Fibre Reinforced and  
High-Strength Concrete

July 1995

Carl Bro Civil & Transportation a/s  
Consulting Engineers and Planners



Claus Vestergaard Nielsen  
Ph.D. Thesis - EF 457

**ASK** Attegang for Baserede Konsultationer  
Department of Structural Engineering  
Danmarks Tekniske Universitet • Technical University of Denmark

**ATV** Attegang for Tekniske Videnskaber  
Danish Academy of Technical Sciences  
Industrial Research • Rømløse

## Preface

The present report is the *first part* of the thesis required to obtain the Ph.D. degree. The study is carried out as required by the Danish Academy of Technical Sciences (ATV) throughout the period October 1st 1992 to March 31st 1995.

The second part of the thesis is titled:

### Ultra High-Strength Steel Fibre Reinforced Concrete, Part II: Structural Applications of Comprest

Both reports are written so that they can be read separately without any lack of information. However, the second part contains a conclusion for the complete thesis.

The project is divided between the Department of Structural Engineering, Technical University of Denmark, under the supervision of Professor, Dr.techn. Mogens Peter Nielsen, and the consulting engineers and planners Carl Bro Civil & Transportation als under the supervision of Managing Director, Professor Bjarne Chr. Jensen. The third party of the project is Aalborg Portland A/S, which is represented by Managing Director Palle Nepper-Christensen from the Cement- and Concrete Laboratory in Aalborg.

I wish to thank the staff at the university, the company and the third party for their help and especially my colleague M.Sc. John Forbes Olesen for fruitful discussions. Furthermore the Cement- and Concrete Laboratory has provided invaluable help by casting all test specimens.

This print of the report includes minor corrections to my original thesis.

Copenhagen  
July 1995

Claus Vestergaard Nielsen

Ultra High-Strength Steel Fibre Reinforced Concrete. Part I. Basic

Strength Properties of Comprest Matrix

Copyright © by Claus Vestergaard Nielsen, 1995

Tryk:

Afdelingen for Bærende Konstruktioner  
Danmarks Tekniske Universitet

Lynøby

ISBN 87-7740-164-6

ISSN 0909-587X

Bogbinder:

H. Meyer, Bygning 101, DTU

## Abstract

The present report contains the basic material properties of the fibre reinforced matrix compressit. Compressit matrix is an ultra high-strength, steel fibre reinforced cementitious matrix, that shows remarkable strength and deformational results. The cement matrix is very dense with a water to binder ratio of 0.18 together with a high content of fibres (up to 10 % by volume), which give it compressive strengths above 150 MPa.

The scope of this report is to collect the strength properties of compressit matrix to be used in a structural design analysis. Both test results obtained throughout the last decade and new results from the present project are included. Furthermore the material properties are related to similar results observed from conventional fibre reinforced concrete and high-strength concretes. The properties include complete stress - strain curves in both uniaxial tension and compression, triaxial compressive tests to determine the strength criterion and finally the fracture energy.

The conclusion of the report is, that even though compressit matrix acts like a high-strength concrete its deformational behaviour is rather like normal-strength concrete, because of the fibres. The uniaxial compressive and tensile strength is satisfactory predicted by direct proportionality with the fibre content and the aspect ratio.

## Resumé

Denne rapport indeholder de basale materiale parametre for fiber armeret compressit matrix. Compressit matrix er betegnelsen for et stålfiberarmet cementbaseret produkt, som udviser forbløfende styrke- og deformationsegenskaber. Cement matrixen er meget tæt med et vand - cement forhold på 0.18, som sammen med et højt indhold af fibre (op til 10 volumen-%) giver trykstyrker over 150 MPa.

Rapportens formål er at samle compressit matrixens styrkeegenskaber til brug i design af bærende konstruktionslementer. Forsøgsresultater fra det sidste år er medtaget sammen med nye resultater opnået i forbindelse med dette projekt. Derudover er materialeegenskaberne sammenlignet med de tilsvarende for fiberarmet beton og højstyrke beton. De egenskaber der behandles er enskset tryk og træk med komplette arbejdskurver, treaksede trykforsøg til fastlæggelse af brudbetingelse samt brudenergi.

Hovedkonklusionen er, at selvom compressit matrix er et højstyrke produkt, så opfører det sig i høj grad som normal beton mht. deformationer pga. fibre. Styrken i enskset tryk og træk er desuden finder proportional med fiberindholdet samt fiberens længde - diameter forhold.

## Table of contents

Notation .....	1
1. Introduction .....	5
1.1 Facts about compressit .....	6
1.2 Scope of present investigation .....	10
1.3 References .....	12
2. Tensile behaviour .....	13
2.1 Review on FRC under tension .....	13
2.1.1 Early investigations concerning FRC .....	13
2.1.2 Single fibre pull-out problem .....	19
2.1.3 Theory for short random fibres .....	29
2.2 Previous investigations on compressit matrix .....	40
2.2.1 Direct tensile tests .....	40
2.2.2 Tensile splitting tests .....	42
2.3 Direct tensile tests on compressit matrix .....	43
2.3.1 Test specimens and method .....	43
2.3.2 Test results .....	45
2.3.3 Tensile strength of compressit matrix .....	58
2.4 Compressit matrix reinforced with both fibres and bars .....	62
2.4.1 Test specimens and method .....	63
2.4.2 Test results .....	64
2.5 Concluding remarks .....	66
2.6 References .....	68
3. Uniaxial compressive behaviour .....	71
3.1 Review on concrete and FRC in uniaxial compression .....	72
3.1.1 Analytical stress - strain curves for concrete .....	72
3.1.2 Stress - strain curves for FRC .....	75
3.1.3 Peak of the compressive stress - strain curve for FRC .....	80
3.1.4 Ductility of FRC under compression .....	83
3.2 Compressit matrix under uniaxial compression .....	84
3.2.1 Test specimens and method .....	85
3.2.2 Test results .....	88
3.2.3 Compressive behaviour of compressit matrix .....	96
3.3 Concluding remarks .....	101

3.4	References .....	103
4.	Multiaxial behaviour .....	105
4.1	Review on concrete and FRC under multiaxial stresses .....	106
4.1.1	Continuum mechanics .....	106
4.1.2	Failure criteria applied to concrete .....	108
4.1.3	Multiaxial strength of concrete .....	112
4.1.4	Multiaxial constitutive relations for concrete .....	119
4.1.5	FRC under multiaxial stresses .....	121
4.2	Compressit matrix under multiaxial compression .....	124
4.2.1	Test specimens and method .....	124
4.2.2	Test results .....	125
4.2.3	Failure criterion for compressit matrix .....	129
4.3	Concluding remarks .....	131
4.4	References .....	132
5.	Fracture energy .....	135
5.1	Review on fracture energy for concrete and FRC .....	135
5.1.1	Three-point bend test on notched beam .....	137
5.1.2	$G_f$ -results for HSC and FRC .....	141
5.2	$G_f$ -tests on compressit matrix .....	142
5.2.1	Test specimens and method .....	143
5.2.2	Test results .....	143
5.3	Concluding remarks .....	146
5.4	References .....	147
6.	Conclusions .....	149
7.	Chronological reference list .....	153

## Appendices

A1	Direct tensile tests, test method and $\sigma_f/\sigma_{cr} - w$ relationships .....	163
A1.1	Test specimens and method .....	163
A1.2	Recorded $\sigma_f/\sigma_{cr} - w$ relationships .....	165
A2	Uniaxial compressive tests, test method and stress - strain relationships .....	175
A2.1	Test specimens and method .....	175
A2.2	Recorded stress - strain curves .....	177
A3	Triaxial compressive tests .....	185
A3.1	Triaxial cell and test method .....	185
A3.2	Preparation of test specimens .....	187

## Notation

Throughout this report SI units are used and in the following a list of the most important symbols are given. Furthermore most of the symbols are described in the text, when they occur.

### Abbreviations

Compressit	Compact reinforced composite.
c.o.v.	Coefficient of variation.
FCM	Fictitious crack model.
FRC	Fibre reinforced concrete.
HSC	High-strength concrete.
LEFM	Linear elastic fracture mechanics.
NSC	Normal-strength concrete.

### Roman letters

$a$	In Chapter 2: Length of debonded zone of matrix - fibre interface. In Chapter 3: Length of micro crack.
$a_0$	Notch depth in $G_r$ -test.
$A_f$	Cross-sectional area of fibre.
$A_{notch}$	Area of cross-section of notched test specimen.
$b$	Beam width.
$c$	Cohesion.
$CMOD$	Crack mouth opening displacement.
$d_s$	Maximum aggregate size.
$d_f$	Fibre diameter.
$e_i, i, j$	Orthogonal unit length vectors.
$E$	Modulus of elasticity.
$E_{notch}$	Initial slope of stress - strain curve recorded from notched test specimen.
$E_{peak}$	Secant modulus of compressive stress - strain curve, corresponding to peak.
$f$	Snubbing coefficient, $f \geq 0$ .
$F$	Tensile load at fibre end.
$F(\alpha)$	Function depending on dimensions, $\alpha = a_0/h$ .
$F_0$	Fibre load at completed debonding.
$f_{bisc}$	Biaxial compressive strength for stress ratio equal to 1.
$f_c$	Uniaxial compressive strength.

$f_s$	Tensile splitting strength.
$f_t$	Direct tensile strength.
$f_y$	Yield strength.
$g$	Snubbing coefficient, $g \geq 1$ .
$G, G_c$	Linear-elastic and secant shear modulus respectively.
$G_s$	Critical value of the surface energy.
$G_F$	Fracture energy per unit crack area.
$h$	Beam depth.
$I_s, I_0, I_{30}$	Toughness indices according to ASTM C1018.
$k$	In Chapter 2: Shear lag stiffness. In Chapter 3 and 4: Parameter in the Coulomb failure criterion, $k \geq 1$ .
$K, K_u$	Stress intensity factors.
$K, K_c$	Linear-elastic and secant bulk modulus respectively.
$l_s$	Characteristic length.
$L$	In Chapter 2: Embedment length of fibre, $0 \leq L \leq L/2$ . In Chapter 5: Load span of three-point loaded beam.
$L_{cr}$	Critical fibre length.
$L_f$	Fibre length.
$N$	Number of aligned fibres per unit area.
$N_A$	Number of random short fibres per unit area.
$N_v$	Number of random short fibres per unit volume.
$P$	Beam load.
$P(x)$	Tensile fibre force at position $x$ .
$r$	Length of deviatoric stress vector.
$s$	Slip of the embedded fibre end.
$u(x)$	Fibre displacement at position $x$ .
$U$	Fibre end displacement.
$U_0$	Fibre end displacement at completed debonding.
$v_0$	Volume fraction of fibres with inclination angle $\theta$ .
$V_f$	Fibre content by volume.
$w$	Crack width.
$w_{1/2}$	Crack width corresponding to a bridging stress equal to half the cracking stress.
$w_0^*$	Crack width at completed debonding.
$w_0$	Crack width corresponding to the post-cracking stress.
$W$	Energy density.
$W_f$	Fibre content by weight.
$X, Y$	Strains and stresses respectively normalized by respect to their peak values.
$z$	Distance from geometric centre of fibre to crack plane.

Greek letters

$\epsilon$	Longitudinal strain.
$\epsilon_0$	Hydrostatic strain.
$\epsilon_c$	Compressive strain at peak load.
$\epsilon_{cr}$	Strain at cracking.
$\epsilon_{ij}$	Second order strain tensor ( $i, j = 1, 2, 3$ ).
$\gamma_0$	Octahedral deviatoric strain.
$\delta$	Deflection of three-point loaded beam.
$\delta_{ij}$	The Kronecker delta.
$\eta_1$	Length efficiency factor.
$\eta_0$	Orientation efficiency factor.
$\theta$	In Chapter 2: Inclination of fibre to crack plane normal. In Chapter 4: Angle in the deviatoric stress plane.
$\nu$	The Poisson ratio.
$\sigma$	Position on the hydrostatic stress axis.
$\sigma_1, \sigma_2, \sigma_3$	Normal stress.
$\sigma_0$	Hydrostatic stress.
$\sigma_B$	Principal stresses.
$\sigma_1, \sigma_2, \sigma_3$	Normal stress from fibres bridging a crack.
$\sigma_r$	Cracking stress.
$\sigma_z$	Ultimate tensile stress of fibre.
$\sigma_{ij}$	Second order stress tensor ( $i, j = 1, 2, 3$ ).
$\sigma_{sc}$	Post-cracking strength.
$\tau$	Bond shear stress at the matrix - fibre interface.
$\tau_0$	Octahedral deviatoric stress.
$\tau_{cr}$	Critical bond shear stress at the matrix - fibre interface.
$\tau_s$	Frictional bond shear stress at the matrix - fibre interface.
$\phi$	Angle of friction.
$\phi$	Geometrical reinforcement ratio.
$\phi_f$	Geometrical fibre reinforcement ratio.

# 1. Introduction

Throughout the last decade efforts have been made to develop concrete with increasing strength. Research programmes all over the world are investigating numerous topics connected with *high-strength* concrete or *high-performance* concrete herein abbreviated as HSC, contrary to *normal-strength* concrete (NSC).

No unique definition of HSC exists, but most investigations separate HSC from NSC by means of the uniaxial compressive strength  $f_c$  determined after 28 days. In Denmark the term HSC is used for concrete with  $f_c$  higher than 50 MPa because this limits the range of the Danish concrete code<sup>1</sup>. In Norway however strengths as high as 105 MPa are permitted, which is exceptional in the world today, and in USA the transition from NSC to HSC happens at 41 MPa according to the American Concrete Institute.

At a recent symposium held in Lillehammer, Norway ('Third International Symposium on Utilization of High-Strength Concrete') during the period June 20th to 24th 1993, approximately 150 papers from all over the world concerning HSC were presented. The trends were as follows

- In Japan focus is put on HSC for high-rise buildings. Much attention is paid to the post-peak behaviour of confined concrete columns, due to earthquake loads.
- In North America the investigations mainly concerned structural behaviour of e.g. beams.
- In Europe the attention concentrated on Norway, who has done a lot of research with emphasis on fracture mechanics, due to their huge off-shore gravity platform. In France the investigations focused on rheology and mix-design.

Of course these points only reflect a small part of the contributions to the symposium. Many papers contained a comparison of various material properties such as splitting strength, modulus of elasticity and fracture energy as function of both compressive strength, concrete mix and curing conditions.

A topic that demands a lot of research is the *increased brittleness* of HSC compared to NSC. The brittleness is often measured on plain beams subjected to 3-point bending as recommended by RILEM, the so-called  $G_f$ -tests. An example of the problems concerned with the increased brittleness is spalling of the cover from columns confined by steel stirrups, the cover simply spalls off at early load stages and leave the stirrups exposed.

In order to utilize the increased compressive strength the demands for ductile reinforcement increases to prevent catastrophic failures.

<sup>1</sup>Dansk Ingeniørforenings Code of Practice for the Structural Use of Concrete, DS 411.



The concept of *fiber reinforced concrete* (FRC) has been known and investigated for many years, but as for HSC the commercial use is still limited. Numerous fibre products exist such as glass fibres, asbestos fibres and carbon fibres.

Observations that are always reported from tests on FRC are *increased ductility* and *reduced crack widths*. While the latter is very important in the service limit state, where the fibres have crack arresting effect, the first observation has not been paid much attention so far, even though the ductility increases significantly by adding fibres to the matrix.

The present report concerns solely with steel fibres in an attempt to connect the best properties from both FRC and HSC by means of short steel fibres mixed into a high-strength matrix.

The main disadvantages of normal steel fibre reinforced concretes are

- The *material costs* increases significantly because of the steel fibres. The material price is often doubled or tripled even at small amounts of fibres.
- The mixing process gets more difficult because it is essential, that the fibres are spread out in the matrix to work properly. This demands for longer mixing with advanced vibration, which makes in-situ casting more difficult.

However, as stated in the following the mixing difficulties are overcome in case of compressit matrix, allowing for very high amounts of fibres to be added.

## 1.1 Facts about compressit

The name *compressit* is an abbreviation of compact reinforced composite and it means an ultra high-strength steel fibre reinforced concrete additionally reinforced with conventional steel bars. The term *compact reinforced* refer to the conventional steel bar reinforcement, while the term *composite* represents the steel fibre reinforced matrix. The compressit concept is patented by Aalborg Portland A/S in Aalborg, Denmark and is closely related to the binder product *Densit*<sup>2</sup>, also patented.

Thus, the name compressit represents a *total concept* rather than just a concrete material. This report deals solely with the material behaviour of the *compressit matrix*, i.e. without any conventional reinforcement bars. It is attempted to use the term compressit matrix throughout the investigation in order to avoid misunderstandings. In the following some historical background together with the principal material data are provided.

<sup>2</sup>Registered trademark of Densit A/S, Aalborg, Denmark.

**Historical background.** The principles leading to the high-strength products from Aalborg Portland A/S are mainly due to the senior research engineer H.H. Baché at the Cement and Concrete Laboratory, being the inventor of both *Densit* and *compressit*.

In the sixties HSC-research concentrated on developing concrete with water cement ratio *w/c* less than 0.3, which was the lower limit for concrete mixes at that time. By use of vibratory compaction the cement particles were forced closer together, obtaining *w/c* as low as 0.2. However, the compaction techniques were not practicable for concrete.

Then the research focused on how to compact the cement by filling the pores with ultra-fine particles. The difficulties in packing the particles densely enough originated from the surface forces between the particles. Around 1970 effective dispersants, that made it possible to produce mixes with strengths higher than 100 MPa, appeared.

At Aalborg Portland A/S these dispersants (in particular superplasticizers) were used to develop a binder with optimum packing. This so-called DSP materials (densified cement/ultra fine particle based materials) consisted of approximately 30 % microsilica with particle size 100 times smaller than ordinary cement particles. Since 1978 these DSP materials have been used commercially under the name *Densit* and they show compressive strengths between 100 and 200 MPa. In *Baché (1987)* the DSP materials are described in details.

The start of compressit (or CRC as it was abbreviated until 1990) was in 1986. It initiated from the fact that the DSP materials were very brittle, which was counteracted by adding short steel fibres. It was expected, that the dense matrix provided excellent bond characteristics for the fibres and furthermore the high viscosity of the matrix made it possible to add high amounts of fibres. For ordinary concretes a fibre content of 2 - 3 % forms the practical upper limit, while compressit goes as high as 12 %, but usually 6 % is used. In *Baché (1987)* the basic principles behind the compressit concept are given.

Since 1986 several tests have been conducted on compressit including beams in shear and bending, slabs subjected to explosions together with numerous tests on the material properties. These tests all show very promising strengths and especially a very high ductility. Aalborg Portland A/S is involved in EC-projects and works closely with the Building Department at Aalborg University and the Carl Bro Group in investigating compressit.

**Mix description.** The mix typically used for compressit matrix consists of concrete with a maximum *aggregate size* as low as 4 mm, because of the compact reinforcement arrangement with closely spaced steel bars. The mix ingredients are given in table 1.1 for a matrix with approximately 6 % steel fibres by volume and a water to binder ratio of 0.18.

The *Densit binder* consists of approximately 20 % microsilica and the rest is ordinary Portland cement. Furthermore the binder includes superplasticizer. The mix design given in table 1.1 naturally can be changed according to special demands for fibres and aggregate, but the listed values apply to the major part of all existing compressit investigations.

## 1. Introduction

The *mixing* of the matrix takes place in a *paddle mixer* in the laboratory (up to 50 litres). First all the ingredients except fibres and water are mixed for 2 minutes. Then water is added followed by 10 minutes of mixing. Finally fibres are added over a period of approximately 1 minute followed by 5 minutes of mixing before the matrix is ready for casting.

Ingredient	Quantity (kg)	Density (kg/m <sup>3</sup> )
Densit binder	34	Cement: 3150 Microsilica: 2250
Quartz sand:		
0 - 0,25 mm	7	2640
0,25 - 1 mm	12	2640
1 - 4 mm	24	2670
Tap water	6	1000
Steel fibres	17	7500

Table 1.1: Typical compressit mix with 6 % steel fibres. The water to binder ratio is equal to approximately 0.18.

During *casting* vibrations varying from 50 to 150 Hz are used and because of the dense nature of the matrix the casting must be carefully undertaken in order to allow the air trapped inside the matrix to escape.

The water content in the compressit mix is very low and in order to minimize the *evaporation* from the cast specimens all exposed surfaces are covered with wet towels and plastic. One day after casting the specimens are usually demoulded and the following *curing* varies according to the given conditions:

- 1 to 5 days in water at 80° C.
- About 5 days in a heat cabinet at 45° C.
- 28 days in water at 20° C.

All the given curings are followed by at least a week in the laboratory wrapped in wet towels at about 20° C before testing. Pilot tests with varying curing conditions show that one day in the hot water results in strengths higher than the more normal approach with 28 days in water. However, the heat curing is only applied in situations with special demands for minimizing time consumption. Furthermore the accelerated curing ensures, that the strength development

## 1.1 Facts about compressit

during testing is insignificant and no dependence of the curing time is included in the test results.

The curing and casting procedures described above are especially aimed at laboratory tests on relatively small specimens. However in case of compressit structural elements the proper procedures should be developed.

**Material properties.** In the following some typical properties of the compressit matrix are listed in table 1.2. The values refer to the range of compressit matrices with varying fibre type and content.

Fibre content (%)	Density (kg/m <sup>3</sup> )	Compressive strength (MPa)	Flexural modulus of elasticity (GPa)	Flexure strength (N/mm <sup>2</sup> )
0 - 10	2500 - 3500	150 - 250	40 - 60	0.1 - 25

Table 1.2: Typical material properties for compressit matrix.

The fibres in question are all *straight steel fibres*, the so-called Dramnix fibre<sup>3</sup>. A total of 3 different Dramnix fibre types have been used in material tests on compressit matrix as shown in table 1.3.

Fibre name Dramnix	Length (mm)	Diameter (mm)	Aspect ratio (L/D)	Tensile strength (MPa)	Note
OL 6/15 HC	6	0.15	40	2950	Brass-coated, high carbon.
OL 13/15 HC	13	0.15	87	2950	Ditto.
OL 12/40	12	0.40	30	1350	Low carbon.

Table 1.3: Dramnix fibre types and properties. The fibres are loose and straight indicated by the designation OL.

The geometrical fibre dimensions given above have tolerances of  $\pm 1$  mm on the length and  $\pm 0.01$  mm on the diameter for fibre type OL 6/15 HC and OL 13/15 HC, while the

<sup>3</sup>Registered trademark of N.V. Beckaert S.A. Building Products, Belgium.

## 1. Introduction

tolerances on fibre type OL 12/40 are  $\pm 2$  mm and  $\pm 0.02$  mm respectively.

Two of the fibre types in table 1.3 have diameter 0.15 mm (only the length separates these two types) and they are made out of high quality steel. These fibres cost about 3 times as much as the third type (with diameter 0.4 mm). So far mostly the fibre type OL 6/15 HC has been applied to compressive matrix because the specimens have been relatively small. In the future however, the longer and cheaper fibre type OL 12/40 is preferred for structural use.

**Steel bar reinforcement.** The compressive concept also includes a compact arrangement of steel bars beside the fibre reinforcement. It is obvious that in order to utilize the high compressive strength of the matrix, high quality steel bars are needed. These bars often consist of *deformed steel bars* of kamsteel with a *guaranteed yield strength* of approximately 550 MPa (Ks 550). However, also high-strength steel products such as prestress wires and Drywidag bars are used.

**Anchorage tests** performed with kamsteel bars indicate, that the necessary anchorage length is only one third of the length required for bars embedded in ordinary concrete according to the Danish concrete code (DS 411). Furthermore the demands for sufficient cover thickness are expected to be easily obtained, because the compressive matrix is very dense (durable) and the fibres prevent cracks.

## 1.2 Scope of present investigation

The normal approach, when the *ultimate limit state* is considered for reinforced concrete structures, is to neglect the tensile strength of the concrete matrix. This limit state is defined as the load level at which failure occurs, i.e. the maximum allowable load sustained by the structure. Throughout this report various names such as yield load, ultimate load and bearing capacity are used for this particular state.

The normal procedure in concrete structural design is to let the reinforcement bars sustain tension, while the concrete carry compressive stresses. This approach has proven good results through many years. However since fibre reinforced concrete has appeared, the question whether concrete tensile strength should be taken into account, has risen. No clear answer is given to that question, but it is evident from numerous tests that incorporation of fibres to concrete *increase the bearing capacity* of reinforced concrete structures, even though the compressive strength is hardly affected.

Throughout the last two decades *fracture mechanical* methods have been developed, where the tensile characteristics are essential for the response of the structure. A well-known approach, meant for concrete, is the so-called *flexious crack method* (FCM), which is developed by professor Hilleborg at the University of Lund, see e.g. Hilleborg (1980). The

## 1.2 Scope of present investigation

method is based on tensile stress - crack opening relationships and states, that stress can be transferred across a crack even though it is open.

Thus, the tensile behaviour is modelled by a continuum mechanics description, i.e. a  $\sigma - \epsilon$  relationship, until *crack localization* occurs. After this localization a  $\sigma - w$  relationship is applied, where  $w$  is the crack opening, and the area under this curve corresponds to the so-called *fracture energy*  $G_f$ .

The FCM requires numerical calculations, which means that the calculations are very time consuming. Furthermore the position of the cracks is generally unknown and therefore several calculations are necessary to obtain the correct behaviour. In order to obtain the stress - crack width relationship for the material in question, tensile tests are necessary and no such standard tests exist like for the compressive strength. In order to make it possible to use the method a simple 3-point bending test, which can be performed almost everywhere, is proposed by RILEM to determine  $G_f$ .

Another theory, which has proven good results throughout many years, is the *theory of plasticity*. Expressions for the ultimate bearing capacity of several structural members such as beams and slabs exist. The fact that concrete is not an ideal plastic material is dealt with by reducing the compressive strength empirically. Most practical solutions neglect the tensile strength of concrete, but this simplification is not necessary.

Bearing in mind that fibres increase the fracture energy of concrete considerably and that the FCM-solution tends toward the plastic solution when  $G_f$  increases, it is obvious to apply the theory of plasticity to FRC-structures.

The present report does not include structural considerations, but establish the *basic material properties* for the compressive matrix. These properties are divided into 4 main parts:

- Uniaxial tensile behaviour considered in Chapter 2.
- Uniaxial compressive behaviour considered in Chapter 3.
- Multiaxial behaviour considered in Chapter 4, including a failure criterion.
- Fracture energy is considered in Chapter 5.

Each chapter includes both *test results* obtained from compressive matrix with varying fibre content and type, and comparisons with existing models for FRC. Thus the chapters are divided into 2 parts. The first part of each chapter contains a general review on the existing knowledge concerning concrete with emphasis on FRC and HSC. Then the second part contains a description of tests performed on compressive matrix. These tests primarily include those performed in connection to the present Ph.D.-project with the details given in Appendices 1 to 3.

## 1. Introduction

The end of each chapter contains a summary of the most important conclusions and characteristics for compressive matrix, together with a reference list. Finally the whole report is ended with a conclusion and a complete chronological reference list.

## 1.3 References

- Baehre, H.H. (1981), *Densified Cement/Ultra-Fine Particle-Based Materials*, Paper presented at The Second International Conference on Superplasticizers in Concrete, June 10 - 12, Ottawa, Canada, Also CBL Report No. 40, Aalborg Portland A/S, 35 pp.
- Baehre, H.H. (1987), *Compact Reinforced Composite, Basic Principles*, CBL Report No. 41, Aalborg Portland A/S, 87 pp.
- Hillerborg, A. (1980), 'Analysis of Fracture by means of the Fictitious Crack Model Particularly for Fibre Reinforced Concrete', *International Journal of Cement Composites*, Vol. 2, No. 4, pp. 177-184.

## 2. Tensile behaviour

The most pronounced effects of adding steel fibres to concrete mixes are the *increased energy dissipation* and the *crack arresting effect*. These subjects primarily concern the conditions of crack opening and are naturally related closely to the tensile behaviour of FRC. The energy dissipation is mainly connected with pull-out of fibres crossing a crack and furthermore these fibres reduce crack growth.

This chapter is divided into two parts: the first part describes theoretical approaches to predict the tensile properties of FRC and the second part reports tensile test results obtained with compressive matrix and applies the theoretical models.

Most theoretical models are based on a *micromechanical approach*, where the behaviour of a single fibre embedded in matrix is considered separately and then further extended to several fibres bridging a crack with random embedment and orientation. The latter is typically treated by means of statistical methods.

### 2.1 Review on FRC under tension

Throughout the last two decades different theoretical models have been proposed in order to predict the tensile strength and the tensile stress - strain curve of FRC. These models approach the problem from slightly different angles and introduce various refinements to the theory. However the final expressions turn out to be quite similar despite of the model.

In the following a description of some of the most important theoretical approaches is given followed by comparisons with existing test results including compressive results.

#### 2.1.1 Early investigations concerning FRC

One of the first models to predict the tensile strength as a function of fibres is reported in Romaldi & Barson (1963) and Romaldi & Mandel (1964). Both use *fracture mechanics* to calculate the strength as a function of the *spacing* between short random steel fibres. A circular internal crack perpendicular to the tensile stress is considered, and stress intensity factors corresponding to the external stress and the fibre bridging stress are given.

The critical fracture energy depends on the fibre spacing, which is assumed to be equal to the critical flaw size. When the elastic energy release equals a critical value, needed to initiate crack growth, the crack becomes unstable. The model states that for constant  $V_f$  the cracking strength is significantly increased with decreasing fibre spacing. The fibre spacing measure is defined as  $1.38d_f/V_f$ , which gives the average distance between the geometric centers of

the fibres.

However the assumption that fibre spacing strongly influences the first-cracking stress is now generally rejected, see e.g. Shah (1991). Instead it is recognized, that the fibres change the overall behaviour of FRC, while the first cracking stress is mainly governed by the matrix material.

**ACK-model.** An early classic investigation is named the *ACK-model* after Aveston, Cooper and Kelly, see e.g. Aveston & Kelly (1973) and Hamant (1978), pp. 16-22. Their model, which is developed in the early seventies, concerns *continuous aligned long fibres* directed in the tensile stress direction. The theory primarily focus on the state of *multiple cracking*.

The model assumes a single-valued matrix cracking stress, i.e. independent of fibre geometry and content. Here we shall only consider the *unbonded case*, where the interfacial bond between fibre and matrix is equal to a constant shear stress  $\tau$ . Refinements have been applied in order to include the debonding process of the fibre-matrix interface, see Aveston & Kelly (1973).

In figure 2.1 an idealized tensile stress - strain relationship is shown. The fibre content by volume is denoted  $V_f$  and a unit area cross-section, normal to the aligned fibres, is considered. This gives a total of  $N$  fibres crossing this section:

$$N = \frac{V_f}{A_f} = \frac{4V_f}{\pi d_f^2} \quad (2.1)$$

In the following subscript  $f$ ,  $m$  and  $c$  denotes fibre, matrix and composite respectively, while  $u$  denotes ultimate. The composite stress increases linear-elastic until matrix cracking:

$$\sigma_c = E_c \epsilon_c, \quad \epsilon_c \leq \epsilon_{cm} \quad (2.2)$$

where  $E_c$  is given by the so-called *Voight-method*. This method gives the stiffness of the composite assuming that the strains of the composite is identical to those of the matrix and the fibres. Thus, it is analogous to a system of two springs with different stiffness connected in parallel:

$$E_c = E_f V_f + E_m (1 - V_f) \quad (2.3)$$

When the stress reaches the value  $E_c \epsilon_{cm}$  the matrix cracks. The matrix stress is then taken by the fibres alone in the cracked section and provided, that the fibres are strong enough the increase in fibre stress is  $\Delta\sigma_f = \sigma_{cm}(1 - V_f)/V_f$ .

This fibre stress is transferred back into the matrix over the length  $x'$  by the shear stress  $\tau$ . The minimum value of  $x'$  is calculated from a simple force balance between the matrix

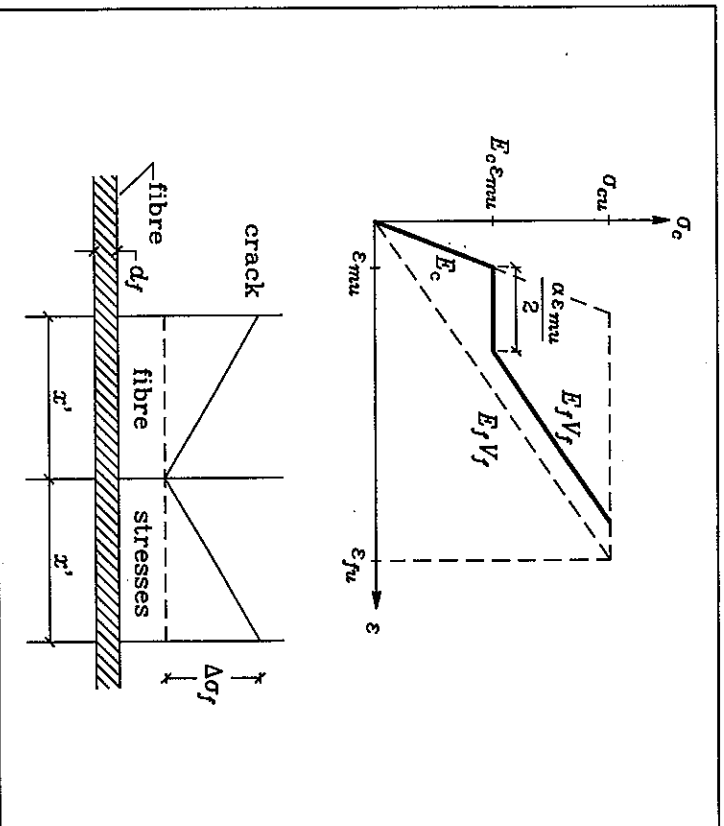


Figure 2.1: Idealized stress - strain relationship for ACK-model. Furthermore the fibre stresses are outlined between 2 cracks. cracking load and the transferred load per unit area cross-section:

$$x' = \frac{1 - V_f}{V_f} \frac{\sigma_{cm} d_f}{4\tau} \quad (2.4)$$

The matrix material cracks subsequently with distance  $x'$  under constant stress  $E_c \epsilon_{cm}$  symbolized by the horizontal line in figure 2.1. The fibre stress varies linearly as shown in figure 2.1 with amplitude  $\Delta\sigma_f$ . This gives an extension per unit length of the fibres equal to  $\Delta\epsilon_f = \frac{1}{2} \Delta\sigma_f / E_f = \alpha \epsilon_{cm} / 2$ , where  $\alpha$  is the ratio  $(1 - V_f) E_m / (V_f E_f)$ .

After total debonding of the matrix, only the fibres carry the stress and the ultimate composite stress is calculated as

$$\sigma_{cu} = \sigma_{\mu} Y_f \quad (2.5)$$

The dashed lines in figure 2.1 symbolize the triangle, where stress - strain curves being observed in practice will fall within because of the variability in matrix strength and bond strength. The lower limit corresponds to the situation without matrix contribution at all, cf. Hannant (1978).

**ACK-model applied to short aligned fibres.** If similar techniques are used for *non-continuous fibres*, the distance between the cracks decreases because of reduced efficiency of the fibres. The number of fibres crossing an arbitrary cross-section of unit area is still given in eq. (2.1).

The shortest embedment length of the fibres crossing a crack plane is assumed to be distributed uniformly within the range  $0 - L_f/2$ . The number of fibres with embedment length greater than  $x_c$  is  $N(1 - 2x_c/L_f)$  and the remaining  $2Nx_c/L_f$  fibres have one end less than  $x_c$  from the crack plane.

Like in the previous case the stresses are transferred from the fibres to the matrix until it cracks at distance  $x_c$ . However, some of the fibres are pulled out and a force balance gives

$$x_c/x' = L_f/x' - \frac{1}{2} \sqrt{(L_f/x')^2 - 4L_f/x'} \quad (2.6)$$

where  $x'$  is the crack distance given in eq. (2.4). When  $L_f$  increases the ratio  $x_c/x'$  goes toward 1 as it should be.

In order to calculate the *ultimate composite strength*, assuming fibre breaking rather than pull-out, the *critical fibre length* is calculated:

$$\pi d_f r \frac{L_{cr}}{2} = \frac{\pi d_f^2 \sigma_{\mu}}{4} \approx L_{cr} = \frac{\sigma_{\mu} d_f}{2\tau} \quad (2.7)$$

which is the fibre length, that is required to break a fibre, which is embedded by half its length, rather than pull it out of the embedment.

If  $L_f > L_{cr}$  and the shortest embedment length is uniformly distributed from 0 to  $L_f/2$ , the number of fibres being pulled out is  $NL_{cr}/L_f$ , while the rest breaks. Therefore we have two contributions to the strength:

$$\sigma_{cu} = \pi d_f r \frac{L_{cr}}{4} \frac{NL_{cr}}{L_f} + \frac{\pi d_f^2 \sigma_{\mu} N}{4} \left(1 - \frac{L_{cr}}{L_f}\right)$$

The first term on the right hand side is the pull-out resistance of the fibres with mean

embedment length  $L_{cr}/4$  and the second term represents the fibres that are breaking. If  $\tau$  is substituted with eq. (2.7) and  $N$  with eq. (2.1) we get

$$\sigma_{cu} = \left(1 - \frac{L_{cr}}{2L_f}\right) Y_f \rho_{\mu} \quad (2.8)$$

where the brackets contain the so-called *length efficiency factor* for  $L_f > L_{cr}$ .

**Efficiency factors  $\eta_l$  and  $\eta_o$ .** In the situation with continuous aligned fibres, the effect of the fibres is *optimum*. When the fibre length gets finite the ultimate strength decreases because some fibres always slip out of the matrix instead of breaking, as previously described.

The disturbance caused by finite fibre lengths and non-aligned fibres is often handled by applying the *efficiency factors* for length and orientation  $\eta_l$  and  $\eta_o$ , respectively. They are defined as the reduced fibre stress, resulting from finite fibre length and non-aligned fibres, related to the stress under optimum conditions.

The *length efficiency factor* in eq. (2.8) reads

$$\eta_l = 1 - \frac{L_{cr}}{2L_f}, \quad L_f \geq L_{cr} \quad (2.9)$$

and from a similar approach in Krenchel (1964), pp. 23-24, where the frictional shear strength during pull-out is neglected, we obtain

$$\eta_l = 1 - \frac{L_{cr}}{L_f}, \quad L_f \geq L_{cr} \quad (2.10)$$

In case of *fibres shorter than the critical length*, no fibres break and we obtain

$$\sigma_{cu} = \frac{L_f}{2L_{cr}} Y_f \rho_{\mu} = \eta_l Y_f \rho_{\mu}, \quad L_f \leq L_{cr} \quad (2.11)$$

It is generally assumed that  $\eta_l$  is near unity in the *elastic region* of the composite, see e.g. Hannant (1978), p. 12 and Laws (1971). Therefore  $\eta_l$  is only applied in the cracked state.

The *orientation efficiency factor* is basically related to the elastic behaviour of a composite to include the reduced stress contribution (and stiffness) from fibres non-aligned with the load axis. This is due to the assumption, that fibres only sustain stresses along their axis.

In figure 2.2a a situation is outlined with a fibre inclined at the angle  $\theta$  to the load axis. When the composite is extended  $\epsilon_c$  we get the fibre extension  $\epsilon_f = \epsilon_c \cos^2 \theta$ . The fibre stress  $\sigma_f$  contributes to the composite stress with  $\sigma_f \cos^3 \theta$ . Combining these expressions through

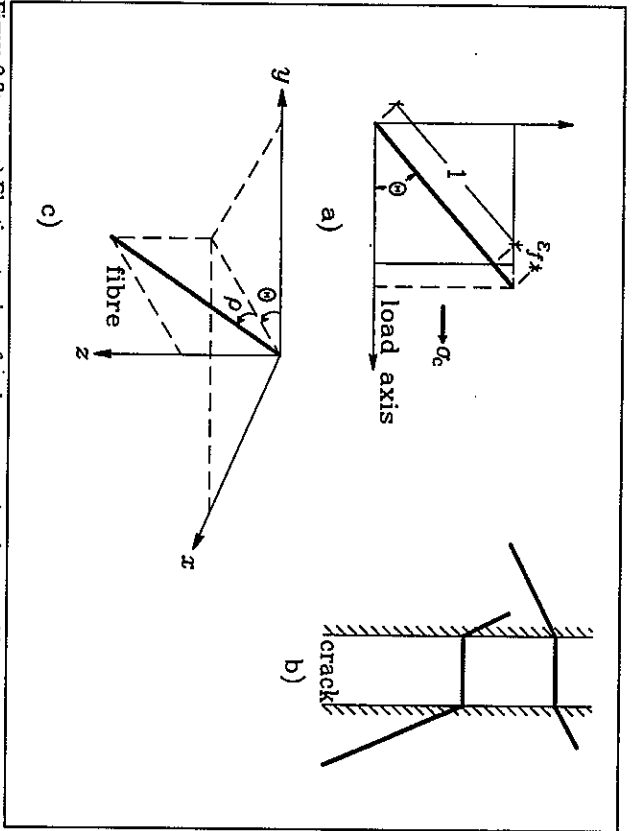


Figure 2.2: a) Elastic extension of a plane composite element with an inclined fibre. b) Inclined fibre aligned across a crack c) Definitions of angles describing a fibre in space.

\$Q\_f = E\_f \epsilon\_f\$, the fibre contribution to the composite stress reads \$E\_f \epsilon\_f \cos^2 \theta\$, see Krenchel (1964). After a sum up over all the fibres in a cross-section we get the following expression

$$\eta_o = \sum V_f \cos^4 \theta \quad (2.12)$$

where \$V\_f\$ is the volume of fibres, having inclination \$\theta\$, related to the total fibre volume. If all the fibres are aligned with angle \$\theta\$, we get \$\eta\_o = \cos^4 \theta\$ and if \$\theta = 0\$ we get \$\eta\_o = 1\$ as it should be.

For the case with fibres *randomized in all directions* the fraction of fibres within the infinitesimal range \$d\theta\$ is \$d\theta \sin \theta\$ and the sum in eq. (2.12) is made as an integration:

$$\eta_o = \int_0^{\pi/2} \sin \theta \cos^4 \theta \, d\theta = \frac{1}{5} \quad (2.13)$$

The stiffness of the composite is reduced corresponding to

$$E_c = \eta_o E_f V_f + E_m (1 - V_f) \quad (2.14)$$

of the Voight modulus given in eq. (2.3).

When the matrix starts cracking, the orientation efficiency factor changes because the fibres tend to align across the crack width, see figure 2.2b. The inclination causes the fibre bond to increase because of the side pressure imposed by the surrounding matrix. In Section 2.1.3 a model including this effect is discussed.

A very simple model assumes that the pull-out strength of an inclined fibre only depends on its length projected on the load axis. Romualdi & Mandel (1964) apply this approach in calculating their fibre spacing parameter as mentioned earlier. The fibre orientation in space is determined by the angles \$\theta\$ and \$\rho\$, see figure 2.2c, which are uniformly distributed between 0 and \$\pi/2\$. A fibre of unit length is projected on the \$y\$-axis, yielding the projection length \$\cos \theta \cos \rho\$. The *mean projection length* of all the fibres which also equals the efficiency factor, is calculated as

$$\eta_o = \frac{\int \int \cos \theta \cos \rho \, d\theta \, d\rho}{\int \int d\theta \, d\rho} = 0.405 \quad (2.15)$$

where the integrations are performed from 0 to \$\pi/2\$. The numerator equals the total sum of all the projection lengths and the denominator equals the number of these lengths.

2.1.2 Single fibre pull-out problem

**Shear lag model.** The behaviour of FRC is obviously closely related to the characteristics of the *fibre - matrix interface*. When short fibres are considered this interface fails progressively followed by fibre pull-out. It is assumed that *debonding* happens along this interface for an embedded fibre and that stresses are transferred along the interface only, i.e. no stress transfer from the fibre end to the matrix. Furthermore it should be noted, that *transverse deformations* are not taken into account in the following. Figure 2.3 shows the model adopted, a so-called shear lag model.

The displacement of the fibre is denoted \$u\$ and from Hooke's law we have the constitutive relation for the fibre written as \$P = E\_f A\_f du/dx\$, where \$P\$ is the tensile normal force in the fibre at position \$x\$ measured from the embedded end.

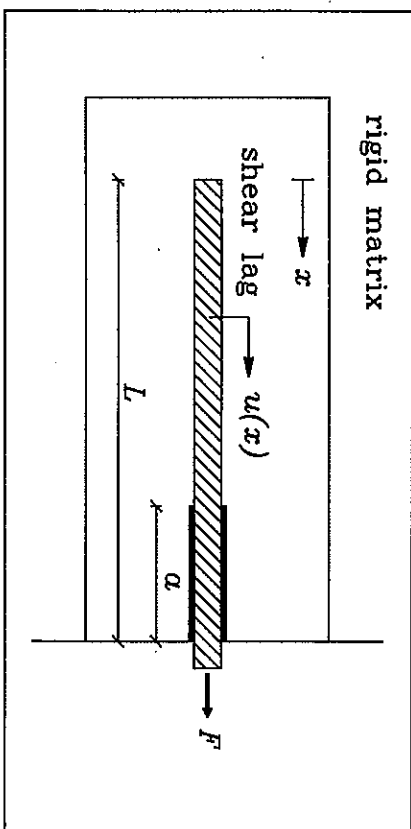


Figure 2.3: Shear lag model with a single fibre embedded in matrix.

If the constitutive relation is inserted in the equilibrium equation between  $P$  and  $\tau$ , which is the interface bond stress we get:

$$\frac{d^2 u}{dx^2} - \frac{4\tau}{EA_f} = 0 \quad (2.16)$$

As constitutive equation for the shear lag a linear-elastic relationship is often proposed with shear lag stiffness  $k$ :

$$\tau = ku \quad (2.17)$$

which is inserted in eq. (2.16) to obtain the second order differential equation that governs the axial displacement  $u$ . In the debonding zone  $L-a \leq x \leq L$  it is assumed, that  $\tau$  is constant and equal to  $\tau^*$ , i.e. a frictional shear resistance.

A total of 4 boundary conditions are needed to solve the problem. The first 2 state, that the load transfer is completed at the embedded end ( $du/dx = 0$  at  $x = 0$ ) and, that the fibre load at the free end equals  $F$  ( $EA_f du/dx = 0$  at  $x = L$ ). The remaining conditions are displacement and strain compatibility, which is required at  $x = L - a$ .

The solution to the problem is given in Stang et al. (1990) and it is based on the work of Lawrence (1972) and Laws (1982). Only a brief survey of the solution is reported here with emphasis on the conditions at the free fibre end, i.e. a prediction of corresponding fibre loads  $F$  and fibre end displacements  $U$ .

The fibre end displacement  $U$  depends on the debonding length  $a$  and the fibre load  $P$  through the following expression

20

$$U = u(x=L) = \frac{F}{EA_f} \left[ \frac{\cosh(\omega(L-a))}{\omega} + a \right] - \pi d_f^2 a \left[ \frac{\cosh(\omega(L-a))}{\omega} + \frac{a}{2} \right] \quad (2.18)$$

$$\omega^2 = \frac{4k}{EA_f}$$

When the solution for  $u(x)$  is known also the bond shear stress field is given through eq. (2.16), which yields

$$\tau = \omega \left( \frac{F}{\pi d_f} - a\tau^* \right) \frac{\cosh(\omega x)}{\sinh(\omega(L-a))}, \quad 0 \leq x \leq L-a \quad (2.19)$$

for the bonded part of the fibre and  $\tau = \tau^*$  for the debonded part. At  $x = L-a$  a discontinuity in  $\tau$  exists. The shear stress increases along the fibre to its maximum value at this point of discontinuity.

**Interfacial bond stress.** From the literature a lot of models exist to relate experimental observed results from single fibre pull-out tests to theoretical bond strengths. Here only a brief summary is given concerning the most popular approaches. Readers are referred to Gray (1984a) and (1984b), where an extensive review of pull-out theories is given, including applications to existing test results with steel fibres.

The various theories apply the so-called *stress criterion* for failure, where debonding is initiated, when the stress  $\tau$  exceeds a *critical value*  $\tau_c$ . After debonding has started the bond stress consists of a *constant frictional stress*  $\tau^*$  over the debonded zone. There are however different opinions, whether these bond strengths are material constants and how they are deduced from experiments.

A simple model proposed by Greszczuk in 1969 states, that the maximum shear stress occurs at the point where the fibre enters the matrix, i.e. at  $x = L$ . Greszczuk relates this maximum shear stress to an *average shear stress* along the interface, which is defined as the maximum pull-out load during a test divided with the surface area of the embedded fibre. Thus, Greszczuk assumes that when debonding is initiated at  $x = L$ , the maximum fibre load is reached and that the frictional bond strength can be neglected.

The experimental method to determine  $\tau_c$  is to register the average shear strength from several embedment lengths. When the average shear strengths are depicted as a function of the embedment length  $L$ , an extrapolation is performed to  $L = 0$ , which gives  $\tau_c$ , that initiates debonding, see Gray (1984a).

Lawrence (1972) includes a frictional shear strength  $\tau^*$  and concludes, that the debonding

21



process can be *stable* until a certain debonding length is reached. The term *stable* refers to the situation where an increase in debonding length  $a$  takes an increasing fibre load, i.e.  $dF/da > 0$ . This directly implies that debonding is *unstable* right from the start for the Greszczuk-model.

Lawrence (1972) gives the following 3 possibilities:

- $\tau_c/r^* = \infty$ , i.e. the Greszczuk-assumption, results in *unstable debonding*.
- $1 < \tau_c/r^* < \infty$  means that there exists a minimum embedment length  $L_{min}$  for stable debonding. If  $L < L_{min}$  debonding is unstable as above, otherwise it is stable until a critical debonding length.
- $\tau_c/r^* = 1$  means identical critical and frictional bond shear strengths and results in *stable debonding*.

According to Lawrence (1972) the strengths are experimentally determined from observed maximum pull-out loads for different embedment lengths. A graphical representation of these observations gives a curve with decreasing slope until it tends to be linear. The point where this curve gets linear determines  $\tau_c$  and  $L_{min}$ , while the slope of the linear part determines the frictional shear strength. A curve showing linear behaviour all the way represents the case  $\tau_c/r^* = 1$ , see Gray (1984a).

In Gray (1984b) a test series with about 40 specimens divided on 5 different embedment lengths is reported ( $L = 25, 50, 75, 100$  and  $125$  mm). The steel fibres are brass-coated with  $d_f = 0.38$  mm and a tensile strength of 2250 MPa, embedded in ordinary Portland mortar mix. It should be noted that the tests show great scatter with coefficients of variation ranging from about 20 to 40 % determined from at least 8 repetitions.

Gray finds that  $\tau_c = 3.3$  MPa according to the Greszczuk-model where no frictional bond is included. This value is determined from extrapolation of the measured average bond strengths.

The Lawrence-model however results in  $\tau_c = 45$  MPa and  $r^* = 1.3$  MPa, i.e.  $\tau_c/r^* \approx 35$ , and the minimum embedment length for stable debonding is 2.2 mm.

Gray (1984b) also includes a couple of other models refining the theory, but these models also differ as much as indicated above (One goes as high as  $\tau_c = 95$  MPa). The conclusions given in Gray (1984b) do not deal with these differences in theoretical predictions even though they differ by one order of magnitude. However he concludes, that bond strength seems to consist of both adhesional and frictional shear and only for very low embedment lengths the test results indicate, that there is no frictional resistance. Another important conclusion is, that bond strengths determined from various tests and analyses are very difficult to compare.

**Solutions to the single fibre pull-out problem.** Combining the contents of the previous two sections, concerning the shear lag model and the bond strength of the interface, gives a final solution to the problem. Stang et al. (1990) assume, that the ratio between the frictional strength and the critical shear stress, that initiates debonding, is denoted  $D$ , i.e.  $\tau^*/\tau_c = D$  with  $0 \leq D \leq 1$ .

The fibre load  $F$ , that corresponds to the debonding length  $a$ , yields directly from eq. (2.19) with  $\tau = \tau_c$  for  $x = L-a$ :

$$F = \pi d_f r_c^* \left( Du + \frac{\tanh(\omega(L-a))}{\omega} \right) \quad (2.20)$$

with  $\omega$  defined in eq. (2.18). The fibre load that initiates the debonding process is calculated for  $a = 0$ :

$$F_{ini} = \frac{\pi d_f r_c^* \tanh(\omega L)}{\omega} \quad (2.21)$$

and the corresponding fibre end displacement is found by inserting this value into eq. (2.18) for  $a = 0$ :

$$U_{ini} = \frac{\pi d_f r_c^*}{k} \quad (2.22)$$

where  $k$  is the shear lag stiffness defined in eq. (2.17).

Because of the linear-elastic shear lag, the  $F - U$  relationship increases linearly until the initiation of debonding. Thereafter the relationship is established by calculating subsequent values of  $F$  and  $U$  (eqs. (2.20) and (2.18) respectively) for increasing  $a$ -values from 0 to  $L$ .

The maximum value of  $F$  is obtained by differentiating eq. (2.20) by respect to  $a$  and equating the derivative to 0:

$$\frac{dF}{da} = 0 \Rightarrow L-a_c = \frac{\operatorname{arccosh}(1/D)}{\omega} \quad (2.23)$$

which gives the *critical debonding length* at which the debonding process gets unstable.

In Gopalaraman & Shah (1987) a similar approach as in Stang et al. (1990) is taken, cf. figure 2.3. Second order differential equations for the fibre force  $P$  are solved, assuming that the disturbance from the fibre reaches a certain distance into the surrounding matrix. This distance is taken as half the spacing between the fibre centers. Gopalaraman & Shah report, that using square packing of the fibres the distance is equal to  $0.5d_f(\pi d_f^2/V_f)$ , which is similar to the fibre spacing given in Romualdi & Mandel (1964). However Gopalaraman & Shah conclude, that the sensitivity of the final solution to the fibre spacing is not significant for

practical FRC-mixes.

The relation between the fibre load  $F$  and the debonding length  $a$ , according to Gopalaraman & Shah (1987), reads

$$F = \frac{\pi d r_c \left( D \operatorname{cosh}(\beta(L-a)) + \frac{\sinh(\beta(L-a))}{\beta} \right)}{(1-\alpha) \operatorname{cosh}(\beta(L-a)) + \alpha} \quad (2.24)$$

where

$$\alpha = \frac{A E_f}{A_m E_m}, \quad \beta^2 = \frac{2\pi G_m}{\ln \left( \frac{1}{2} \sqrt{\frac{\pi}{V_f}} \right) A E_f} \quad (2.25)$$

The symbol  $A_m$  denotes the matrix cross-sectional area, that surrounds each fibre and  $G_m$  is the linear-elastic shear modulus of the matrix.

A comparison with the previous solution given in eq. (2.20), where the extent of the surrounding shear lag is neglected and only taken into account through the stiffness  $k$ , gives a close similarity. If  $\alpha$  is neglected and  $\beta$  is replaced by  $\omega$  the two solutions are identical. Furthermore Gopalaraman & Shah (1987) proposes that the debonding length corresponding to maximum  $F$  can be calculated approximately from eq. (2.23) with  $\omega$  replaced by  $\beta$  under the assumption that  $(1-\alpha) \operatorname{cosh}(\beta(L-a)) \gg \alpha$ , which is true for practical FRC.

The model presented by *Lim et al.* (1987) takes the same approach as the latter, but in contrast to the fibre spacing concept, the surrounding matrix is taken into account by means of efficiency factors  $\eta_1$  and  $\eta_0$ . The fibre content is reduced by multiplying it by these factors representing the fibre randomness in length and orientation. Furthermore the matrix shear stiffness is modelled by a constant  $k$ .

*Lim et al.* (1987) introduce a bond shear model, where the frictional bond strength is equal to the critical shear strength, i.e.  $\tau^* = \tau_{\sigma}$  or  $D = 1$ . This model results in a stable debonding process all the way and the maximum pull-out load occurs, when debonding has completed, i.e.  $a_{\sigma} = L$ .

The reported relation between  $F$  and  $a$  is identical to that in Gopalaraman & Shah (1987), see eq. (2.24) with  $D = 1$ , and the constants  $\alpha$  and  $\beta$  are defined by

$$\alpha = \frac{\eta_1 \eta_0 E_f Y_f}{E_m (1-Y_f) + \eta_1 \eta_0 E_f Y_f}, \quad \beta^2 = \frac{4k E_m (1-Y_f) + \eta_1 \eta_0 E_f Y_f}{E_f Y_f E_m (1-Y_f)} \quad (2.26)$$

As it appears from the above there exists plenty of models describing both the interfacial properties and the fibre response to tensile loading for fibres embedded in a cementitious

material. The scope of these models differs of course according to the intended accuracy of the model. The question whether the matrix deformations should be taken into account when a fibre is pulled out cannot be given a clear answer, because it depends on the actual fibre stiffness and length, e.g. if short steel fibres with high stiffness are considered the matrix contribution can be significant.

An obvious difficulty in describing the fibre response is the bond shear problem. Pull-out experiments with a single fibre are difficult to perform like indicated by the relatively few existing tests. Furthermore the interpretation of the observed pull-out loads may result in very different bond strengths, beside the fact, that the test results are known to show great scatter.

In the following a very simple approach to the single fibre pull-out problem is given because it is the authors belief, that refinements are more useful at a later step of the calculations, when the structural capacity is considered. This is of course a choice, that must be taken in each individual case.

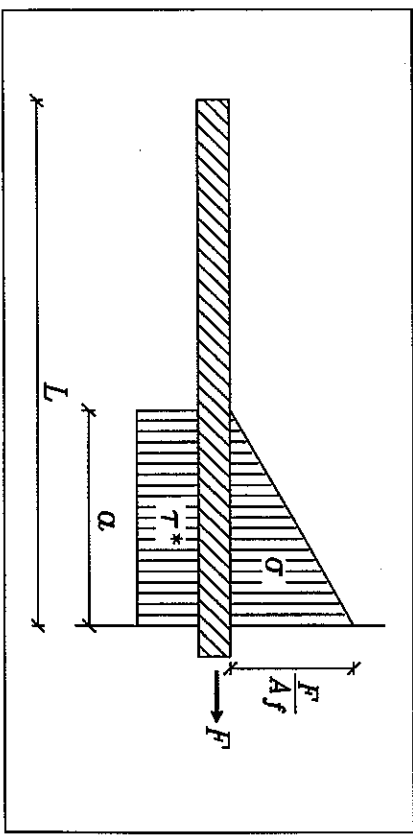


Figure 2.4: Special case of the shear lag model in figure 2.3. Rigid shear lag and only shear transfer under debonding.

**Simple solution to the single fibre pull-out problem.** This model assumes a rigid shear lag and that the fibre - matrix interface starts to debond, when the shear stresses grow to a certain critical value. The debonding zone transfers a constant shear stress equal to the critical value. This means that the fibre load is transferred along the debonded zone only, see figure 2.4.

In order to solve the problem by means of the equations previously established we apply the condition  $k \rightarrow \infty$ , which causes  $\omega \rightarrow \infty$ . It is clear, that debonding starts right from the beginning, cf. eqs. (2.21) and (2.22), because  $\tanh(\infty) = 1$ . The  $F - a$  relationship taken from eq. (2.20) reads

$$F = \pi d_j \tau^* \sigma$$

where  $\tau^* = \tau^*$  is the frictional bond shear strength ( $D = 1$ ). This expression is substituted into eq. (2.18) giving the  $U - a$  relationship:

$$U = \frac{\pi d_j \tau^* a^2}{2EA_f} \quad \Rightarrow \quad a = \sqrt{\frac{E A_f U}{2\tau^*}}$$

Finally these two expressions are combined into

$$F = \pi \sqrt{E A_f^3 \tau^* U/2} \quad (2.27)$$

with the maximum fibre load equal to  $F_{max} = \pi d_j L \tau^*$  at total debonding.

Even though this solution simplifies the pull-out behaviour and generally is known to be too rough, its advantages are several: The simple expressions are good as the first approximation in an analysis. Furthermore it is recognized to reflect the correct qualitative behaviour and the importance of the various fibre parameters.

In Li (1992) the simple theory is applied to investigate the complete stress - strain curve in the post-cracking domain of FRC as discussed in the following section.

**Fracture mechanical approach.** To end the description of the single fibre pull-out problem a fracture mechanical method to predict the fibre load is given. The method is based on Stang et al. (1990) and it is characterized by the assumption, that the *propagation of the debonding zone requires a certain energy*, opposite to the stress criterion just described.

The energy available for crack growth in the debonding zone is equal to the difference between the *elastic strain energy* stored in the system, together with the *frictional energy* and the *external work* performed on the system by the fibre load  $F$ . The shear lag model from figure 2.3 is used, giving the 3 following contributions to the elastic strain energy:

- The first part is stored in the debonded part of the fibre.
- The second part is stored in the debonded part of the shear lag.
- The third part is stored in the bonded system, i.e.  $0 \leq x \leq L-a$ .

The first and the third part are easily obtained because the fibre displacements  $u(x)$  are known together with the corresponding fibre forces  $F(x)$ . The second part concerning the debonded part of the shear lag cannot be calculated exactly within the theory presented here, because

the displacements of the shear lag is undetermined along the debonding zone. Only the frictional shear stress  $\tau^*$  is prescribed in this zone.

Stang et al. (1990) assume, that the debonded matrix interface has a *constant displacement* equal to the fibre displacement in  $x = L-a$ , but this assumption violates the constitutive relation in eq. (2.17). If instead eq. (2.17) is fulfilled ( $\alpha = \tau^*/k$ ) in the debonded zone there exists a *displacement discontinuity* at  $x = L-a$ .

The *work of friction* along the debonded interface is equal to the product of the constant shear load and the relative displacement between matrix and fibre. Once again the assumptions presented above are necessary to calculate an approximate value of the frictional energy.

The energy available for crack development, when the displacement of the fibre end is increased by  $dU$  reads

$$dW = F dU - dW_e - dW_f$$

where  $W_e$  and  $W_f$  are the strain energy and frictional energy respectively. The *energy release rate* (energy per unit new debonding length) is

$$\frac{dW}{da} = F \frac{dU}{da} - \frac{dW_e}{da} - \frac{dW_f}{da} \quad (2.28)$$

When this rate equals a *critical value* debonding is initiated. Stang et al. (1990) presents two solutions according to the assumptions concerning the debonded part of the shear lag.

Compared to eq. (2.20) a certain similarity between the shear lag solution and the fracture mechanical solution is discovered, but as stated in Stang et al. (1990) the fracture mechanical approach uncouples the parameters describing the adhesion and the frictional bond, while the stress criterion couples these parameters through  $D$ .

By numerical calculations it is found that the critical energy release affects both the fibre load, that initiates debonding, and the maximum fibre load, while  $\tau^*$  mainly affects the latter.

**Fibre pull-out after completed debonding.** After the debonding process has ended, whether it has been stable or not, the embedded fibre still has load capacity left. Now the fibre is pulled out of the matrix under *constant frictional bond shear stress*  $\tau^*$ , see figure 2.5. At total debonding the fibre load is denoted  $F_0$ :

$$F_0 = \pi d_j \tau^* \quad (2.29)$$

which coincides with the maximum load in the special case  $D = 1$ . Thereafter the embedded length decreases as the *fibre end slip out of the matrix* followed by decreasing load.

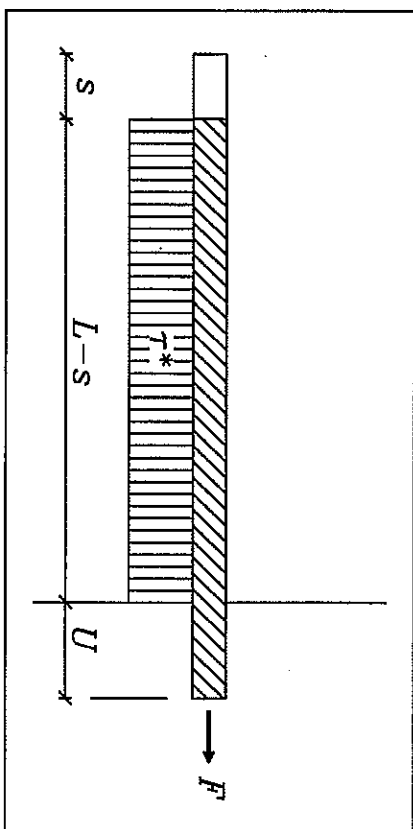


Figure 2.5: Fibre pull-out under constant frictional shear stress.

Simultaneously the fibre is *elastically contracted* because of the load reduction. The fibre end displacement consists of the following contributions:

$$U = U_0 - U_d + s, \quad 0 \leq s \leq L \quad (2.30)$$

where  $U_0$  is the displacement at total debonding, i.e. corresponding to  $F_0$ ,  $s$  is the *fibre end slip* and  $U_d$  is the contraction caused by the load decreasing from its maximum value  $F_0$  to  $F(s)$ . The *equation of equilibrium* reads  $F(s) = \pi d_f L \tau^*$  and the elastic contraction is calculated as

$$U_d = \frac{1}{2} \frac{\pi d_f \tau^*}{E_f A_f} (L^2 - (L-s)^2) = \frac{2\tau^*}{E_f d_f} (2Ls - s^2)$$

Inserting  $U_d$  in eq. (2.30) yields

$$U = U_0 + s - \frac{2\tau^*(2Ls - s^2)}{E_f d_f}, \quad 0 \leq s \leq L \quad (2.31)$$

which is reduced to  $U = U_0 + s$  when the elastic deformations of the fibre are neglected. In Li (1992) this latter assumption is taken, which yields

$$F = \pi d_f L \tau^* \left( 1 - \frac{U - U_0}{L} \right), \quad U_0 \leq U \leq L \quad (2.32)$$

i.e. a linearly decreasing  $F - U$  relationship.

### 2.1.3 Theory for short random fibres

After the discussion of the mechanics of a single straight fibre being pulled out of a matrix embedment, the theories are extrapolated to a bigger scale, where the fibre reinforced material is considered a *continuum*. It is assumed, that the fibres are totally *randomized* by respect to both orientation and position in a FRC structure.

The properties of steel fibre reinforced concrete with short fibres, i.e. shorter than the critical length, and randomly mixed in the matrix show several advantages, e.g.

- The dissipated energy during debonding and especially during fibre pull-out is much higher, than if the fibres break.
- The mixing/casting process is easier, when there is no constraints on the fibre orientation.
- Finally the material properties can be considered isotropic, which simplifies the design calculations.

Several early investigations are mainly concerned about the tensile behaviour in the elastic region, and therefore only consider the cracking strength, see Section 2.1.1. Another interesting area however, is the post-crack behaviour, which is strongly influenced by the fibres. During fibre debonding and pull-out the major part of the energy dissipation happens. Furthermore one of the conditions for multiple cracking, i.e. whether the bridging fibres can sustain stresses higher than the matrix cracking strength, are directly related to the post-cracking region. The major part of the investigations of the post-cracking behaviour of FRC focus on the post-crack strength, which is reflected in the following.

**Basic definitions.** A volume element of FRC with dimensions  $A_f L_f$  is considered, containing all the fibres crossing the crack plane  $A_c$ . The content by volume of straight fibres is  $V_f$  with fibre diameter  $d_f$  and length  $l_f$ .

Figure 2.6 shows a fibre arbitrary located with its center at distance  $z$  from the crack plane and orientation angle  $\theta$  to the crack plane normal. The central distance and the orientation angle are uniformly random distributed within the ranges from 0 to  $L_f/2$  and from 0 to  $\pi/2$  respectively. In figure 2.5 the probability density functions for  $z$  and  $\theta$  are shown.

The shortest of the two embedment lengths of a fibre is equal to

$$L = \frac{l_f}{2} - \frac{z}{\cos\theta} \geq 0, \quad 0 \leq \theta < \frac{\pi}{2}$$

resulting in the following constraint on  $\theta$  in order to make a fibre with central distance  $z$  to bridge the crack plane:

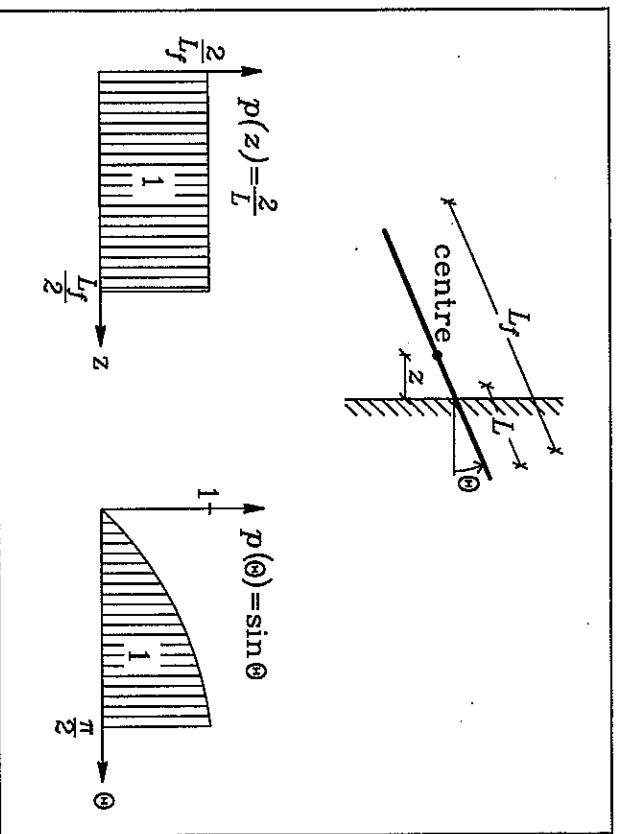


Figure 2.6: Probability density functions for the distance  $z$  and the orientation angle  $\theta$  of a random fibre.

$$\cos\theta \approx 2z/L_f \Rightarrow \theta \leq \arccos(2z/L_f)$$

The total number of fibres in the volume element is  $N_{total} = A_c V_f / A_f$  and the number of fibres  $dN$  located within the intervals  $\theta$  to  $\theta + d\theta$  and  $z$  to  $z + dz$  is calculated from

$$dN = N_{total} p(\theta) d\theta p(z) dz, \quad \begin{cases} 0 \leq z \leq L_f/2 \\ 0 \leq \theta \leq \arccos(2z/L_f) \end{cases} \quad (2.33)$$

The number of fibres crossing the crack plane  $A_c$  is calculated by integration:

$$N_c = N_{total} \int_0^{L_f/2} \int_0^{\arccos(2z/L_f)} \sin\theta d\theta dz = \frac{N_{total}}{2}$$

The number of fibres per unit volume and per unit area crack plane  $N_v$  and  $N_A$  respectively are hereby given as:

$$N_v = \frac{N_{total}}{A L_f} = \frac{4V_f}{\pi d_f^2 L_f}, \quad N_A = \frac{N_{total}}{2A_c} = \frac{2V_f}{\pi d_f^2} \quad (2.34)$$

By comparing  $N_v$  with  $N$  given in eq. (2.1), which applies to aligned fibres, it appears, that the randomness in fibre direction halves the number of fibres crossing a cross-section.

**Theoretical model of the complete post-crack behaviour:** Most approaches to predict the complete post-cracking behaviour by means of the fibre bridging stresses vs. the crack openings relationship, use empirical expressions obtained by mathematical curve fitting. In Li (1992) however, a simple model is presented. This model uses the simple solution for a single fibre pull-out, neglecting matrix stiffness and only considering frictional bond. Equations (2.27) and (2.32), for the ascending and the descending part of the fibre load - crack opening relationship for a fibre with its shortest embedment length  $L$  give

$$F(w) = \begin{cases} \frac{\pi}{2} \sqrt{E_f d_f^3} \tau^* w, & 0 \leq w \leq w_0 = \frac{4\tau^* L^2}{E_f d_f} \\ \pi d_f L \tau^* \left(1 - \frac{w-w_0}{L}\right), & w_0 \leq w \leq L \end{cases} \quad (2.35)$$

where  $\tau^*$  is the frictional bond and  $w_0$  corresponds to completed debonding. It appears from eq. (2.35), that the crack width  $w$  is introduced instead of the fibre end displacement  $U$ . The relation between  $w$  and  $U$  is simply  $w = 2U$ , while debonding takes place, because the elastic extension of the fibre happens on both sides of the crack. At complete debonding only the shortest embedded length starts to slip out of the matrix, giving  $w = U$  for the descending part.

Li (1992) takes the fibre orientation angle  $\theta$  into account by applying an empirical relation originally suggested by Morton & Groves (1976). When a fibre with inclination angle  $\theta$  crosses a crack, it is aligned after the load direction normal to the crack plane, see figure 2.2b. Experiments performed on polypropylene fibres show an increasing  $F$  when  $\theta$  increases from 0. This so-called *snubbing effect* is modelled by

$$F(w, \theta) = F(w) \exp(f\theta), \quad 0 \leq \theta < \pi/2, \quad f \geq 0$$

where the snubbing coefficient  $f$  is determined experimentally. Unfortunately no tests with steel fibres under various  $\theta$  are known to the author.

The fibre bridging stress  $\sigma_b$  is calculated by sum up all the fibre loads across a unit crack area. By use of the same principles as in the previous section the bridging stress is given as

$$\sigma_g(w) = \frac{\int F(w, \theta) dN}{A_c} = \frac{4V_f L_f}{\pi d_f^2} \int_0^{2} \int_0^{\arccos(2w/L_f)} F(w, \theta) \sin \theta d\theta dz$$

where  $A_c$  is the crack area,  $dN$  is given in eq. (2.33) and the integrations represent the sum of all fibre loads with varying embedment lengths and orientation angles. The integration is performed in two steps: The first step includes the fibres with embedment lengths not fully debonded, while the other concerns fibre pull-out i.e. the calculation includes fibres passing from debonding to pull-out, see Li (1992) for further details. The solution reads

$$\frac{\sigma_g(w)}{\frac{g\tau^* V_f L_f}{2 E_f d_f}} = \begin{cases} \begin{cases} 2 \sqrt{\frac{w}{w_0^*} - \frac{w}{w_0^*}} & 0 \leq w \leq w_0^* \\ \frac{4}{L_f} \left( \frac{L_f}{2} - w \right)^2 & w_0^* \leq w \leq \frac{L_f}{2} \end{cases} \end{cases} \quad (2.36)$$

where  $w_0^*$  is the value of  $w_0$ , that corresponds to  $L = L_f/2$ :

$$w_0^* = \frac{\tau^* L_f^2}{E_f d_f} \quad (2.37)$$

A new snubbing coefficient  $g$  is introduced, defined by

$$g = \frac{2(1 + \exp(\pi f/2))}{4 + f^2}, \quad g \geq 1, \quad f \geq 0 \quad (2.38)$$

where the situation without snubbing effect corresponds to the lower limits for  $f$  and  $g$ .

It should be noted, that the solution in eq. (2.36) assumes, that  $w_0^* < L_f/2$ . The maximum bridging stress occurs at  $w = w_0^*$  or actually a little bit before, and corresponds to the so-called *post-cracking strength*, denoted  $\sigma_{pc}$ :

$$\sigma_{pc} = \frac{g\tau^* V_f L_f}{2 E_f d_f} \quad (2.39)$$

In Section 2.1.2 Lim et al. (1987) introduces *efficiency factors*  $\eta_1$  and  $\eta_0$  to take the effects of fibre length and orientation into account. One fibre with embedment length  $L_f/2$  is considered and the randomness in both embedment length and fibre orientation is included by reducing the fibre content by multiplying it by the efficiency factors ( $\eta_1 \eta_0 V_f$ ) and thus the fibre bridging stress reads

$$\sigma_g(w) = \eta_1 \eta_0 V_f \frac{F(w)}{A_f} \quad (2.40)$$

where  $F(w)$  is the fibre load in a single fibre at crack width  $w$ , calculated from the expressions in eqs. (2.24) and (2.26), i.e. stepwise with increasing debonding length  $\alpha$ .

The *length efficiency factor* is given as

$$\eta_1 = \begin{cases} \frac{1}{2} & \text{for } L_f \leq L_{cr} \\ 1 - \frac{L_{cr}}{2L_f} & \text{for } L_f > L_{cr} \end{cases} \quad (2.41)$$

which coincides with eq. (2.9) for  $L_f \geq L_{cr}$ . The value  $\eta_1 = 0.5$  is taken because the reference value of the fibre stress corresponds to the case of continuous fibres. By comparison of eq. (2.1) and eq. (2.34) it is recalled, that in the case of continuous fibres there is exactly twice as many fibres crossing an arbitrary cross-section as in case of finite fibre lengths and therefore  $\eta_1$  equals 0.5, when fibre pull-out is considered.

The *orientation efficiency factor* in eq. (2.40) has the following values

$$\eta_0 = \begin{cases} 0.14, & \text{Elastic region} \\ 0.41, & \text{After matrix cracking} \end{cases} \quad (2.42)$$

The final solution suggested in Lim et al. (1987) does not include any simple expressions like in eq. (2.36), but instead a simplified relationship is given:

- From the cracking strength, which is assumed higher than the post-cracking strength ( $\sigma_{cr} \geq \sigma_{pc}$ ), the bridging stresses drop to the post-crack strength given by

$$\sigma_{pc} = 2\eta_1 \eta_0 \tau^* V_f \frac{L_f}{d_f} = 0.41 \tau^* V_f \frac{L_f}{d_f} \quad (2.43)$$

and the corresponding crack width reads

$$w_0^* = \frac{\tau^* L_f^2}{E_f d_f} + \frac{2\tau^*}{k} \quad (2.44)$$

**Theoretical models of the post-crack strength.** In the following the maximum stress, observed in the post-cracking region, is considered, i.e. the peak value of the bridging stress - crack opening curve. Especially for high contents of steel fibres, this strength is interesting because it can exceed the cracking strength of the composite. Two models based on statistics are presented briefly, giving predictions of both the mean value of the post-cracking strength

and the variance of this value, but first a very simple approach is taken.

The simple approach corresponds to the maximum pull-out load of a fibre, where only frictional bond strength is included, i.e.  $F_{max} = \pi d_f \tau^* L$  with  $L$  symbolizing the embedment length. The embedment length is uniformly distributed between 0 and  $L_f/2$ , cf. Figure 2.6, with mean value  $L_f/4$ . The maximum value of the post-crack strength sustained by the bridging fibres is calculated as the number of fibres crossing a unit area crack plane multiplied by the mean pull-out load per fibre, see e.g. Hannant (1978):

$$\sigma_{pc} = N_A F_{max}(L=L_f/4) = \frac{2V_f}{\pi d_f^2} \pi d_f \frac{L_f}{4} \tau^* = \frac{1}{2} \tau^* V_f \frac{L_f}{d_f} \quad (2.45)$$

One of the earliest investigations of the post-crack strength of FRC is reported in Naaman *et al.* (1974). The model is based on the statistical concept of the *weakest link*, meaning that a tensile member is considered as a chain consisting of  $n$  links. When one link fails (the weakest cross-section of the member) the whole chain breaks.

The statistical theory is not discussed here, but an important assumption is, that the fibres are distributed in the matrix according to a Poisson process with parameter  $N_v$ , cf. eq. (2.34). The simplest case is a chain with  $n = 1$ , resulting in a mean value and variance equal to

$$E[\sigma_{pc}] = \frac{1}{\pi} \tau^* V_f \frac{L_f}{d_f}, \quad \text{Var}[\sigma_{pc}] = \frac{\pi}{A_c} (\tau^*)^2 V_f \frac{L_f^2}{8} \left( \frac{1}{8} - \frac{1}{3\pi^2} \right) \quad (2.46)$$

where  $\tau^*$  is the average bond shear strength and  $A_c$  is the cross-sectional area of the tensile member. When the number  $n$  increases, the mean strength decreases because the possibility of an exceptionally weak link grows. This dependency is calculated numerically by Naaman *et al.*

Naaman *et al.* (1974) report, that  $\tau^*$ , measured from a single fibre pull-out test, should be reduced with the number of fibres. This reduction is due to the interference of the stress fields along the fibres. A suggestion, based on tests with 0.25 mm diameter steel fibres, reads  $\tau_s^* = \tau^* - 0.52N_v$ , where  $N_v$  is the number of fibres per unit cross-sectional area given in eq. (2.34).

The coefficient of variation can be estimated from eq. (2.46):

$$c.o.v. = \frac{\sqrt{\text{Var}[\sigma_{pc}]} }{E[\sigma_{pc}]} \approx \frac{5.5d_f}{\sqrt{A_c} V_f}$$

and using, that the minimum cross-sectional dimension in direct tensile tests is typically 3 times the fibre length, i.e.  $A_c = 9L_f^2$ , we get

$$c.o.v. \approx \frac{1.8 d_f}{\sqrt{V_f} L_f} \quad (2.47)$$

For typical values of  $V_f$  the first term is of magnitude 10 and if fibres with  $L_f/d_f = 50$  are considered, then the coefficient of variation is approximately 20 %.

Another statistical approach to predict the post-crack strength is given in Gasparini *et al.* (1989), where the *Poisson process* is assumed to describe the occurrences of fibres. The Poisson process is characterized by identical mean and variance.

Gasparini *et al.* (1989) assume, that the fibre pull-out strength only depends on the *effective embedment length*, defined as the projection of the embedment length on the load direction. If the effective embedment length is given for a fibre it is assumed, that the occurrence of such fibres on a unit cross-sectional area follows the Poisson distribution with mean and variance equal to  $N_v L$ , where  $L$  denotes the given projected embedment length. It is crucial for the model that the process of fibre occurrences unconditional this length is not a Poisson process, see Gasparini *et al.* (1989) for further details.

By assuming that the embedment length of fibres with projected length  $L$  is uniformly distributed between 0 and  $L/2$  and given the probability density function for both the projected embedment length and the occurrence of fibres, conditioned the projected length  $L$ , the mean and variance of the post-crack strength are given as

$$E[\sigma_{pc}] = \frac{1}{4} \tau^* V_f \frac{L_f}{d_f}, \quad \text{Var}[\sigma_{pc}] = \frac{1}{48} \left( \tau^* V_f \frac{L_f}{d_f} \right)^2 \quad (2.48)$$

with the coefficient of variation simply derived as

$$c.o.v. \approx \frac{4}{\sqrt{48}} = 0.577 \quad (2.49)$$

which seems higher than that obtained by Naaman *et al.* (1974).

The different models all suggest similar expressions for the post-crack strength, directly proportional to the bond shear strength and the fibre reinforcement index:

$$\sigma_{pc} = \alpha \tau^* V_f \frac{L_f}{d_f} \quad (2.50)$$

with  $\alpha$  being the constant of proportionality and  $\tau^*$  being determined from a single fibre pull-out test. In table 2.1 a survey of the different proposals is given.

Investigator	Suggested $\alpha$ value	Equation	Note
Naaman, Moavzenadeh & McGary (1974)	0.32	(2.46)	Depends on $n$ .
Hannant (1978)	0.50	(2.45)	-
Lim, Paramasivam & Lee (1987)	0.41	(2.43)	Using efficiency factors.
Gasparini, Verma & Abdallah (1989)	0.25	(2.48)	-
Li (1992)	0.5g	(2.39)	The factor $g$ is defined in eq. (2.51), $g \geq 1$ .

Table 2.1: Suggested values for  $\alpha$  in eq. (2.50), expressing the post-cracking strength.

It is clear from the table that the suggested  $\alpha$ -values have great range, varying from 0.25 to more than 0.5. Furthermore from the predictions of the variances to be expected on  $\sigma_{ps}$  of eqs. (2.47) and (2.49) and those experienced on measurements of  $\tau^*$ , there is no reason to believe, that tests performed with normal accuracy can be expected to distinguish between the different suggestions.

Relatively few experiments exist, investigating the post-crack strength of FRC. Most existing test results do not distinguish between the cracking strength and the post-crack strength, because the amount of fibres is insufficient to separate the fibre contribution from the matrix contribution. However, in figure 2.7 post-crack test results from Naaman et al. (1974) and Lim et al. (1987) are given. The strengths are normalized by respect to the bond strength, measured on single pull-out tests on fibres.

Naaman et al. (1974) represent more than 100 tests with specimens of the *dog-bone type*, i.e. specimens with a weak midsection. The cross-sectional dimensions are 50.8 x 38.1 mm at the notched sections and 50.8 x 50.8 mm elsewhere. Each specimen contains 3 notched sections in order to model a chain with 3 links.

The test programme, listed in table 2.2, consists of 4 different fibres and 3 different contents for each fibre type. From 54 *single fibre pull-out tests*, an experimental value of  $\tau^*$  is determined to 2.6 MPa with *c.o.v.* equal to 54%. The mortar matrix used in the experiments has water to cement ratio 0.6.

Also Lim et al. (1987) use dog-bone specimens, but *without notches*. The midsection has cross-sectional dimensions 83 x 83 mm. A total of 8 different mixes are used, like it appears from table 2.2, all having water to cement ratio 0.5. Both straight and hooked steel fibres are

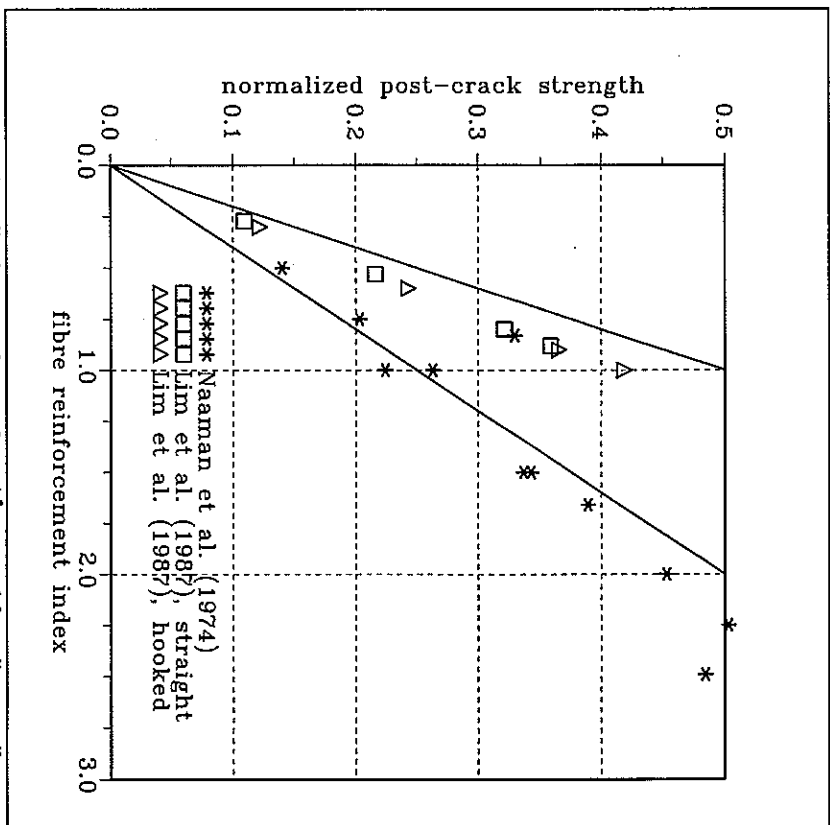


Figure 2.7: Normalized post-crack strengths  $\sigma_{ps}/\tau^*$  measured from direct tensile tests.

The solid lines have slopes  $\alpha = 0.25$  and  $\alpha = 0.5$ .

used and from each mix single fibre pull-out tests are performed. The obtained bond strengths lie within 2 - 3 MPa for the straight fibres and approximately the double for the hooked fibres. The coefficients of variation on these measurements vary from 10 to 20%.

The results depicted in figure 2.7 represent fibre reinforcement indices as high as 3, which is generally considered to be the practical upper limit. Furthermore two lines are drawn in figure 2.7 representing the slopes  $\alpha = 0.25$  and  $\alpha = 0.5$ . It seems that the best prediction of the results from Naaman et al. (1974) correspond to  $\alpha = 0.25$ , while the results from Lim et al. (1987) are higher. The proposal by Li (1992) seems to overpredict the post-cracking strength.



Naaman et al (1974) report coefficients of variation on the experimental post-crack strength varying from 25 % to more than 70 % determined from at least 8 test results. This indicates that the estimate of approximately 58 % predicted by Gasparini et al. (1989), cf. eq. (2.49), is not overpredicted.

Investigator	Fibre type	Crack width (mm)	Fibre length (mm)	V <sub>c</sub> (%)		
				Exp.	Pred.	
Naaman, Moavenzadeh & McGarry (1974)	Straight steel, brass-plated, low carbon	0.25	12.7	1	0.50	
				2	1.00	
				3	1.50	
		0.25	19.1	1	0.75	
				2	1.50	
				3	2.25	
	0.25	25.4	1	1.00		
			2	2.00		
			3	3.00		
			0.15	12.7	1	0.83
					2	1.66
					3	2.49
Lim, Paramasivam & Lee (1987)	Straight steel	0.57	30	0.5	0.27	
				1.0	0.53	
				1.5	0.80	
	0.57	50	1.0	0.88		
			0.5	0.30		
			1.0	0.60		
Hooked steel	0.50	30	1.0	0.60		
			1.5	0.90		
			1.0	1.00		

Table 2.2: Survey over fibre types and -dimensions used in direct tensile tests.

In Li (1992) the model using  $\alpha = 0.5g$  is compared to test results, which have not been

available to the author. These results go as high as  $V_c(L_f/d) = 1$ , and give satisfactory agreement under the assumption that  $\tau^* = 4 \text{ MPa}$  (no single fibre pull-out test performed) and  $g = 2.3$ , i.e.  $\alpha\tau^* = 4.6 \text{ MPa}$ .

**Fracture energy.** During fibre pull-out energy is dissipated at the interfaces between fibre and matrix. This energy dissipation is significantly higher, than the energy dissipation observed without fibres. The *dissipated energy* is divided with the crack area introducing the *fracture energy*  $G_f$ , interpreted as the energy required to produce a unit area new crack surface.

A direct tensile test results in a well-defined crack area, thus it is easy to calculate the fracture energy. If the complete  $\sigma_f - w$  relationship is known. If the fracture energy is divided into 2 parts, representing the contribution from the *debonding* process and *pull-out* process, it is found, that the first part is negligible compared to the second. Li (1992) finds by integration of the expression in eq. (2.36), that

$$G_f = \int_0^{l_f} \sigma_B(w) dw = \frac{l_f}{6} \sigma_{pc} \quad (2.51)$$

which is identical to the expression given in Naaman et al. (1974) from the weakest link concept. Thus, the theoretical fracture energy is directly proportional to the bond strength, the fibre reinforcement index and the fibre length.

**The softening behaviour of cementitious matrix.** Even though a crack is formed and the displacements are localized in a narrow zone, the matrix still transfer stress. This transfer is due to *aggregate interlock* and naturally forms a descending stress - crack width curve. Only *empirical suggestions* for the matrix softening exist, where the curves registered through experiments are fitted with mathematical expressions. An expression proposed by Stang (1992) reads

$$\sigma_A = \frac{\sigma_c}{1 + (w/w_{1/2})^p} \quad (2.52)$$

where the two parameters  $p$  and  $w_{1/2}$  are fitted by means of an experimental  $\sigma_A - w$  relationship. The crack width  $w_{1/2}$  corresponds to the crack width, where the aggregate bridging stress  $\sigma_A$  has decreased to half the cracking strength.

Another empirical relationship suggested by Gopalaraman & Shah (1987) has the following form

## 2. Tensile behaviour

$$\sigma_1 = \sigma_c \exp(-q w^p) \quad (2.53)$$

in which  $p$  and  $q$  are the fitting parameters. Stang (1992) reports that the parameter  $p$  is close to unity for most concretes and, that  $w_c$  is 0.01 - 0.02 mm for normal concrete.

The contribution from the aggregate interlock should of course be added to the fibre bridging contribution for every value of the crack opening  $w$  in order to obtain the correct bridging stress relationship. However in most FRC-mixes the fibre content is very low, making it difficult to separate the two contributions.

## 2.2 Previous investigations on compressit matrix

### 2.2.1 Direct tensile tests

Because of the difficulties generally connected with measurements of the uniaxial tensile strength of concrete, only a few tests have been performed on compressit matrix. In the following these tests are briefly discussed and the main results are given. Common to all the tests is, that they are performed under *deformation control* in a universal 500 kN Instron test machine. Furthermore the specimens are of the *dog-bone type* with a weak middle section, but with different dimensions.

The term deformation control means, that the cross-head of the test machine moves with constant speed, which is chosen manually. The stiffness of the machine is important in order to obtain a complete stress - strain curve. During loading elastic strain energy is stored in the test machine as well as in the specimen. When localized cracking starts in the specimen at peak load, *unstable failure* happens if

- The slope of the descending part of the stress - strain curve is too steep, resulting in a sudden release of the elastic energy, i.e. the test machine is not stiff enough to follow the descending part.

Otherwise the descending part is registered until the carrying capacity vanishes. A method to obtain stable behaviour, even though the test machine lacks stiffness, is to load the specimen in parallel with a steel bar, which results in a continuous increasing load, i.e. a normal load controlled experiment, which is considerably easier to perform.

In the M.Sc.-thesis *Aarup & Pedersen (1987)* nine specimens are tested. The mid-section has cross-sectional dimensions 32 x 32 mm and contains 2 opposite saw-cut notches with depth 3 mm. The specimens are saw-cut from beams and in order to investigate the influence of *casting direction*, beams have been cast both horizontally and vertically. However, no

### 2.2 Previous investigations on compressit matrix

significant differences in tensile strength because of casting direction are observed. The mean values of the tensile strength are listed in table 2.3. The *connections* between specimen and test machine consist of steel plates glued on the ends of the test specimen. In each of these plates a threaded bar is screwed and locked in the hydraulic jaws of the test machine, i.e. an attempt to obtain a rotationally stiff connection.

In *Heshe (1988)* only three specimens, with rectangular cross-section (61 x 41 mm), are tested. The connections are similar to those mentioned above, but a hinge is inserted in each end of the specimen. This hinge allow rotations to happen in the test specimen.

Finally 7 tests have been performed using *cylindrical specimens*, where the top and the bottom of the mould serve as connections to the test machine. Like in the previous case hinges are inserted in the connections, which simplifies the procedure to centre the load. These tests are reported in *Heshe & Nielsen (1992a)* and the results are given in table 2.3.

The *initial modulus of elasticity E*, measured on the linear part of the stress - strain curve, is given in table 2.3 together with the tensile strengths obtained from direct tensile tests on compressit matrix.

Investigator	No. of specimens	$f_{t,0}$ (MPa)	$f_{t,0}$ (MPa)	Tensile strength (MPa)	Initial modulus (GPa)
Aarup & Pedersen (1987)	9	6	40	6.5 (12.7)	-
Heshe (1988)	3	6	40	9.4 (2.2)	58
Heshe & Nielsen (1992a)	7	6	40	6.3 (9.5)	40

Table 2.3:

Survey of tensile test results obtained from direct tensile tests with dog-bone specimens. The steel fibres used are Dramix OL 6/15 HC. The listed tensile strengths represent mean values with the coefficients of variation given in brackets.

Throughout all the mentioned test series, corresponding values of the tensile load, longitudinal strain and cross-head displacement are registered. The observed stress-strain relationships however, show *unstable behaviour* on the descending part, indicating that the test machine is not stiff enough to follow this branch. This results in sudden failures, when the deformations localize in a narrow crack zone, followed by the load dropping to zero almost immediately.

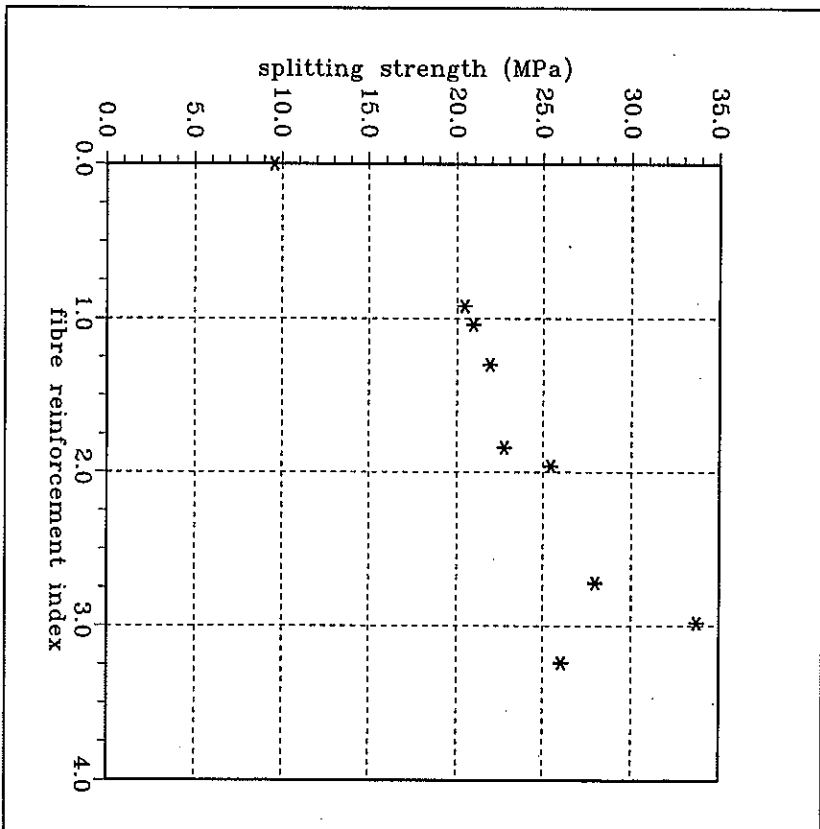


Figure 2.8: Experimental  $f_s - V_f(V_f/d_f)$  relationship from compressive cylinders with varying fibre lengths and contents. Each data point represents 3 tests.

A better way to perform a direct tensile test, in order to obtain a complete stress - strain relationship, is to use a feedback signal in a *closed-loop control*. In Section 2.3 tests performed by controlling the crack opening, instead of the cross-head displacements, are presented and the results are compared to those given in the present section.

### 2.2.2 Tensile splitting tests

A well-known indirect test method to determine the tensile strength of concrete is the *splitting test*, where a cylinder is loaded along two diametrical lines until it cracks along the connecting

diameter. In Hansen (1983), which contains some of the earliest tests on compressive matrix, a total of 27 cylinders with height 90 mm and diameter 45 mm are tested, see test results in figure 2.8.

An *elastic solution* to the splitting problem gives an almost uniform tensile stress  $f_s = P/(rwh)$ , where  $P$  is the load,  $r$  is the cylinder diameter and  $h$  is the height, along the splitting diameter. For ordinary concrete the ultimate *splitting stress* is typically found to be about 2/3 higher than the direct tensile strength. Thus the splitting test forms a simple way to predict the tensile strength because it is performed under load control like a compressive test.

The tests in Hansen (1983) cover 3 different lengths of the straight brass-coated Dexam steel fibres (3, 6 and 12.7 mm) all having diameter 0.15 mm and furthermore they include 3 different fibre contents for each fibre length.

### 2.3 Direct tensile tests on compressive matrix

In this section direct tensile tests, which are performed during the present project, are presented. The tests have been carried out at the Building Materials Laboratory at Technical University of Denmark. The test method is originally developed in connection to the Ph.D.-thesis Aarre (1992) and is only briefly discussed here, while more informations can be found in the thesis.

The scope of the experiments is to establish relations between the tensile characteristics of compressive matrix and the steel fiber characteristics such as fiber content and aspect ratio. This is primarily obtained by measuring  $\sigma_g - w$  relationships on notched specimens, where  $\sigma_g$  is the bridging stress sustained by the fibres (and aggregate interlock) and  $w$  is the crack width. The experiments are controlled by comparing a feed-back signal from two extensometers, measuring the crack opening, with a control signal, that prescribes a constant rate of increase. This method is very effective, but requires a sufficiently fast datalogger in order to perform the signal comparisons with the necessary quickness. Furthermore the specimens are notched so that the localization of the deformations is forced to occur within the measuring length of the extensometers.

#### 2.3.1 Test specimens and method

Detailed information about the tests is given in Appendix 1. The experiment tries to create a uniform tensile stress state at each cross-section of the specimen by *preventing rotation*, i.e. the connections between the specimen and the test machine are stiff enough to ensure, that each cross-section is uniformly extended. This is obtained by gluing two steel blocks to the specimen ends and by using relatively short specimens.

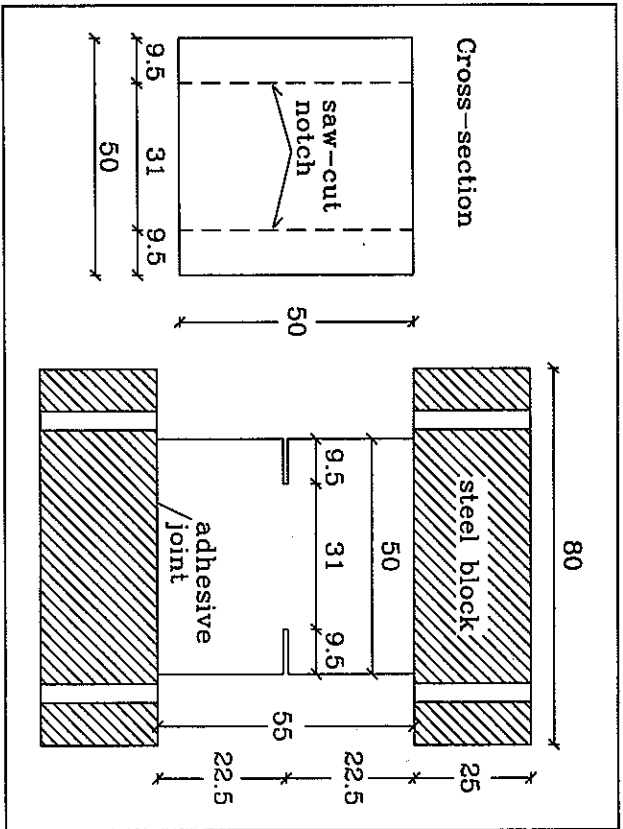


Figure 2.9: Test specimens for direct tensile tests on compressive matrix.

The test specimens consist of small prisms either provided with saw-cut notches or without notches. The specimen dimensions are given in figure 2.9. The specimen *shape and size* are chosen from the following considerations:

- The specimen should fit a 100 kN Instron test machine.
- The smallest width of the cross-section should be at least 3 times the fibre length and 3 times the maximum aggregate size.
- The ratio between specimen length and width should not exceed approximately 2 in order to secure the necessary rotational stability; cf. Aarre (1992).

From figure 2.9 it appears the minimum width is 31 mm, which is less than 3 times the fibre length. However, this is allowed to ensure failure at the notched cross-section at high fibre contents.

The test programme covers 8 different compressive matrices and in table 2.4 a survey of these mixes is given. The specimens are named UT for uniaxial tension followed by a number giving the aspect ratio of the fibre type, that is added to the mix.

Specimen name	$L_f/d_f$	$V_f$ (%)	$V_f(L_f/d_f)$	Fibre type-Diameter
UT0	-	0	0	-
		3	0.9	
UT30	30	6	1.8	OL 12/40
		9	2.7	
		3	1.2	
UT40	40	6	2.4	OL 6/15 HC
		9	3.6	
UT87	87	3	2.6	OL 13/15 HC

Table 2.4: Survey of the 8 different compressive matrices composed from 3 different fibre types (straight Drammix steel fibres). Fibre characteristics in table 1.3.

From the test executions it turns out, that the two opposite notches shown in figure 2.9 are not enough to ensure that cracking actually happens in this cross-section, when the fibre reinforcement index gets too high. Therefore extra notches are saw-cut in the 2 remaining sides. Thus, the following 2 specimen configurations exist:

- Specimens with two opposite notches, when the fibre reinforcement index is lower than 2, resulting in a notched cross-sectional area of 60 % of the original area.
  - Specimens with notches on all 4 sides, when the fibre reinforcement index is higher than 2, leaving only 36 % of the cross-sectional area to carry the stresses.
- The two extensometers are placed on opposite sides of the specimen, measuring the deformations of the central part of the specimen. If the final crack occurs outside the measuring length of these extensometers, the test control fails. This is the case for the unnotched specimens, where the failure happens in the adhesive joint.

### 2.3.2 Test results

Values of the tensile force and the extensometer strain measurements have been recorded from all tests. The *notched* prisms were supposed to supply the *stress - crack width relationship*, i.e. the part after the displacement localization. The *unnotched* prisms were meant to give *complete stress - strain curves*, i.e. both an ascending and a descending part. In

Figure 2.10 these 2 possibilities are outlined.

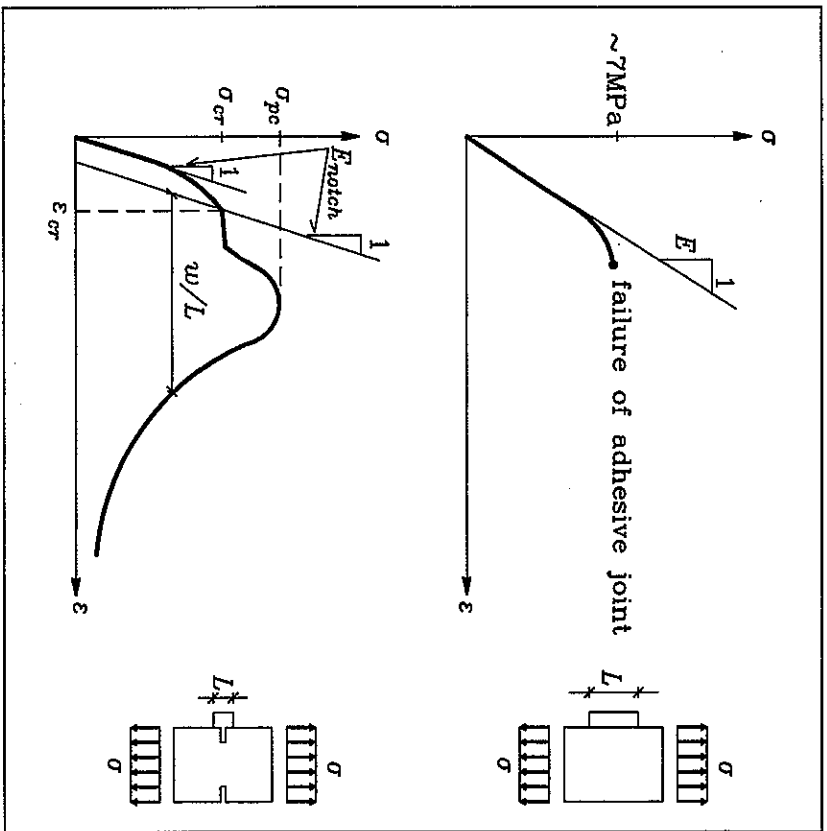


Figure 2.10: Characteristics of tensile stress - strain curves obtained from extensometer measurements on both unnotched and notched specimens. The term stress - strain curve is used about the complete test recording, knowing that the deformations localize in narrow failure zones (cracks) and therefore makes it doubtful to consider strains instead of displacements.

It turned out to be practically impossible to record the complete stress - strain curves for the unnotched specimens. Even though the ends of the prisms and the steel blocks were sand-blasted before gluing them together, it always appeared to be the adhesive joints, that failed rather than the cross-sections in between. Therefore it was impossible to record the descending

part of the stress - strain curve, i.e. the unnotched prisms only determine the initial modulus of elasticity. It was found that the adhesive joint had a tensile strength of about 7 MPa, which coincides with the cracking strength of the matrix as described later. In order to obtain a complete stress - strain curve with compressive matrix, using unnotched prisms, a much stronger glue is needed, or perhaps specimens of the traditional dog-bone type.

The notched specimens, on the contrary, showed behaviour as outlined in figure 2.10. After the deformations localize in the notched cross-section, the material appears to yield followed by "strain hardening" as recognized from reinforcement steel. The yield point is interpreted as initiation of cracking and is defined by the cracking stress  $\sigma_{cr}$ . The following peak is termed the post-cracking stress  $\sigma_{pc}$  and it is due to the steel fibres bridging the crack. Of course the latter observation does not apply for matrix without fibres, in this case the bridging stress descends right after cracking, with the descending stresses sustained by aggregate interlock, i.e. so-called strain softening.

In the following presentation of the results in tables and figures, no attempt has been done to separate the stress contributions from matrix and fibres, which is justified later on.

**Experimental  $\sigma_g - w$  relationships.** In order to obtain the stress - crack width relationships from the notched specimens, the elastic part of the strains is subtracted from all the values, that follow cracking as shown in figure 2.10. Thus it is assumed, that the unnotched cross-sections are not damaged, when the notched section cracks, i.e. the unnotched cross-sections follow the linear-elastic stress - strain curve with slope corresponding to the initial stiffness  $E_{notch}$ , while the cracked section follows the post-crack curve.

This gives the following relation between the crack width  $w$  and the measured strains  $\epsilon$ :

$$w(\sigma_g) = L \left( \epsilon(\sigma_g) - \epsilon_{cr} - \frac{\sigma_g - \sigma_{cr}}{E_{notch}} \right) \quad (2.54)$$

with symbols taken from figure 2.10.

In each individual case the  $\sigma_g - w$  relationship is calculated from this equation after determining the cracking point ( $\epsilon_{cr}, \sigma_{cr}$ ) and the initial slope  $E_{notch}$  manually from the stress-strain recordings. When the  $\sigma_g - w$  curve is obtained, the fracture energy termed  $G_f$  is calculated as shown by the integration in eq. (2.51). It is interpreted as the energy dissipated per unit crack area during the test and it is represented by the area below the complete  $\sigma_g - w$  curve.

Typical post-cracking relationships are shown in Appendix 1 for each of the 8 compressive matrices. It appears that at least 3 tests are carried out for each matrix, except for UT40 with 9 % fibres, where only 2 tests succeeded. In figure 2.11 and 2.12 characteristic  $\sigma_g/\sigma_c - w$  curves are given, with the bridging stress normalized by respect to the cracking strength, i.e. all the curves start at (0,1).

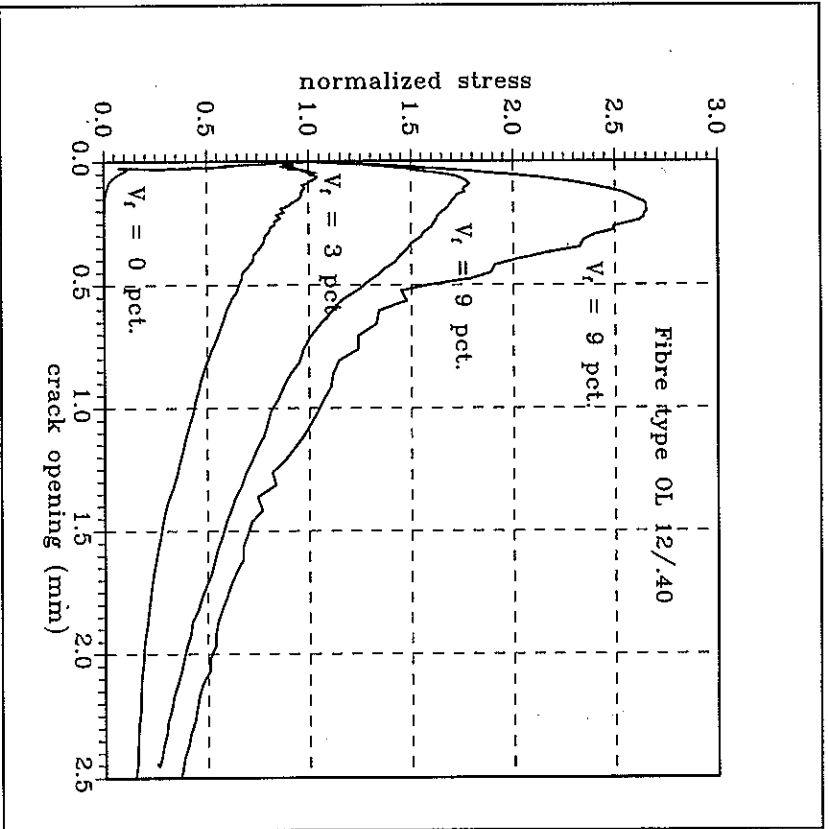


Figure 2.11: Characteristic  $\sigma_f/\sigma_{cr} - w$  curves for notched specimens of type UT30.

It is obvious from the two figures, that there are great differences between both the post-cracking stresses and the energy dissipation for the various compressit matrices, caused by changing fibre content and geometry. The cracking stress only varies slightly with the fibre content, making the normalized curves directly comparable. Furthermore Appendix 1 shows, that there exists great variations within each mix, leading to relatively large coefficients of variation on the test results.

The maximum crack opening of 2.5 mm corresponds to the range of the extensometers and cannot be exceeded. This means that the longest fibres (OL 12/40 and OL 13/15 HC with  $L_f$  equal to 12 and 13 mm respectively) are not fully pulled out, when the test is stopped, because their maximum embedment lengths of  $L_f/2$  are not exceeded. Therefore the bridging

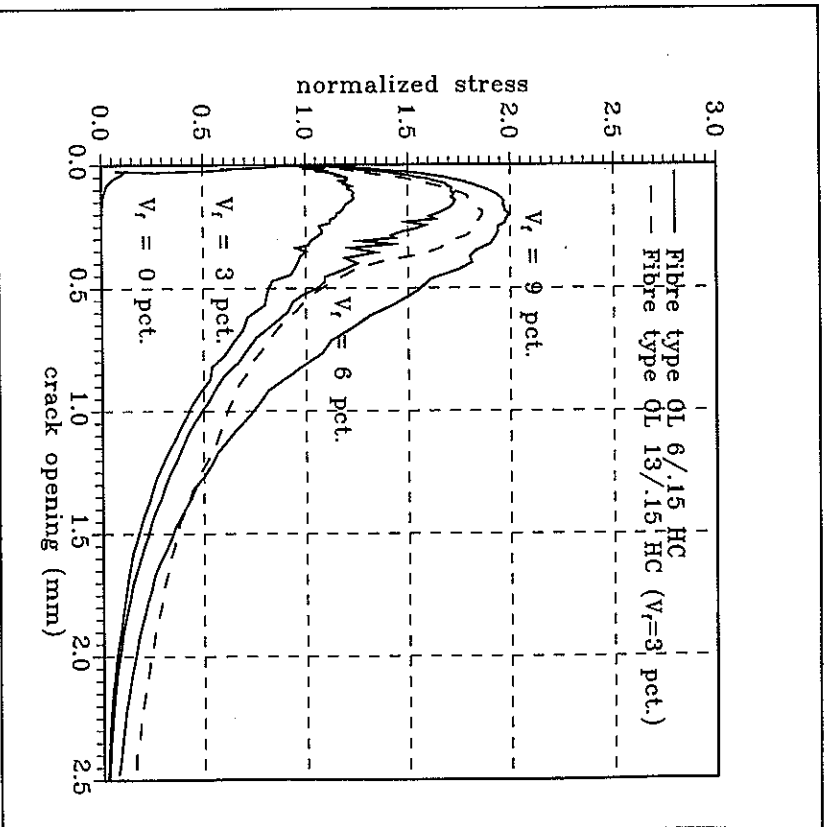


Figure 2.12: Characteristic  $\sigma_f/\sigma_{cr} - w$  curves for notched specimens of type UT40 and UT87.

stress has not dropped to zero except for the UT40-specimens with fibre length 6 mm. As a consequence of this the calculated  $G_f$ -values do not represent the correct values because of the incomplete tail of some of the curves. However this is assumed to be of minor importance, considering the relatively high variations in the test results.

Like it appear from figure 2.11 and 2.12, only the lowest fibre contents ( $V_f = 3\%$ ) show an actual drop in stresses after cracking. The typical behaviour is a slight disturbance of the stress-strain curve, disclosing that cracking starts, before the stresses continue to increase.

## 2. Tensile behaviour

**Statistical definitions.** In order to interpret the test results properly the observed experimental variations are taken into account. In this section the basic definitions, concerning the statistics involved in evaluating the results, are given.

An estimation of the uncertainty of a variable  $x$  on basis of  $n$  samples is typically taken as its *sample variance*  $s^2$  and the *coefficient of variation* is defined as the square root of this sample variance divided with the *sample mean*  $x_m$ :

$$c.o.v. = \frac{\sqrt{s^2}}{x_m} = \frac{\sqrt{\frac{1}{n-1} \sum_{i=1}^n (x_i - x_m)^2}}{\frac{1}{n} \sum_{i=1}^n x_i} \quad (2.55)$$

If the samples are assumed *independent* and *normal distributed* with mean  $\mu$  and variance  $\sigma^2$  it can be shown, that the sample mean and variance are the best estimates for these two parameters. Furthermore the *double-sided 95 % confidence interval* for  $\mu$  is given as

$$x_m \pm t_{97.5\%}(n-1) \sqrt{\frac{s^2}{n}} \quad (2.56)$$

where  $t_{97.5\%}(n-1)$  is the fractile of the  $t$ -distribution with  $n-1$  degrees of freedom, that corresponds to 97.5 % of the probability mass. Thus, instead of estimating a single value of the variable  $x$  by its sample mean (for instance  $x$  is a material property such as strength) the confidence interval gives a range containing the mean value of  $x$  with 95 % probability. When  $n$  increases the interval gets more narrow. It is noted, that the probability level is chosen by the investigator, but a value of 95 % is generally accepted.

If we have several groups of samples with different mean values, but assume equal variance, a *stronger estimate* for the variance is given by

$$s_0^2 = \frac{(n-1) \sum_{i=1}^m s_i^2}{m(n-1)} \quad (2.57)$$

where  $s_i^2$  is the sample variance corresponding to the  $i$ th group and  $m$  is the number of groups. The corresponding double-sided 95 % confidence interval for  $\mu$  is expressed as

## 2.3 Direct tensile tests on compressive matrix

with  $x_m$  being the sample mean of the  $i$ th group.

$$x_m \pm t_{97.5\%}(m(n-1)) \sqrt{\frac{s_0^2}{n}} \quad (2.58)$$

For instance with two sample groups, representing two different values of a parameter, the confidence intervals given above are compared. In order to conclude whether the difference in the observed sample means is caused by random errors and uncertainties, or if it is caused by the parameter change in, the confidence intervals are compared. If the intervals do not overlap the effect of the parameter is concluded to be significant.

In terms of the present investigation we change the mix parameters (fibre content and geometry) and measure the material properties. These measurements include errors, e.g. originating from inaccurate equipment and the inhomogeneous nature of concrete materials, which are reflected in the coefficients of variation. If these errors are assumed to be independent of the mix parameters eq. (2.58) is applied in order to investigate whether a change in parameters effects the material property significantly.

**Mean values of the test results.** In table 2.5 the main results of the tensile tests are given in terms of the cracking stress  $\sigma_c$ , the initial modulus of elasticity  $E$ , the post cracking stress  $\sigma_p$  and the fracture energy  $G_f$ . The modulus of elasticity is determined from unnotched specimens with 3 repetitions in each case, while the other material properties are measured on notched specimens. The area below the  $\sigma_g - w$  curve is calculated numerically using the trapezoidal rule, where the relationship in between two observations is assumed linear. The values in brackets are the coefficients of variation calculated from eq. (2.55).

**Initial modulus of elasticity  $E$ .** When the elastic region of the stress - strain relationship is considered for FRC, the so-called *law of mixtures* is often applied. The two different phases (matrix and steel) are assumed to act together, neglecting the effect of the Poisson's ratio. The so-called *Voight model*, which assumes, that the strains are equal in the two phases, reads:

$$E = E_f Y_f + E_m (1 - Y_f) \quad (2.59)$$

making an *upper limit*, because the orientation of the fibres, relative to the load axis, is not taken into account, cf. eq. (2.14).

Fibre type	Fibre content (pct.)	Number of specimens	Measured modulus (GPa)		Predicted modulus (GPa)		Difference (GPa)		
			Mean	95% CI	Eq. (2.59)	Eq. (2.60)			
UT10	-	0	44.9	(5.5)	5.3	(12.2)	-	0.151	
			44.0	(3.4)	6.8	(21.4)	7.8	(38.3)	8.2
			50.2	(16.4)	7.0	(15.6)	13.8	(3.2)	14.2
UT30	30	6	55.2	(4.8)	7.4	(11.8)	18.7	(1.8)	20.2
			50.7	(6.6)	6.0	(8.8)	6.6	(15.3)	5.5
			50.5	(5.4)	7.5	(8.2)	10.0	(29.7)	9.8
UT40	40	9	49.9	(6.8)	8.2	(5.8)	15.7	(10.0)	14.0
			52.6	(4.6)	7.2	(9.3)	12.5	(11.8)	12.0
			52.6	(4.6)	7.2	(9.3)	12.5	(11.8)	12.0
UT87	87	3	52.6	(4.6)	7.2	(9.3)	12.5	(11.8)	12.0
			52.6	(4.6)	7.2	(9.3)	12.5	(11.8)	12.0
			52.6	(4.6)	7.2	(9.3)	12.5	(11.8)	12.0

Table 2.5: Test results from direct tensile tests. All values are mean values and the brackets contain the coefficients of variation.

Another approach is the *Reuss model*, which is analogous to a system of two linear-elastic springs, representing the two phases, in a series connection, i.e. the stresses are assumed equal. This model gives the following expression for the modulus of elasticity:

$$\frac{1}{E} = \frac{V_f}{E_f} + \frac{1-V_f}{E_m} \quad \Leftrightarrow \quad E = \frac{E_m E_f}{E_f + V_f(E_m - E_f)} \quad (2.60)$$

representing a *lower limit*. In Baalbaki et al. (1992) several models are presented, combining these two models.

In figure 2.13 the *E*-values from table 2.5 are depicted with varying fibre content together with the two predictions from eq. (2.59) and (2.60). The material parameters are chosen as  $E_f = 200$  GPa and  $E_m = 45$  GPa.

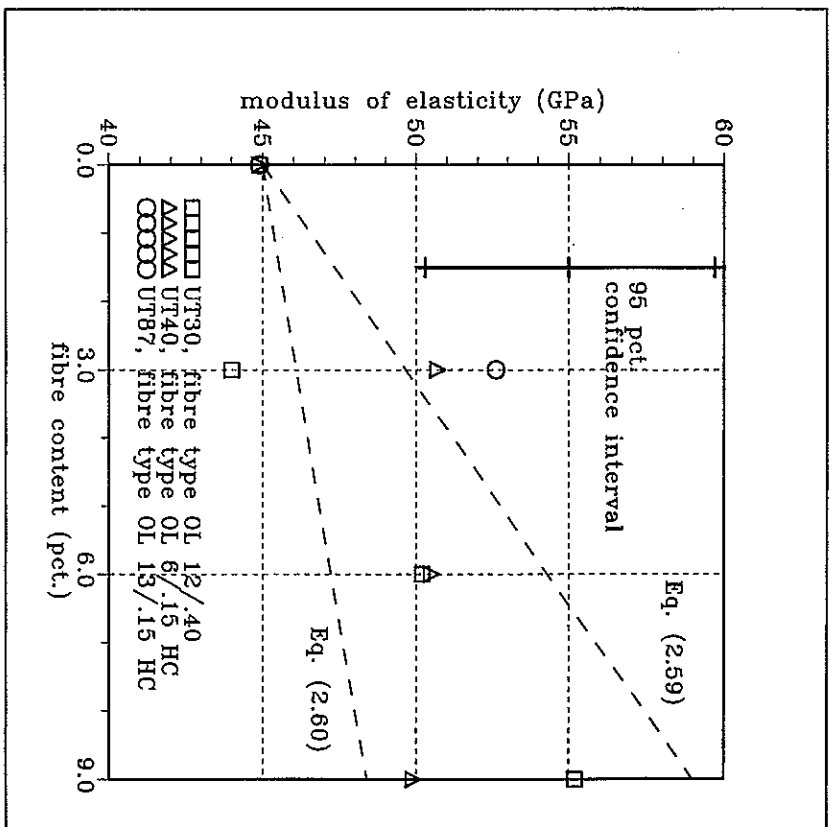


Figure 2.13: Mean values of the initial modulus of elasticity given in table 2.5. Also shown is the double-sided 95 % confidence interval for the expected modulus.

A simple *statistical analysis* performed on the measured *E*-values gives the 95 % confidence interval, which is inserted in figure 2.13. By calculating the sample variance from eq. (2.57) with  $n = 3$  and  $m = 8$ , the width of the confidence interval is determined to 9.4 GPa using eq. (2.58). By applying the confidence interval to the measured mean values it is clear, that both the Reuss and Voigt model predict the modulus of elasticity within acceptable accuracy. However a mean value of the two models seems to give the best agreement. Furthermore it is evident, that only in case of very high fibre contents, the modulus is increased significantly because of the presence of fibres.



Cracking stress  $\sigma_{cr}$ . As explained in Section 2.2, the general assumption concerning FRC is, that the cracking stress does not differ much from the strength of the unreinforced matrix. This assumption originates from the law of mixtures, where the contributions from matrix and fibres are separated, see e.g. Haanant (1978), p. 11.

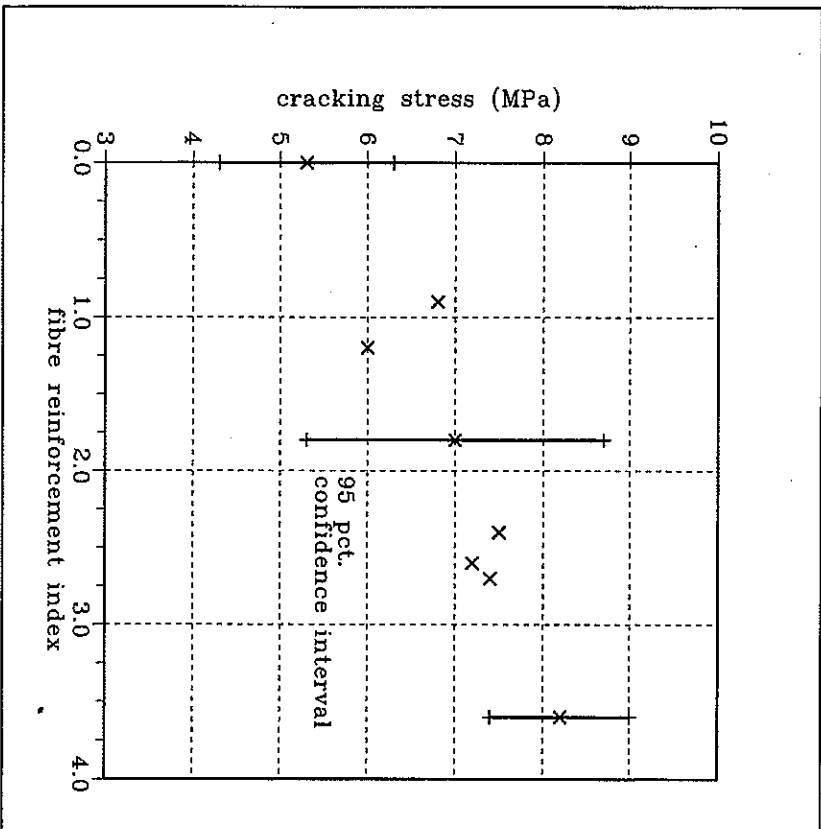


Figure 2.14: Experimental  $\sigma_{cr} - V_f(L_f/d_f)$  relationship from table 2.5, including 3 typical double-sided 95 % confidence intervals.

The cracking stresses, given in table 2.5, show an increasing strength with fibre content. Figure 2.14 gives the relationship between  $\sigma_{cr}$  and the fibre reinforcement index together with 3 representative 95 % confidence intervals, calculated on basis of eq. (2.56) with  $n = 4$ .

It is clear that the cracking stress is influenced by the steel fibres, but it also seems, that the

effect is only significant, when large differences in fibre reinforcement index are compared. Thus, a comparison of the confidence intervals for  $V_f(L_f/d_f) = 0$  and  $V_f(L_f/d_f) = 1.8$  shows, that the uncertainties on the measurements are too high to conclude any fibre effect. Therefore the cracking strength of compressive matrix is considered a *single value* in the following. If all the measured  $\sigma_{cr}$ -values are taken into account a mean value of 6.9 MPa is obtained, with the coefficient of variation equal to 16.6 %.

It is likely that there exists a strain value for the matrix material at which the deformations localize into discrete cracks. Unfortunately the strains, measured on the notched specimens, do not represent a uniform strain field because of the notch. Therefore the  $E$ -values, measured on unnotched specimens, are used to determine  $\epsilon_{cr}$ , assuming that the stress - strain curve is linear until cracking, an assumption which is generally accepted.

An analysis of the *cracking strains* gives a mean value of  $\epsilon_{cr} = \sigma_{cr}/E = 0.14$  %. This value coincides satisfactorily with previous observations of the ultimate tensile strain equal to approximately 0.2 % obtained in Heshe (1988) and in Heshe & Nielsen (1992a) by means of electrical resistance strain gages.

If the cracking stresses from table 2.5 are compared to the tensile strengths in table 2.3 it appears, that the  $f_t$ -values reported in previous investigations on compressive matrix correspond to the cracking strength obtained in the present test programme. It is recalled from Section 2.2, that the previous investigations are performed under simple deformation control, i.e. without any feed-back signal. It is probably, that the stiffness of the test machine is insufficient and causes, that the post-cracking behaviour is not recorded properly because of unstable crack growth. Thus, the cracking strength is interpreted as the ultimate strength.

**Post-cracking stress  $\sigma_{pc}$ .** The maximum stress sustained by the steel fibres alone as they bridge the crack is termed the post-cracking strength. From the post-cracking curves in figure 2.11 and 2.12  $\sigma_{pc}$  occurs for a crack opening of approximately 0.2 mm and by comparison with the behaviour observed for plain compressive matrix without fibres, it is obvious that only the fibres contribute to the post-cracking stresses. The aggregate interlock has completely vanished.

In figure 2.15,  $\sigma_{pc}$  is depicted with varying values of the fibre reinforcement index. From statistical considerations similar to those performed on  $E$ , a double-sided 95 % confidence interval is calculated, giving a total width of 4.1 MPa, see figure 2.15. Also the mean value of the cracking stress  $\sigma_{cr} = 6.9$  MPa is shown.

It is evident, that the specimens of type UT30 and UT40 are difficult to separate for identical fibre content, because their confidence intervals overlap, but UT30 tends to show the highest strengths. However it is undoubtful, that the fibre reinforcement index has a significant effect on the post-cracking strength.

A very simple criterion for so-called *multiple cracking* is, that the post-cracking strength is

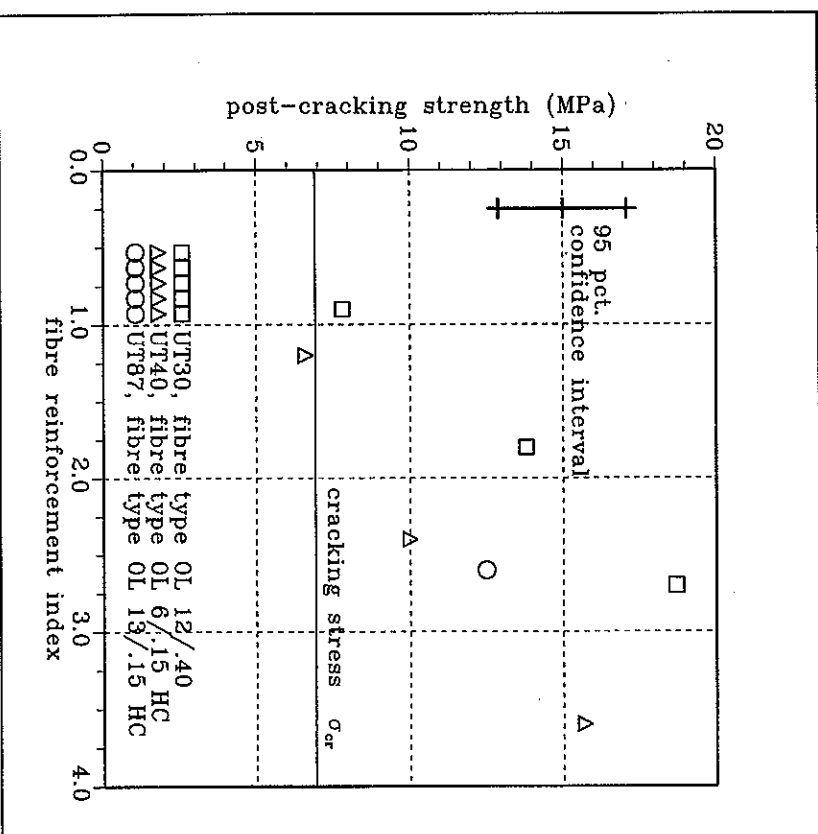


Figure 2.15: Experimental  $\sigma_{pc} - V_f(L_f/d)$  relationship from table 2.5, including the double-sided 95 % confidence interval for  $\sigma_{pc}$ .

higher than the cracking strength. From figure 2.14 it is recalled, that  $\sigma_c$  is not significantly influenced by the fibres. Therefore the relationship in figure 2.15 indicates, that the minimum fibre reinforcement index to ensure multiple cracking is approximately 1, corresponding to  $V_f \approx 3\%$  of OL 12/.40 fibres.

**Fracture energy  $G_f$ .** Values of the fracture energy are calculated as given in eq. (2.51) and from table 2.5 it is clear, that they are subject to great scatter. In figure 2.16 the  $G_f - V_f(L_f/d)$  relationship is shown, including the double-sided 95 % confidence interval.

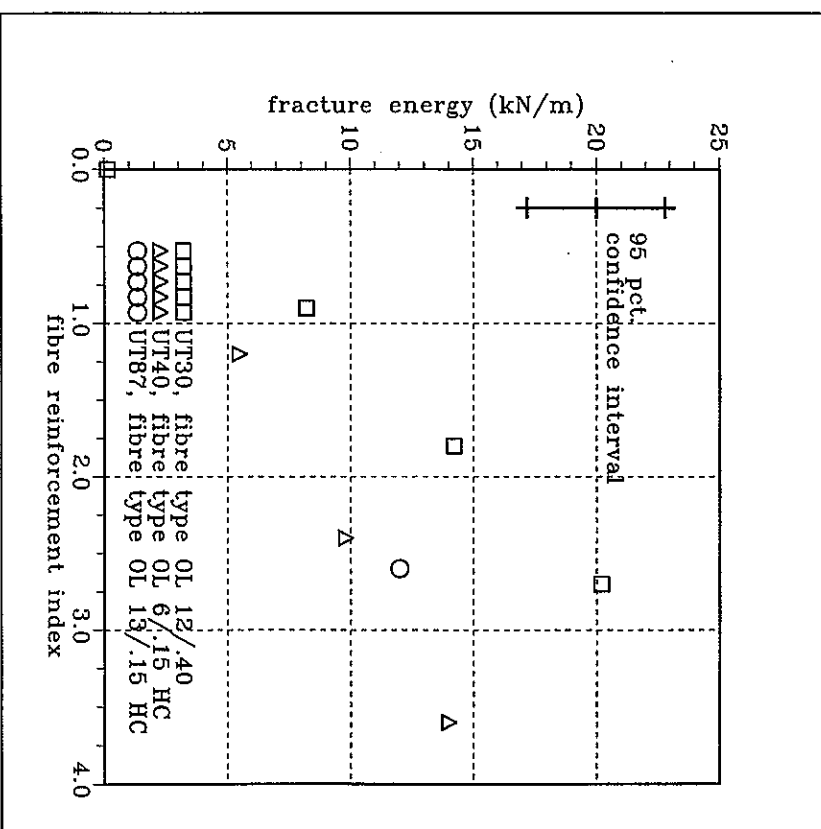


Figure 2.16: Experimental  $G_f - V_f(L_f/d)$  relationship from table 2.5, including the double-sided 95 % confidence interval for  $G_f$ .

Like it is mentioned earlier, the lack of data covering the last part of the  $\sigma_c - w$  curve (i.e. the part exceeding  $w = 2.5$  mm), is assumed to be insignificant, when the  $G_f$ -values are compared. A rough estimate, modelling the missing tail with a linear decreasing part between  $w = 2.5$  mm and  $L_f/2$ , indicates, that the contribution neglected under this assumption is approximately 3 kN/m except for UT30 with  $V_f \approx 9\%$ , where it is approximately 7 kN/m. It is chosen to neglect these contributions, but in the following analysis it is noted, that the  $G_f$ -values represent a *lower limit*. A further investigation of the fracture energies are performed in Section 5.2.

## 2.3.3 Tensile strength of compressit matrix

Based on the test results presented in the previous section, the tensile strength characteristics of compressit matrix are summarized. A simple and straightforward approach is to interpret the fibres as conventional reinforcement. By assuming that the steel fibres control the post-cracking strength a tensile strength prediction, similar to those given in Section 2.1.3, is obtained by considering the fibres as conventional steel bars.

When a cross-section contains steel bars, the *geometrical reinforcement ratio*  $\phi$  is defined as the cross-sectional area of the steel divided with the total cross-sectional area. The tensile strength of the cross-section is calculated as

$$f_t = \phi f_y \quad (2.61)$$

where  $f_y$  is the *yield strength* of the steel bars. Thus  $f_t$  is the strength of the bars, uniformly distributed over the total area assuming, that the concrete does not contribute to the tensile strength.

For *fibres* randomly located in a structure, the number of fibres crossing an arbitrary cross-section per unit area is given in Section 2.1.3 as  $N_A = 2Y_f/(\pi d_f^2)$ . Thus, the geometrical reinforcement ratio of the fibre reinforcement is given by

$$\phi_f = N_A A_f = \frac{Y_f}{d_f} \quad (2.62)$$

Under the assumption that the fibre length is shorter than the critical length, defined in eq. (2.7), the mean value of the yield strength of a fibre is related to its effective bond shear strength  $\tau$ :

$$f_{f'} = \frac{\pi d_f^2 \tau \frac{L_f}{4}}{A_f} = \tau \frac{L_f}{d_f}$$

where the numerator is the mean pull-out force of a single fibre, having embedment length  $L_f/4$ . Finally the tensile strength of the fibre reinforced composite is calculated as

$$f_t = \sigma_{pc} = \phi_f f_{f'} = \frac{1}{2} \tau Y_f \frac{L_f}{d_f} \quad (2.63)$$

The *effective bond strength*  $\tau$  of the fibre - matrix interface includes the effect of fibres, that are inclined to the crack plane and therefore it is not identical to the single fibre bond strength  $\tau^*$ . In order to compare with the expressions proposed in table 2.1 we use the relation  $\alpha \tau^* = \tau/2$ , cf. eq. (2.50).

In figure 2.15 the dependence of the post-cracking strength on the fibre reinforcement index indicates, that *direct proportionality* is satisfactory. If  $\sigma_{pc}$  is expressed as in eq. (2.63), the effective shear strength  $\tau$  is determined as half the slope in figure 2.15.

From figure 2.15 it appears, that there exist different slopes for the fibre types, corresponding to either the thin fibre type with diameter 0.15 mm (used for UT40 and UT87), or to the fibre with diameter 0.4 mm used for UT30. The two slopes from figure 2.15 are calculated to equal

- an effective bond strength  $\tau = 9.4$  MPa for the fibre with diameter 0.15 mm.
- an effective bond strength  $\tau = 15.7$  MPa for the fibre with diameter 0.4 mm.

In figure 2.17 the tensile strengths are shown together with the two lines, symbolizing the following expressions:

$$f_t = \frac{1}{2} Y_f \frac{L_f}{d_f} \begin{cases} 9.4 \text{ MPa}, & d_f = 0.15 \text{ mm} \\ 15.7 \text{ MPa}, & d_f = 0.4 \text{ mm} \end{cases} \quad (2.64)$$

From the figure it appears, that for fibre reinforcement indices below 2, the difference between the two fibre types, caused by the different bond strengths, are difficult to detect experimentally because of the experimental scatter. Therefore the expressions in eq. (2.64) are satisfactory for most practical needs with a mean value of  $\tau$  instead of distinguishing between the fibre types.

The *splitting strengths*  $f_s$ , determined in Section 2.2.2 and reported in Hønsen (1983), seem to predict the effect of the fibre reinforcement index similar to the description above. In figure 2.8 the dependency of  $f_s$  on the fibre reinforcement index is given. This dependency is modelled satisfactorily by a straight line, reading

$$f_s = \left( 13.4 + 5.5 Y_f \frac{L_f}{d_f} \right) \text{ MPa} \quad (2.65)$$

obtained from a linear regression analysis with the coefficient of correlation equal to 0.9.

Even though the splitting strength seems to overestimate the tensile strength of the plain compressit matrix without fibres by a factor 2, which is also the case for normal concrete splitting strength. The slope of the relationship coincides with that given in eq. (2.64).

There has been no attempts to determine the single fibre pull-out strength in the present test programme. Therefore it is not possible to perform a direct comparison with the model predictions presented in Section 2.1.3, which are based on  $\tau^*$ , see e.g. table 2.1. In figure 2.7 existing post-cracking strengths, normalized by respect to the single fibre bond strength  $\tau^*$ , are depicted with the parameter  $\alpha$  from eq. (2.50) being the slope of the straight line expressing the normalized post-cracking strength.

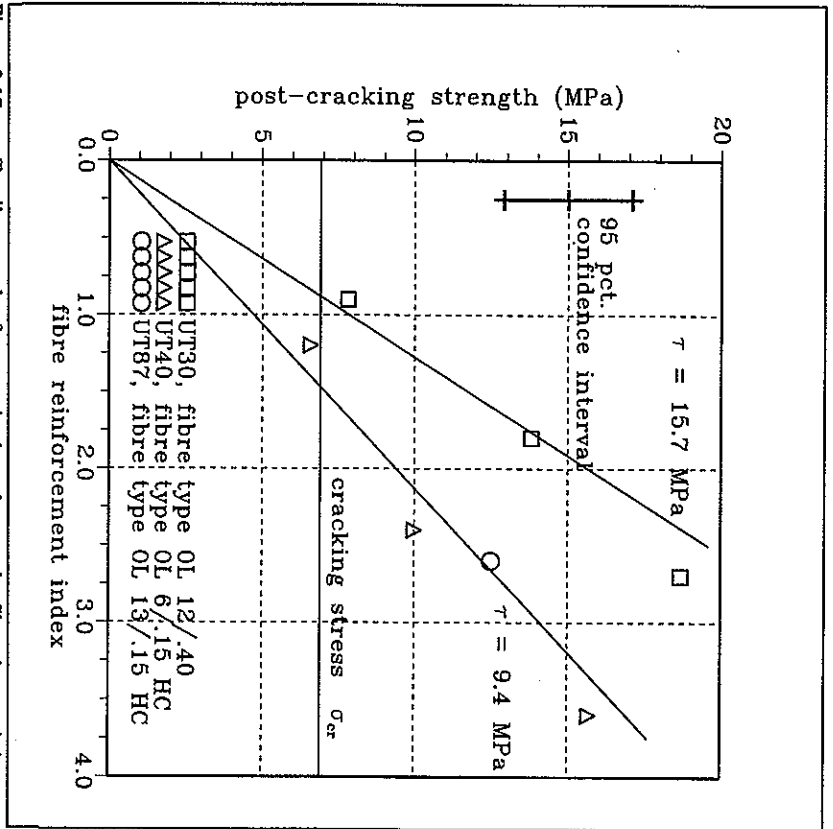


Figure 2.17: Tensile strength of compressive concrete, dependent on the fibre characteristics.

UT30 contains fibres of type OL 12/40, while UT40 and UT87 contain fibres of type OL 6/15 HC and OL 13/15 HC respectively.

$$\tau/2 = \alpha \tau^* \quad \tau = 1.3 \text{ MPa}$$

From the test results in Naaman et al. (1974) the slope  $\alpha = 0.25$  seems satisfactory and the bond strength is reported to  $\tau^* = 2.6$  MPa, which yields an effective bond shear strength  $\tau$ :

Similarly the results in Lim et al. (1987) are analysed and yields  $\tau = 2.1$  MPa for straight fibres and approximately the double for hooked-end fibres.

By comparing these effective bond strengths from normal FRC tests with eq. (2.64), it is

obvious, that the compressive fibre - matrix interface is extremely strong.

**Characteristics of the  $\sigma_c - w$  relationship for compressive.** From the post-cracking curves in Appendix I it is clear, that the fibres affect the tensile behaviour strongly. For the matrix without fibres the post-cracking curves descend very rapidly, which is similar to curves measured on both normal and high-strength concrete.

When fibres are added the curves are lifted considerably, increasing the fracture energy more than a 100 times. For instance the crack width, corresponding to half the cracking stress, is increased from approximately 0.02 mm for plain matrix to approximately 2 mm for fibre reinforced matrix.

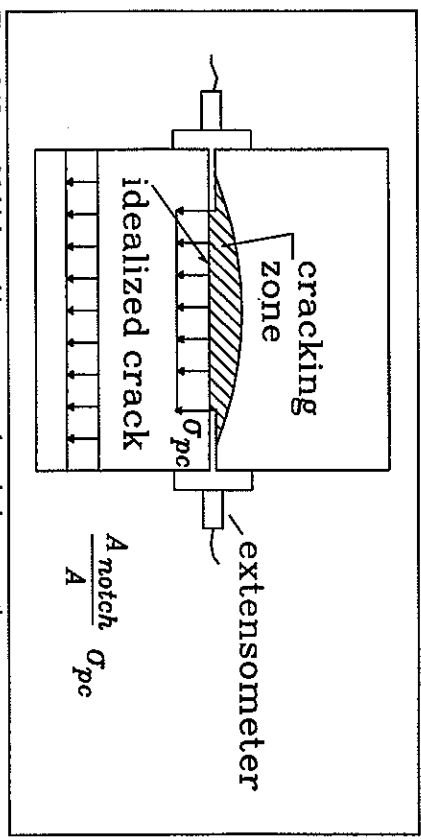


Figure 2.18: Multiple cracking zone around notched cross-section.

The occurrence of the maximum post-cracking stress is registered to lie between  $w = 0.1$  and  $w = 0.2$  mm, cf. figure 2.11 and 2.12. If crack widths of this magnitude are compared to the model prediction suggested in Li (1992), see eq. (2.37):  $w_0^* = \tau^2 L_f^2 / (E_f d_f)$ , a very poor agreement is found.

By inserting the parameters corresponding to the present steel fibres, the predicted crack widths are 5 to 10 times smaller, than those observed in the tests. It is recalled, that the prediction given in eq. (2.37) is interpreted as elastic elongation of the debonded part of the embedded fibres. A plausible explanation for the great difference between the observations and the model prediction is, that the  $\sigma_c - w$  relationship for compressive matrix does not represent a single crack. Because of the post-cracking stresses, that exceed the cracking strength of the matrix, a system of cracks may develop around the notched cross-section as indicated in figure 2.18. This means that even though only one crack is visible (located in the notched section), there might be cracks inside the specimen, that contribute to the extensometer displacements.

Practical considerations for compressit matrix. The limit for application of FRC is often determined by its *workability* during mixing and casting. In practice the upper limit for the fibre reinforcement index is typically within the range 1 - 2. For compressit matrix the practical *upper limit* is about 2, even though compressit mixes with fibre reinforcement indices as high as 4 have been cast. When these limits are reached it gets difficult to mix the fibres properly and the risk of fibre bundles increases.

The possibility of *multiple cracking* is controlled by  $\sigma_{pc} > \sigma_{cr}$ , which is mainly limited by the maximum attainable fibre reinforcement index. For ordinary FRC the cracking strength of the matrix is typically about 4 MPa, while the post-cracking strength of fibres bridging a crack is of magnitude  $\sigma_{pc} = Y_f(L_f/d_f)$  MPa. These values demand a fibre reinforcement index higher than 4 in order to obtain multiple cracking. For compressit matrix the high bond strength provides the post-cracking strength to increase significantly, making it possible to reduce the initiation of multiple cracking to  $Y_f(L_f/d_f) \approx 1$ , cf. figure 2.17.

Considering the high bond strength of the compressit matrix, care should be taken to avoid fibre breaking instead of pull-out by choosing the fibre length property. The *critical length* is given in eq. (2.7):  $L_{cr} = \sigma_{cr}d_f/(2\tau)$ , where  $\tau$  is taken as the effective bond shear strength. By inserting the tensile strength of the fibres, see table 1.3, together with the bond strengths given in eq. (2.64) we get

$$L_{cr} = \begin{cases} 23.5 \text{ mm}, & d_f = 0.15 \text{ mm} \\ 17.2 \text{ mm}, & d_f = 0.4 \text{ mm} \end{cases} \quad (2.66)$$

It is recalled, that the thin fibres (OL 6/15 HC and OL 13/15 HC) are the most expensive and it seems that in order fully utilize their bond capacity the fibre length should be increased considerably. For the other (cheaper) fibre type OL 12/40, the actual fibre length matches its critical length very well, making this fibre the most attractive for compressit.

## 2.4 Compressit matrix reinforced with both fibres and bars

In the following section a description of tensile tests with steel bars embedded in compressit matrix. They serve to investigate, whether the tensile strength of compressit matrix contributes to the tensile behaviour of the member.

One of the basic principles of the compressit concept, described in Baehre (1987), concerns the interaction between the main reinforcement and the fibre reinforced matrix. It is well-known, that the *brittleness* of a structure increases with both the material strength and the size. Naturally the fibres decrease the brittleness, because they increase the fracture energy, but also the compact main reinforcement is meant to decrease the brittleness. The main

reinforcement primarily increases the overall ductility of the structure because of its plastic behaviour, but it also effects the matrix brittleness. The compact steel arrangement divide the matrix into smaller *sub-volumes*, i.e. it decreases the characteristic dimension, that is a part of the so-called brittleness number, see Section 5.1.2. Thus, instead of a brittle high-strength matrix, that cracks easily around the bars, we have a ductile steel fibre reinforced matrix, that follows the bar deformations and keeps its coherence.

### 2.4.1 Test specimens and method

Two different types of experiments are performed with fibre reinforced compressit matrix and varying contents of main reinforcement. The specimens vary considerably in their design.

In *Heshe & Nielsen (1992a)* a total of 8 specimens are reported, covering 4 different reinforcement degrees and containing 6 % steel fibres of type OL 6/15 HC. The tests are a continuation of the tensile tests mentioned in Section 2.2.1, determining the tensile strength of plain compressit matrix.

The specimens are of the dog-bone type, i.e. cylindrical with a mid-sectional diameter equal to 76 mm. The steel bars are arranged concentric with a diametrical distance of 56 mm. These bars are Danish tenor steel (T350) with a guaranteed 0.2 % proof-stress of 550 MPa. In table 2.6 the material characteristics of the steel bars are given.

The specimens are instrumented with electrical resistance strain gages both on the surface of the cylinders and on the reinforcement bars. A comparison between these two strain measurements shows, that the bars and the matrix deform identically. Furthermore the cross-head displacements of the test machine are registered.

The M.Sc.-thesis *Duedahl & Nielsen (1993)* includes a total of 14 disc-shaped specimens with dimensions 300 × 75 × 12 mm. The specimens have especially designed fittings glued on both ends to connect it with a universal test machine at the laboratory of the Department of Building Technology and Structural Engineering at Aalborg University.

Inside the specimens up to 5 steel wires with diameter 5 mm are embedded. Tests with both threaded wires and high-strength cold-drawn wires are performed, see table 2.6. The test series includes 2 fibre contents, viz. 2 and 6 % of the fibre type OL 6/15 HC. From the cross-sectional dimensions of 12 × 75 mm it seems, that the small depth causes the fibres to align in the plane of the specimen. Thus, it is questionable to state, that the fibres have random orientation.

Before gluing the aluminium fittings to the specimen ends, both surfaces are sandblasted to increase the adhesive joint strength. Two LYDT's are mounted on the specimen sides in order to measure the deformations over a distance of 180 mm.

Investigator	Number of specimens	Matrix modulus (MPa)	Matrix yield strength (MPa)	Matrix ultimate strength (MPa)	Matrix elongation at break (%)	Reinforcement yield strength (MPa)	Reinforcement ultimate strength (MPa)	Reinforcement elongation at break (%)
Heshe & Nielsen (1992a)	6	-	210	-	739	6 mm tendon bars.		
Duedahl & Nielsen (1993)	2, 6	483	197	2.45	682	3 mm threaded wire.		
		464	193	2.40	681	5 mm threaded wire.		
		1757	203	8.66	1892	5 mm cold-drawn wire.		

Table 2.6: Survey of material characteristics for the test specimens. The steel fibres are straight and brass-coated Dramix OL 6/15 HC.

2.4.2 Test results

For the 7 tests reported in Heshe & Nielsen (1992a) complete tensile curves are observed, with 2 or 3 major cracks developing until the steel bars start to break. All tests end with *rupture* of the tendon bars and no failures are observed in the bond zone. In Duedahl & Nielsen (1993) all the tests end with *splintering cracks* along the wires followed by a pull-out failure or eventually by a failure of the adhesive joints. Therefore the following description primarily concerns the linear-elastic region of the stress - strain relationship of the steel bars.

In figure 2.19 a *qualitative* stress - strain curve, that represents the complete range of tests, is shown. The reinforcement ratio is denoted  $\phi$ .

It is assumed, that the matrix and the steel bars deform together, corresponding to perfectly bond, which is confirmed by strain measurements on the specimen surface and on the steel bars. The tensile stress  $\sigma_t$  is uniformly distributed across the complete cross-section of the specimen, while the stresses in the matrix and in the bars are denoted  $\sigma_m$  and  $\sigma_s$  respectively. In the linear-elastic region of both the matrix and the main reinforcement the *constitutive relation* reads:

$$\sigma_t = (1-\phi)\sigma_m + \phi\sigma_s = E_t \epsilon, \quad E_t = (1-\phi)E_m + \phi E_s \quad (2.67)$$

The modulus of elasticity  $E_t$  of the compressit matrix is presented in the previous section, see e.g. figure 2.13, and it is of magnitude 50 GPa, while  $E_s$  is equal to approximately 200 GPa.

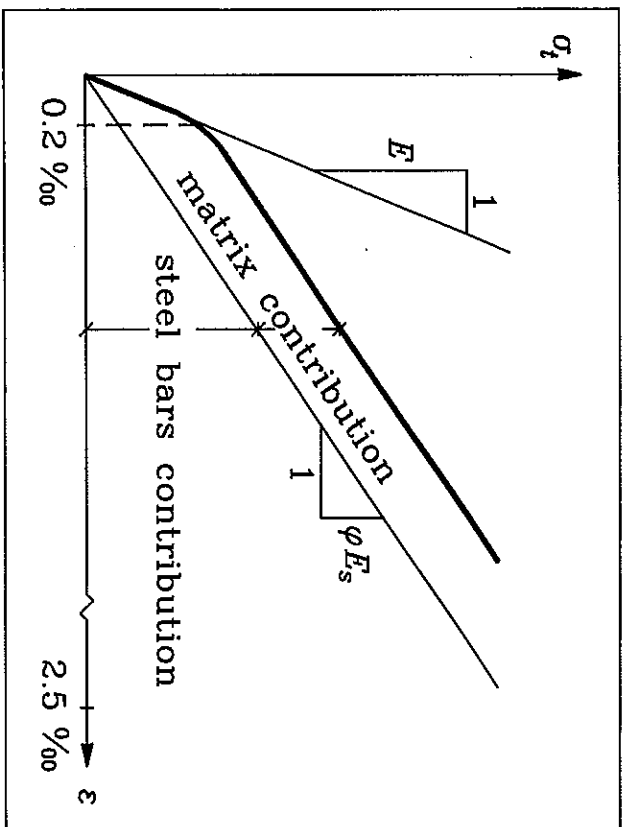


Figure 2.19: Qualitatively stress - strain relationship.

The *reinforcement ratios* applied in the two investigations range from 2.5, 3.1, 3.7 and 4.4 % in Heshe & Nielsen (1992a), while Duedahl & Nielsen (1993) uses 8 different  $\phi$ -values within the interval 1.1 - 10.9 % in their test programme.

The  $\sigma_t - \epsilon$  relationships start with a straight line governed by eq. (2.67), where both the matrix and the steel bars contribute to the stiffness. When the strain reaches approximately 0.2 % the slope of the curve decreases to a value, that represents the stiffness of the bars. The tensile strain value  $\epsilon = 0.2$  % corresponds to the *cracking strain* of the matrix and marks, that localization begins. However, still no visible cracks exist on the specimen surface.

While the loading continues, the load sustained by the matrix is kept constant, under increasing strains. This situation corresponds to *yielding* of the matrix and it continues until the steel bars start to yield (normally at  $\epsilon \approx 2$  to 3 %). By using a magnifying glass (25x), cracks are detected on the specimen surface, when the strains are equal to approximately 1.5 %.

In table 2.7 the observed matrix yield stresses are listed. It is noted, that the stresses are obtained as the difference between the total load and the load taken by the bars, divided by the net cross-sectional area of the compressit matrix.

Author	Fibre content (%)	Vertical strain (mm/mm)	Yield stress (MPa)
Heshe & Nielsen (1992a)	6	-5	Tenor bars. ( $2.5 \leq \phi \leq 4.4$ )
Duedahl & Nielsen (1993)	2	-5	Threaded. ( $1.1 \leq \phi \leq 7.7$ )
		-5	Cold-drawn. ( $4.4 \leq \phi \leq 10.9$ )
		up to 13	Threaded. ( $1.1 \leq \phi \leq 7.7$ )
	6	-7	Cold-drawn. ( $4.4 \leq \phi \leq 10.9$ )

Table 2.7: Observed yield stresses of compressit matrix during linear-elastic extension of the embedded steel bars, i.e. until  $\epsilon \approx 2\%$ . The steel fibres are Dramix OL 6/15 HC.

It appears that stresses as high as 13 MPa is observed, but it is likely, that this value is due to the fact, that the fibre orientation is not totally random. It seems more reasonable to use the *cracking strength* of the compressit matrix as its yield strength instead of using the post-cracking strength.

## 2.5 Concluding remarks

From Section 2.1.2 and 2.1.3, where a number of investigations of the behaviour of FRC under tensile loading are included, a general problem seems to exist. This problem is closely related to the fact, that the tensile test methods and specimens differ significantly, because no standard procedures exist for tension tests of concrete. Therefore the results from various investigations are hardly comparable. Furthermore the test results show great experimental scatter, which is also expected from the theoretical models. The scatter makes it difficult to observe any significant fibre effects. Thus, in order to observe significant fibre effects the fibre content should be higher, than what is practically obtainable in many cases.

The *micro mechanical* shear lag models, concerning the pull-out behaviour of a single fibre, which is extrapolated to a continuum by means of statistical considerations, do not necessarily improve their practical benefit by increasing the degree of complexity. It is evident that it is not enough to know the single fibre pull-out strength to predict the tensile post-cracking behaviour of FRC. The strength dependency on the qualitatively important parameters such as fibre content and aspect ratio is well-known, but still the models need empirical fitting to take the interaction between fibres (fibre spacing) and the properties of the matrix mix (e.g.

aggregate type and matrix density) into account.

The presence of great experimental scatter does not encourage to further refinements of the micro mechanical models. Instead a simple model is necessary together with proper experimental calibration.

When FRC-mixes with relatively small amounts of fibres are concerned, the choice of model is very important, because the stress contribution from the fibres is almost negligible compared to that of the plain matrix. For instance if the strength model in eq. (2.63) is assumed and the cracking strength is misinterpreted as the post-cracking strength. Then the effective shear strength of the fibre - matrix interface is overpredicted. Therefore several investigations simply apply the *empirical* post-crack relationships similar to those in eqs. (2.52) and (2.53) in order to model the post-crack behaviour. This approach does not include any parameters, characterizing the fibres except for the empirical parameters, which are fitted to vary with different fibre geometry and content (e.g.  $w_f$  increases significantly with the fibre reinforcement index).

The experiments with *compressit matrix* under direct tension show *multiple cracking* behaviour ( $\sigma_c \geq \sigma_{cr}$ ) for values of the fibre reinforcement index higher than 1, which corresponds to a fibre content of approximately 3 % of the Dramix fibres typically used for compressit.

The *cracking strength* seems to increase slightly with the fibre reinforcement index, but due to the experimental scatter a value of  $\sigma_{cr} = 7$  MPa is proposed, see figure 2.17. Also the *initial modulus of elasticity* increases slightly with increased fibre content, following the law of mixtures. The value for plain compressit matrix without fibres is approximately 50 GPa. If the tensile behaviour until first cracking is assumed linear-elastic, a value of the *cracking strain*  $\epsilon_{cr}$ , corresponding to the cracking strength, is determined to lie between 0.1 and 0.2 %.

After matrix cracking is initiated the stress continues to increase until the *tensile strength*  $f_t$  governed by the fibres crossing the crack is reached. Basically two types of fibres with different diameters (0.15 and 0.4 mm) are utilized. In table 2.8 the strength characteristics and the geometry of the fibre types are given.

It is concluded, that the fibre type OL 12/40 is the most attractive for compressit purposes, because it costs less than the other fibre type, which is of high quality steel, and its length is close to the optimum with respect to fibre pull-out. In cases where special demands for shorter fibres exist, e.g. with very close spacing of reinforcement bars or needs for small cover thickness, the fibre type OL 6/15 HC should be applied.

Test results described in Section 2.4 indicate, that in case of compressit matrix reinforced with continuous *steel bars*, the matrix seems to yield throughout the entire linear-elastic range of the steel bars, i.e. until the tensile strains exceed 2 %. The *yield stresses*, observed for the compressit matrix, is subject to great experimental scatter, but it seems, that a constant value equal to the matrix cracking strength is reasonable. Therefore it is concluded that even though the compressit matrix is found to produce very high post-cracking strengths (2 to 3 times the

## 2. Tensile behaviour

cracking strength) as a result of the fibre reinforcement, it seems impossible to take more than the cracking strength into practical consideration.

	OL 12/40	OL 6/15 HC	OL 13/15 HC						
	0.40	0.15	0.15	30	15.7	7.9 $V_f(L_f/d_f)$	17.2	Cheapest fibre.	
				40	9.4	4.7 $V_f(L_f/d_f)$	23.5	High quality fibre.	
				87					

Table 2.8: Strength characteristics for the fibre types applied to compress. The fibres are straight steel fibres.

## 2.6 References

- Aarre, T. (1992), *Tensile characteristics of FRC with special emphasis on its applicability in a continuous pavement*, Ph.D.-thesis, Serie R, No. 301, Department of Structural Engineering, Technical University of Denmark, Lyngby, 167 pp.
- Aarp, B.K. & C.E. Pedersen (1987), *Brudmekanik anvendt på CRC-beton*, in Danish, M.Sc.-thesis, Department of Building Technology and Structural Engineering, Aalborg University, Aalborg, 156 pp.
- Aveston, J. & A. Kelly (1973), 'Theory of Multiple Fracture of Fibrous Composites', *Journal of Materials Science*, Vol. 8, pp. 352-362.
- Baalbaki, W., P.-C. Aïcin & G. Bailly (1992), 'On Predicting Modulus of Elasticity in High-Strength Concrete', *ACI Materials Journal*, Vol. 89, No. 5, pp. 517-520.
- Bacbe, H.H. (1987), *Compact Reinforced Composite, Basic Principles*, CBL Report No. 41, Aalborg Portland A/S, 87 pp.
- Duedahl, T. & M.S. Nielsen (1993), *Beregningsmodel til Bestemmelse af Spændings- og Deformationsstandene for Bøjningspåvirkede CRC-Bjælker*, in Danish, M.Sc.-thesis, Department of Building Technology and Structural Engineering, Aalborg University, Aalborg, 109 pp.

## 2.6 References

- Gasparini, D.A., D. Verma & A. Abdallah (1989), 'Postcracking Tensile Strength of Fiber Reinforced Concrete', *ACI Materials Journal*, Vol. 86, pp. 10-15.
- Gopalaraman, V.S. & S.P. Shah (1987), 'Tensile Failure of Steel Fiber-Reinforced Mortar', *Journal of Engineering Mechanics*, ASCE, Vol. 113, No. 5, pp. 635-652.
- Gray, R.J. (1984a), 'Analysis of the Effect of Embedded Fibre Length on Fibre Debonding and Pull-Out from an Elastic Matrix. Part 1: Review of Theories', *Journal of Materials Science*, Vol. 19, pp. 861-870.
- Gray, R.J. (1984b), 'Analysis of the Effect of Embedded Fibre Length on Fibre Debonding and Pull-Out from an Elastic Matrix. Part 2: Application to a Steel Fibre-Cementitious Matrix Composite System', *Journal of Materials Science*, Vol. 19, pp. 1680-1691.
- Hannant, D.J. (1978), *Fibre Cements and Fibre Concretes*, John Wiley & Sons, xiii + 219 pp.
- Hansen, A.S. (1983), *Undersøgelse af de Mekaniske Egenskaber for Stålfiberarmet DENSIT*, in Danish, M.Sc.-thesis, Department of Civil Engineering, Building Materials Laboratory, Technical University of Denmark, Lyngby, 59 pp.
- Heshe, G. (1988), 'Experimental Research on Compact Reinforced Composite (CRC)', *Bygningsstatiske Meddelelser*, Vol. 59, No. 1, Danish Society for Structural Science and Engineering, 79 pp.
- Heshe, G. & C.V. Nielsen (1992a), *EU 264 - COMPRESIT, Subtask 1.6 - Behaviour in Tension*, NOVIT's Udviklingsfond, Aalborg, 27 pp.
- Krenchel, H. (1964), *Fibre Reinforcement*, Akademisk Forlag, Copenhagen, 159 pp.
- Lawrence, P. (1972), 'Some Theoretical Considerations of Fibre Pull-Out from an Elastic Matrix', *Journal of Materials Science*, Vol. 7, pp. 1-6.
- Laws, V. (1971), 'The Efficiency of Fibrous Reinforcement of Brittle Matrices', *Journal of Physics D: Applied Physics*, Vol. 4, pp. 1737-1746.
- Laws, V. (1982), 'Micromechanical Aspects of Fibre-cement Bond', *Composites*, Vol. 13, pp. 145-151.
- Li, V.C. (1992), 'Postcrack Sealing Relations for Fiber Reinforced Cementitious Composites', *Journal of Materials in Civil Engineering*, ASCE, Vol. 4, No. 1, pp. 41-57.
- Lim, T.Y., P. Paramasivan & S.L. Lee (1987), 'Analytical Model for Tensile Behaviour of Steel-Fiber Concrete', *ACI Materials Journal*, Vol. 84, pp. 286-298.



## 2. Tensile behaviour

- Morton, J. & G.W. Groves (1976), 'The Effect of Metal Wires on the Fracture of Brittle Matrix Composite', *Journal of Materials Science*, Vol. 11, pp. 617-622.
- Naaman, A.E., F. Moavenzadeh & F.J. McGarry (1974), 'Probabilistic Analysis of Fiber-Reinforced Concrete', *Journal of the Engineering Mechanics Division*, ASCE, Vol. 100, No. EM2, pp. 397-413.
- Romualdi, J.P. & G.B. Batson (1963), 'Mechanics of Crack Arrest in Concrete', *Journal of the Engineering Mechanics Division*, ASCE, Vol. 89, No. EM3, pp. 147-168.
- Romualdi, J.P. & J.A. Mandel (1964), 'Tensile Strength of Concrete Affected By Uniformly Distributed and Closely Spaced Short Lengths of Wire Reinforcement', *ACI Journal*, Vol. 61, pp. 657-671.
- Shah, S.P. (1991), 'Do Fibers Increase the Tensile Strength of Cement-Based Matrixes?', *ACI Materials Journal*, Vol. 88, pp. 595-602.
- Stang, H. (1992), 'Evaluation of Properties of Cementitious Fiber Composite Materials', in *High Performance Fiber Reinforced Cement Composites* (Eds. H.W. Reinhardt & A.E. Naaman), Proceedings of the International RILEM/ACI Workshop, pp. 388-406.
- Stang, H., Z. Li & S.P. Shah (1990), 'Pullout Problem: Stress versus Fracture Mechanical Approach', *Journal of Engineering Mechanics*, ASCE, Vol. 116, No. 10, pp. 2136-2150.

## 3. Uniaxial compressive behaviour

The most important property of concrete materials is undoubtedly the *uniaxial compressive strength*. Throughout the world this parameter is known to reflect the quality of a concrete mix and it classifies the concrete as normal or high-strength as mentioned in Chapter 1.

The most important factors, influencing the compressive strength  $f_c$  are

- The cement content given by the *water - cement ratio* (w/c). A lower ratio yields higher strength.
- The *curing* conditions (humidity, temperature and age).

The strength is often determined on cylinders ( $\phi 100 \times 200$  mm or  $\phi 150 \times 300$  mm) or 100 mm cubes and the procedure is standardized in most countries. It is well-known that the cube strength is higher than the cylinder strength (about 20 % higher).

This chapter concerns the complete compressive stress - strain relationship and not solely the strength. First a brief review on existing stress - strain models for concrete is given, followed by compressive test results obtained on compressive matrix.

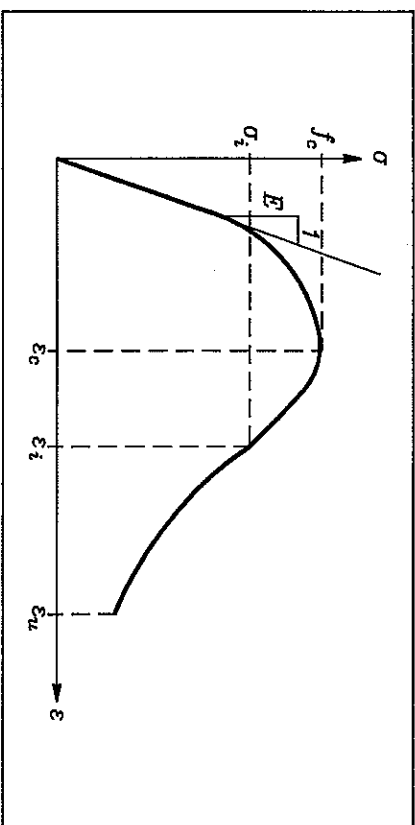


Figure 3.1: Qualitative stress - strain curve for concrete.

## 3.1 Review on concrete and FRC in uniaxial compression

The compressive stress - strain relationship is recognized to be difficult to record experimentally, because it requires a certain *stiffness* of the test machine. The test must be deformation controlled and if the stiffness is too small, the failure is *unstable*. There are methods to compensate for this lack of stiffness, by using closed-loop control with a feedback signal, or by loading the concrete cylinder in parallel with steel columns.

Another difficulty in determining the complete stress - strain curve is, that the result of a compressive test is known to depend on both the test set-up (e.g. dependent on whether there are intermediary layers between the loading plates and the specimen in order to eliminate friction) and the measuring techniques (e.g. whether the strains are measured directly on the specimen or taken as the overall deformations). Therefore the experimental results are difficult to compare and it is questionable whether the compression curve is a material property.

## 3.1.1 Analytical stress - strain curves for concrete

Knowing that concrete is a very complex material, no simple theory exists to include the effects of all the parameters, known to influence the compressive behaviour. All approaches are *empirical* and they all apply mathematical expressions with varying degree of accuracy to predict the experimental stress - strain curve.

In figure 3.1 a compressive stress - strain curve is shown with generally accepted symbols included. The *peak point* is represented by  $(\epsilon_p, f_p)$ , while  $(\epsilon_s, \sigma)$  denotes the *inflection point* on the descending branch, where the negative slope starts to increase. The curve is characterized by an *ascending part* until the peak, including a linear elastic portion up to approximately 60 % of the peak stress. After the peak point the curve descends with a considerably long tail, but in most cases this tail is cut off at a reasonable value.

For NSC the peak strain is approximately 2 % and the ultimate strain according to the Danish concrete code<sup>1</sup> is 3.5 %, when the compressive stress block for beams subjected to bending is considered.

In *Sargin (1971)* a very extensive review on the various approaches is given together with a proposal, which has been used widely since. *Sargin (1971)* gives at least 4 requirements for the mathematical stress - strain expression to fulfil:

- Obviously the curve passes through the origin.

<sup>1</sup>Dansk Ingeniørforenings Code of Practice for the Structural Use of Concrete, DS 411.

- The initial slope is equal to the initial modulus of elasticity  $E$ .

- The slope at the peak point is zero.

- The curve passes through the experimental determined peak point and at least one point at the descending part.

*Sargin* proposes the following expression

$$Y = \frac{AX + (D-1)X^2}{1 + (A-2)X + DX^2}, \quad \begin{cases} X = \frac{\epsilon}{\epsilon_c} \\ Y = \frac{\sigma}{f_c} \end{cases} \quad (3.1)$$

where  $X$  and  $Y$  are normalized strains and stresses respectively. The expression ensures the curve to pass through both the origin and the peak point, i.e.  $(0,0)$  and  $(1,1)$ . Furthermore it also results in a horizontal slope at the peak point, i.e.  $dY/dX = 0$  at  $X = 1$ .

The constant  $A$  is determined from the initial slope:

$$\frac{dY}{dX}(X=0) = \frac{E}{E_{peak}} \quad \Leftrightarrow \quad A = \frac{E}{E_{peak}}, \quad E_{peak} = \frac{f_c}{\epsilon_c} \quad (3.2)$$

where  $E_{peak}$  is the secant modulus at the peak point. The other constant  $D$  controls the descending part of the curve (the descending branch is lifted by increasing  $D$ ), and it is determined by an experimental data point at the descending part. Thus, in order to obtain a complete  $\sigma - \epsilon$  relationship from eq. (3.1), 4 parameters are necessary, i.e.  $f_c$ ,  $\epsilon_c$ ,  $E$  and an arbitrary point  $(\epsilon_s, \sigma)_{desc}$ . The *Sargin* expression forms the basis for the CEB<sup>2</sup> model code proposal from 1990.

*Wang et al. (1978)* have modified the above solution and end up with *separate expressions* for the ascending and the descending part. Instead of eq. (3.1) the following expressions are proposed, where  $i = 1,2$  correspond to the ascending and the descending part respectively, i.e. a total of 8 constants have to be determined empirically.

$$Y = \frac{A_i X + B_i X^2}{1 + C_i X + D_i X^2}, \quad i = 1,2 \quad (3.3)$$

The condition for the initial slope in eq. (3.2) still applies for  $A_i$ , but in order to determine the 3 remaining constants for the *ascending part* we require

<sup>2</sup>Comite Euro-International du Beton.

$$Y(X=1) = 1, \quad \frac{dY}{dX}(X=1) = 0 \quad (3.4)$$

which yields  $B_1 = D_1 - 1$  and  $C_1 = A_1 - 2$ . Furthermore it is required, that the curve is straight until  $Y = 0.45$ , i.e. it passes through the point  $(0.45f_c/E, 0.45)$ , which determines  $D_1$ . Thus, the physical parameters necessary to determine the ascending part are  $f_c$ ,  $\epsilon_c$  and  $E$ .

The descending part also needs 4 conditions to determine the constants and two of them are identical to eq. (3.4) at the peak point. Furthermore the curve passes through the inflection point  $(\epsilon_i/f_c, \sigma_i/f_c)$ , and through an arbitrary point of the descending part. The complete solution is not given here, but it is described in Fanella & Naaman (1985).

The approach in Wang et al. (1978) is related to practical concrete mixes through the compressive strength. The parameters that determine the 8 constants ( $\epsilon_c, f_c, E, \epsilon_i, \sigma_i$  and an arbitrary point of the descending part) are all related to  $f_c$  by means of *linear regression analysis* on a large number of tests, covering strengths from 20 MPa to 70 MPa. Some of the coefficients of correlation are poor, especially for the strains, indicating that  $\epsilon_c$  and  $\epsilon_i$  are only slightly influenced by the compressive strength.

Another empirical approach to model the stress - strain behaviour of concrete is given in Carreira & Chu (1985). This model applies a *single expression* to describe both the ascending and the descending part:

$$Y = \frac{\beta X}{\beta - 1 + X^\beta} \quad (3.5)$$

where  $\beta$  is determined from the initial modulus of elasticity, cf. eq. (3.2):

$$\frac{dY}{dX}(X=0) = \frac{E}{E_{peak}} \quad \Leftrightarrow \quad \beta = \frac{E}{E - E_{peak}} \approx 1 \quad (3.6)$$

The lower limit corresponds to a perfectly rigid-plastic stress - strain curve, while  $\beta \rightarrow \infty$  corresponds to a perfectly linear-elastic material.

The simplicity of eq. (3.5) is remarkable, considering that  $\beta$  is fitted to obtain the correct initial slope and simultaneously controls the descending part. From existing test data Carreira & Chu propose different relations between  $E/E_{peak}$  (or  $\beta$ ) and the compressive strength, by fitting test results with  $f_c$  varying between 10 and 70 MPa. The parameter  $\beta$  seems to vary between 2 for low-strength concrete and approximately 8 for HSC. However, a relatively large part of the test recordings only contains a very small part of the descending stress - strain curve.

In the discussion of the article by Carreira & Chu, given by Tomaszewicz (1986), a modification of eq. (3.5) is proposed. For the descending branch, the exponent  $\beta$  in the

denominator should be replaced by  $\beta f_c/20$  ( $f_c$  in MPa). This modification takes into account, that the descending part of the curve tends to be very steep, when HSC is considered.

**Application of empirical models to HSC.** Investigations of the uniaxial stress - strain behaviour of HSC (with strengths up to 120 MPa) are performed at the Department of Structural Engineering at Technical University of Denmark, see e.g. Olsen (1990) and Dahl (1992).

Both investigations use a test setup with concrete cylinders ( $\phi 100 \times 200$  mm) loaded in parallel with steel columns. By choosing the stiffness of this system properly it is possible to obtain both the ascending and the descending part of the compressive concrete curve, while the total compressive load, applied to the system, increases continuously, i.e. a *load controlled* test execution. The strains of the ascending branch are measured by means of electrical resistance gages, placed on the middle-third of the cylinder, while the descending branch is measured from the overall deformations of the cylinder, divided by its height.

Both Olsen (1990) and Dahl (1992) conclude, that the advanced model in eq. (3.3), involving 8 constants, gives very good agreement to the test results, but it is too complicated for practical use. Instead they propose the CEB-model, which is based on the Sargin-expression in eq. (3.1), because it is more simple and shows satisfactory agreement.

Dahl (1992) reports that the CEB-model matches the ascending branch almost perfectly, when the correct peak strains are applied. Also the descending branch is satisfactory, even though it is almost vertical after peak. The strain at peak stress is found in the vicinity of 3‰ for HSC, while the CEB-model suggests  $\epsilon_c = 2.2$ ‰ with practically no dependence of  $f_c$ .

### 3.1.2 Stress - strain curves for FRC

When the compressive behaviour of FRC is considered, the existing investigations mainly conclude, that the uniaxial strength is only *slightly influenced* by the presence of fibres. The investigations are few and they include relatively small fibre contents. However, the majority finds that the *ductility*, measured as the area under the stress - strain curve, increases significantly with the fibre content.

The earliest investigations concerning the compressive strength of concrete mixed with randomly short fibres are Chen & Carson (1971), Edgington & Hannant (1972) and Hughes & Fatuh (1977).

Edgington & Hannant (1972) mainly consider the effect of vibration during casting on the fibre orientation and state, that the fibres tend to align randomly in the planes perpendicular to the direction of vibration (and gravity). This statement is based on observed stress - strain curves with different load directions relative to the casting/vibrating direction.

In *Chen & Carson (1971)* and *Hughes & Farnih (1977)*, numerous compressive tests are reported, using standard cylinders and cubes respectively. The tests cover a wide range of fibre types (straight, hooked and crimped steel fibres), fibre geometries and contents (up to 2% by volume). The general conclusion is, that the compressive strength increases less than 10%, when fibres are added to the plain matrix. However, *Chen & Carson* observe an optimum fibre content of approximately 0.75% for mortar, yielding an increase in strength of 60%.

**Empirical stress - strain models.** As mentioned there exists a very limited number of investigations concerning the complete stress - strain relationship for FRC. All observations include a remarkable increase in ductility, while both the initial stiffness and the strength are only slightly influenced, which naturally leads to the fact, that the fibres primarily affect the descending branch.

In *Fanella & Naaman (1985)* an extensive test programme is reported, including various fibre types, geometries and contents. The fibres are straight brass-coated steel fibres added to mortar mixes ( $w/c = 0.5$  and  $0.35$ ), covering 3 different strengths ( $f_c = 50, 60$  and  $70$  MPa), 3 aspect ratios ( $L_f/d_f = 47, 83$  and  $100$ ) and 3 fibre contents ( $V_f = 1, 2$  and  $3\%$ ). The tests are closed-loop controlled by the cross-head displacement of the test machine, i.e. the strains are calculated from the overall deformations of the cylinder. The cylinder dimensions are  $\phi 76 \times 152$  mm and the tests are terminated, when the strains exceed  $15.4\%$ .

The modified *Sargin-model* proposed by *Wang et al. (1978)*, see eq. (3.3), is proposed. The four constants describing the ascending part of the stress - strain curve are determined from the initial modulus of elasticity and the peak point. The descending branch is governed by four other constants, ensuring that the curve passes through two experimental data points together with the peak point. *Fanella & Naaman (1985)* propose expressions, obtained from linear regression analysis, that give the relations between the physical parameters ( $E, f_c, \epsilon_c$ , and two data points on the descending branch) and the fibre reinforcement index. Unfortunately the coefficients of variation for the regression lines are not provided in the article.

*Fanella & Naaman* observe a significant fibre effect on the descending part of the curves. The fibre reinforcement index is varied between  $0.83$  and  $2.49$  for the different mortar mixes, resulting in stress - strain curves, where the descending branches are lifted significantly compared to the case without fibres.

In *Ezeldin & Balaguru (1992)* the simple model in eq. (3.5) is applied, including only one constant to be determined empirically. The experimental investigation is performed on  $\phi 100 \times 200$  mm cylinders, reinforced with low-carbon hooked-end steel fibres collated into bundles. Three different aspect ratios ( $L_f/d_f = 60, 75$  and  $100$ ) and 3 fibre contents ( $V_f = 0.4, 0.6$  and  $0.8\%$ ) are applied together with NSC ( $f_c \approx 40$  MPa) and silica fume HSC ( $f_c \approx 75$  MPa), having  $w/c$  equal to  $0.46$  and  $0.35$  respectively. The strains are recorded by use of two LVDT's, measuring the compression of the middle half of the cylinder.

By applying regression analysis on the stress - strain curves *Ezeldin & Balaguru (1992)* obtain the following relation between the constant  $\beta$  in eq. (3.5) and the fibre reinforcement index by weight for the NSC mix:

$$\beta = 1.09 + \frac{0.71}{\left(\frac{L_f}{d_f}\right)^{0.09}}, \quad 0.75 \leq W_f \frac{L_f}{d_f} \leq 2.5 \quad (3.7)$$

where  $W_f$  is the fibre content by weight.

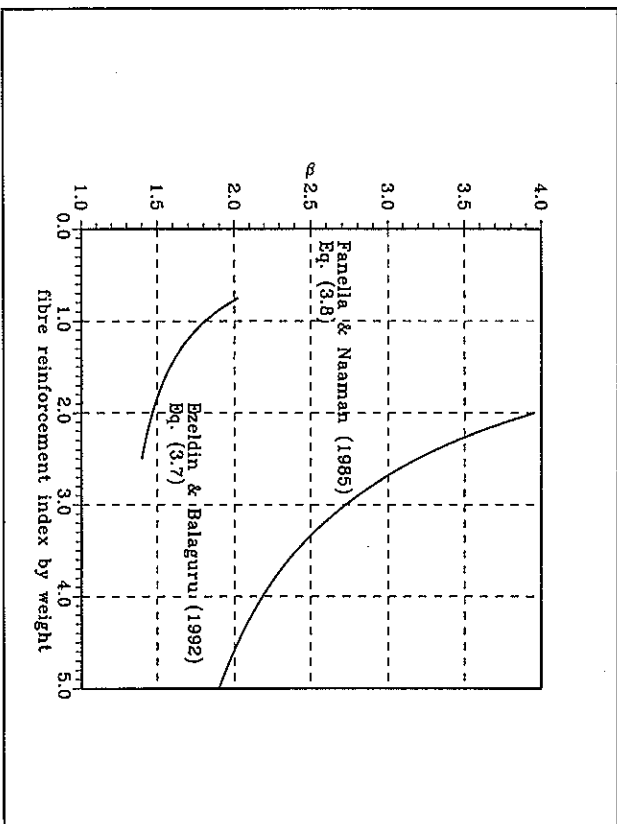


Figure 3.2: Variation of  $\beta$  with  $W_f(L_f/d_f)$  as suggested in *Ezeldin & Balaguru (1992)*.

The fibre content by weight  $W_f$  is related to  $V_f$  by a factor corresponding to the ratio between the densities of the fibres and the matrix, i.e.  $W_f = 3V_f$ . The range of the fibre reinforcement index by weight given in eq. (3.7) corresponds to  $0.2 \leq V_f(L_f/d_f) \leq 0.8$ , which is a rather narrow experimental range.

*Ezeldin & Balaguru* also perform a fitting of  $\beta$  from the results in *Fanella & Naaman (1985)*, dependent on the fibre reinforcement index by weight, see eq. (2.8). It is noted that eq. (3.7) applies for NSC reinforced with hooked-end fibres and that eq. (3.8) applies for high-strength

mortar reinforced with straight fibres. In figure 3.2 the expressions for  $\beta$  are shown for varying fibre reinforcement index by weight.

$$\beta = 1.09 + \frac{7.48}{\left(\frac{W_f L_f}{d_f}\right)^{1.39}}, \quad 2 \leq \frac{W_f L_f}{d_f} \leq 5 \quad (3.8)$$

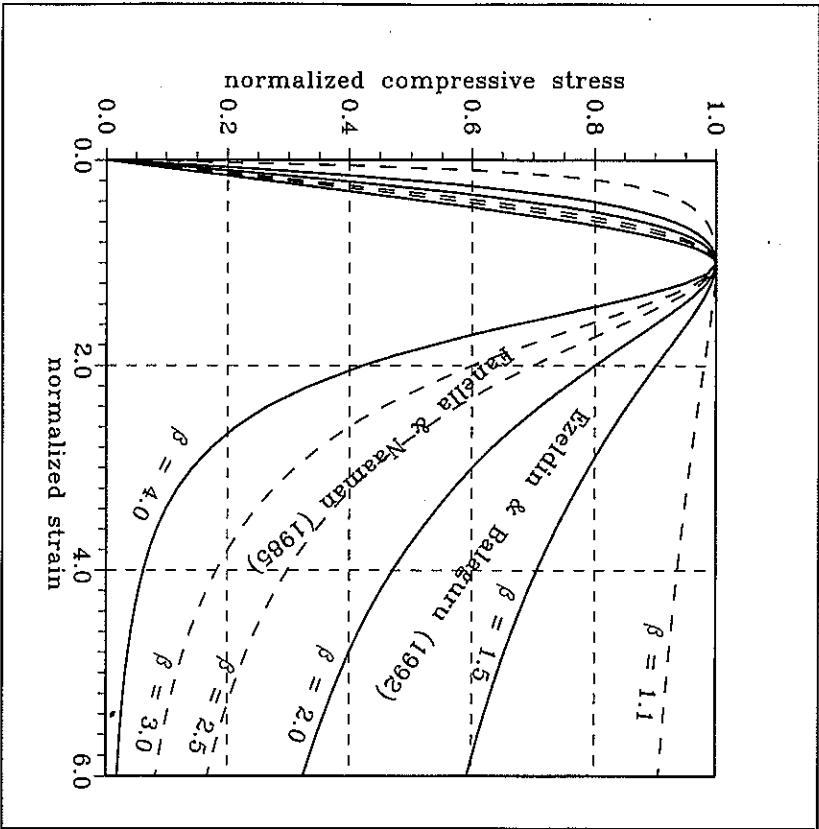


Figure 3.3: Theoretical  $\sigma/\sigma_c - \epsilon/\epsilon_c$  curves with varying  $\beta$ . The analytical expression is given in eq. (3.5).

In figure 3.3 examples of the theoretical normalized stress - strain curves, expressed by eq. (3.5), are shown with  $\beta$  varying according to figure 3.2. In the figure the two areas,

corresponding to the domains of the two investigations, are separated by the bold lines. It is clear, that the normalized descending curves registered in Panella & Naaman (1985) are lowest because the  $\beta$ -values are higher. However, by comparing the domain for Panella & Naaman (1985) in figure 3.3, with their actual stress - strain recordings included in their article, it appears, that the lower limit for  $\beta$  ( $\approx 2$ ) should be rather 1.5 in order to find satisfactory agreement.

It is well-known, that it is difficult to compare two different investigations directly, because the shape of the stress - strain curves depend on a lot of factors beside the fibres. It is evident that a comparison between Ezeldin & Balaguru (1992) and Panella & Naaman (1985) is questionable, because of different materials and strengths together with different strain measurements and test set-up. However, both investigations conclude significant influence of the fibres on the descending branch.

**Fracture mechanical model.** A plane crack, inclined the angle  $\theta$  to the remote compressive stress  $\sigma$ , is considered in an infinite body, see figure 3.4.

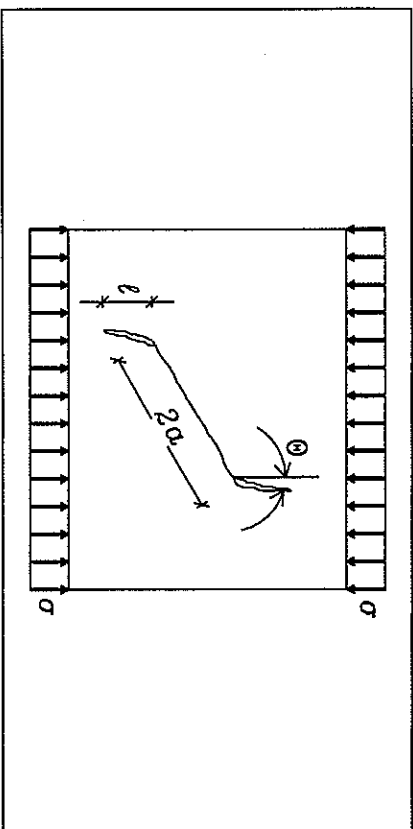


Figure 3.4: Wing cracks initiated from a micro crack inclined  $\theta$  to the load direction.

From linear elastic fracture mechanics we know, that a singular stress field exists near the crack tip. The remote compressive stress results in frictional shear stresses in the micro crack, caused by sliding of the crack surfaces, governed by the coefficient of friction. The stress intensity factor, describing the stresses near the crack tip, has the form

$$K_{II} \propto \tau\sqrt{a} \quad (3.9)$$

When this stress intensity factor reaches a critical value, which is determined experimentally, the vertical wing cracks start to grow.

The Ph.D.-thesis *Glavind (1992)* investigates the compressive stress - strain curve for concrete by means of growing wing cracks. When fibres are added to the concrete they influence the behaviour, because they contribute with *bridging stresses* both when the inclined crack slides and when the wing cracks open.

*Glavind (1992)* uses the fibre bridging stresses modelled by the shear lag model described in Section 2.1.2 and 2.1.3. The solution to the problem is not given here, but the calculations result in a  $\sigma - l$  relationship, where  $l$  is the *wing crack length*. The procedure is given below:

- First the sliding displacement of the inclined micro crack is increased stepwise. For each step the frictional shear stress and the corresponding fibre bridging stress are determined. This is repeated until the stress intensity factor equals its critical value, i.e. initiation of wing cracks.
- Then for each value of the sliding displacement, the wing crack length is increased stepwise until the stress intensity factor equals its critical value. This procedure is repeated until the compressive stress has vanished or until the wing crack length has reached a certain value.

For each step the remote compressive stress is calculated, dependent on the sliding displacement and the wing crack length. The wing crack opening is directly related to the sliding displacement by the factor  $\sin\theta$ .

In order to obtain a peak on the  $\sigma - l$  relationship it is necessary to include a measure for the interaction between the wing cracks, i.e. a measure for the density of the micro cracks. Otherwise the crack continues to grow, like if it is located in an infinite body.

As a part of the investigation, the model is compared to compressive tests, using HSC reinforced with straight steel fibres ( $L_f = 12.5$  mm,  $d_f = 0.4$  mm and  $V_f = 0, 1$  and  $3\%$ ). This comparison shows very close accordance between the proposed  $\sigma - l$  curves and the experimental  $\sigma - \epsilon$  curves and the same applies for the test results by *Fanella & Naaman (1985)*.

Thus, *Glavind (1992)* concludes, that the wing crack model includes the different fibre effects satisfactory, but it also contains a lot of parameters to be fitted empirically. For instance the length and the density of the micro cracks, together with the critical stress intensity factor are needed. Furthermore the theoretical wing crack lengths have to be interpreted as strains.

### 3.1.3 Peak of the compressive stress - strain curve for FRC

The three previously mentioned investigations all include experimental values of the corresponding uniaxial compressive strengths and strains with varying fibre content. In figure 3.5 the compressive strengths are depicted as a function of the fibre reinforcement index.

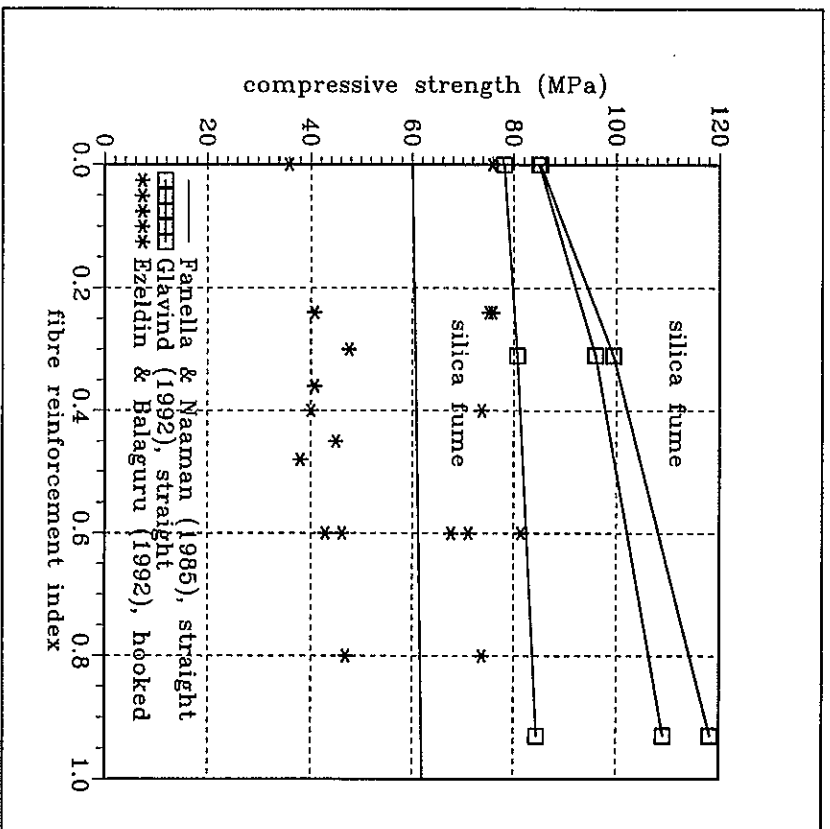


Figure 3.5: Experimental  $f_c - V_f(L_f/d_f)$  relationship for FRC reinforced with steel fibres.

It is obvious that the *silica fume* increases the strength considerably, and from the results in *Glavind (1992)* it also seems to amplify the effect of the fibres. For *Ezeidin & Balaguru (1992)* the fibre effect is questionable mainly because the variation of the fibre content are very little. It should be noted, that the author does not know the data points from the *Fanella & Naaman* article, and therefore the suggested regression line is used in the figure.

The *strain at maximum stress* is sometimes difficult to determine, because the deformations tend to localize in inclined crack planes. In *Fanella & Naaman (1985)*, the strains are taken as the overall deformations divided with the cylinder height, and in *Ezeidin & Balaguru (1992)* only the middle half of the cylinder is taken into account. In *Glavind (1992)* electrical resistance gauges are placed on the middle third of the cylinder to measure the strains until

localization occurs, after which the overall deformations are used.

It is generally accepted, that the strains measured over the middle-third of the cylinder are less than the overall strains, which makes comparisons difficult. Fanella & Naaman (1985) suggest, that the difference is approximately 0.4 %.

In figure 3.6 the strains  $\epsilon_p$ , corresponding to the strengths given in figure 3.5, are given. Again only the regression line provided in Fanella & Naaman (1985) is inserted in the figure.

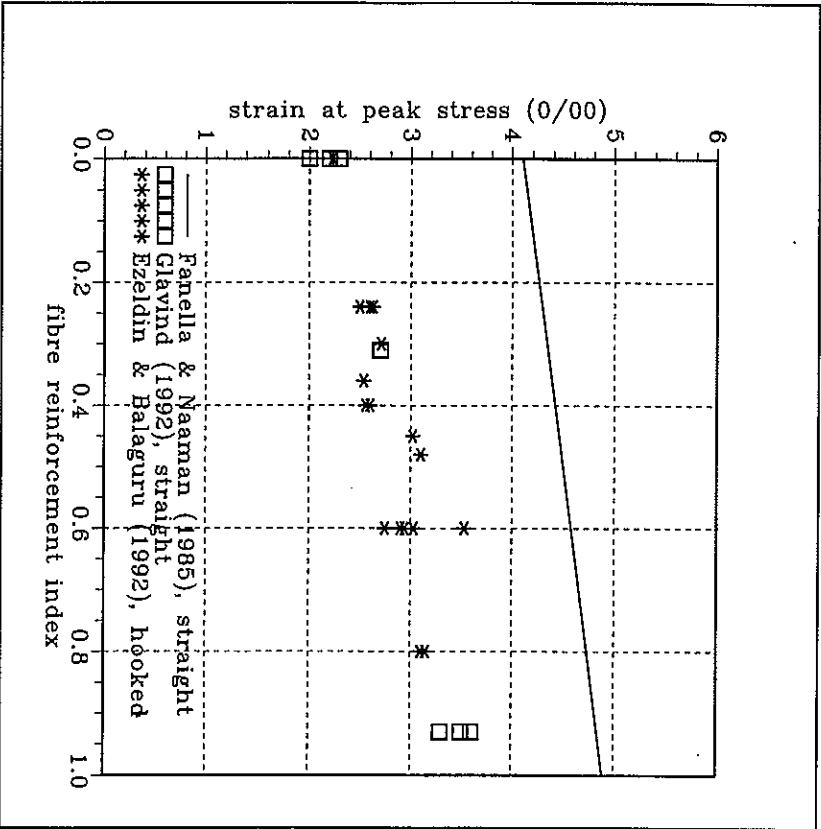


Figure 3.6: Experimental  $\epsilon_p - V_f(L_f/d_f)$  relationship for FRC reinforced with steel fibres. The effect of the fibre reinforcement index seems to be almost identical in the three investigations, corresponding to a slope of approximately 0.8 % as proposed by Fanella &

Naaman (1985). However, the difference in the level of the strains is probably due to the different measuring techniques and the fact, that Fanella & Naaman use mortar instead of concrete.

It is recalled from Section 3.1.1, that Dahl (1992) finds  $\epsilon_p$  close to 3 % for HSC, which corresponds satisfactory with the results in figure 3.6.

### 3.1.4 Ductility of FRC under compression

There exists no clear definition of the ductility or the toughness of concrete subjected to compression. Glavind (1992) defines ductility as the inelastic fraction of the area under the stress - strain curve until crack localization occurs, i.e. the descending branch is neglected. Fanella & Naaman (1985) relate the total area under the stress - strain curve to the special case without fibres (*the toughness index*), and finally Ezelidin & Balaguru (1992) relate the total area to the corresponding area under the *rigid-plastic* stress - strain curve (*the toughness ratio*).

It is evident from the presented test results, that the fibres primarily effect the descending part of the stress - strain relationship and thus, it seems justified to include this part in the comparison of ductilities. However, it is often a problem to determine the complete stress - strain curve experimentally for plain matrix because the test shows *unstable behaviour*. The recent developments of test techniques using closed-loop equipment have reduced the risk of catastrophic failures, but still HSC with  $f_c > 100$  MPa causes problems.

In Ezelidin & Balaguru (1992) the tests with plain matrix are unsuccessful. Therefore, the *toughness ratio* is calculated, using strains up to 15 %, i.e. the rigid-plastic energy density is 0.015f. In figure 3.7 these values are depicted for varying fibre reinforcement index.

In Fanella & Naaman (1985) the *energy density*, defined as the area under the stress - strain curve, is calculated for strains up to 15 % like in Ezelidin & Balaguru (1992). The energy density is divided by the density measured without fibres. Fanella & Naaman (1985) suggest a slightly increasing linear relationship between the toughness index and the fibre reinforcement index (the toughness index varies between 2 and 3, when  $V_f(L_f/d_f)$  varies from 0.8 to 2.5), but the correlation is not good. In figure 3.7 the regression line from Fanella & Naaman is inserted, where the energy density is related to the rigid-plastic energy, i.e. the toughness ratio.

It appears that the number of tests is too limited to obtain any clear relationship from figure 3.7. The toughness ratio seems to increase with the fibre reinforcement index, but it is questionable, whether further adding of fibres has any effect on the toughness ratio.

It is recalled that the toughness or ductility mainly serves as a parameter for comparisons within a test series. From the experiments referred to in this section it is clear, that the fibres increases the ductility significantly even though the scatter is very high.

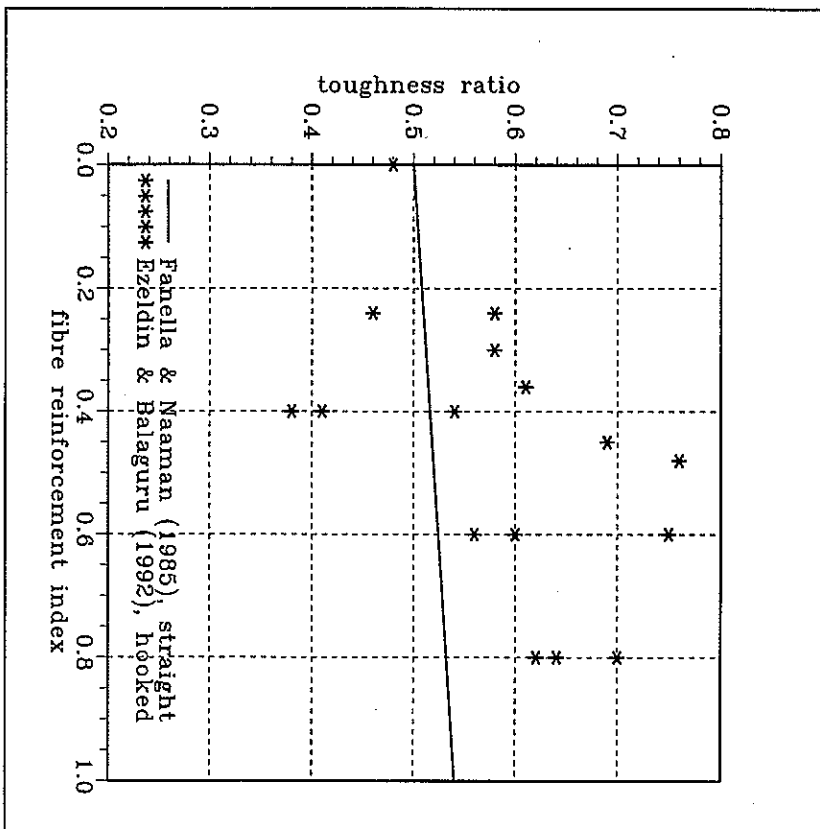


Figure 3.7: Experimental toughness ratios, depending on the fibre reinforcement index.

### 3.2 Compressit matrix under uniaxial compression .

The compressive strength of compressit matrix is well-known because each casting includes 3 standard cylinders ( $\phi 100 \times 200$  mm) as reference. The mean strength of such 3 cylinders is considered to be representative for the whole batch. Normally the *coefficient of variation* is less than 5 %, which is satisfactory. However, in case of plain compressit matrix without fibre reinforcement, the failure is almost catastrophic, resulting in higher experimental scatter on the strengths.

In this chapter two test series are presented:

- The first is performed by I. Al-Shummer at the Cement and Concrete Laboratory in Aalborg during 1988, see Al-Shummer (1989).
- The second test series is performed during the present project at the laboratory of the Department of Structural Engineering, Technical University of Denmark.

Both series use  $\phi 45 \times 90$  mm cylinders because the capacity of the test machines makes it impossible to crush bigger cylinders. The fibre content and geometry are varied and both the ascending and the descending part of the stress - strain relationship are investigated.

#### 3.2.1 Test specimens and method

A total of 10 cylinders are reported in Al-Shummer (1989), covering 5 different fibre contents. In table 3.1 the 5 different compressit mixes are listed and it appears, that the Dramix fibre type OL 6/15 HC is utilized for all the mixes, cf. table 1.3.

The cylinders are cured under water at a temperature of  $80^\circ \text{C}$  for two days in order to accelerate the strength development.

The Al-Shummer tests are performed in a 500 kN universal Instron test machine under deformation control. Signals from two electrical resistance gages on the cylinder surface, measuring the longitudinal strain, and two gages measuring the lateral strain, are recorded during each test. Because of the *insufficient stiffness* of the test machine, the descending part of the stress - strain curve is not registered.

The tests performed in connection to the present project includes both the ascending branch and the descending branch. The test principle is a closed-loop control with the test setup originally developed by Glavind & Stang (1991). In Appendix 2 the test procedure is described in detail.

The cylinders are cast from 8 different compressit mixes, identical to those utilized in Section 2.3 for the direct tensile tests. In table 3.1 the fibre content and type for these mixes are listed. The specimens are named UC for uniaxial compression followed by a number giving the fibre aspect ratio. Each of the 8 compressit matrices are tested by means of 3 cylinders with dimensions  $\phi 45 \times 90$  mm, which gives a total of 24 tests.



Specimen name	$L_0/d_0$	$\epsilon_f$ (%)	$\epsilon_f(L_0/d_0)$	Fibre type Diameter
Al-Shummer (1989)	40	0	0	OL 6/15 HC
		3	1.2	
		6	2.4	
		9	3.6	
		12	4.8	
UC0	-	0	0	-
		3	0.9	
		6	1.8	OL 12/40
UC30	30	9	2.7	
		3	1.2	
		6	2.4	OL 6/15 HC
UC40	40	9	3.6	
		6	2.4	
UC87	87	3	2.6	OL 13/15 HC

Table 3.1: Survey of the compressive mixes used for uniaxial compressive tests. See fibre characteristics in table 1.3.

The test principle is based on the work of Dahl & Brinker (1989), using a combined signal as feedback signal in the closed-loop control. Instead of controlling the test by the longitudinal deformations alone, like in normal deformation control, the transversal strains are included. This means that the *feedback signal* is composed as the sum of the longitudinal and the transversal strain signal:

- At the ascending branch the longitudinal deformations are dominant, which means normal deformation control.
- Around the peak the transversal deformations increase significantly, because of cracking, while the longitudinal deformations are almost constant or even decrease (snap back). However, the feedback signal continues to increase.

Glavind (1992) reports successful tests on the setup, using strengths up to 90 MPa, and concludes that higher strengths require better equipment in order to transmit the feedback

signal sufficiently fast. In the present test programme fibre reinforced matrix strengths above 200 MPa give satisfactory results, but the plain compressive cylinders without fibres (UC0) are impossible to perform because of *explosive failures*.

In Shah et al. (1978) it is emphasized, that problems in establishing stable compressive tests under closed-loop control can occur, either because the overall deformations are used as feedback signal instead of the localized deformations, or because the closed-loop system cannot respond sufficiently quick.

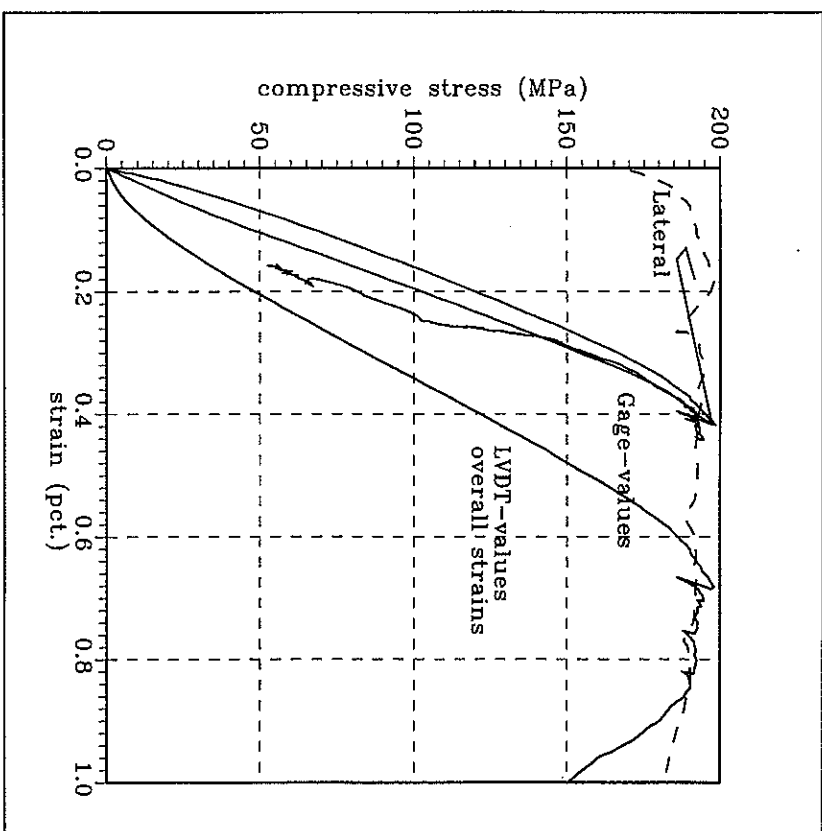


Figure 3.8: Comparison of longitudinal strains, measured by means of electrical strain gages and LVDT's. Also the lateral strains are shown.

## 3.2.2 Test results

In this section we present the results obtained for compressit matrix under uniaxial compression. The tests reported in Al-Shammer (1989) only concern the ascending part of the stress - strain curve, while the other test series consider the complete curve.

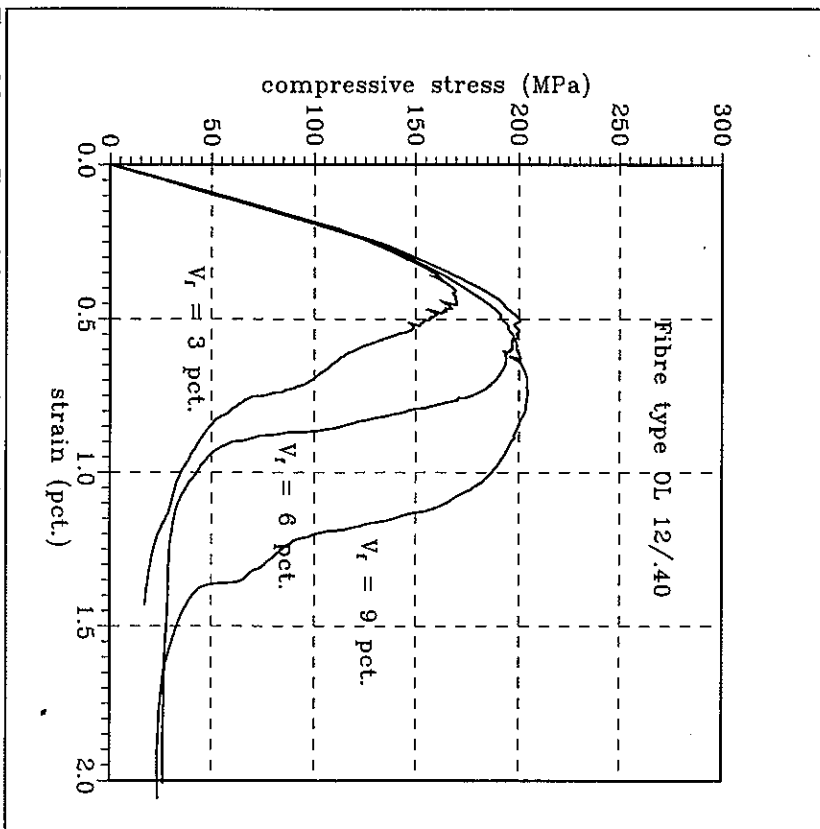


Figure 3.9: Characteristic stress - strain curves for cylinders of type UC30.

**Stress - strain curves.** Each of the matrices UC30, UC40 and UC87, listed in table 3.1, is represented in Appendix 2 with their stress - strain curves. Because of the catastrophic failures of the unreinforced cylinders (UC0), their curves are not shown. Each stress - strain curve is composed by the strains, measured by means of electrical gages, for the ascending part until approximately 75 % of the peak load. Then the overall deformations, measured by means of

the LVDT's, are used for the remaining part of the curve. In figure 3.8 corresponding strain-values, obtained by electrical gage measurements and by overall LVDT measurements, are shown. It is evident, that the gage measurements cannot be used, when the deformations start to localize. The LVDT's measure the compression of the cylinder between the load plates, but they do not include the deformations of the load frame, which is rather soft.

When the deformations localize the strain gages are relieved, which is the case figure 3.8 at  $\epsilon \approx 0.42\%$ , or eventually a crack crosses them, followed by a sudden increase of their signal. The lateral strains, measured by dividing the extension of the circumference by its nominal length, seem to be practically zero until the initiation of cracks, which causes a considerably increase of the lateral signal.

Another observation from figure 3.8 is, that the overall strains are higher than the middle-third strains, which is the general opinion. Especially in the beginning the overall strains increase too much, while the initial slope increases towards the correct modulus of elasticity. This is due to adjustments of the load plates to fit the specimen ends. For instance the specimen ends are not perfectly plane and parallel with each other and furthermore small grains and cement paste are crushed by the load plates. Therefore it seems reasonable to use the gage-signals until crack localization occurs and switch to the LVDT-signals on the descending branch.

In figure 3.9 and 3.10 typical stress - strain curves, taken from Appendix 2, are shown. The effect of the fibre content on both the peak point and the energy dissipation, taken as the area under the curves, is obvious from both figures. It is interesting to notice, that for the fibre content  $V_f = 3\%$  of fibre type OL 6/15 HFC and OL 12/40, the curves show so-called *snap-back*, defined as decreasing strains on the descending branch. Each snap-back represents sudden energy releases through crack development, followed by an increase in the lateral strain, causing the closed-loop control to unload. Ghavind & Slang (1991) suggest, that it is possible to minimize the occurrence of snap-back by means of the composition of the feedback signal, but no investigations seem to concern that problem. Naturally the fibres reduce snap-back because they counteract the crack development.

The differences between the fibre types in figure 3.9 and 3.10 seem to influence the form of the descending part. It appears that UC30 descends with a steeper slope than the others and, that they fall to a load level of about 10 % of the peak load. However, the curves in Appendix 2 show great scatter on the slopes and on the end levels of the descending parts.

The *proportionality limits* for the ascending stress - strain curves also seems to depend on the fibres. The cylinders with  $V_f = 0$  show linear behaviour all along the ascending branch until they fail explosively, leaving only two cones on the load plates. For the smallest fibre content  $V_f = 3\%$  the curves are linear until 70 to 80 % of the peak load and for higher fibre contents the limit is about 60 %. It seems that the proportionality limit is approximately 120 MPa and that the stresses increase beyond this value due to strain hardening of the matrix under development of a crack pattern, that is controlled by the fibres.

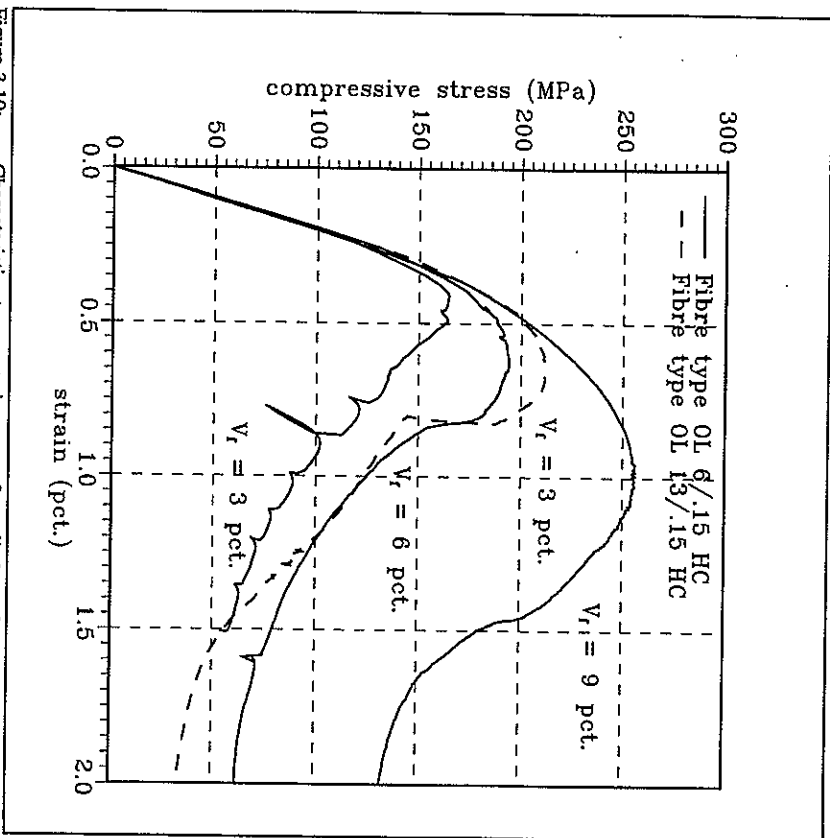


Figure 3.10: Characteristic stress - strain curves for cylinders of type UC40 and UC87. Mean values of the test results. In table 3.2 the main results are given in terms of the initial modulus of elasticity  $E$ , the compressive strength  $f_c$  together with the corresponding strain  $\epsilon_c$  and finally the energy density  $W$ . Each result is a mean value from 3 identical tests and brackets contain the coefficients of variation. The test results from Al-Shunner (1989) do not include coefficients of variation because they only represent two repetitions.

The  $E$ -modulus is determined graphically from the stress - strain curves in Appendix 2 and  $W$  is calculated numerically as the area under the stress - strain curve until the strain 1.5 % by means of the trapezoidal rule. However, because of lack of data the area is only calculated until the strain 1 % for the specimens UC30 and UC40 with fibre content  $V_f = 3\%$ , cf. figure A2.1 and A2.4 in Appendix 2.

Initial modulus of elasticity  $E$ . The  $E$ -values from table 3.2 are depicted in figure 3.11 as a function of the fibre content. The figure also contains the tensile moduli of elasticity presented in Section 2.3, see table 2.5.

Specimen	Fibre content (%)	Repetitions	Compressive strength $f_c$ (MPa)		Initial modulus of elasticity $E$ (GPa)		Energy density $W$ (MJ/m <sup>3</sup> )	
			Mean	COV (%)	Mean	COV (%)	Mean	COV (%)
Al-Shunner (1989)	40	0	0	49.6	148.5	0.31	-	
		3	1.2	51.1	176.5	0.37	-	
		6	2.4	53.9	192.5	0.43	-	
	30	9	3.6	53.7	209.0	0.40	-	
		12	4.8	60.6	294.5	0.62	-	
		-	0	0	51.8	168.0	0.33	-
UC0	3	0	0	51.8	168.0	0.33	-	
		3	0.9	50.7	170.0	0.43	1188	
		6	1.8	55.6	194.3	0.53	1684	
	9	2.7	50.8	197.3	0.73	2191		
		3	1.2	53.2	164.3	0.40	1412	
		6	2.4	51.0	195.7	0.65	2146	
UC40	6	2.4	51.0	195.7	0.65	2146		
		9	3.6	51.0	257.3	1.04	2971	
		3	1.2	53.2	164.3	0.40	1412	
	9	2.7	50.8	197.3	0.73	2191		
		3	1.2	53.2	164.3	0.40	1412	
		6	2.4	51.0	195.7	0.65	2146	
UC87	3	2.6	51.0	208.0	0.62	1910		
		3	2.6	51.0	208.0	0.62	1910	
		3	2.6	51.0	208.0	0.62	1910	
	9	3.6	51.0	257.3	1.04	2971		
		9	3.6	51.0	257.3	1.04	2971	
		3	1.2	53.2	164.3	0.40	1412	

Table 3.2: Test results from uniaxial compressive tests. All values are mean values and the brackets contain the coefficients of variation.

### 3. Uniaxial compressive behaviour

It is evident from figure 3.11, that the initial moduli of elasticity measured under uniaxial compression and tension are directly comparable. The results show a certain increase with fibre content as predicted by the law of mixtures, but this effect is exceeded by the variations due to various castings. A value of  $E = 50$  GPa seems reasonable for practical use without taking the fibre effect into consideration.

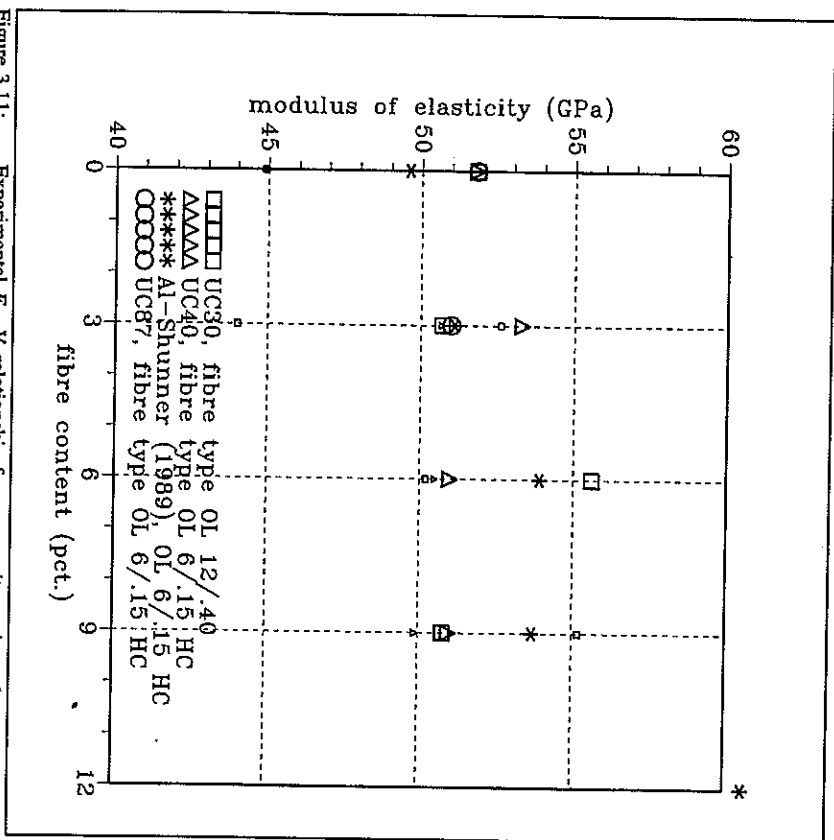


Figure 3.11: Experimental  $E - V_f$  relationship for compressit matrix under compression. The small symbols represents the direct tensile tests, cf. figure 2.13.

Peak point of the stress - strain curve. From figure 3.9 and 3.10 the fibre effect on the peak point is unquestionable. Both the ultimate stress and the corresponding strain increase with the fibre content and the aspect ratio. In figure 3.12 and 3.13 the strength  $f_c$  and the peak strain  $\epsilon_c$  are depicted as a function of the fibre reinforcement index.

### 3.2 Compressit matrix under uniaxial compression

The double-sided 95 % confidence intervals for the mean values of  $f_c$  and  $\epsilon_c$  are calculated from the techniques described in Section 2.3.2. These intervals are calculated solely from the results obtained in the present test programme and they have the widths 16.6 MPa and 0.1 % for the mean values of  $f_c$  and  $\epsilon_c$ , respectively.

In figure 3.12 the only unexpected difference is found for UC40 with  $V_f = 9\%$ , where  $f_c = 257.3$  MPa, while Al-Shunner finds  $f_c = 209.0$  MPa. In figure 3.13 the strains from Al-Shunner (1989) seem to underestimate  $\epsilon_c$ . This is probably due to the fact that Al-Shunner measures the strains by means of electrical gages, while the other data points are overall strains.

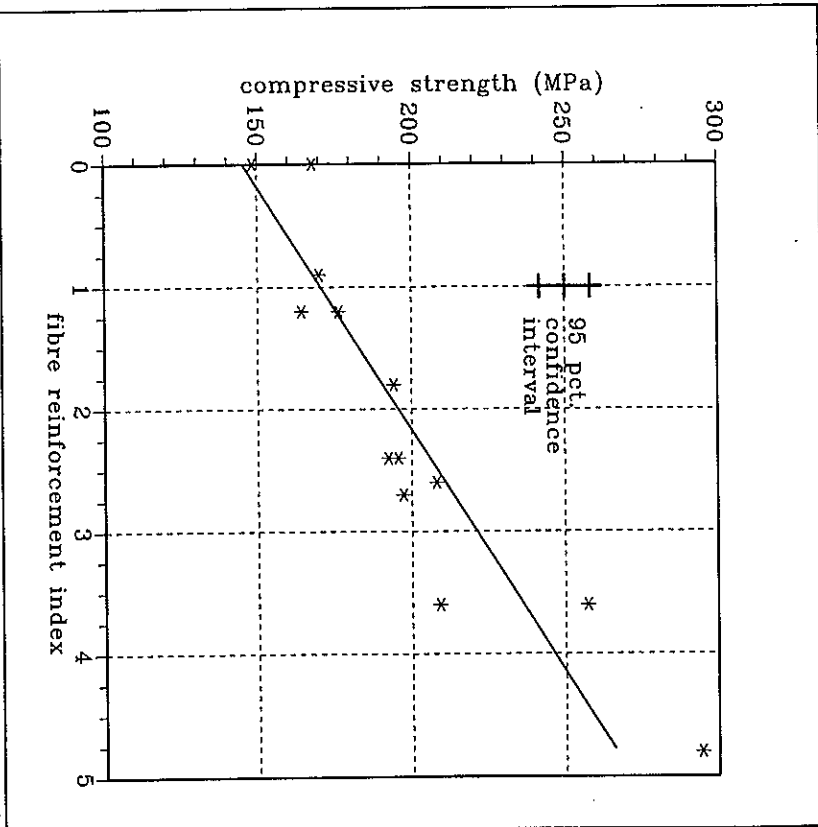


Figure 3.12: Experimental  $f_c - V_f(L_f/d_f)$  relationship from table 3.2, including the double-sided 95 % confidence interval for the mean value of  $f_c$ .

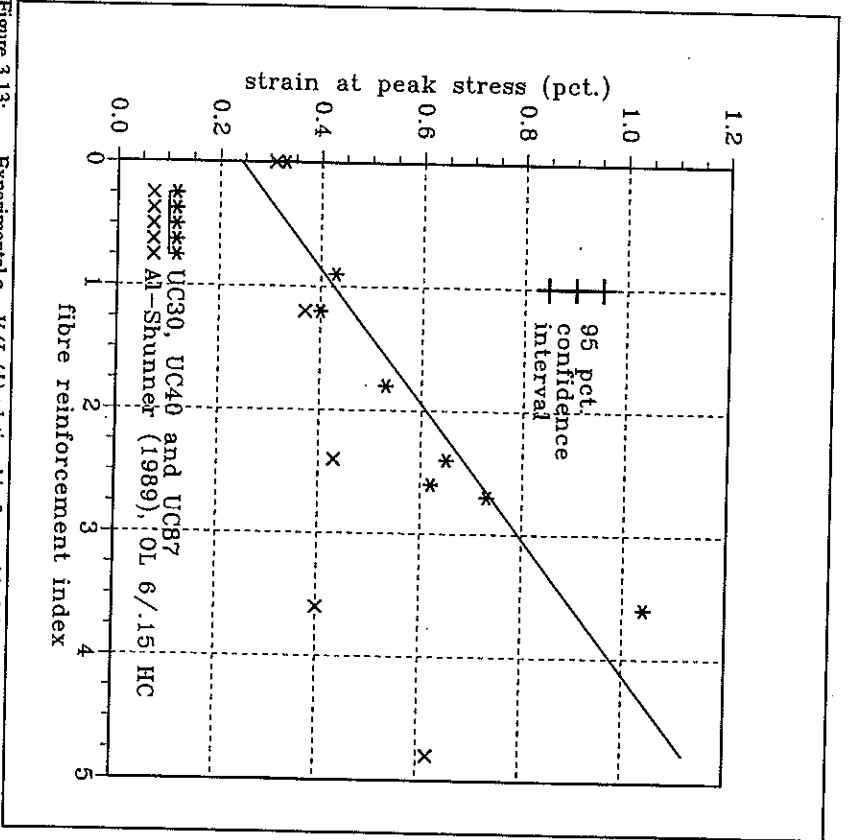


Figure 3.13: Experimental  $\epsilon_c - V_f(L_f/d_f)$  relationship from table 3.2, including the double-sided 95 % confidence interval for the mean value of  $\epsilon_c$ . The compressive strength  $f_c$  and the strain  $\epsilon_c$  are satisfactory described by linear regression lines, which are inserted in the figures:

$$f_c = \left( 145 + 25 V_f \frac{L_f}{d_f} \right) \text{MPa} \quad \left. \begin{array}{l} 0 \leq V_f \frac{L_f}{d_f} \leq 5 \end{array} \right\} \quad (3.10)$$

$$\epsilon_c = \left( 0.24 + 0.18 V_f \frac{L_f}{d_f} \right) \% \quad \left. \begin{array}{l} 0 \leq V_f \frac{L_f}{d_f} \leq 5 \end{array} \right\}$$

where the coefficients of correlation is equal to 0.91 and 0.94 respectively. The regression analysis is performed on all the strengths in table 3.2, but excluding the strains from Al-Shunner (1989).

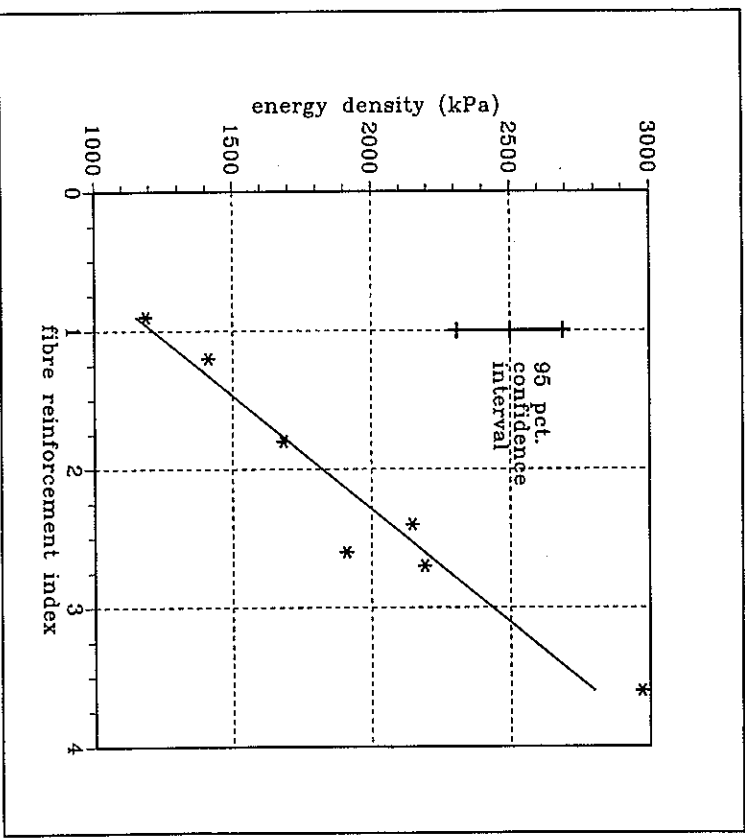


Figure 3.14: Experimental  $W - V_f(L_f/d_f)$  relationship from table 3.2, including the double-sided 95 % confidence interval for the mean value of  $W$ .

### 3. Uniaxial compressive behaviour

Energy density  $W$ . From figure 3.14, where  $W$  is depicted as a function of  $V_f(L_f/d_f)$ , it appears, that the energy density increases almost linearly with the fibre reinforcement index. A linear regression analysis yields the expression

$$W = \left( 605 + 610 V_f \frac{L_f}{d_f} \right) \text{ kN/m}^2, \quad 1 \leq V_f \frac{L_f}{d_f} \leq 4 \quad (3.11)$$

with the coefficient of correlation equal to 0.97.

#### 3.2.3 Compressive behaviour of compressit matrix

Based on the test results from the previous section, the compressive characteristics of compressit matrix are reported. Linear expressions with respect to the fibre reinforcement index are found to give satisfactorily agreement. These expressions for compressit matrix are listed in table 3.3. The findings for compressit matrix is compared to other compressive results on FRC, cf. Section 3.1.2.

Material	Plain matrix	Fibre-reinforced matrix	Strength limit	Equation
$f_c$	145 MPa	25 MPa	$0 \leq V_f(L_f/d_f) \leq 5$	(3.10)
$\epsilon_c$	0.24 %	0.18 %	$0 \leq V_f(L_f/d_f) \leq 4$	(3.10)
$W$	605 kN/m <sup>2</sup>	610 kN/m <sup>2</sup>	$1 \leq V_f(L_f/d_f) \leq 4$	(3.11)

Table 3.3: Compressive characteristics of the tests with compressit matrix.

Uniaxial compressive strength  $f_c$ . The tests show, that the cylinder strength  $f_c$  is satisfactory expressed as a linear function of the fibre reinforcement index, see figure 3.12. If the expression for  $f_c$  is compared to the experimental investigations in figure 3.5 it is recalled, that Famella & Naaman (1985) and Ezzeldin & Balaguru (1992) hardly register any fibre effect, but nevertheless they propose linear regression lines. The former gives a slope on the  $f_c - V_f(L_f/d_f)$  relationship equal to 1.9 MPa, while the latter suggests 1.1 MPa, but the coefficients of correlation are poor.

However, the HSC reinforced with steel fibres, reported in Glavind (1992), see figure 3.5, seems to include a fibre effect of the same magnitude as observed for compressit matrix. It is probably, that this effect is caused by the presence of silica fume, which increases the fibre bond considerably.

If the knowledge of the tensile strength of compressit matrix is taken into account by means of eq. (2.64):

### 3.2 Compressit matrix under uniaxial compression

$$f_c = 6 V_f \frac{L_f}{d_f} \text{ MPa}, \quad 1 \leq V_f \frac{L_f}{d_f} \leq 4 \quad (3.12)$$

where  $f_c$  represents the mean value of the experimental post-cracking strength of compressit matrix, cf. figure 2.15. By inserting eq. (3.12) into eq. (3.10) we get

$$f_c = f_{c0} + 4 f_t \quad (3.13)$$

where  $f_{c0}$  is the strength of the plain matrix without fibres (within the range 140 - 150 MPa).

This expression corresponds remarkably to the plastic solution given in Nielsen (1984), p. 130 and originally developed in Exner (1983):

$$p = f_c + k f_t \quad (3.14)$$

where  $p$  is an upper-bound carrying capacity of a concrete cylinder with uniaxial compressive and tensile strength  $f_c$  and  $f_t$  respectively. The solution corresponds to a rigid-plastic material following the modified Coulomb failure criterion governed by the cohesion  $c$ , the angle of friction  $\phi$  and the tensile strength. The constant  $k$  depends on the angle of friction through  $(1+\sin\phi)/(1-\sin\phi)$ . For normal concrete several tests show, that  $\phi = 37^\circ$ , which gives  $k$  equal to 4 just like the constant in eq. (3.13), which is obtained empirically.

Like it is stated in Exner (1983) the theoretical solution in eq. (3.14) gives too high values because  $f_c$  is defined as the uniaxial strength of a cylinder and thus  $p = f_c$ . This is a consequence of the upper-bound solution technique due to an incorrect failure mechanism.

The second term in eq. (3.14) represents the contribution from the tensile strength, when vertical cracks originate from the cylinder axis, because of the outward directed radial displacements. Thus, the tensile strength provided by the steel fibres acts as confinement to the cylinders, which seems plausible.

Strain corresponding to  $f_c$ . The tests show that  $\epsilon_c$  increases significantly with the fibre reinforcement index, see figure 3.13. The peak strain for the plain compressit matrix without fibres corresponds very well with the values usually obtained for concrete, i.e. within the interval 2 to 3 ‰.

The slope of the linear expression in eq. (3.10) is a little bit higher than those suggested in Famella & Naaman (1985) and Ezzeldin & Balaguru (1992), which are 0.08 % and 0.14 % respectively, see figure 3.6. However, there seems to be satisfactory agreement between the different investigations, even though the compressive strength varies between 40 and 200 MPa and the strain measurements use different techniques.

**Ductility.** The area under a certain part of the stress - strain curve is only useful for comparisons between tests performed under the same conditions. The energy density  $W$ , measured on compressive cylinders up to compressive strains of about 1.5 %, is strongly affected by the fibres, see figure 3.14. Unfortunately no tests have succeeded without fibres, but a comparison of the constant term in eq. (3.11) ( $= 605 \text{ kN/m}^2$ ) with the test results in Dahl & Brincker (1989) shows, that the energy density for plain compressive matrix without fibres is also reasonably predicted by the linear expression. Dahl & Brincker (1989) investigate HSC cylinders with strengths ranging from 70 to 150 MPa and find energy densities ranging from 500 to 700  $\text{kJ/m}^2$ , which support the compressive results.

If the so-called toughness ratio, defined as  $W$  divided by the area under the corresponding rigid-plastic stress - strain curve, is calculated and compared to figure 3.7 no clear pattern is found. The values vary from 0.6 to 0.9, but no significant influence of the fibre reinforcement is found. A similar conclusion is found for the results in figure 3.7.

**Complete stress - strain curves.** From the curves in Appendix 2, that represent the data recordings from the test series, it is evident, that the descending branches are subject to relatively high experimental scatter, when identical tests are compared. The peak point is well-determined, while the descending tail shows various slopes and end levels. Therefore it seems pointless to search for a unique relationship between the fibre characteristics and the descending branch on basis of the available test recordings.

The general observation is, that when the strains exceed 3 to 4 times the peak strain the stresses become almost constant at a level of 10 to 40 % of the strength. A normalized stress - strain relationship ( $Y - X$  relationship) of the representative curves in figure 3.9 and 3.10 indicates, that the curves only vary within a relatively narrow region, see figure 3.15.

In figure 3.15 the 7 curves from figure 3.9 and 3.10 are depicted together as data points in a  $X - Y$  diagram. The figure also contains two theoretical curves, obtained from the simple expression in eq. (3.5), proposed by Carreira & Chu (1985):

$$Y = \frac{\beta X}{\beta - 1 + X^\beta}, \quad \beta \geq 1, \quad X = \epsilon/\epsilon_c, \quad Y = \sigma/f_c \quad (3.5)$$

The upper curve in figure 3.15 is calculated for  $\beta = 2.5$  and represents an upper limit for the experimental descending branches obtained for compressive matrix with high fibre volumes. The lower curve represents the situation with a very steep descending branch for low fibre contents. The lower curve is calculated for  $\beta = 4$  for the ascending part, while the expression is slightly modified for the descending part. This modification follows the proposal given by Tomaszewicz (1986), where the exponent in the denominator of eq. (3.5) is increased in order to obtain a steeper descending part, which is necessary for HSC. Instead of using  $\beta = 4$  the exponent is increased by 20 % to 4.8 for the descending part, i.e. for  $X \geq 1$ . It is noted, that Tomaszewicz proposes an even higher value for the exponent in the case of HSC without fibres, cf. Section 3.1.1.

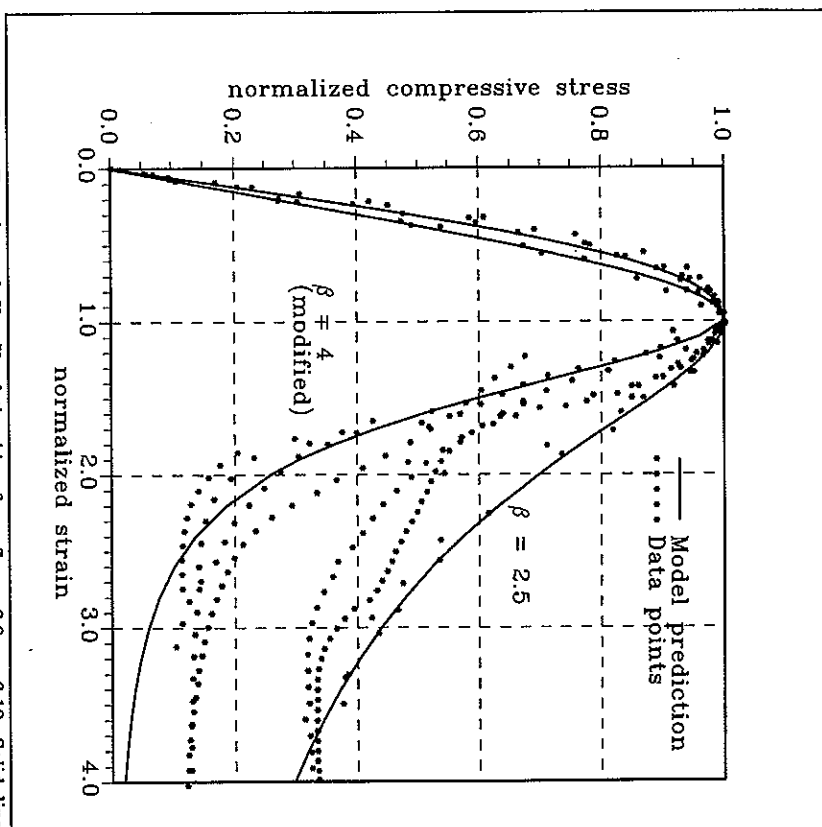


Figure 3.15: - Experimental  $Y - X$  relationships from figure 3.9 and 3.10. Solid lines represent model predictions given by eq. (3.5).

If instead the parameter  $\beta$  is determined from the initial modulus of elasticity and the peak point as stated in eq. (3.6), the experimental values fall within the interval  $2 < \beta < 4.5$ , which agrees satisfactorily with the range given in figure 3.15.

A comparison with the proposals in Ezeildin & Balaguru (1992), which are shown in figure 3.2, indicates that compressive matrix follows the same normalized stress - strain curves as reported for other FRC materials. However, the peak point is significantly altered by the fibres, which is not the case for most FRC investigations.

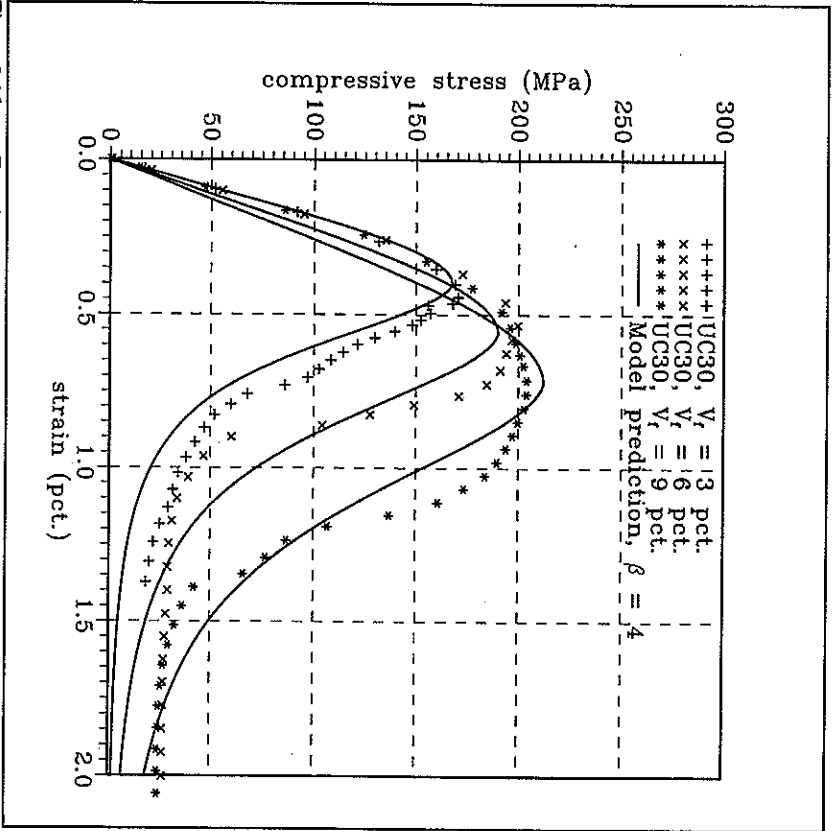


Figure 3.16: Experimental stress-strain relationships taken from figure 3.9. Model predictions given by eq. (3.5).

Finally figure 3.16 and 3.17 contain stress - strain curves together with the model prediction.

It is noted, that the peak points are not actually taken from the test data, but estimated from eq. (3.10), corresponding to the actual fibre reinforcement index. It seems possible to predict the shape of the complete stress - strain curves satisfactory, by means of the simple one-parameter expression in eq. (3.5) together with the peak stress and strain.

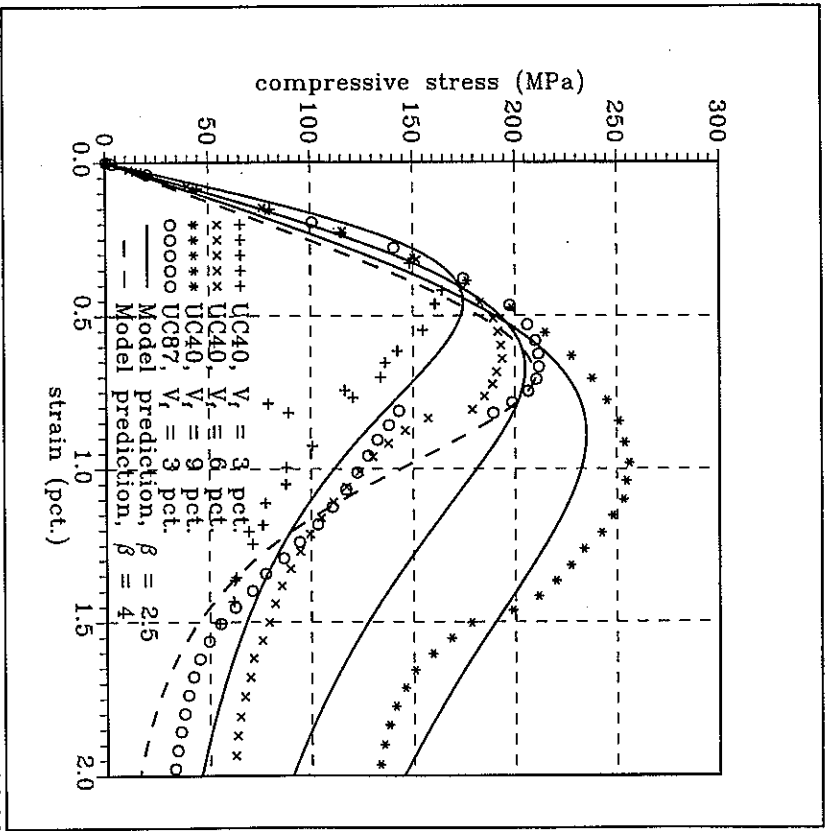


Figure 3.17: Experimental stress - strain relationships taken from figure 3.10. Model predictions given by eq. (3.5).

### 3.3 Concluding remarks

There exists only a very limited number of theoretical models to predict the shape of the compressive stress - strain relationship for concrete. The number of factors influencing this curve is numerous:

- The curing conditions.



- Whether the specimens are cylindrical or cubes.
- The presence of intermediary layers to minimize friction.

Beside these parameters, that influence the behaviour, there exist the question, whether the deformations registered after the occurrence of localized cracks, should be interpreted as overall strains. It is well-known, that the deformations after peak are concentrated in narrow crack zones and therefore the overall strains depend on the specimen height.

In Section 3.1.2 a model based on fracture mechanics is presented, utilizing the fact, that brittle materials develop splitting cracks parallel with the compressive load. The criterion for crack growth is a critical stress intensity factor and the effect of fibres is included by taking the bridging stresses from fibres crossing a crack into account. The model is very complicated and not yet ready for practical use. However, its qualitative description of the behaviour of FRC under compression seems to be good.

The empirical models, which describe the stress - strain curve by means of mathematical expressions, are widely used. It is obvious, that the accuracy of the models increase with the number of parameters. Practically every model ends up in describing the stress - strain relationship solely as a function of the compressive strength.

For FRC the presence of fibres increases the area under the stress - strain curve considerably. The investigations indicate, that when steel fibres are added to HSC the shape of the stress - strain curve tend to be similar to the curves for NSC (in a normalized stress diagram), i.e. the steepness of the descending branch is decreased. However, the question whether it is possible to add fibres until the descending branch gets almost horizontal is not answered. Both Fanelia & Naaman (1985) and Ezzeldin & Balaguru (1992) find, that the specimens reinforced with moderate amounts of fibres still carry 80 % of their capacity, when the strains exceed 3 times the value at peak stress.

Composit matrix is a ultra high-strength matrix with  $f_c > 140$  MPa and the compression tests do not indicate, that the descending branch is altered significantly when the fibre content is varied between 3 and 9 % by volume. However, the presence of fibres influences the compressive stress - strain curve to show a shape similar to that observed from NSC. Thus, the brittleness of the high-strength matrix is effectively reduced by the fibres. This is also supported by the fact, that plain compressit cylinders without fibres showed very explosive failures, while the fibres ensured, that the cylinder kept its coherency after the peak load.

Furthermore the steel fibres affect the strength and the strain capacities considerably and not only marginally. The increase in strength from the fibres is directly related to the post-cracking tensile strength, observed in the previous chapter, by considering the fibres as confinement.

### 3.4 References

- Al-Shunaber, I. (1989) *Statusrapport, Effekten på Densit of Væretende Indhold af Metafibre*, in Danish, Preliminary Report, The Cement and Concrete Laboratory, Aalborg Portland A/S, 14 pp.
- Carreira, D.J. & K.-H. Chu (1985), 'Stress - Strain Relationship for Plain Concrete in Compression', *ACI Journal*, Vol. 82, pp. 797-804.
- Chen, W.-F. & J.L. Carson (1971), 'Stress - Strain Properties of Random Wire Reinforced Concrete', *ACI Journal*, Vol. 68, pp. 933-936.
- Dahl, H. & R. Brincker (1989), 'Fracture Energy of High-Strength Concrete in Compression', in *Fracture of Concrete and Rock, Recent Developments* (Eds. S.P. Shah, S.E. Swartz & B. Bar), Elsevier Applied Science, pp. 523-536.
- Dahl, K.K.B. (1992), *Uniaxial Stress - Strain Curves for Normal and High Strength Concrete*, Serie R, No. 282, Department of Structural Engineering, Technical University of Denmark, Lyngby, 96 pp.
- Eggington, J. & D.J. Hannant (1972), 'Steel Fibre Reinforced Concrete. The Effect on Fibre Orientation of Compaction by Vibration', *Materials and Structures*, RILEM, Vol. 5, No. 25, pp. 41-44.
- Exner, H. (1983), *Plasticitæsteori for Coulomb Materialer*, in Danish, Ph.D.-thesis, Serie R, No. 175, Department of Structural Engineering, Technical University of Denmark, Lyngby, 258 pp.
- Ezzeldin, A.S. & P.N. Balaguru (1992), 'Normal- and High-Strength Fiber-Reinforced Concrete under Compression', *Journal of Materials in Civil Engineering*, ASCE, Vol. 4, No. 4, pp. 415-429.
- Fanelia, D.A. & A.E. Naaman (1985), 'Stress - Strain Properties of Fiber Reinforced Mortar in Compression', *ACI Journal*, Vol. 82, pp. 475-483.
- Glavind, M. (1992), *Evaluation of the Compressive Behaviour of Fiber Reinforced High Strength Concrete*, Ph.D.-thesis, Serie R, No. 302, Department of Structural Engineering, Technical University of Denmark, Lyngby, 144 pp.
- Hansen, A.S. (1983), *Undersøgelse af de Mekaniske Egenskaber for Stålfiberarmet DENST*, in Danish, M.Sc.-thesis, Department of Civil Engineering, Building Materials Laboratory, Technical University of Denmark, Lyngby, 59 pp.

### 3. Uniaxial compressive behaviour

- Hughes, B.P. & N.I. Fatuhi (1977), 'Stress - Strain Curves for Fibre Reinforced Concrete in Compression', *Cement and Concrete Research*, Vol. 7, pp. 173-184.
- Nielsen, M.P. (1984), *Limit Analysis and Concrete Plasticity*, Prentice-Hall Inc., Englewood Cliffs, New Jersey, xii + 420 pp.
- Olsen, N.H. (1990), *Design Proposal for High Strength Concrete Sections Subjected to Flexural and Axial Loads*, Part of Ph.D. thesis, Serie R, No. 233, Department of Structural Engineering, Technical University of Denmark, Lyngby, 91 pp.
- Sargin, M. (1971), *Stress - Strain Relationships for Concrete and the Analysis of Structural Concrete Sections*, Study No. 4, Solid Mechanics Division, University of Waterloo, Canada, xxvi + 167 pp.
- Shah, S.P., P. Stroeven, D. Daluisen & P. Van Stekelenburg (1978), 'Complete Stress - Strain Curves for Steel Fibre Reinforced Concrete in Uniaxial Tension and Compression', in *Testing and Test Methods of Fibre Cement Composites*, The Construction Press, Lancaster, pp. 399-408.
- Tomaszewicz, A. (1986), Discussion on paper by Carreira & Chu (1985), *ACI Journal*, Vol. 83, pp. 872-873.
- Wang, P.T., S.P. Shah & A.E. Naaman (1978), 'Stress - Strain Curves of Normal and Lightweight Concrete in Compression', *ACI Journal*, Vol. 75, pp. 603-611.

### 4. Multiaxial behaviour

Even though the uniaxial compressive strength of concrete is recognized to be the most important material property, the multiaxial strength is also extensively investigated. It is well-known, that concrete structures show an increasing compressive capacity, when a certain confinement is provided. For fibre reinforced concrete the fibres act as confinement across the cracks and therefore it is possible, that the findings from normal concrete are applicable to FRC.

Throughout this chapter it is assumed that *compressive concrete stresses are positive* and furthermore the principal stresses are arranged so that  $\sigma_1 \geq \sigma_2 \geq \sigma_3$ .

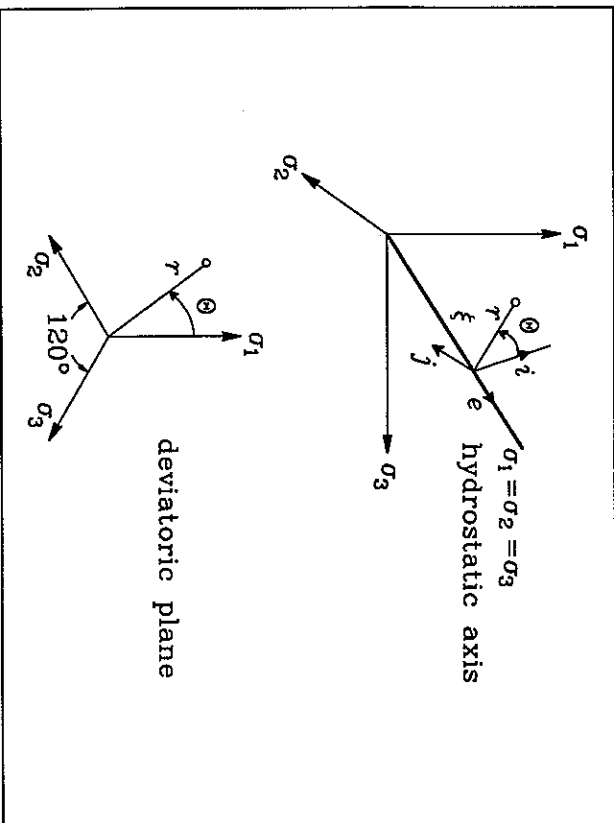


Figure 4.1: Principal stress coordinate system and deviatoric stress plane.

## 4.1 Review on concrete and FRC under multiaxial stresses

### 4.1.1 Continuum mechanics

Before considering the special characteristics for concrete tested under multiaxial stress states we give some important definitions. The stresses are formulated in the so-called *octahedral components* and the constitutive relations for a *linear-elastic isotropic material* are provided.

**State of stress.** The state of stress in an isotropic material is uniquely described by the *principal stresses*  $\sigma_1, \sigma_2$  and  $\sigma_3$ . In figure 4.1 each stress state is defined as a point in an orthogonal  $\sigma_1, \sigma_2, \sigma_3$  - coordinate system. The stress state is given by a vector, containing the 3 principal stresses and it can be divided into a hydrostatic and a deviatoric part:

$$\sigma = \xi e + r(i \cos\theta + j \sin\theta) \quad (4.1)$$

where  $e, i$  and  $j$  are unit length vectors, forming an orthogonal coordinate system with  $e$  along the hydrostatic axis ( $\sigma_1 = \sigma_2 = \sigma_3$ ) and  $i$  and  $j$  lying in the deviatoric plane, see figure 4.1.

The hydrostatic part of the stresses are determined by the parameter  $\xi$ , which can be both positive and negative, and the deviatoric part by the distance  $r$  and the angle  $\theta$  with  $i$ . The relations between the two stress descriptions are formulated as

$$\begin{bmatrix} \sigma_1 \\ \sigma_2 \\ \sigma_3 \end{bmatrix} = \frac{1}{\sqrt{6}} \begin{bmatrix} \sqrt{2} & 2 & 0 \\ \sqrt{2} & -1 & \sqrt{3} \\ \sqrt{2} & -1 & -\sqrt{3} \end{bmatrix} \begin{bmatrix} \xi \\ r \cos\theta \\ r \sin\theta \end{bmatrix} \Leftrightarrow \begin{bmatrix} \xi \\ r \cos\theta \\ r \sin\theta \end{bmatrix} = \frac{1}{6} \begin{bmatrix} 2\sqrt{3} & 2\sqrt{3} & 2\sqrt{3} \\ 2\sqrt{6} & -\sqrt{6} & -\sqrt{6} \\ 0 & 3\sqrt{2} & -3\sqrt{2} \end{bmatrix} \begin{bmatrix} \sigma_1 \\ \sigma_2 \\ \sigma_3 \end{bmatrix} \quad (4.2)$$

Another notation that is often applied is the so-called *octahedral stresses*  $\sigma_0$  and  $\tau_0$ , or the *stress invariants*  $I_1$  and  $J_2$ , defined by the following equations.

$$\begin{aligned} \sigma_0 &= \frac{\sigma_1 + \sigma_2 + \sigma_3}{3} = \frac{\xi}{\sqrt{3}} \\ \tau_0 &= \frac{\sqrt{(\sigma_1 - \sigma_2)^2 + (\sigma_2 - \sigma_3)^2 + (\sigma_3 - \sigma_1)^2}}{3} = \frac{r}{\sqrt{3}} \\ \sin\theta &= \frac{\sigma_2 - \sigma_3}{\sqrt{2}r} \end{aligned} \quad (4.3)$$

$$I_1 = 3\sigma_0 = \sqrt{3}\xi, \quad J_2 = \frac{3\tau_0^2}{2} = \frac{r^2}{2} \quad (4.4)$$

Thus, each stress state is completely determined by the principal stresses, by the octahedral stresses, or by the stress invariants and the deviatoric angle  $\theta$ .

Finally it is recalled, that the principal stresses are determined from an arbitrary stress tensor  $\sigma_{ij}$  by solving the roots of the third-order polynomial:

$$\det(\sigma_{ij} - \sigma \delta_{ij}) = 0, \quad i, j = 1, 2, 3 \quad (4.5)$$

where  $\delta_{ij}$  is the so-called Kronecker delta, defined by

$$\delta_{ij} = \begin{cases} 1, & i = j \\ 0, & i \neq j \end{cases} \quad (4.6)$$

**Constitutive relations for an isotropic linear-elastic material.** The constitutive relations connect the stresses and the strains of a material, i.e. they describe the stiffness. Here we consider the simplest case, where the material generates its original form after each loading. The relations do not include any time dependence such as creep and shrinkage and the material properties are independent of the direction considered.

For this type of material only 2 material constants are necessary to determine the relations between  $\sigma_{ij}$  and  $\epsilon_{ij}$  ( $i, j = 1, 2, 3$ ). Hooke's law applies the *modulus of elasticity*  $E$  and the *Poisson ratio*  $\nu$  as material constants. The general form of the constitutive relations is written as

$$\sigma_{ij} = \frac{E}{1+\nu} \left( \epsilon_{ij} + \frac{\nu}{1-2\nu} \epsilon_{kk} \delta_{ij} \right) \Leftrightarrow E \epsilon_{ij} = (1+\nu) \sigma_{ij} - \nu \sigma_{kk} \delta_{ij} \quad (4.7)$$

where the *summation convention* is applied.

If the stresses and the strains are divided into their hydrostatic and deviatoric parts, as explained in the previous section, the constitutive relations are simplified significantly because these 2 parts are totally uncoupled:

$$\sigma_0 = 3K\epsilon_0, \quad \tau_0 = 2G\gamma_0 \quad (4.8)$$

where  $\sigma_0$  and  $\tau_0$  are the octahedral stresses defined by eq. (4.3), and  $\epsilon_0$  and  $\gamma_0$  are the corresponding octahedral strains defined similarly. The *bulk modulus*  $K$  and the *shear modulus*  $G$  are related to  $E$  and  $\nu$  by

$$K = \frac{E}{3(1-2\nu)}, \quad G = \frac{E}{2(1+\nu)} \quad (4.9)$$

The first relation in eq. (4.8) expresses the change in volume from a hydrostatic pressure, while the second relation concerns the distortion of a volume element.

4.1.2 Failure criteria applied to concrete

The typical way of formulating a failure criterion is to consider a *failure surface* in the  $\sigma_1, \sigma_2, \sigma_3$  - coordinate system:

$$f(\sigma_1, \sigma_2, \sigma_3) = f(\xi, r, \theta) = f(I_1, I_2, \theta) = 0 \quad (4.10)$$

When this condition is met by a stress state, the material fails, otherwise  $f < 0$  and the stress state is safe. In Dahl (1990) an extensive review on existing failure criteria is given, see also Chen (1982), pp. 201-250. The main characteristics of the failure surface are the following

- It is periodic in the deviatoric stress plane with a period of 60°, corresponding to the 6 combinations of the principal stresses.
- It is convex and of course the stress free state is contained in the safe region.
- It is open ended, so that pure hydrostatic compression cannot cause failure, but it is closed in the tensile region.

The deviatoric stress plane contains 6 different regions, corresponding to the different combinations of the three principal stresses. Here we only consider the region  $0 \leq \theta \leq 60^\circ$ , corresponding to  $\sigma_1 \geq \sigma_2 \geq \sigma_3$ , see figure 4.1.

Most failure surfaces are described in terms of the octahedral stresses, because it gives the simplest description of the complex criteria. Thus, the description is divided into an analytical model of the meridians, i.e. the dependence between  $r$  and  $\xi$ , and a model of the shape of the surface in the deviatoric plane, i.e. the  $r - \theta$  dependence.

Like it appears from the following various investigators have proposed failure criteria of increasing complexity in order to match the experimental results. In table 4.1 a survey of some of the most important criteria for concrete is given, see the expressions in Dahl (1990).

The most simple criterion is the *Rankine criterion*, which states that failure only occurs, when the tensile strength of the material is exceeded, i.e. a separation failure. The only parameter necessary to determine this criterion is the tensile strength  $f_t$  and therefore the model is termed a *one-parameter model*. The Rankine criterion makes a pyramid in a  $\sigma_1, \sigma_2, \sigma_3$  - system with its 3 sides being perpendicular to the axes and with its top at  $\sigma_1 = \sigma_2 = \sigma_3 = -f_t$ .

Criterion	No. of parameters	Meridian	Deviatoric plane	Physical properties needed
Rankine	1	Straight	Straight	$f_t$
Coulomb	2	Straight	Straight	$f_c, \phi$
William-Warke	3	Straight	Elliptical	$f_c, f_t, f_{tcr}$
Ottosen	4	Parabolic	Membrane analogy	$f_c, f_t, f_{tcr}$ and an arbitrary point

Table 4.1: Survey of typical failure criteria for concrete.

The *Coulomb criterion* assumes, that failure is governed by frictional resistance. This model is described separately later in this section, because it is often applied to concrete, especially in connection with the *theory of plasticity* for reinforced concrete structures.

The so-called *William-Warke criterion* is a *three-parameter model*, where the deviatoric curve is a quarter of an ellipse. This elliptical curve is determined by means of two parameters and the third parameter determines the slope of the straight meridians.

Finally the most advanced criterion to be used in practice is included, which is the *four parameter Ottosen criterion*. The meridians are parabolic, which demands two parameters, and the deviatoric curve is determined by solving the problem of a *membrane*, simply supported along the 3 sides of an equilateral triangle and subjected to uniform pressure. The solution is rather complicated, see e.g. Dahl (1990) or Ottosen (1977). It is noted that the Ottosen criterion forms the basis for the failure criterion proposed by the CEB.

**Modified Coulomb criterion.** The most common failure criterion applied to concrete is the *Coulomb friction hypothesis*, which states that failure occurs, when the shear stress at a section exceeds a cohesive and a frictional resistance:

$$|\tau| = c + \sigma \tan \phi \quad (4.11)$$

where  $c$  is the *cohesion* and  $\phi$  is the *angle of friction*. This expression appears as a straight line inclined the angle  $\phi$  to the  $\sigma$ -axis in a Mohr diagram. The Coulomb criterion can be expressed in terms of the principal stresses, which yields

<sup>1</sup>Comité Euro-International du Béton.

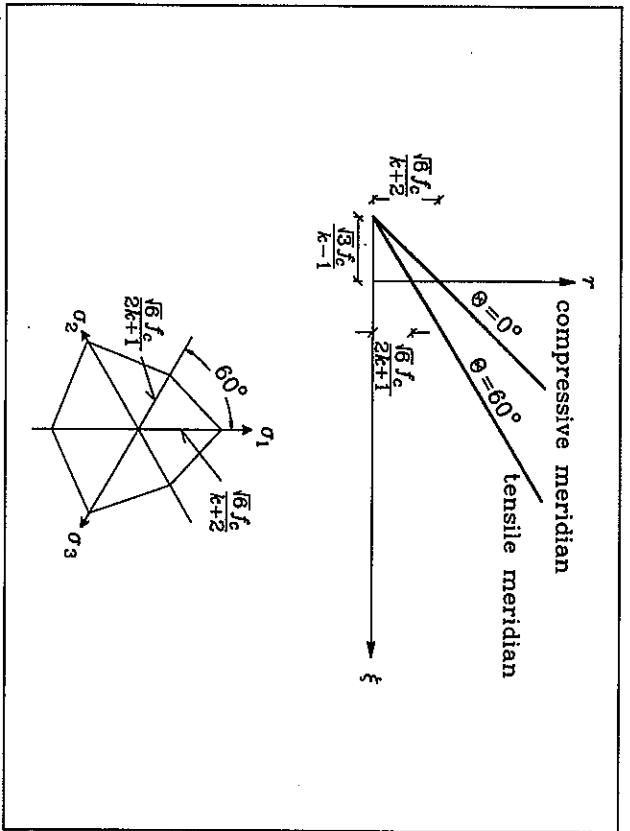


Figure 4.2: Failure surface for Coulomb material. The  $\xi$ -axis is the hydrostatic axis and  $r$  is the distance in the deviatoric plane.

$$f(\sigma_1, \sigma_2, \sigma_3) = \sigma_1 - (k\sigma_2 + f) = 0, \quad \sigma_1 \geq \sigma_2 \geq \sigma_3 \quad (4.12)$$

where the parameter  $k$  depends solely on the angle of friction:

$$k = \frac{1 + \sin\phi}{1 - \sin\phi} \quad (4.13)$$

Expressing the Coulomb criterion in terms of the octahedral stresses we get the following equation by substituting  $\sigma_1$  and  $\sigma_3$  by means of eq. (4.2):

$$f(\xi, r, \theta) = -\sqrt{2}(k-1)\xi + ((k+2)\cos\theta + \sqrt{3}\sin\theta)r - \sqrt{6}f_c = 0, \quad 0^\circ \leq \theta \leq 60^\circ \quad (4.14)$$

In figure 4.2 this failure surface is depicted by means of the straight meridians at  $\theta$  equal to  $0$  and  $60^\circ$  together with the deviatoric plane for  $\xi = 0$ .

However, it is generally accepted, that concrete materials do not fail by means of friction

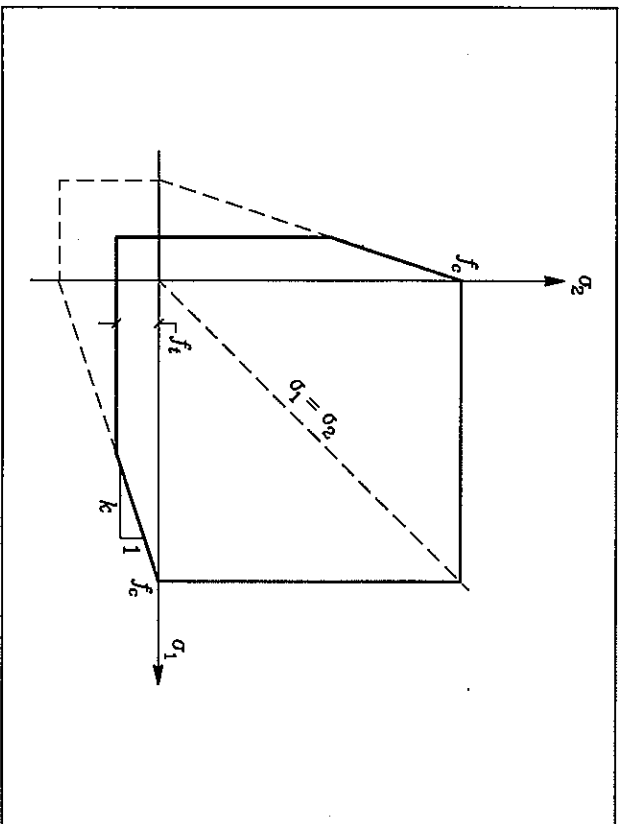


Figure 4.3: Modified Coulomb failure criterion for plane stress condition. The dashed lines represent the Coulomb criterion without tension cut-off at  $\sigma_3 = -f_r$ .

under high tensile stresses. Therefore a so-called *tension cut-off* is applied to the Coulomb criterion, resulting in the *modified Coulomb criterion*. This modification consists of the Rankine failure criterion, i.e. a separation failure, when the tensile strength  $f_t$  of the material is exceeded. Thus,  $\sigma_3$  should not exceed the uniaxial tensile strength:

$$f(\sigma_1, \sigma_2, \sigma_3) = -(\sigma_3 + f) = 0, \quad \sigma_1 \geq \sigma_2 \geq \sigma_3 \quad (4.15)$$

$$\dagger f(\xi, r, \theta) = -\sqrt{2}\xi + (\cos\theta + \sqrt{3}\sin\theta)r - \sqrt{6}f_c = 0, \quad 0^\circ \leq \theta \leq 60^\circ$$

The condition for a tensile sliding failure region instead of a separation failure is  $f_c/f_t \leq k$ , which is not interesting for practical considerations of concrete.

In figure 4.3 the modified Coulomb criterion is depicted for the special case of *plane stress*, i.e. the trace of the failure surface at the plane  $\sigma_3 = 0$ . From eq. (4.12) it appears that the intermediate principal stress  $\sigma_2$  does not influence the failure criterion, which seems to be a rough assumption, but nevertheless the criterion shows the necessary accuracy for most practical purposes. In the biaxial plane of figure 4.3 the independence of the intermediate principal stress causes the biaxial compressive strength to equal the uniaxial strength under

all conditions. In the next section this property is investigated further.

For further description of the modified Coulomb failure criterion the reader is referred to *Neilson (1984)*, pp. 15-35, which contains an extensive treatment of the theory of plasticity applied to concrete, utilizing the modified Coulomb criterion.

#### 4.1.3 Multiaxial strength of concrete

In order to determine the characteristics of concrete subjected to multiaxial stresses many attempts exist to establish a well-defined state of stress in experiments. This is mainly done by using one of the following techniques, see e.g. *Dahl (1990)*:

- Loading cubes in 2 or 3 orthogonal directions, ensuring that the friction between load plates and specimen is minimized.
- Loading cylinders vertically together with an external fluid pressure on the specimen sides.
- Loading hollow cylinders (tubes) vertically together with internal/external pressure or torsion.

It is generally known that the problems concerning *boundary constraints* are significant, see e.g. *Van Mier & Vank (1991)*. Both the strength and in particular the post-peak behaviour are sensitive to the method of eliminating boundary friction. Many laboratories utilize *steel brushes* on their load plates in order to obtain free deformations perpendicular to the load direction. Tests involving *fluid pressure* do not have these problems, because there is no mechanical contact. However, it is necessary to prevent the fluid to enter the permeable concrete specimens, by covering them with rubber membranes.

Also the load path causes problems, because it is uncertain whether the order in which the different stresses are applied has any influence. The most important *load paths* are

- Separated hydrostatic and deviatoric loading. First the hydrostatic pressure ( $\sigma_1 = \sigma_2 = \sigma_3$ ) is increased until a specified level. Then the stresses are varied within the deviatoric plane corresponding to a prescribed value of  $\theta$ , cf. figure 4.1.
- Triaxial loading. First the hydrostatic pressure is increased until a specified level. Then one of the principal stresses is either increased or decreased until failure.
- Proportional loading, where the ratios between the principal stresses are kept constant throughout the test until failure.

*Dahl (1990)* concludes, that no clear indication exists, whether any of the load paths is preferable, when the ultimate strength is considered. *Kotsovos (1979a)* states that the load path

influences the early stages of cracking inside the specimens, but not the ultimate stages.

The most popular load path is the triaxial *compressive meridian*, which corresponds to  $\theta = 0^\circ$  in figure 4.1. After the specified hydrostatic level is obtained the principal stress  $\sigma_1$  is increased further, i.e. uniaxial compressive stress imposed to a hydrostatic pressure ( $\sigma_1 \geq \sigma_2 = \sigma_3$ ). Analogous to this is the *tensile meridian*, which corresponds to uniaxial tension imposed to a hydrostatic pressure, i.e.  $\theta = 60^\circ$  or  $\sigma_1 = \sigma_2 \geq \sigma_3$ .

Besides the review given in *Dahl (1990)* an extensive evaluation of numerous investigations is provided in *Wastels (1979)*, including 91 references. Also *Hannant (1974)* includes a great collection of strength results and presents them in both biaxial and triaxial diagrams.

**Biaxial strength of concrete.** A classic test series, investigating the biaxial strength of concrete at the University of Munich is reported in *Kupfer et al. (1969)*. The investigation of biaxial strengths of  $200 \times 200 \times 50$  mm concrete discs with 3 different concrete strengths (20, 30 and 60 MPa) is reported, including 4 different biaxial stress ratios within each of the regions compression - compression, compression - tension and tension - tension. Load plates with steel brushes are utilized in order to minimize friction. The use of steel brushes is originally developed by H.K. Hilsdorf in connection to this test series.

*Kupfer et al.* report a maximum *compressive biaxial strength* of approximately  $1.3f_c$ , when the stress ratio is  $\sigma_2/\sigma_1 = 0.5$ . The stresses are normalized with respect to the uniaxial compressive strength  $f_c$ , i.e. the strength observed at  $\sigma_2/\sigma_1 = 0$ . The biaxial strength  $f_{br}$  at  $\sigma_2/\sigma_1 = 1$  is approximately  $1.15f_c$ . Finally the effect of steel brushes is investigated, resulting in a considerably strength increase, when dry load plates are used instead of brushes.

Throughout the seventies biaxial tests have been performed at the Cornell University. Several tests on  $127 \times 127 \times 13$  mm specimens are executed, using steel brush plates. *Liu et al. (1972)* report results in the compression - compression region and later on *Tasayfi et al. (1979)* include the remaining tensile regions. Based on their ultimate biaxial strength results a *failure surface* is proposed, which also match satisfactory with the results in *Kupfer et al. (1969)*. In figure 4.4 this proposal, which consists of straight lines, is given.

The figure also includes the *biaxial design proposal* suggested by *Hannant (1974)*, which is based on most test results available up to 1973. Like it is meant to be this failure criterion seems to be on the safe side.

The test series reported in *Neilson (1972)* includes a total of 22 stress ratios covering all biaxial regions. The specimens have the dimensions  $177 \times 177 \times 126$  mm and are loaded by brush plates. From the results a parabolic envelope in the compression - compression region is proposed, but also a simple bi-linear expression is given. In figure 4.4 this bi-linear suggestion is inserted.

In *Gerstle et al. (1978)* a co-operative test programme, where identical concrete and mortar

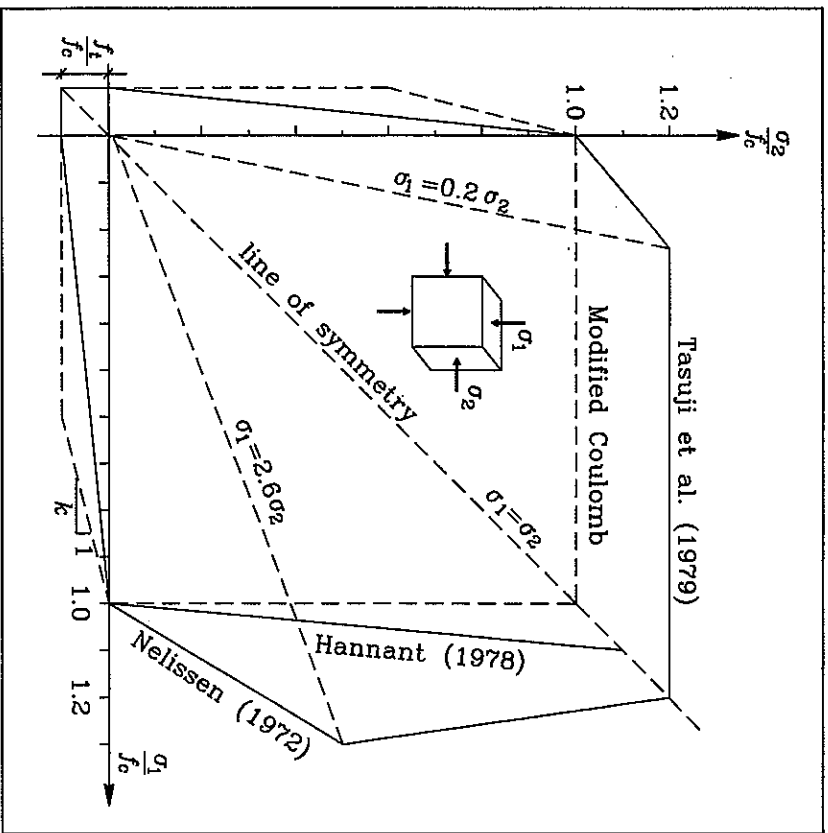


Figure 4.4: Proposals of the biaxial strength of concrete. The dashed lines symbolize the modified Coulomb criterion.

mixes are tested under multiaxial stresses at 7 laboratories all over the world, is presented. The various laboratories have different test methods, different equipment and different specimens, but the specimens are cast and cured identically.

The biaxial tests are all performed in the compression - compression region and show great scatter between the various laboratories. The biaxial strength normalized with respect to the uniaxial strength varies from approximately 1 to more than 2. The highest strengths correspond to the highest degree of friction between load plates and test specimen. If the results with constrained boundary conditions are neglected the results agree very well with

figure 4.4.

Kotsovos (1979b) proposes a failure criterion, where the 3-parameter William-Wanke criterion is modified. Instead of using linear meridians Kotsovos fits the meridian to experimental results obtained at the Imperial College in London in connection to the co-operative project. As it is expected the model seems to predict the biaxial strength envelope satisfactory, but still the experimental scatter is rather high to prefer this relatively complex criterion instead of those suggested in figure 4.4.

From figure 4.4 it is evident that even though there are differences in test results, most investigators agree, that the compressive biaxial strength is 10 to 30 % higher than the uniaxial strength. Furthermore it is recommended, that the boundary constraints are minimized in order to obtain comparative results. In the tension - tension region the biaxial strength is constantly equal to the direct tensile strength of concrete (often taken as 5 % of the compressive strength). Finally the compression - tension region is typically modelled by a straight line from the uniaxial tensile strength to the uniaxial compressive strength, which also agrees satisfactory with the modified Coulomb criterion. In the compression - compression region however, the Coulomb criterion is on the safe side, modelling the biaxial strength equal to the uniaxial strength.

**Triaxial strength of concrete.** Most of the triaxial tests performed on concrete concern multiaxial compression with all principal stresses higher than zero. In Dahl (1990) the most important test series with NSC (strengths ranging from 10 to 60 MPa) are included with the triaxial strengths tabulated.

It is generally accepted, that NSC is satisfactorily described by the modified Coulomb criterion given in eq. (4.12), see e.g. Nielsen (1984), pp. 24-29. In the compressive region the major principle stress  $\sigma_1$ , depicted as a function of the minor stress  $\sigma_2$ , forms a straight line with slope  $k = (1 + \sin\varphi)/(1 - \sin\varphi)$ , where  $\varphi$  is the angle of friction. For NSC it is found, that  $k = 4$ , which corresponds to  $\tan\varphi = 0.75$  and  $\varphi = 37^\circ$ , agrees very well with the test results.

As it appears from eq. (4.12) the modified Coulomb criterion is independent of the intermediate principle stress  $\sigma_2$ . Thus, the results obtained from triaxial tests along the compressive meridian ( $\theta = 0^\circ$ ) and the tensile meridian ( $\theta = 60^\circ$ ) should be equal in a  $\sigma_1 - \sigma_3$  system. Figure 4.5 contains results obtained both along the compressive and the tensile meridian.

The figure includes results from the classic investigation by Richart, Brandtzeig & Brown (1928), using  $\phi 100 \times 200$  mm cylinders subjected to hydraulic oil pressure on the sides together with a vertical load. The compressive meridian is obtained by first increasing the hydrostatic pressure followed by increasing the vertical load until failure. For the tensile meridian the vertical load is raised to a prescribed level, followed by an increasing oil pressure until failure. Two different uniaxial strengths are included ( $f_c = 18$  and 25 MPa).

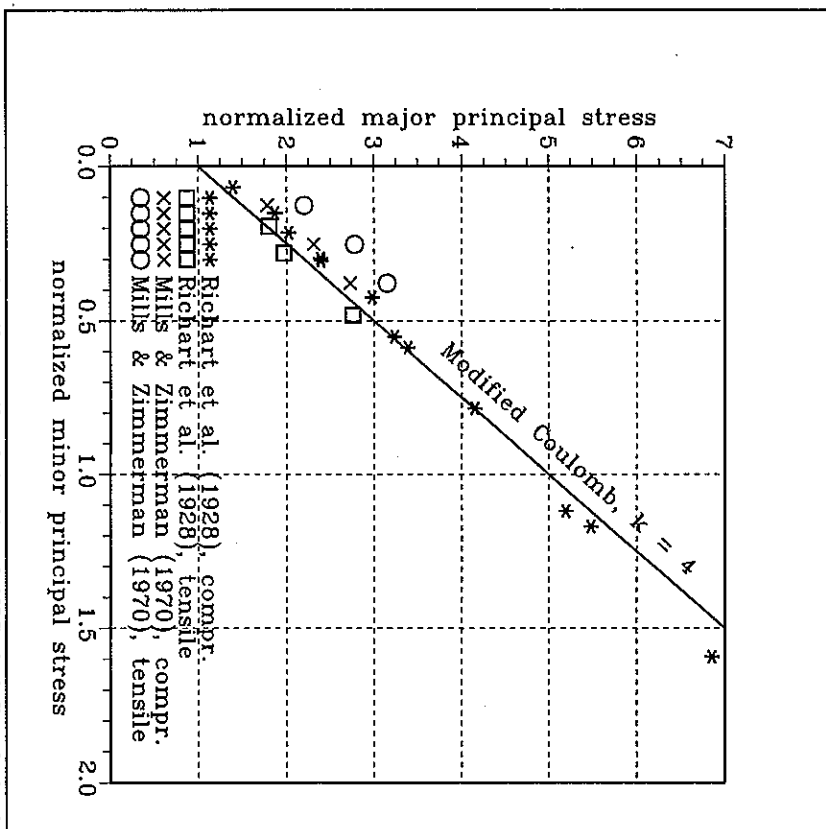


Figure 4.5: Experimental  $\sigma_1/f_c - \sigma_2/f_c$  relationship of NSC, including both the compressive and the tensile meridian.

In Mills & Zimmerman (1970) compressive loads are applied to 57 mm concrete cubes with a uniaxial strength of 23 MPa. From figure 4.5 it appears, that the 3 points on the tensile meridian is slightly higher than the remaining points, but for practical use the dependence of the intermediate principal stress is assumed to be negligible.

In the co-operative project reported in Gerstle *et al.* (1978) no specific proposal for the failure criterion is given. Of course the results from various laboratories differ considerably, but again it is noted, that the deformational constraints on the specimens should be minimized. All the tests are performed by increasing the hydrostatic pressure to a given level and then increasing

the deviatoric stress alone, following one of three stress paths ( $\theta = 0, 30$  or  $60^\circ$  in figure 4.1). The test results are given in terms of the octahedral stresses  $\sigma_0$  and  $\tau_0$ . It is recalled that the modified Coulomb criterion results in linear  $\tau_0 - \sigma_0$  relationships dependent on the angle  $\theta$ . For  $k = 4$  the compressive, the shear and the tensile meridian are calculated from eq. (4.14):

$$\frac{\tau_0}{f_c} = \begin{cases} 0.236 + 0.707 \frac{\sigma_0}{f_c}, & \theta = 0^\circ \\ 0.163 + 0.490 \frac{\sigma_0}{f_c}, & \theta = 30^\circ \\ 0.157 + 0.471 \frac{\sigma_0}{f_c}, & \theta = 60^\circ \end{cases} \quad k = 4 \quad (4.16)$$

If these expressions are compared to the graphical representation of the test data from the 3 stress paths in Gerstle *et al.* (1978) a satisfactory agreement is found, when the experimental scatter is taken into account.

The number of tests covering the *tensile regions* of the triaxial stress combinations are limited, partly because of the difficulties and experimental scatter normally connected with tensile testing and partly because the tensile strength of concrete is often neglected. However, like in the case of biaxial tests the modified Coulomb failure criterion with its tension cut-off seems to be in agreement with the experimental results.

**Application of failure criterion to HSC.** By an extensive experimental programme at the Department of Structural Engineering at Technical University of Denmark, Dahl (1992a) investigates the failure criterion for HSC. The uniaxial strength range from 10 to 110 MPa and the tests are performed in a *triaxial cell* with oil pressure on the sides of  $\phi 100 \times 200$  mm cylinders. The test method is further described in Section 4.2 and Appendix 3. It is noted that all tests are performed along the *compressive meridian*.

Dahl (1992a) concludes, that the four-parameter *Otosen failure surface*, see e.g. Otosen (1977), correlates well with the triaxial test results of HSC up to  $f_c = 100$  MPa and he performs an empirical fitting of the four parameters. However, Dahl also admits that this model is rather complicated in practice and therefore he suggests a criterion based on the modified Coulomb criterion. A bi-linear curve is proposed in the compressive  $\sigma_1 - \sigma_2$  diagram instead of a single the straight line with slope  $k = 4$ . In figure 4.6 this proposal is shown together with test results from both NSC and HSC. For minor principal stresses up to  $0.5f_c$  the slope  $k = 4$  is applied and thereafter the slope decreases to 3.

In Lahlou *et al.* (1992) HSC with  $f_c$  between 50 and 115 MPa is investigated by means of a triaxial cell similar to that in Dahl (1992a). The triaxial strengths along the compressive meridian are determined on  $\phi 100 \times 200$  mm cylinders and furthermore  $\phi 54 \times 118$  mm



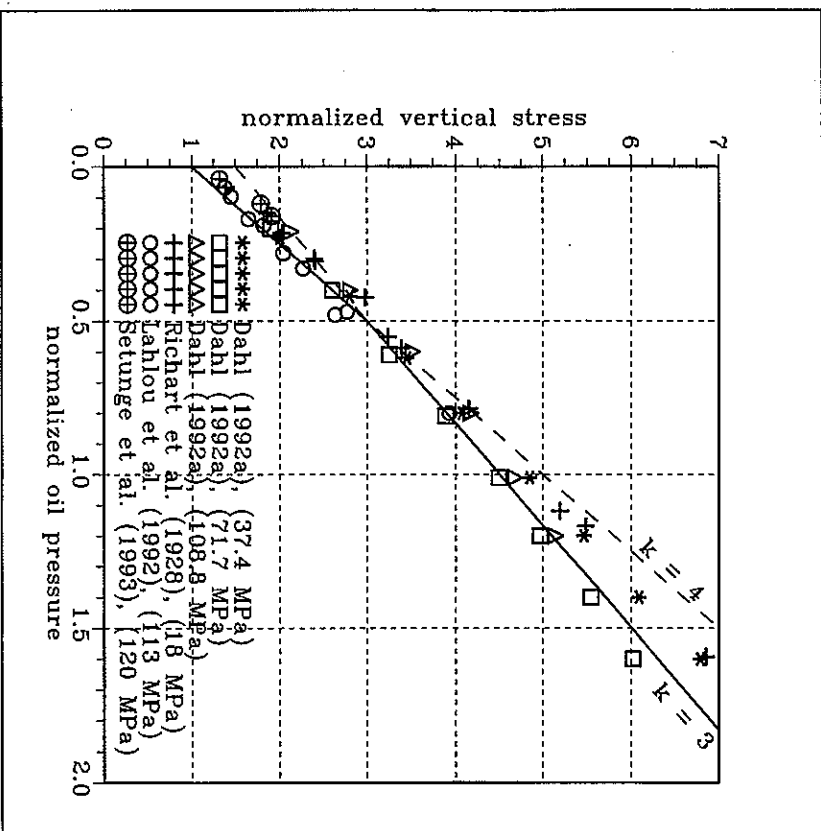


Figure 4.6: The so-called two-stage model of the failure criterion for HSC suggested by Dahl (1992a) in a  $\sigma_1/f_c - \sigma_2/f_c$  coordinate system. The brackets give  $f_c$  by cylinders confined by steel tubes of varying thickness are tested. The concrete mixes have water to binder ratios of 0.23 to 0.5 and the 115 MPa mix contains silica fume. The steel tube confinement, determined by assuming yielding of the steel, correlates well with the corresponding oil pressures. In figure 4.6 the test results from Lahlou et al. (1992) are included and it is observed, that they correspond to the two-stage model for oil pressures below  $0.5f_c$ .

Finally figure 4.6 also includes test results from Setunge et al. (1993). The compressive strength range from 90 to 130 MPa and the triaxial strengths are obtained in a triaxial cell on  $\phi 100 \times 200$  mm cylinder under low confinement stresses. The concrete mixes have water to

binder ratio of 0.26 to 0.35 and include silica fume. The investigation includes the effect of varying aggregate types, but no significant effect is observed.

The data of figure 4.6 is further treated in Section 4.2 in connection with the triaxial test results on compressive matrix.

#### 4.1.4 Multiaxial constitutive relations for concrete

Like for the multiaxial strength of concrete several attempts have been made to model the stress - strain behaviour under multiaxial loading. This is however a difficult task because the stress path is essential. Most models are based on the linear-elastic relations in Section 4.1.1 for an isotropic material, while others use empirical relations like those described in Chapter 3 for the uniaxial stress - strain curves.

Only a few investigations concern the complete stress - strain relationship because the boundary conditions and the specimen size are known to influence the shape of the descending branch, see e.g. Van Mier & Vook (1991). Difficulties also arise with the determination of the peak point of the stress - strain curve, because confinement provide the specimens with great ductility. Some investigators therefore use the point, where the volume strain starts to decrease, i.e. the initiation of volume expansion, as an indication of failure.

In the present section only a very brief description of the different attempts is given. For a more extensive overview the reader is referred to e.g. Chen & Ting (1980).

**Biaxial behaviour.** In Liu et al. (1972) a proposal based on the so-called *Sargin model*, see eq. (3.1), is suggested for the behaviour up to the peak stresses. If the linear-elastic stress - strain expression in eq. (4.7) is considered for biaxial stresses, i.e.  $\sigma_3 = 0$ , we obtain

$$\sigma_1 = \frac{E\epsilon_1}{1-\nu\alpha}, \quad \alpha = \frac{\sigma_2}{\sigma_1}$$

where the stress direction in question is altered by interchanging the indices 1 and 2.

Application of the empirical Sargin model with  $D = 1$  to the biaxial case reads

$$Y_b = \frac{AX_b}{1 + (A-2)X_b + X_b^2}, \quad \begin{cases} X_b = \frac{\epsilon_1}{\epsilon_{1c}} \\ Y_b = \frac{\sigma_1}{\sigma_{1c}} \end{cases} \quad (4.17)$$

where the biaxial principal stresses and strains are normalized by respect to their values at the

peak point. It is recalled that this expression ensures, that the  $\sigma_1 - \epsilon_1$  curve passes through both the origin and the peak point and shows a horizontal slope at the peak. In order to obtain the correct initial slope, which is given by  $E/(1-\nu\alpha)$ , the constant  $A$  is determined by

$$A = \frac{E}{E_{peak}(1-\nu\alpha)}, \quad E_{peak} = \frac{\sigma_{1c}}{\epsilon_{1c}} \quad (4.18)$$

The parameters needed to determine the stress - strain curve for a given value of the biaxial stress ratio  $\alpha$ , are the uniaxial constants  $E$  and  $\nu$  together with the peak stresses and strains. The biaxial strength envelopes shown in figure 4.4 give the peak stresses as a function of  $\alpha$  and Tasuji et al. (1979) suggest linear relationships between the peak strains and stresses, based on their experimental results on  $127 \times 127 \times 13$  mm concrete discs.

In Kupfer & Gerstle (1973) the experimental programme of Kupfer et al. (1969) is investigated. The stress - strain model is based on the octahedral linear-elastic stress - strain expressions of eq. (4.8):  $\sigma_0 = 3K\epsilon_0$  and  $\tau_0 = 2G\gamma_0$ , where  $K$  and  $G$  are the bulk modulus and the shear modulus respectively.

Kupfer & Gerstle (1973) use the *secant moduli*  $K_s = \sigma_0/(3\epsilon_0)$  and  $G_s = \tau_0/(2\gamma_0)$  to model the non-linear behaviour of concrete, i.e. the moduli vary with the stresses and the strains throughout a test, instead of being constant. By depicting the experimental octahedral strains and stresses as functions of each other it is concluded, that the deviatoric part of the constitutive relationship does not depend on the hydrostatic part, while the opposite does not apply. The proposed expressions are not shown here, but they have the principal form

$$\gamma_0 = \frac{\tau_0}{2G_s(\tau_0)}, \quad \epsilon_0 = \frac{\sigma_0}{3K_s(\sigma_0)} \quad (4.19)$$

where the moduli are matched to the test results by mathematical fitting. It is obvious, that  $K_s$  and  $G_s$  go towards their initial linear-elastic values as the stress state tends to zero.

Contrary to what Kupfer & Gerstle conclude, *Andreas et al. (1977)* state, that there exist unique relationships for both the deviatoric and the hydrostatic part. Using 100 mm concrete cubes in a triaxial cell under fluid pressure, each principal stress can be varied independently. A total of 41 cubes are tested biaxial in the compression - compression region.

In *Gerstle et al. (1980)*, which concerns the deformations obtained under the co-operative test programme, the conclusion is, that the biaxial stress - strain curves are satisfactory described, disregarding any coupling between the deviatoric and the hydrostatic part.

**Triaxial behaviour.** Most investigations of the stress - strain curves under multiaxial stresses apply the method of separating the deviatoric and the hydrostatic parts, but no clear answer exists to the question, whether the two parts interact.

In *Palaniwamy & Shah (1974)* a test series with  $\phi 76 \times 230$  mm cylinders, subjected to hydrostatic oil pressure in a triaxial cell together with increasing vertical load until failure, is reported. All tests follow the compressive meridian. The authors propose a unique hydrostatic behaviour, while the deviatoric part depends on both  $\sigma_0$  and  $\tau_0$ .

*Cedolin et al. (1977)* investigate triaxial tests performed by Richard et al. (1928) and several others. By depicting the octahedral stresses and strains in all combinations they conclude, that  $K_s$  and  $G_s$  depend solely on  $\epsilon_0$  and  $\gamma_0$  respectively, i.e. no coupling effect.

In the co-operative project described in *Gerstle et al. (1980)* however, the hydrostatic and the deviatoric load paths are separated experimentally. Thus, first the hydrostatic stresses are applied followed by deviatoric stresses under constant hydrostatic stress. In most other investigations the stress path is taken as the so-called triaxial loading, cf. Section 4.1.3.

The results taken from 7 different laboratories show, that the deviatoric stress - strain relation is not influenced by the hydrostatic stress state. However, it is also found that when the deviatoric stress is increased, the hydrostatic strain is influenced. This coupling effect is modelled similar to the expressions in eq. (4.19).

Finally it is noted, that various stress - strain models for triaxial loading include both the ascending and the descending part, see e.g. *Otosen (1979)* and *Ahmad & Shah (1982)*. They are both based on the *Sargin model* in eq. (3.1). Just like in the case of uniaxial compression, four physical parameters in each principal stress direction are needed to determine the curve. These four parameters consist of the *initial stiffness*, the corresponding stress and strain values at the *peak point* and a data point at the *descending part* of the curve. As a part of his Ph.D.-thesis Dahl (1992b) perform a modification of the model in Otosen (1979) in order to match it with his test results for HSC ( $f_c$  up to 110 MPa). The reader is referred to Dahl (1992b) for further details.

#### 4.1.5 FRC under multiaxial stresses

The number of investigations concerning multiaxial loading of fibre reinforced concrete is very limited and only consider compression (especially biaxial compression). Three investigations, concerning biaxial tests of FRC, are known to the author. In table 4.2 a survey of these investigations is given.

The general conclusion is, that the steel fibres mainly influence the failure mode from a typical splitting failure, with cracks parallel to the biaxial stress plane, to inclined shear cracks. Also the biaxial strength is reported to increase compared to plain concrete specimens. In figure 4.7 the biaxial strength envelopes from the results on FRC are shown together with the findings from figure 4.4.

Investigator	Specimen dimensions	Characteristics of FRC mix	Principal stress ratios	Note
Taylor et al. (1975)	50 mm cubes	Round straight steel fibres, $V_f = 2\%$ , $L_f/d_f = 87$ , $f_c = 30$ MPa	0, 0.2, 0.6, 0.8 and 1	Both proportional and sequential loading. Both solid plates and steel brushes.
Yin et al. (1989)	152 x 152 x 38 mm discs	Straight steel fibres, $V_f = 0, 1$ and $2\%$ , $L_f/d_f = 37$ and $48$ , $f_c = 40$ MPa	0, 0.2, 0.5 and 1	Proportional loading. Steel brushes.
Traina & Mansour (1991)	76 mm cubes	Hooked-end and corrugated steel fibres, $V_f = 0, 0.5, 1$ and $1.5\%$ , $L_f/d_f = 60$ and $33$ , $f_c = 40$ MPa	0, 0.5 and 1	Proportional loading. Friction reducing pads.

Table 4.2: Survey on existing biaxial tests involving FRC.

In the early investigation by Taylor et al. (1975) they report, that the use of solid load plates almost doubles the strength compared to steel brushes, which is also concluded in Kupfer et al (1969) on plain concrete. A comparison of the proportional loading and the sequential loading, where the two loads are applied separately, shows a slightly higher strength for the proportional load path. Taylor et al. find a biaxial strength of about  $1.7f_c$  with a fibre reinforcement index equal to 1.7.

In Yin et al. (1989) the fibre reinforcement index varies between 0.4 and 1.0. The increase in uniaxial strength because of the fibres is less than 10 % compared to plain concrete. However, the biaxial strength is increased considerably as it is shown in figure 4.7.

Finally the results of Traina & Mansour (1991) also show a biaxial strength increase with the fibre reinforcement index varying between 0.2 and 0.9, even though the increase is slightly smaller than that obtained by Yin et al.

None of the investigations include any proposals for the biaxial strength envelope, but it appears, that the fibres increase the strength by approximately 25 % compared to plain concrete. This increase is probably due to the confinement effect of the fibres in the stress-free direction.

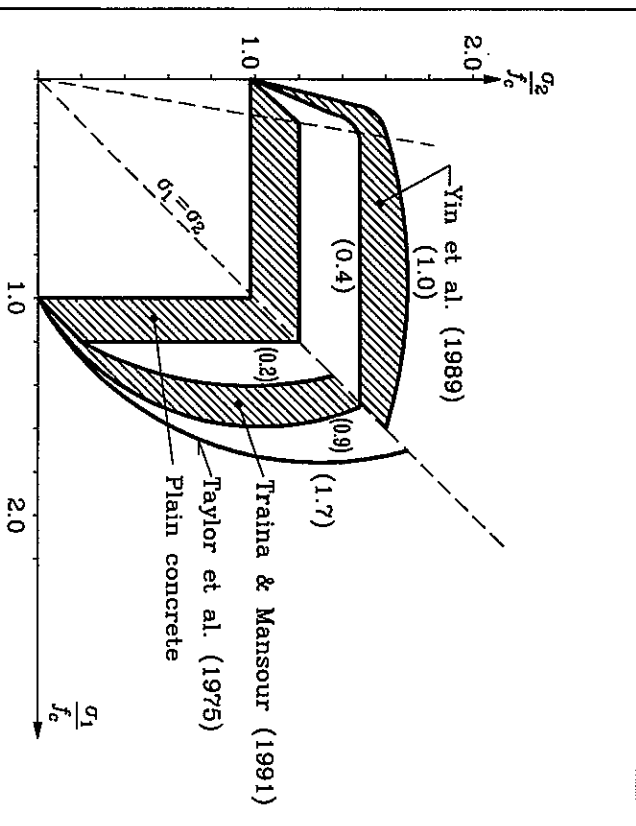


Figure 4.7: Experimental biaxial strengths of FRC. The numbers in brackets represent the fibre reinforcement index  $V_f(L_f/d_f)$ .

The only investigation, available to the author, concerning triaxial stresses in FRC, is reported in the M.Sc.-thesis Egging & Ko (1981). A concrete mix containing 0.6 % by volume of Dramix steel fibres (type ZP 30/40), with hooked ends ( $V_f(L_f/d_f) = 0.45$ ), is tested by means of 100 mm cubes. The uniaxial compressive strength is approximately 60 MPa, which is an increase of 20 % compared to the plain concrete strength.

A triaxial test equipment in Egging & Ko (1981) makes it possible to load each specimen side independently by means of an oil pressure. A total of 3 different hydrostatic stress levels ( $\sigma_0 = 28, 41$  and  $55$  MPa) are tested along the compressive, the tensile and the shear meridian. By comparing the experimental relations between  $\tau_0$  and  $\sigma_0$  to eq. (4.16) it seems reasonable to conclude, that the modified Coulomb criterion applies satisfactory as it does for plain concrete. Egging & Ko perform a fitting of the results to the William-Warner criterion, but conclude that the FRC behaves similar to plain concrete.

## 4.2 Compressit matrix under multiaxial compression

A total of 50 compressit cylinders with dimensions  $\phi 100 \times 200$  mm are subjected to oil pressure together with an axial compressive load. All tests are performed along the compressive meridian, i.e.  $\sigma_1 \geq \sigma_2 = \sigma_3 \geq 0$  ( $\theta = 0^\circ$ ), at the Department of Structural Engineering, Technical University of Denmark. The test equipment is developed by K.K.B. Dahl during his Ph.D. project, see Dahl (1992c). The basic test principles are similar to those described in Newman (1974).

There exist two different test series with compression on compressit matrix:

- In 1992 K.K.B. Dahl performed a series with the results presented in Heshe & Nielsen (1992b).
- During the present project a test series, slightly different from that above, is performed.

The differences between these series consist of the type of fibres and the range of oil pressures applied, but nevertheless the results are directly comparable.

### 4.2.1 Test specimens and method

In Appendix 3 the test procedure and the equipment are presented. For further information the reader is referred to Dahl (1992c). In table 4.3 the fibre characteristics for the two test series are given. The specimen name consists of TC for triaxial compression followed by the aspect ratio of the fibre type in question.

Specimen name	Aspect ratio $L/d$	Fibre content $V_f$ (%)	Fibre reinforcement index $V_f(L/d)$	Fibre type Diameter
TC40 (K.K.B. Dahl)	40	6	2.4	OL 6/15 HC
TC0	-	0	0	-
TC30	30	6	1.8	OL 12/40

Table 4.3: Survey of the compressit mixes used for triaxial compression tests. See fibre characteristics in table 1.3.

A cylinder is fitted in a tight rubber membrane and it is placed in a steel barrel filled with hydraulic oil. The oil pressure is increased, subjecting the cylinder to a hydrostatic pressure. At a specified level the vertical load is applied from an external jack under *load control* until failure.

Both the longitudinal and the circumferential strains are measured by means of electrical resistance gages, but it turns out that most of these gages fail even before the vertical load is applied. This is due to air voids on the cylinder surface under the gages, which are cat-atrophic to the gages. These holes are filled before testing, but it appears that this filling is insufficient or at least it demands great care. Because of this lack of deformational measurements only the *triaxial strength* of the compressit matrix is considered in the following.

### 4.2.2 Test results

In this section the triaxial strength results for compressit matrix are presented. Even though the two test series utilize different compressit mixes the uniaxial strength do not differ significantly. Table 4.4 contains the results normalized by respect to the uniaxial strength. The results for TC40 are obtained from 3 repetitions, but as the coefficients of variation on the strength all are found less than 2 %, see Heshe & Nielsen (1992b), the present project (TC0 and TC30 in table 4.4) only includes 2 repetitions for each confinement pressure.

K.K.B. Dahl applies 6 different oil pressures, varying from 20 to 140 MPa, beside the uniaxial test. This enables the confinement pressure to go up to  $0.85f_c$ . In the present test series the confinement pressure is only raised to 70 MPa and instead the interest is focused on small confinement pressures. For practical purposes it seems relevant to investigate the strength behaviour at relatively small confinement pressures, e.g. in order to model the confinement effect of steel stirrups.

The few tests involving plain compressit matrix without fibres (TC0) are included for reference purpose to HSC. In figure 4.8 the results from the table is depicted in a normalized  $\sigma_1 - \sigma_3$  diagram. The *two-stage model* from figure 4.6 is also inserted in the figure, where the initial line with slope 4 is the usual *Coulomb line* for concrete, but as stated by Dahl (1992a) this line seems too steep when the confinement pressure exceeds  $0.5f_c$ . Thus, the second line of the two-stage model has the slope  $k = 3$ .

From the compressit results in figure 4.8 two observations are obvious:

- It seems that the line with slope  $k = 3$  is valid as low as  $\sigma_3 = 0.1f_c$ .
- Furthermore there seems to be a rather steep line for small values of the confinement pressure, i.e. a strong confinement effect in the beginning.

Series	σ <sub>1</sub> /f <sub>c</sub>	σ <sub>2</sub> /f <sub>c</sub>	σ <sub>3</sub> /f <sub>c</sub>	σ <sub>1</sub> /f <sub>c</sub> (σ <sub>2</sub> /f <sub>c</sub> )	Concrete strength	
					σ <sub>1</sub> /f <sub>c</sub>	σ <sub>2</sub> /f <sub>c</sub>
TC40	40	6	2.4	165.0 (0.5)	0.125	1.84
					0.245	2.29
					0.365	2.69
					0.485	2.98
					0.607	3.23
TC40	40	6	2.4	165.0 (0.5)	0.729	3.62
					0.849	4.05
					0.029	1.26
TC0	-	0	0	170.2 (1.7)	0.059	1.47
					0.080	2.10
					0.034	1.34
					0.065	1.61
TC30	30	6	1.8	164.3 (2.1)	0.120	1.88
					0.180	2.19
					0.240	2.38
					0.370	2.74
TC30	30	6	1.8	164.3 (2.1)	0.400	2.84
					0.430	2.96

Table 4.4: Test results from triaxial compression tests on compressive matrix. All values are mean values and the brackets contain the coefficients of variation.

The steep initial line shows a slope corresponding to  $k = 8$  and the two-stage model seems to be on the safe side. A possible explanation for these observations is, that compressive matrix (and HSC) act as true Coulomb materials for relatively high confinement pressures, showing  $k = 3$ , i.e. the angle of friction is equal to  $30^\circ$ . If the material did act in this manner for decreasing confinement pressures going towards zero, it would produce uniaxial strengths 50% higher than those actually observed.

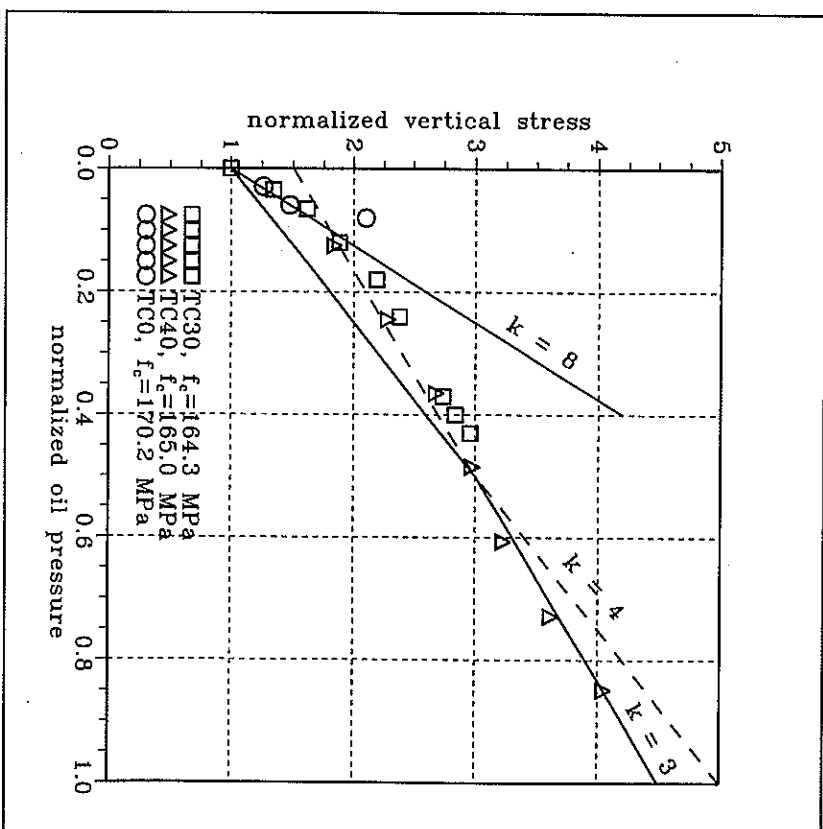


Figure 4.8: Experimental  $\sigma_v/f_c - \sigma_o/f_c$  relationship for compressive matrix. The two-stage model from Dahl (1992a) is also shown.

It is well-known, that HSC shows almost vertical cracks in uniaxial compression instead of inclined shear cracks. Therefore it seems reasonable to believe, that uniaxial failure and failure under small confinements are governed by a rather steep line in a Mohr diagram, see figure 4.9. These splitting cracks are often connected with the increased brittleness of HSC compared with NSC. The strength  $f_c$ , represented by the small circle in figure 4.9, and the cohesion are related through

$$f_c = 2c/\sqrt{k}, \quad k = (1 + \sin\phi)/(1 - \sin\phi) \quad (4.20)$$

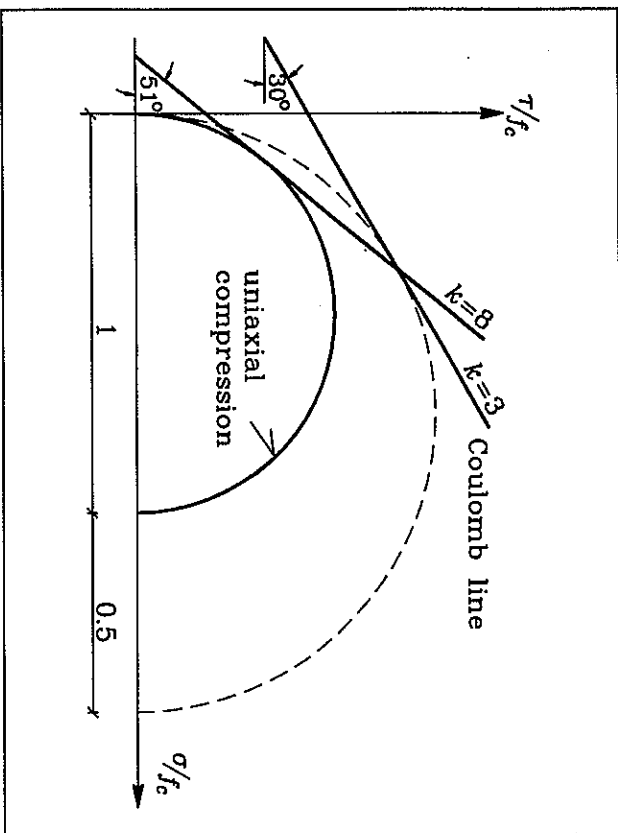


Figure 4.9: Molar diagram for a Coulomb material showing a bi-linear failure criterion. Furthermore the effect of increasing cohesion is illustrated.

It is possible to construct a situation, where the uniaxial strength is identical for the two lines in figure 4.9, which have different slopes, i.e. the uniaxial compression circle tangents both lines:

$$c_2/c_1 = \sqrt{k_1/k_2} \tag{4.21}$$

where subscript 1 and 2 refer to the initial line and the Coulomb line respectively.

In Part II of the thesis<sup>2</sup> the bi-linear failure criterion is treated in a more detailed manner. Furthermore the physical phenomena corresponding to the criterion are discussed.

<sup>2</sup>Structural application of compressit.

### 4.2.3 Failure criterion for compressit matrix

A failure criterion to be used for *design purposes* should of course be on the safe side. Furthermore simplicity is essential, when it comes to practical use. The triaxial tests performed on compressit matrix may justify a change of failure criterion, compared to that normally used for concrete. However, it seems that in case of triaxial compression the fibre effect is insignificant, meaning that the compressit matrix behaves similar to HSC, when the triaxial strength is considered. The fibres undoubtedly have great effect on the deformational characteristic just like in the uniaxial case described in Chapter 3.

A comparison of the triaxial compressit results with results from HSC ( $f_c$  up to 130 MPa) for small values of the confinement pressure ( $\sigma_3$  up to 0.5 $f_c$ ) is given in figure 4.10. The figure clearly shows, that the results of Setunge et al. (1993) indicate the similar trend as observed for compressit matrix. Contrary to this, Lahlou et al. (1992) do not observe an initial increased slope, their results seem to follow the normal Coulomb line.

For high values of the confinement pressure most investigations find, that the angle of friction is reduced from 37° to 30°, i.e.  $k$  decreases from 4 to 3, when HSC is considered instead of NSC. This observation seems reasonable, as it is accepted, that HSC, amongst other things, is characterized by failure zones passing through the aggregate instead of following the mortar-aggregate interfaces. Thus, the coefficient of friction ( $\tan\phi$ ) is reduced because of the smooth failure zones for HSC. The *two-stage failure criterion* proposed by Dahl (1992a) seems reasonable, because it only gives a slight modification of the existing plastic solutions:

$$\frac{\sigma_1}{f_c} = \begin{cases} 1 + 4\frac{\sigma_3}{f_c}, & 0 \leq \frac{\sigma_3}{f_c} \leq 0.5 \\ 1.5 + 3\frac{\sigma_3}{f_c}, & \frac{\sigma_3}{f_c} > 0.5 \end{cases} \tag{4.22}$$

Furthermore it appears to be a safe failure surface for HSC. From the fact that all available HSC test results only cover the compressive meridian, it might be questionably to suggest a value of  $k$  higher than 4, before further experimental evidence is present.

The utilization of the two-stage model on the existing plastic solutions only means small alterations of the theoretical energy dissipation in the lines of discontinuity. In case of *plane stressers*, see e.g. figure 4.4, only the inclination of the failure surface in the compression-tension region depends on the angle of friction, corresponding to the initial slope in eq.(4.22). However, in most practical cases the tensile regions are neglected, resulting in solutions independent of the angle of friction. In case of *plane stressers* on the contrary, the relative displacements in a yield line are limited by the angle of friction. From the fact that the angle of friction is found to change with the minor principal stress in eq. (4.22), the plastic solutions for plane stressers need modifications, e.g. the rotation symmetrical solution for punching shear failure. The energy dissipation formulas are included in Part II of the thesis.

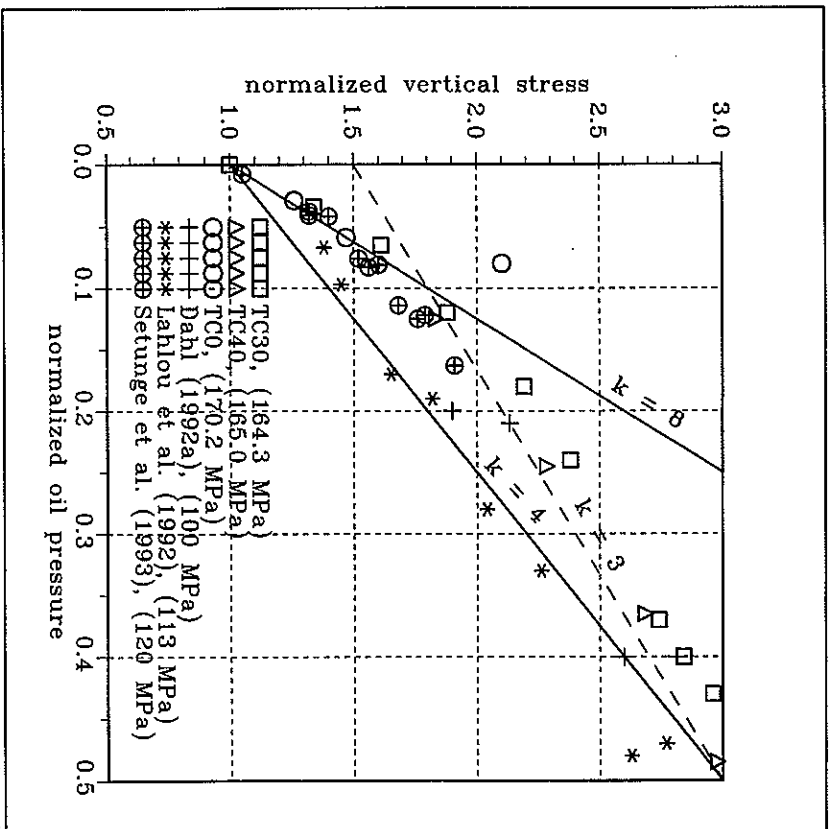


Figure 4.10: Experimental  $\sigma_{ff} - \sigma_{3ff}$  relationship for relatively small values of the oil pressure. The brackets give the uniaxial strength.

In the *tensile regions* doubts still exist, whether the tensile strength  $f_t$  should be included for fibre reinforced concretes. For compressive matrix the test results in Section 2.3 show multiple cracking and  $f_t$  increasing with the fibre reinforcement index. However, the tensile results with combined steel fibres and reinforcement bars in Section 2.4 show, that the compressive matrix only contributes with a tensile stress corresponding to its *cracking strength* (5 to 10 MPa). This contribution represents 3 to 5 % of the compressive strength and therefore it seems unlikely to be advantageous to include this strength into the solutions. Thus, for structural purposes it seems likely, that the zero tension cut-off is applied just like it is done in traditional concrete design.

### 4.3 Concluding remarks

From Section 4.1.5 it appears, that the number of investigations, concerning the effect of fibres on the multiaxial behaviour, is very limited. The general observation for FRC under biaxial compression is, that the strength increases slightly, which is probably due to the confinement effect of the fibres in the stress-free direction. Furthermore the fibres certainly affect both the cracking behaviour and the stress - strain curve, just like in the case of uniaxial compression. However, the triaxial strength of FRC seems to follow the normal concrete behaviour.

Therefore it seems reasonable to consider compressive matrix as a HSC material with compressive strengths above 100 MPa. The angle of friction decreases from  $37^\circ$  for NSC to  $30^\circ$  for HSC, which is explained by the failure zones passing through the aggregates in HSC. The present test results on compressive matrix also show an increased angle of friction (approximately  $51^\circ$ ) for small confinement pressures, which is also observed by another investigation on HSC. This indicates a failure criterion, that results in reduced/effective compressive strengths, compared to the strengths to be expected if the material acted as a *true Coulomb material*. For compressive matrix and other HSC's this true Coulomb strength seems to be 1.5 times the actually measured strength.

In order to obtain a *simple failure criterion* appropriate to both HSC and fibre reinforced compressive matrix, the proposal by Dahl (1992a) is suggested. The *initial* angle of friction correspond to that normally applied to NSC ( $\varphi \approx 37^\circ$ ,  $k = 4$ ), while this angle *reduces* to  $\varphi = 30^\circ$  ( $k = 3$ ), when the minor principal stress exceeds  $0.5f_c$ .

When the tensile strength is considered for compressive matrix, an increase with fibre content is found in Chapter 2. However, it seems reasonable to neglect  $f_t$  because it only contributes with about 5 % of the compressive strength. Tests show that the tensile strength of compressive matrix does not exceed the cracking strength for structural use, but they also show that this tensile strength is present over a remarkable strain range. Thus, the crack pattern is influenced remarkably from the presence of fibres.

It should be emphasized, that the main reason for maintaining the simple straight lines as analytical failure criterion, is to utilize the existing solutions without any major changes. It is obvious to perform an empirical curve fitting to the triaxial data points, in order to obtain a smooth failure surface. This approach is hardly adequate for design purposes, even though it applies to a computer algorithm.

It is recalled, that the discussion of an appropriate failure criterion is continued in Chapter 2 of Part II of the thesis<sup>3</sup>.

<sup>3</sup>Structural Applications of Compress.

## 4.4 References

- Ahmad, S.H. & S.P. Shah (1982), 'Complete Triaxial Stress - Strain Curves for Concrete', *Journal of the Structural Division*, ASCE, Vol. 108, No. ST4, pp. 728-742.
- Andreas, E., K.H. Gerstle & H.-Y. Ko (1977), 'Response of Mortar and Concrete to Biaxial Compression', *Journal of the Engineering Mechanics Division*, ASCE, Vol. 103, No. EM4, pp. 515-526.
- Cedolin, L., Y.R.J. Gunzen & S.D. Poli (1977), 'Triaxial Stress - Strain Relationship for Concrete', *Journal of the Engineering Mechanics Division*, ASCE, Vol. 103, No. EM3, pp. 423-439.
- Chen, W.-F. (1982), *Plasticity in Reinforced Concrete*, McGraw-Hill Book Company, xv + 474 pp.
- Chen, W.-F. & E.C. Ting (1980), 'Constitutive Models for Concrete Structures', *Journal of the Engineering Mechanics Division*, ASCE, Vol. 106, No. EMI, pp. 1-19.
- Dahl, K.K.B. (1990), *Preliminary State-Of-The-Art Report on Multiaxial Strength of Concrete*, Serie R, No. 262, Department of Structural Engineering, Technical University of Denmark, Lyngby, 77 pp.
- Dahl, K.K.B. (1992a), *A Failure Criterion for Normal and High Strength Concrete*, Serie R, No. 286, Department of Structural Engineering, Technical University of Denmark, Lyngby, x + 115 pp.
- Dahl, K.K.B. (1992b), *A Constitutive Model for Normal and High Strength Concrete*, Serie R, No. 287, Department of Structural Engineering, Technical University of Denmark, Lyngby, x + 96 pp.
- Dahl, K.K.B. (1992c), *The Calibration and Use of a Triaxial Cell*, Serie R, No. 285, Department of Structural Engineering, Technical University of Denmark, Lyngby, x + 70 pp.
- Eggins, D.E. & H.-Y. Ko (1981), *Constitutive Relations of Randomly Oriented Steel Fiber Reinforced Concrete Under Multiaxial Loadings*, M.Sc.-thesis, University of Colorado, Boulder, 480 pp.
- Gerstle, K.H., D.L. Linse, P. Bertacchi, M.D. Kotsyvos, H.-Y. Ko, J.B. Newman, P. Rossi, G. Schickert, M.A. Taylor, L.A. Traña, R.M. Zimmerman & R. Bellotti (1978), 'Strength of Concrete Under Multiaxial Stress States', *Douglas McHenry International Symposium on Concrete and Concrete Structures*, ACI Publication, SP-55, pp. 103-

- 131.
- Gerstle, K.H., H. Aschl, R. Bellotti, P. Bertacchi, M.D. Kotsyvos, H.-Y. Ko, D.L. Linse, J.B. Newman, P. Rossi, G. Schickert, M.A. Taylor, L.A. Traña, H. Winkler & R.M. Zimmerman (1980), 'Behaviour of Concrete Under Multiaxial Stress States', *Journal of the Engineering Mechanics Division*, ASCE, Vol. 106, No. EM6, pp. 1383-1403.
- Hannant, D.J. (1974), 'Nomograms for the Failure of Plain Concrete Subjected to Short-Term Multiaxial Stresses', *The Structural Engineer*, Vol. 52, No. 5, pp. 151-165.
- Heshe, G. & C.V. Nielsen (1992b), *EU 264 - COMPRESIT, Subtask 1.4 - Behaviour in Compression, Triaxial Stress State and Short Columns*, NOVIT's Udviklingsfond, Aalborg, 51 pp.
- Kotsyvos, M.D. (1979a), 'Effect of Stress Path on the Behaviour of Concrete Under Triaxial Stress States', *ACI Journal*, Vol. 76, pp. 213-223.
- Kotsyvos, M.D. (1979b), 'A Mathematical Description of the Strength Properties of concrete Under Generalized Stress', *Magazine of Concrete Research*, Vol. 31, No. 108, pp. 151-158.
- Kupfer, H.B. & K.H. Gerstle (1972), 'Behaviour of Concrete Under Biaxial Stresses', *Journal of the Engineering Mechanics Division*, ASCE, Vol. 99, No. EM4, pp. 853-866.
- Kupfer, H., H.K. Hilsdorf & H. Rusch (1969), 'Behaviour of Concrete Under Biaxial Stresses', *ACI Journal*, Vol. 66, pp. 656-666.
- Lahlou, K., P.-C. Aitcin & O. Chaallah (1992), 'Behaviour of High-Strength Concrete Under Confined Stresses', *Cement & Concrete Composites*, Vol. 14, pp. 185-193.
- Lin, T.C.Y., A.H. Nilson & F.O. Slate (1972), 'Stress-Strain Response and Fracture of Concrete in Uniaxial and Biaxial Compression', *ACI Journal*, Vol. 69, pp. 291-295.
- Mills, L.L. & M. Zimmerman (1970), 'Compressive Strength of Plain Concrete Under Multiaxial Loading Conditions', *ACI Journal*, Vol. 67, pp. 802-807.
- Nelissen, L.J.M. (1972), *Biaxial Testing of Normal Concrete*, HERON, Vol. 18, No. 1, 90 pp.
- Newman, J.B. (1974), 'Apparatus for Testing Concrete under Multiaxial States of Stress', *Magazine of Concrete Research*, Vol. 26, No. 89, pp. 229-238.
- Nielsen, M.P. (1984), *Limit Analysis and Concrete Plasticity*, Prentice-Hall Inc., Englewood Cliffs New Jersey, xii + 420 pp.



#### 4. Multiaxial behaviour

- Otosen, N.S. (1977), 'A Failure Criterion for Concrete', *Journal of the Engineering Mechanics Division*, ASCE, Vol. 103, No. EM4, pp. 527-535.
- Otosen, N.S. (1979), 'Constitutive Model for Short - Time Loading of Concrete', *Journal of the Engineering Mechanics Division*, ASCE, Vol. 105, No. EM1, pp. 127-141.
- Palaniswamy, G. & S.P. Shah (1974), 'Fracture and Stress - Strain Relationship of Concrete Under Triaxial Compression', *Journal of the Structural Division*, ASCE, Vol. 100, No. ST5, pp. 901-916.
- Richard, F.E., A. Brandtzaeg & R.L. Brown (1978), *A Study of the Failure of Concrete Under Combined Compressive Stresses*, Bulletin no. 185, Engineering Experiment Station, University of Illinois, Urbana, 104 pp.
- Setunge, S., M.M. Attard & P.L.P. Darvall (1993), 'Ultimate Strength of Confined Very High-Strength Concretes', *ACI Structural Journal*, Vol. 90, pp. 632-641.
- Tasuji, M.E., A.H. Nilson & F.O. Slate (1979), 'Biaxial Stress-Strain Relationships for Concrete', *Magazine of Concrete Research*, Vol. 31, No. 109, pp. 217-224.
- Taylor, M.A., M.K. Tai & M.R. Ramey (1975), 'Biaxial Compressive Behaviour of Fiber Reinforced Mortar', *ACI Journal*, Vol. 72, pp. 496-501.
- Traina, L.A. & S.A. Mansour (1991), 'Biaxial Strength and Deformational Behaviour of Plain and Steel Fiber Concrete', *ACI Materials Journal*, Vol. 88, pp. 354-362.
- Van Mier, J.G.M. & R.A. Vank (1991), 'Fracture of Concrete Under Multiaxial Stress - Recent Developments', 53-MTC Multiaxial Testing of Concrete, Final Report, *Materials and Structures*, RILEM, Vol. 24, pp. 61-65.
- Wasilefs, J. (1979), 'Behaviour of Concrete Under Multiaxial Stresses - A Review', *Cement and Concrete Research*, Vol. 9, pp. 35-44.
- Yin, W.S., E.C.M. Su, M.A. Mansour & T.T.C. Hsu (1989), 'Biaxial Tests of Plain and Fiber Concrete', *ACI Materials Journal*, Vol. 86, pp. 236-243.

## 5. Fracture energy

From the introduction it is recalled, that fracture mechanics applied to concrete structures is in progress. Fracture mechanics concerns the propagation of cracks and therefore it involves the tensile properties of concrete in particular. The fictitious crack method (FCM) by A. Hillerborg applies the so-called fracture energy  $G_f$  as a material property together with the compressive and tensile strengths.

The energy absorption per unit crack area is measured by means of methods, where the crack area is well-defined, e.g. a notched direct tensile test. However, direct tension tests are known to cause trouble in normally equipped laboratories and therefore the RILEM<sup>1</sup> committee TC50-FMC submitted a draft recommendation in 1985. In RILEM (1985) this proposal of a *three-point bend test* on notched beams is described.

In 1990 a new draft recommendation is provided from committee TC89-FMT, see RILEM (1990a) and (1990b). The new proposals try to eliminate the experienced size-effects of the bend test in order to obtain a true material parameter. In the following these recommendations are described together with a method provided by the ASTM<sup>2</sup> to evaluate the *flexural toughness* of FRC.

The  $G_f$ -values normally obtained for HSC are compared to measurements on compressive matrix. It is noted that the  $G_f$ -tests on compressive matrix are not performed strictly in accordance with the RILEM proposals, but for comparison the results are useful.

### 5.1 Review on fracture energy for concrete and FRC

Before considering the  $G_f$ -tests on notched beams, a few fracture mechanical definitions are given, see e.g. Broek (1986) or Hellan (1985). Fracture mechanics concern the conditions near a *crack tip* in a continuum. A *linear elastic* solution of the stress field at a distance  $r$  from the tip shows a *stress singularity*, which is written on the form

$$\sigma \propto \frac{K}{\sqrt{r}}, \quad r > 0 \quad (5.1)$$

where  $K$  is the so-called *stress intensity factor*, which depends on loading and geometry. Only a few exact solutions exist to problems with a small crack in infinitely large bodies, but

<sup>1</sup>The International Union of Testing and Research Laboratories for Materials and Structures.

<sup>2</sup>The American Society for Testing and Materials.

several solutions are evaluated to specific geometries and loadings. From eq. (5.1) it appears, that LEFM result in stresses, increasing toward infinity at the crack tip, which is of course impossible in practice.

In 1921 A.A. Griffith stated, that a crack develops, when the energy dissipated in producing new crack surface exceeds a critical value  $G_c$ . In LEFM all energy is absorbed in the crack surfaces, i.e.  $G_f = G_c$ . However, in the fifties G.R. Irwin and E. Orowan showed, that most of the energy is dissipated in plastic zones around the cracks, when building materials are considered, i.e.  $G_f = G_c + \text{plastic energy absorption}$ .

$G_f$  is often considered a material constant and according to LEFM it is related to the critical stress intensity factor by

$$K_{Ic}^2 = EG_f \tag{5.2}$$

where subscript  $I$  denotes failure mode I, i.e. crack opening.

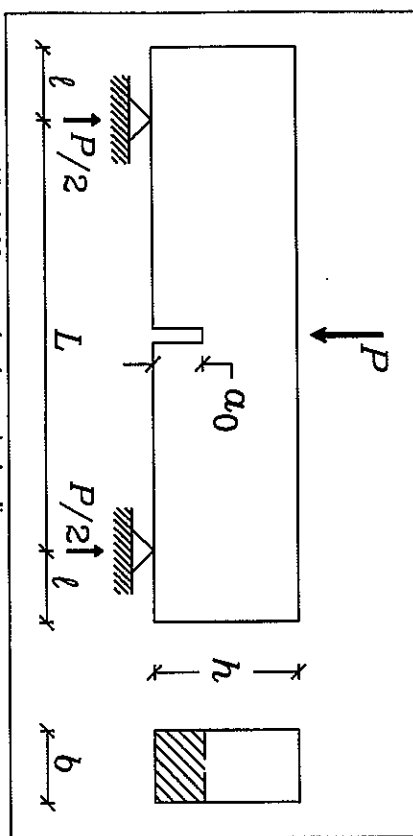


Figure 5.1: Notched beam under three-point bending.

For the special case of a notched beam, with symbols given in figure 5.1, the stress intensity factor is written as

$$K_I = \frac{3}{2} \frac{P}{hb} \frac{L}{h} \sqrt{\pi a_0} F(\alpha), \quad \alpha = \frac{a_0}{h} \tag{5.3}$$

where the function  $F(\alpha)$  depends on the geometry of the notch:

The critical factor  $K_{Ic}$  is determined by inserting the maximum beam load in eq. (5.3). It is recalled that LEFM is only correct in case of infinitely large beams, where the plastic energy dissipation gets negligible compared to the surface energy.

5.1.1 Three-point bend test on notched beam

**The Hillerborg proposal.** The first recommendation in RILEM (1985) is based solely on the FCM described in Hillerborg (1985). The three-point bend test is preferred instead of a direct tension test because: "It is much easier to perform stable bending tests on notched specimens. The simplest possible test of this type is the three-point bend test on a notched beam."

A beam is broken into two halves and the work applied by the force  $P$  is divided by the crack area  $b(h-a_0)$ . The work, represented by the area under the load - deflection curve, is modified to take account for the self-weight induced deflection. An extra contribution to the work is calculated as  $mg\delta_0$ , where  $m$  is the beam weight within the load span,  $g$  is the acceleration of gravity ( $= 9.82$  m per square second) and  $\delta_0$  is the recorded deflection at final failure.

It is well-known, that the self-weight induced bending moment at mid-span vanishes, if the length  $l$  is equal to half the load span, cf. figure 5.1. However, Hillerborg (1985) states that such an experimental elimination of the self-weight influence complicates the test execution, because the  $P - \delta$  curve tends to get a very long tail, which makes it difficult to determine, when the test ends.

The recommended beam sizes are listed in table 5.2. The dimensions are mainly chosen from the following requirements:

- The beam should be easy to handle, i.e. not too heavy.
- The smallest dimension should be at least 3 times the maximum aggregate size.
- The influence of energy absorption outside the notched section should be minimized.
- The stiffness demand for the test equipment should be obtainable at most laboratories.

Hillerborg performs a sensitivity analysis on strength results obtained from FCM with varying  $G_f$ . He concludes that the strength is only about one third as sensitive to a variation of  $G_f$  as it is to variations of the other material parameters of concrete structures. Therefore the errors in  $G_f$ -tests, e.g. originating from size-effects, are acceptable within normal engineering accuracy.

An experimental study at 12 different laboratories throughout the world indicates a certain influence of beam size. The increase in  $G_f$  is approximately 30 %, when the beam depth  $h$  increases by a factor 3.

The influence of specimen size is e.g. investigated by M. Eliecs, G.V. Guinea and J. Planas in 3 articles from 1992, see Eliecs et al. (1992), Guinea et al. (1992) and Planas et al. (1992). They investigate the influence of *experimental procedures*, the influence of *bulk energy dissipation* and the influence of ignoring the last part of the  $P - \delta$  tail. By means of bend tests, which are not necessarily according to RILEM (1985), they conclude, that a true beam size independent  $G_f$ -value is attainable if the following contributions to the energy absorption are considered:

- The energy dissipation in the supports by means of friction, (rolling supports are preferred).
- The energy dissipation in the bulk are analyzed by means of finite element computations. An upper bound of about 5 % of  $G_f$  is reported to dissipate in the bulk of the beams.
- The neglected energy from the tail of the load - deflection curve. This contribution is concluded to cause the greatest misinterpretation of  $G_f$ .

However, no specific proposals to improve the experimental procedure of the bend test are provided.

**The effective crack length approach.** In the latest draft recommendation in RILEM (1990a), the *two-parameter model* is presented. The basis for the theory originates from Jeng & Shah (1985). Instead of a  $P - \delta$  curve a  $P - CMOD$  relationship is required, where  $CMOD$  is the *crack mouth opening displacement*. Furthermore an unloading cycle is necessary near the peak load, meaning that this proposal demands considerably more from the laboratories, than that of RILEM (1985).

From the initial stiffness and the unloading stiffness of the notched beam, the critical crack length  $a_c$  is determined from *LEFM-expressions*. The critical (effective) crack length consists of the initial length  $a_0$  and the stable crack growth until peak load. When  $a_c$  is determined, the critical stress intensity factor is calculated from eq. (5.3) with  $\alpha = a_c/h$  and  $P$  corresponding to the observed peak load. Finally  $G_f$  is calculated by means of eq. (5.2).

The specimen size for the two-parameter model are given in table 5.2 together with those proposed by the other methods.

In *Karihaloo & Nallathambi (1989)* a model similar to the previous is suggested. However, their *effective crack model* only requires the experimental  $P - \delta$  relationship until peak, i.e. no stiffness requirements for the test equipment. The value of the critical crack

length at peak load is determined by means of regression analysis performed on existing test results. The subsequent calculation of  $G_f$  is similar to the two-parameter model.

**The size-effect method.** The second suggestion in RILEM (1990b) is based on the *size-effect law* by Z.P. Bazant, see e.g. Bazant et al. (1986). The generalized size-effect law has the form

$$\sigma_N = G_f \left( 1 + \frac{h}{A} \right)^{-1/2}$$

where  $\sigma_N$  is the nominal stress at failure,  $A$  and  $C$  are empirical constants,  $h$  is a characteristic dimension and  $f_t$  is the tensile strength. If this equation is applied to the three-point bend test we get

$$\left( \frac{hb}{P_{max}} \right)^2 = Ah + C \quad (5.5)$$

where  $P_{max}$  is the peak load and  $A$  and  $C$  are empirical constants, but not identical to those in the previous expression.

The test method consists of bend tests with *various beam depths* (at least 3 different beam depths), but having geometrically similar load spans and notch depths. A linear regression analysis is performed on the peak loads, resulting in estimates of the constants  $A$  and  $C$  of eq. (5.5).

The method utilizes that the LEFM is correct for *large specimens* and an extrapolation is performed from the experimental beam sizes. First eq. (5.3) is rewritten into

$$K_{Ic}^2 \left( \frac{hb}{P_{max}} \right)^2 \frac{1}{h} = \left( \frac{L}{h} \right)^2 \pi \alpha \left( \frac{3}{2} F(\alpha) \right)^2, \quad \alpha = \frac{a_0}{h}$$

In the special case with  $h \rightarrow \infty$  this expression is inserted into eq. (5.2)

$$G_f = \left( \frac{L}{h} \right)^2 \pi \alpha \frac{\left( \frac{3}{2} F(\alpha_0) \right)^2}{EA}, \quad \alpha = \frac{a_0}{h} \quad (5.6)$$

where  $A$  is the slope obtained from the regression analysis. As a consequence of this test principle, the demands for the beam size are rather few, see table 5.2.

**Comparison of various  $G_f$ -tests.** The experimental data necessary in order to determine the fracture energy differ significantly between the various proposals. In table 5.1 a survey of the

demands for each method is given.

Method	Necessary data recordings and control	Calculations
Fictitious crack model RILEM (1985)	Complete $P - \delta$ curve. Deformation control.	Area under $P - \delta$ curve divided by crack area.
Two-parameter model RILEM (1990a)	Complete $P - CMOD$ curve including unloading near the peak. Crack opening control.	Critical crack length by means of unloading stiffness. Equation (5.3) gives $K_c$ .
Size-effect method RILEM (1990b)	Peak loads for at least 3 different beam depths. Load control.	Linear regression analysis by means of eqs. (5.5) and (5.6).

Table 5.1: Survey of RILEM methods to determine  $G_f$ . It is noted, that each method take account of the beam weight by increasing the experimentally observed load, corresponding to the weight within the load span.

It is obvious that the two-parameter model is the most difficult to accomplish, because it requires clip gage measurements of the crack opening together with an unloading cycle. The size-effect law only demands load controlled bend tests, but it uses various beam sizes, which can cause practical problems.

The *beam dimensions* recommended for the methods are listed in table 5.2. The cross-sectional dimensions in the table represent the smallest aggregate sizes in case of the FCM and the two-parameter model. Both models increase  $h \times b$  up to  $400 \times 200$  mm and  $250 \times 150$  mm respectively, when  $d_a$  increases to approximately 50 mm. However, it seems unfortunately from a practical point of view, that the beam sizes are changed so that the existing moulds must be replaced at many laboratories.

Method	Depth	Load span	Notch	Width	Total length
		$L/h$	$a/h$	$b$	$L$
Fictitious crack model	100 mm	8	0.5	100 mm	840 mm
Two-parameter model	150 mm	4	0.33	80 mm	700 mm
Size-effect method	$\geq 3d_a$	$\geq 2.5$	$\geq 0.15$ $\leq 0.5$	$\geq 3d_a$	-

Table 5.2: Beam dimension for RILEM recommendations. The symbols are taken from figure 5.1. The maximum aggregate size is denoted  $d_a$ .

It is notable that the proposed load span is decreased significantly from 1985 to 1990. The load span  $L/h = 8$  according to RILEM (1985) is probably due to low stiffness requirements for the test equipment.

In Karhaloo & Nallathambi (1991) the methods are extensively compared. It is concluded that the new recommendations yield almost identical results without any significant influence of the beam size. Furthermore it is noticed, that the size-effect method is very sensitive to the slope  $A$  of eq. (5.5). Thus, great care should be taken in performing an adequate regression analysis.

### 5.1.2 $G_f$ -results for HSC and FRC

Since the first RILEM proposal there is performed numerous bend tests on notched concrete beams. The general conclusion is, that  $G_f$  increases with compressive strength, but the rate decreases.

A. Hillerborg defines a measure of ductility as a *characteristic length* in the following way. The elastic energy stored in a specimen just before tensile failure is proportional to  $l_{ch} f_c^2/E$  and the energy required to produce a crack is proportional to  $l_{ch}^2 G_f$ . The ratio of these two energies is  $l_{ch} f_c^2/(EG_f)$  and it indicates the brittleness of the material. The characteristic length  $l_{ch}$  on the other hand, indicates the ductility and it is defined as

$$l_{ch} = \frac{EG_f}{f_c^2} \quad (5.7)$$

Thus, it increases with the ductility of the material. In Baache (1987) a similar definition of the so-called *brittleness number* is presented as  $l_{ch}^2/G_f$ , where a small value indicates a high degree of ductility. The characteristic length is typically decreasing from 500 - 600 mm for NSC to 200 - 300 mm for HSC.

In Giaccio *et al.* (1993) HSC beams are tested according to RILEM (1985). The tests cover various aggregate types and water to cement ratios from 0.28. The compressive strength ranges from 70 to 107 MPa. Within this strength range the fracture energy  $G_f$  increases slightly from 150 N/m to 200 N/m. A mix of NSC with  $f_c = 23$  MPa yields  $G_f = 135$  N/m.

Byngar *et al.* (1993) compare existing bend tests with RILEM (1985) and RILEM (1990b). The conclusion is, that the  $G_f$  calculated by means of the size-effect method is smaller than the fracture energy under a load - deflection curve (approximately 50 N/m compared to 80 N/m).

In Hillerborg (1980) it is stated, that the proper determination of  $G_f$  for FRC is a *direct tensile test*, where the stress - crack width curve is obtained. This is due to the fact, that the fracture zone for FRC is much larger than for plain concrete. Therefore it takes very large beams to

determine a true fracture energy for FRC. In *Li & Hashida (1992)* this problem is investigated for *polyethylene fibre reinforced mortar* ( $V_f = 2\%$  and  $L/d_f = 316$ ). Two test methods are applied: a direct tensile test on notched prisms and a double cantilever beam, being split from one end by two opposite forces.

The direct tensile test is assumed to determine the true  $G_f$ , where all energy is dissipated in the crack plane, while the double cantilever beam also includes so-called off-crack plane dissipation around the crack tip. The true  $G_f$  is measured to 122 N/m, while the double cantilever beam energy absorption increases significantly with specimen size up to twice this value. Thus, the off-crack plane energy seems to equal the in-crack plane energy in this case.

Finally a test method from the ASTM to determine a *toughness index* for FRC is briefly reviewed, see ASTM C1018 (1989). A FRC beam is loaded in its *third-points* and a complete load-deflection curve is recorded. The *first crack point* is observed and the toughness indices  $I_3$ ,  $I_5$  and  $I_{30}$  are defined as the area under the load-deflection curve up to 3, 5.5 and 15.5 times the first crack deflection respectively, divided by the area up to the first crack. In case of true *elastic-plastic* behaviour the values of  $I_3$ ,  $I_5$  and  $I_{30}$  are 5, 10 and 30 respectively.

ASTM C1018 (1989) requires the beam depth and the beam width to be at least 3 times the fibre length. The preferred beam dimensions are  $100 \times 100 \times 350$  mm with a load span of 300 mm.

*Gopalaraman et al. (1991)* investigate the influence of the steel fibre reinforcement index on the toughness indices. Two beam sizes are used under third-point loading, having dimensions  $102 \times 102 \times 356$  mm and  $152 \times 152 \times 533$  mm (load spans equal to 305 and 457 mm). By varying  $V_f(L_f/d_f)$  between 0.25 and 1, the conclusion is, that the toughness indices are rather insensitive to the fibre content and aspect ratio.

In *Johnston & Skarandahl (1992)* a total of 107 beams are tested according to ASTM C1018. The beam dimensions are  $150 \times 100 \times 800$  mm with a load span of 750 mm. Five different steel fibres are applied with aspect ratios ranging from 37 to 125 with the fibre contents up to 1.3% ( $0 \leq V_f(L_f/d_f) \leq 1$ ). They find a significantly increasing effect on the toughness indices from both aspect ratio and fibre content.

## 5.2 $G_f$ -tests on compressit matrix

The only measurements of the fracture energy, performed in the present project, are the direct tensile tests described in Section 2.3, cf. table 2.5. Previous investigations of compressit matrix under three-point bend tests exist and they are described in the following sections.

### 5.2.1 Test specimens and method

It is noted that the bend tests on compressit matrix do not follow the RILEM recommendations for beam dimensions, but still the results are useful for comparisons.

*Hansen (1983)* utilizes beams with  $b = h = 50$  mm,  $a_0/h = 0.5$  and  $L/h = 2.1$ , cf. figure 5.1. A total of 9 different compressit mixes are tested by means of 3 different fibre lengths ( $L_f = 3, 6$  and  $12.7$  mm and  $d_f = 0.15$  mm) and various fibre contents.

In *Søndergård & Jensen (1986)* the Dramix fibre OL 6/15 HC is applied for 4 fibre contents ( $V_f = 0, 2, 4$  and  $6\%$ ). The beams are identical to those in Hansen (1983), but the load span is  $L/h = 5$ , corresponding to zero self-weight induced bending at mid-span.

Finally *Al-Shammer (1989)* test beams with  $b = 55$  mm,  $h = 50$  mm,  $a_0/h = 0.5$  and  $L/h = 8.4$ . The fibres are Dramix OL 6/15 HC with  $V_f = 0, 3, 6, 9$  and  $12\%$ .

By a comparison with the RILEM recommendations in table 5.2 it is evident, that the beams are too small, having cross-sectional dimensions only about half of what is normally applied. However, according to the size-effect method the only restriction is 3 times the maximum aggregate size, or according to ASTM C1018 it is 3 times the fibre length. For compressit matrix  $d_a$  is only 4 mm, leaving the smallest beam dimension ( $= 25$  mm) more than 3 times this value, and the fibre length of 6 mm is also applicable to this dimension.

### 5.2.2 Test results

In table 5.3 the test results are given in terms of  $G_f$ . The values are calculated as the area under the load-deflection curve, divided by the crack area  $b(h-d_0)$ . Because of the low self-weight (approximately 4 kg) of the beams, no load compensation is taken into account. The results from the direct tensile tests are shown in table 2.5.

It is clear that the fracture energy increases remarkably with both the aspect ratio and the fibre content. However, it is recalled, that the bend tests on FRC beams probably overpredict  $G_f$ , because the size of the fracture zone is relatively large compared to the crack.

According to eq. (2.51), the micro mechanical models of fibres crossing a crack suggest, that the fracture energy dissipated during fibre pull-out is proportional to the fibre-matrix shear strength, the fibre reinforcement index and the fibre length:

$$G_f \approx \tau \frac{L_f}{d_f} L_f \quad (5.8)$$

Author (Year)	No. of tests	G <sub>F</sub> /L <sub>I</sub> (MPa)		G <sub>F</sub> (N/m)
		Mean	95% CI	
Hansen (1983)	104	0	0	0.73 (9.9)
		6.5	1.3	5.8 (19.9)
	20	16.2	3.2	13.5 (11.7)
		2.3	0.9	11.1 (10.6)
	40	4.6	1.8	19.3 (18.2)
		6.8	2.7	27.3 (37.9)
	84.7	1.2	1.0	31.4 (13.0)
		2.3	2.0	35.9 (12.0)
		3.5	3.0	28.1 (25.5)
	Søndergård & Jensen (1986)	250	0	0
2			0.8	8.2 (14.9)
40		4	1.6	12.2 (11.4)
		6	2.4	13.4 (14.6)
Al-Shunier (1989)	420	0	0	0.12 (-)
		3	1.2	6.1 (44.0)
	40	6	2.4	9.9 (2.9)
		9	3.6	17.3 (-)
	12	4.8	24.9 (15.1)	

Table 5.3: Test results from three-point bend tests on compressive matrix. All values are mean values and the brackets contain the coefficients of variation.

The values of table 5.3 and 2.5 are not directly comparable because the fibre content and length vary. Instead figure 5.2 contains the results, where  $G_F$  is divided with  $L_I$  and depicted as a function of the fibre reinforcement index. The experimental slope that appears in the figure should equal one sixth of the effective shear strength of the fibre - matrix interface, see eq. (2.51). This value corresponds to a slope of approximately 1 MPa in figure 5.2, which seems reasonable.

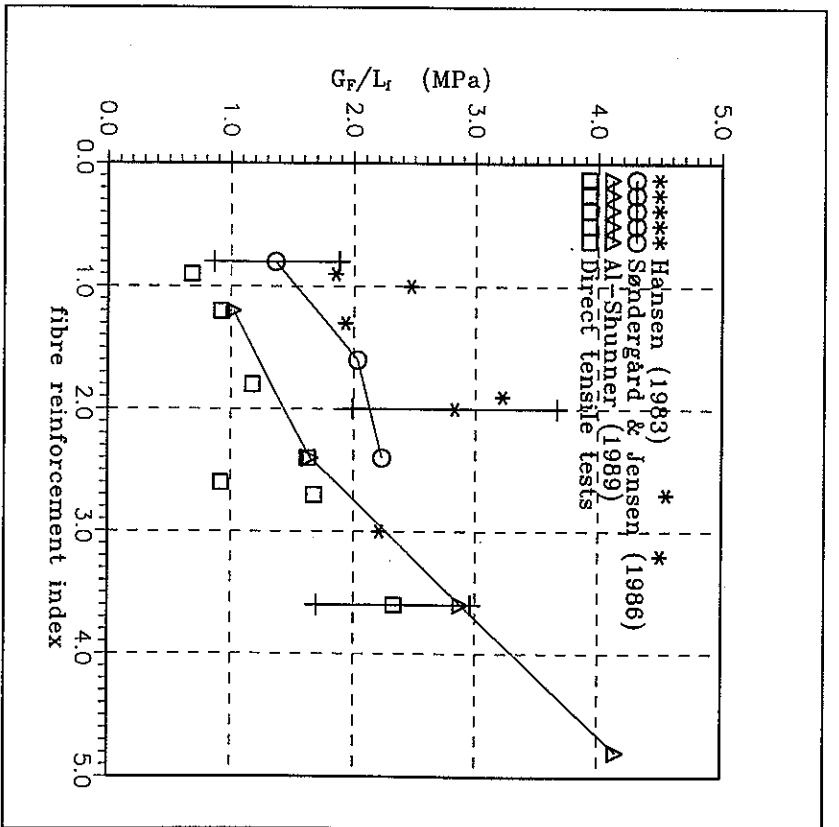


Figure 5.2: Experimental  $G_F/L_I - Y_f(L_f/d)$  relationship, including typically 95 % double-sided confidence intervals.

From the tables 5.3 and 2.5 it is evident, that the results show great scatter with coefficients of variation from 10 to 20 % and even higher. In figure 5.2 this is indicated by means of 3 double-sided 95 % confidence intervals, calculated according to eq. (2.56).

The general trend of the results, despite of the experimental scatter, is that the direct tensile test results yield the lowest values as it is expected. However, it is recalled from Section 2.3.2, that the direct tensile tests do not include the complete fibre pull-out (it is recalled that the direct tensile tests are terminated at a crack opening of 12.5 mm). Therefore they are lower bound predictions of  $G_F$ .

Only the results by Hansen (1983) seem to overpredict  $G_f$  which is probably due to the extremely short load span. Otherwise the results in figure 5.2 correspond to a slope of approximately 1 MPa, i.e.  $G_f/l_d = V_f(l_f/d)$  MPa, as it should be.

It is interesting to note, that the values obtained from plain compressive matrix without fibres correspond very well to those obtained on HSC, i.e. ranging from 100 to 200 N/m.

If the  $G_f$ -values for compressive matrix is inserted in the definition for  $l_a$  in eq. (5.7), we get  $l_a = 1000 V_f(l_f/d)/l_f$ , where the cracking strength of approximately 7 MPa is applied as  $f_c$ . Thus, characteristic lengths of several metres are easily obtained by adding fibres, while plain compressive matrix only gives  $l_a = 100$  mm.

### 5.3 Concluding remarks

The  $G_f$ -tests proposed by RILEM are described in Section 5.1. Despite of the various opinions, whether the fracture energy is a true material constant, or if it is size dependent, it seems to increase slightly with the compressive strength. For HSC  $G_f$  is 100 - 200 N/m and together with the tensile strength it forms the basis for the fictitious crack model on concrete structures.

To the author it seems, that the interest in determining a true material parameter overshadow the fact, that the experimental scatter on  $G_f$  is rather high. Therefore it appears that more effort is needed in the application of a quantified fracture energy to practical concrete structural design.

For FRC materials and in particular compressive matrix, the fracture energy increases strongly with the fibre content and indeed with the fibre length, see eq. (5.8). However, it is questionable to originate the fracture energy solely to a single crack plane. Instead the energy dissipation is expected to happen over a large fracture zone, making  $G_f$  strongly size dependent for FRC. A better way to determine fracture energy on FRC, is a complete direct tensile test, which again is rather complicated for many laboratories.

The fracture energy obtained for compressive matrix are easily raised from about 0.1 kN/m for the plain matrix to 5 - 20 kN/m by adding steel fibres, i.e. an increase of more than 50 times.

### 5.4 References

- Al-Shunaber, I. (1989), *Statusrapport, Effekten på Densitet og Vægt af Væretende Indhold af Metafibre*, in Danish, Preliminary Report, The Cement and Concrete Laboratory, Aalborg Portland A/S, 14 pp.
- ASTM C1018 (1989), 'Standard Test Method for Flexural Toughness and First-Crack Strength of Fiber-Reinforced Concrete (Using Beam With Third-Point Loading)' *Annual Book of ASTM Standards, Vol. 04.02*.
- Bache, H.H. (1987), *Compact Reinforced Composite, Basic Principles*, CBL Report No. 41, Aalborg Portland A/S, 87 pp.
- Bazant, Z.P., J.-K. Kim & P.A. Pfeiffer (1986), 'Nonlinear Fracture Properties from Size Effect Tests', *Journal of Structural Engineering*, ASCE, Vol. 112, No. 2, pp. 290-307.
- Broek, D. (1986), *Elementary Engineering Fracture Mechanics*, 4th Ed., Martinus Nijhoff Publishers.
- Elices, M., G.V. Guinea & J. Planas (1992), 'Measurement of the Fracture Energy Using Three-Point Bend Tests: Part 3 - Influence of Cutting the P - δ Tail', *Materials and Structures*, RILEM, Vol. 25, pp. 327-334.
- Giaccio, G., C. Rocco & R. Zerbino (1993), 'The Fracture Energy ( $G_f$ ) of High-Strength Concrete', *Materials and Structures*, RILEM, Vol. 26, pp. 381-386.
- Gopalaraman, V.S., S.P. Shah, G.B. Batson, M.E. Criswell, V. Ramakrishnan & M. Wecharatana (1991), 'Fracture Toughness of Fiber Reinforced Concrete', *ACI Materials Journal*, Vol. 88, pp. 339-353.
- Guinea, G.V., J. Planas & M. Elices (1992), 'Measurement of the Fracture Energy Using Three-Point Bend Tests: Part 1 - Influence of Experimental Procedures', *Materials and Structures*, RILEM, Vol. 25, pp. 212-218.
- Hansen, A.S. (1983), *Undersøgelse af de Mechaniske Egenskaber for Stålfiberrærret DENSIT*, in Danish, M.Sc.-thesis, Department of Civil Engineering, Building Materials Laboratory, Technical University of Denmark, Lyngby, 59 pp.
- Hellan, K. (1985), *Introduction to Fracture Mechanics*, McGraw-Hill Book Co., Singapore, x + 302 pp.
- Hilteborg, A. (1980), 'Analysis of Fracture by means of the Fictitious Crack Model, Particularly for Fibre Reinforced Concrete', *International Journal of Cement*

## 5. Fracture energy

- Composites, Vol. 2, No. 4, pp. 177-184.
- Hilleborg, A. (1985), 'The Theoretical Basis of a Method to Determine the Fracture Energy  $G_f$  of Concrete', *Materials and Structures*, RILEM, Vol. 18, pp. 291-296.
- Iyengar, K.T.S.R., B.K. Raghuprasad, T.S. Nagaraj & B. Patel (1993), 'Prediction of Load-Deflection Behaviour Using Fracture Energy  $G_f$ : A Comparative Study of Two Fracture Models for Concrete', *Engineering Fracture Mechanics*, Vol. 46, No. 1, pp. 27-33.
- Jeng, Y. & S.P. Shah (1985), 'Two Parameter Fracture Model for Concrete', *Journal of Engineering Mechanics*, ASCE, Vol. 111, No. 10, pp. 1227-1241.
- Johnson, C.D. & A. Skarendahl (1992), 'Comparative Flexural Performance Evaluation of Steel Fibre-Reinforced Concretes According to ASTM C1018 Shows Importance of Fibre Parameters', *Materials and Structures*, RILEM, Vol. 25, pp. 191-200.
- Karhaloo, B.L. & P. Nallathambi (1989), 'Fracture Toughness of Plain Concrete from Three-Point Bend Specimens', *Materials and Structures*, RILEM, Vol. 22, pp. 185-193.
- Karhaloo, B.L. & P. Nallathambi (1991), 'Notched Beam Test: Mode I Fracture Toughness', in *Fracture Mechanics Test Methods for Concrete* (Eds. S.P. Shah & A. Carpinteri), RILEM Report 5, pp. 1-86.
- Li, V.C. & T. Hashida (1992), *Ductile Fracture in Cementitious Materials?*, UMCBE Report No. 92-6, Department of Civil Engineering, University of Michigan, USA, 10 pp.
- Planas, J., M. Eliecs & G.V. Guinea (1992), 'Measurement of the Fracture Energy Using Three-Point Bend Tests: Part 2 - Influence of Bulk Energy Dissipation', *Materials and Structures*, RILEM, Vol. 25, pp. 305-312.
- RILEM (1985), 'Determination of the Fracture Energy of Mortar and Concrete by Means of Three-Point Bend Tests on Notched Beams', Draft recommendation, TC50-FMC Fracture Mechanics of Concrete, *Materials and Structures*, Vol. 18, pp. 285-290.
- RILEM (1990a), 'Determination of Fracture Parameters ( $K_{Ic}$  and CTOD<sub>I</sub>) of Plain Concrete Using Three-Point Bend Tests', Draft recommendation, TC89-FMT Fracture Mechanics of Concrete - Test Methods, *Materials and Structures*, Vol. 23, pp. 457-460.
- RILEM (1990b), 'Size-Effect Method for Determining Fracture Energy and Process Zone Size of Concrete', Draft recommendation, TC89-FMT Fracture Mechanics of Concrete - Test Methods, *Materials and Structures*, Vol. 23, pp. 461-465.
- Søndergaard, J. & H.J. Jensen (1986), *Revenubredelse i Armeret Højslyrkebeton*, in Danish, M.Bc.-thesis, Technical School of Esbjerg.

## 6. Conclusions

This conclusion is a summary of some of the most important observations concerning the strength properties of compressive matrix.

It is recalled from Chapter 1, that compressive matrix is a very dense matrix with *microsilica*, having a water to binder ratio of approximately 0.18 by weight. The steel fibre reinforcement normally used is straight Dramix fibres 12 mm long with aspect ratio  $L_f/d_f$  equal to 30, but other fibres are also applicable.

In the following the mechanical properties of compressive matrix are summarized. All properties are measured on fully hardened specimens so that no strength development is included.

**Uniaxial tension and compression.** In Chapter 2 and 3 it is shown experimentally, that the uniaxial tensile and compressive strength increases with the fibre parameters. A satisfactory linear relationship is found, depending on the *fibre reinforcement index*  $V_f(L_f/d_f)$ . In table 6.1 the most important experimental relations are listed.

Material property	Plain concrete	Fibre effect	Note
Tensile cracking stress $\sigma_{cr}$ (MPa)	7	Insignificant	Figure 2.14
Tensile cracking strain $\epsilon_{cr}$ (%)	0.2	Insignificant	-
Tensile strength $f_t$ (MPa)	7	$6 V_f(L_f/d_f)$	Eq. (2.64)
Modulus of elasticity $E$ (GPa)	50	Insignificant	Figure 3.11
Compressive strength $f_c$ (MPa)	145	$25 V_f(L_f/d_f)$	Eq. (3.10)
Compressive strain $\epsilon_c$ (%)	2.4	$1.8 V_f(L_f/d_f)$	Eq. (3.10)
Fracture energy $G_f$ (kJ/m)	0.1	$1 V_f(L_f/d_f)L_f/\text{mm}$	Figure 5.2

Table 6.1: Survey of material properties for compressive matrix subjected to uniaxial tension and compression.

The increase of the tensile strength is directly connected with pull-out of the fibres, bridging a crack, while the increase of the compressive strength is interpreted as a confinement effect from the fibres.

The relatively high fibre - matrix shear strength of approximately 10 to 15 MPa, makes it possible to utilize the steel fibres to their limit:

- For fibre lengths higher than approximately 20 mm the steel fibres are broken rather



than pulled out of the matrix, even though they are high-quality fibres, cf. table 1.3 and eq. (2.66).

- The post-cracking strength from fibres crossing an open crack exceeds the cracking strength of the matrix at a fibre reinforcement index of approximately 1. Thus, at a fibre content around 3 % of the normal fibre type.

The fact that the tensile strength exceeds the plain matrix cracking strength, when the fibre reinforcement index exceeds a value of approximately 1, provides the material with a remarkable tensile *strain capacity*. However it appears, that the tensile strength of compressive matrix acting together with steel bars in structural elements does not exceed the cracking strength. Instead the fibres ensure a strain capacity so that visible cracking is avoided.

By adding fibres to compressive matrix the *fracture energy* is increased from 0.1 kN/m, which is normal for HSC, to values a 100 times higher. This huge increase in energy dissipation, provided by the fibres, is also reflected by the uniaxial compressive stress - strain curves. It is well-known, that HSC shows rather unstable behaviour at its descending branch of the stress - strain curve, but it appears, that compressive matrix follows a curve, that is qualitatively identical to that of NSC, despite the fact, that the strength is more than 3 times higher.

In Section 3.2.3 a simple analytical uniaxial compressive stress - strain relationship is proposed.

**Triaxial strength criterion.** In Chapter 4 the failure criterion is evaluated for compressive matrix. All test results are performed along the compressive meridian, where uniaxial compression is imposed on a hydrostatic compression state. Therefore caution must be shown in suggesting a complete three-dimensional failure surface before the other stress combinations are investigated further. A slight modification of the existing *Coulomb failure criterion* is proposed, see eq. (4.22).

The triaxial compressive test observations for compressive matrix are similar to what is found for HSC by other investigators. The effect of the minor principal compressive stress is described satisfactorily by an *angle of friction*  $\phi$  equal to 30° instead of 37°, which is normally applied to NSC. However, if this relationship is extrapolated to the uniaxial stress state, where the minor principal stress equals zero, it predicts strengths, that are about 50 % higher than what is actually registered in a uniaxial compression test.

To take this observation into account, the Coulomb criterion is modified for small values of the minor principal stress in order to predict the correct uniaxial strength. It seems that the angle of friction should be increased to about 51° for small values of the confinement pressure. The proper application of a failure criterion to compressive matrix and other HSC

matrices is further discussed in Part II of the thesis!

The question whether the *tensile strength* should be applied to a strength criterion, still needs *structural* considerations to be answered clearly. However it seems, that the fibres rather contribute to the ductility (ensure stable crack growth and delay discrete cracking), than to the tensile strength in case of structural design. It is a fact, that the tensile cracking strength of the compressive matrix only makes a few percent of the compressive strength and therefore it might complicate the calculations more than it benefits them, to include the tensile strength into the design situation.

## 7. Chronological reference list

- Richard, F.E., Brandtzaeg & R.L. Brown (1928), *A Study of the Failure of Concrete Under Combined Compressive Stresses*, Bulletin no. 185, Engineering Experiment Station, University of Illinois, Urbana, 104 pp.
- Romaldi, J.P. & G.B. Batson (1963), 'Mechanics of Crack Arrest in Concrete', *Journal of the Engineering Mechanics Division*, ASCE, Vol. 89, No. EM3, pp. 147-168.
- Krenchel, H. (1964), *Fibre Reinforcement*, Akademisk Forlag, Copenhagen, 159 pp.
- Romaldi, J.P. & J.A. Mandel (1964), 'Tensile Strength of Concrete Affected By Uniformly Distributed and Closely Spaced Short Lengths of Wire Reinforcement', *Journal of the ACI*, Vol. 61, pp. 657-671.
- Kupfer, H., H.K. Hilsdorf & H. Rusch (1969), 'Behaviour of Concrete Under Biaxial Stresses', *ACI Journal*, Vol. 66, pp. 656-666.
- Mills, L.L. & M. Zimmerman (1970), 'Compressive Strength of Plain Concrete Under Multiaxial Loading Conditions', *ACI Journal*, Vol. 67, pp. 802-807.
- Chen, W.-F. & J.L. Carson (1971), 'Stress - Strain Properties of Random Wire Reinforced Concrete', *ACI Journal*, Vol. 68, pp. 933-936.
- Laws, V. (1971), 'The Efficiency of Fibrous Reinforcement of Brittle Matrices', *Journal of Physics D: Applied Physics*, Vol. 4, pp. 1737-1746.
- Sargin, M. (1971), *Stress - Strain Relationships for Concrete and the Analysis of Structural Concrete Sections*, Study No. 4, Solid Mechanics Division, University of Waterloo, Canada, xxvi + 167 pp.
- Edgington, J. & D.J. Hannant (1972), 'Steel Fibre Reinforced Concrete. The Effect on Fibre Orientation of Compaction by Vibration', *Materials and Structures*, RILEM, Vol. 5, No. 25, pp. 41-44.
- Lawrence, P. (1972), 'Some Theoretical Considerations of Fibre Pull-Out from an Elastic Matrix' *Journal of Materials Science*, Vol. 7, pp. 1-6.
- Lin, T.C.Y., A.H. Nilson & F.O. Slate (1972), 'Stress-Strain Response and Fracture of Concrete in Uniaxial and Biaxial Compression', *ACI Journal*, Vol. 69, pp. 291-295.
- Neissen, L.J.M. (1972), *Biaxial Testing of Normal Concrete*, HERON, Vol. 18, No. 1, 90 pp.
- Aveston J. & A. Kelly (1973), 'Theory of Multiple Fracture of Fibrous Composites', *Journal of Materials Science*, Vol. 8, pp. 352-362.

- Kupfer, H.B. & K.H. Gerstle (1973), 'Behaviour of Concrete Under Biaxial Stresses', *Journal of the Engineering Mechanics Division*, ASCE, Vol. 99, No. EM4, pp. 853-866.
- Hannant, D.J. (1974), 'Nomograms for the Failure of Plain Concrete Subjected to Short-Term Multiaxial Stresses', *The Structural Engineer*, Vol. 52, No. 5, pp. 151-165.
- Naaman, A.E., F. Moavenzadeh & F.J. McGarry (1974), 'Probabilistic Analysis of Fiber-Reinforced Concrete', *Journal of the Engineering Mechanics Division*, ASCE, Vol. 100, No. EM2, pp. 397-413.
- Newman, J.B. (1974), 'Apparatus for Testing Concrete under Multiaxial States of Stress', *Magazine of Concrete Research*, Vol. 26, No. 89, pp. 229-238.
- Palaniswamy, G. & S.P. Shah (1974), 'Fracture and Stress - Strain Relationship of Concrete Under Triaxial Compression', *Journal of the Structural Division*, ASCE, Vol. 100, No. ST5, pp. 901-916.
- Taylor, M.A., M.K. Tai & M.R. Ramey (1975), 'Biaxial Compressive Behaviour of Fiber Reinforced Mortar', *ACI Journal*, Vol. 72, pp. 496-501.
- Morton, J. & G.W. Groves (1976), 'The Effect of Metal Wires on the Fracture of Brittle Matrix Composite', *Journal of Materials Science*, Vol. 11, pp. 617-622.
- Andreas, E., K.H. Gerstle & H.-Y. Ko (1977), 'Response of Mortar and Concrete to Biaxial Compression', *Journal of the Engineering Mechanics Division*, ASCE, Vol. 103, No. EM4, pp. 515-526.
- Cedolin, L., Y.R.J. Cruzen & S.D. Poli (1977), 'Triaxial Stress - Strain Relationship for Concrete', *Journal of the Engineering Mechanics Division*, ASCE, Vol. 103, No. EM3, pp. 423-439.
- Hughes, B.P. & N.I. Fattuhi (1977), 'Stress - Strain Curves for Fibre Reinforced Concrete in Compression', *Cement and Concrete Research*, Vol. 7, pp. 173-184.
- Otosen, N.S. (1977), 'A Failure Criterion for Concrete', *Journal of the Engineering Mechanics Division*, ASCE, Vol. 103, No. EM4, pp. 527-535.
- Gerstle, K.H., D.L. Linse, P. Bertacchi, M.D. Koisovos, H.-Y. Ko, J.B. Newman, P. Rossi, G. Schickert, M.A. Taylor, L.A. Traina, R.M. Zimmerman & R. Bellotti (1978), 'Strength of Concrete Under Multiaxial Stress States', *Douglas McHenry International Symposium on Concrete and Concrete Structures*, ACI Publication, SP-55, pp. 103-131.
- Hannant, D.J. (1978), *Fibre Cements and Fibre Concretes*, John Wiley & Sons, xiii + 219 pp.

- Shah, S.P., P. Stroeven, D. Dalhuisen & P. Van Stekelenburg (1978), 'Complete Stress - Strain Curves for Steel Fibre Reinforced Concrete in Uniaxial Tension and Compression', *Testing and Test Methods of Fibre Cement Composites*, The Construction Press, Lancaster, pp. 399-408.
- Wang, P.T., S.P. Shah & A.E. Naaman (1978), 'Stress - Strain Curves of Normal and Lightweight Concrete in Compression', *ACI Journal*, Vol. 75, pp. 603-611.
- Koisovos, M.D. (1979a), 'Effect of Stress Path on the Behaviour of Concrete Under Triaxial Stress States', *ACI Journal*, Vol. 76, pp. 213-223.
- Koisovos, M.D. (1979b), 'A Mathematical Description of the Strength Properties of concrete Under Generalized Stress', *Magazine of Concrete Research*, Vol. 31, No. 108, pp. 151-158.
- Otosen, N.S. (1979), 'Constitutive Model for Short - Time Loading of Concrete', *Journal of the Engineering Mechanics Division*, ASCE, Vol. 105, No. EM1, pp. 127-141.
- Tasuji, M.E., A.H. Nilson & F.O. Slate (1979), 'Biaxial Stress-Strain Relationships for Concrete', *Magazine of Concrete Research*, Vol. 31, No. 109, pp. 217-224.
- Wastels, J. (1979), 'Behaviour of Concrete Under Multiaxial Stresses - A Review', *Cement and Concrete Research*, Vol. 9, pp. 35-44.
- Chen, W.-F. & E.C. Ting (1980), 'Constitutive Models for Concrete Structures', *Journal of the Engineering Mechanics Division*, ASCE, Vol. 106, No. EM1, pp. 1-19.
- Gerstle, K.H., H. Aschl, R. Bellotti, P. Bertacchi, M.D. Koisovos, H.-Y. Ko, D.L. Linse, J.B. Newman, P. Rossi, G. Schickert, M.A. Taylor, L.A. Traina, H. Winkler & R.M. Zimmerman (1980), 'Behaviour of Concrete Under Multiaxial Stress States', *Journal of the Engineering Mechanics Division*, ASCE, Vol. 106, No. EM6, pp. 1383-1403.
- Hillerborg, A. (1980), 'Analysis of fracture by means of the fictitious crack model particularly for fibre reinforced concrete', *International Journal of Cement Composites*, Vol. 2, No. 4, pp. 177-184.
- Bache, H.H. (1981), *Densified Cement/Ultra-Fine Particle-Based Materials*, Paper presented at The Second International Conference on Superplasticizers in Concrete, June 10-12, Ottawa, Canada, Also CBL Report No. 40, Aalborg Portland A/S, 35 pp.
- Egging, D.E. & H.-Y. Ko (1981), *Constitutive Relations of Randomly Oriented Steel Fiber Reinforced Concrete Under Multiaxial Loadings*, M.Sc.-thesis, University of Colorado, Boulder, 480 pp.

- Ahmad, S.H. & S.P. Shah (1982), 'Complete Triaxial Stress - Strain Curves for Concrete', *Journal of the Structural Division*, ASCE, Vol. 108, No. ST4, pp. 728-742.
- Chen, W.-F. (1982), *Plasticity in Reinforced Concrete*, McGraw-Hill Book Company, xv + 474 pp.
- Laws, V. (1982), 'Micromechanical Aspects of Fibre-cement Bond', *Composites*, Vol. 13, pp. 145-151.
- Exner, H. (1983), *Plasticitetsteori for Coulomb Materialer*, in Danish, Ph.D.-thesis, Serie R, No. 175, Department of Structural Engineering, Technical University of Denmark, Lyngby, 258 pp.
- Hansen, A.S. (1983), *Undersøgelse af de Mekaniske Egenskaber for Stålfiberrammeret DENSIT*, in Danish, M.Sc.-thesis, Department of Civil Engineering, Building Materials Laboratory, Technical University of Denmark, Lyngby, 59 pp.
- Gray, R.J. (1984a), 'Analysis of the Effect of Embedded Fibre Length on Fibre Debonding and Pull-Out from an Elastic Matrix. Part 1: Review of Theories', *Journal of Materials Science*, Vol. 19, pp. 861-870.
- Gray, R.J. (1984b), 'Analysis of the Effect of Embedded Fibre Length on Fibre Debonding and Pull-Out from an Elastic Matrix. Part 2: Application to a Steel Fibre-Cementitious Matrix Composite System', *Journal of Materials Science*, Vol. 19, pp. 1680-1691.
- Nielsen, M.P. (1984), *Limit Analysis and Concrete Plasticity*, Prentice-Hall Inc., Englewood Cliffs, New Jersey, xii + 420 pp.
- Carreira, D.J. & K.-H. Chu (1985), 'Stress - Strain Relationship for Plain Concrete in Compression', *ACI Journal*, Vol. 82, pp. 797-804.
- Farella, D.A. & A.E. Naaman (1985), 'Stress - Strain Properties of Fiber Reinforced Mortar in Compression', *ACI Journal*, Vol. 82, pp. 475-483.
- Hellan, K. (1985), *Introduction to Fracture Mechanics*, McGraw-Hill Book Co., Singapore, x + 302 pp.
- Hilleborg, A. (1985), 'The Theoretical Basis of a Method to Determine the Fracture Energy  $G_f$  of Concrete', *Materials and Structures*, RILEM, Vol. 18, pp. 291-296.
- Jeng, Y. & S.P. Shah (1985), 'Two Parameter Fracture Model for Concrete', *Journal of Engineering Mechanics*, ASCE, Vol. 111, No. 10, pp. 1227-1241.

- RILEM (1985), 'Determination of the Fracture Energy of Mortar and Concrete by Means of Three-Point Bend Tests on Notched Beams', Draft recommendation, TCS0-FMC Fracture Mechanics of Concrete, *Materials and Structures*, RILEM, Vol. 18, pp. 285-290.
- Bazant, Z.P., J.-K. Kim & P.A. Pfeiffer (1986), 'Nonlinear Fracture Properties from Size Effect Tests', *Journal of Structural Engineering*, ASCE, Vol. 112, No. 2, pp. 290-307.
- Broek, D. (1986), *Elementary Engineering Fracture Mechanics*, Martinus Nijhoff Publishers.
- Søndergård, J. & H.J. Jensen (1986), *Revetudbredelse i Armeret Højsykebeton*, in Danish, M.Bc.-thesis, Technical School of Esbjerg.
- Tomaszewicz, A. (1986), Discussion on paper by Carreira & Chu (1985), *ACI Journal*, Vol. 83, pp. 872-873.
- Aarup, B.K. & C.E. Pedersen (1987), *Brudmekanik anvendt på CRC-beton*, in Danish, M.Sc.-thesis, Aalborg University, Aalborg, 156 pp.
- Bache, H.H. (1987), *Compact Reinforced Composite, Basic Principles*, CBL Report No. 41, Aalborg Portland A/S, 87 pp.
- Gopalaraman, V.S. & S.P. Shah (1987), 'Tensile Failure of Steel Fiber-Reinforced Mortar', *Journal of Engineering Mechanics*, ASCE, Vol. 113, No. 5, pp. 635-652.
- Lim, T.Y., P. Paramasivam & S.L. Lee (1987), 'Analytical Model for Tensile Behaviour of Steel-Fiber Concrete', *ACI Materials Journal*, Vol. 84, pp. 286-298.
- Heshe, G. (1988), 'Experimental Research on Compact Reinforced Composite (CRC)', *Bygningssstatistiske Meddelelser*, Vol. 59, No. 1, Danish Society for Structural Science and Engineering, 79 pp.
- Al-Shunimer, I. (1989), *Statusrapport, Effekten på Densit af Varierende Indhold af Metal fibre*, in Danish, Preliminary Report, The Cement and Concrete Laboratory, Aalborg Portland A/S, 14 pp.
- ASTM C1018 (1989), 'Standard Test Method for Flexural Toughness and First-Crack Strength of Fiber-Reinforced Concrete (Using Beam With Third-Point Loading)' *Annual Book of ASTM Standards*, Vol. 04.02.
- Dahl, H. & R. Brincker (1989), 'Fracture Energy of High-Strength Concrete in Compression', in *Fracture of Concrete and Rock, Recent Developments* (Eds. S.P. Shah, S.E. Swartz & B. Barr), Elsevier Applied Science, pp. 523-536.

- Gasparini, D.A., D. Verma & A. Abdallah (1989), 'Postcracking Tensile Strength of Fiber Reinforced Concrete', *ACI Materials Journal*, Vol. 86, pp. 10-15.
- Karhaloo, B.L. & P. Nallathambi (1989), 'Fracture Toughness of Plain Concrete from Three-Point Bend Specimens', *Materials and Structures*, RILEM, Vol. 22, pp. 185-193.
- Yin, W.S., E.C.M. Su, M.A. Mansur & T.T.C. Hsu (1989), 'Biaxial Tests of Plain and Fiber Concrete', *ACI Materials Journal*, Vol. 86, pp. 236-243.
- Dahl, K.K.B. (1990), *Preliminary State-Of-The-Art Report on Multiaxial Strength of Concrete*, Serie R, No. 262, Department of Structural Engineering, Technical University of Denmark, Lyngby, 77 pp.
- Olsen, N.H. (1990), *Design Proposal for High Strength Concrete Sections Subjected to Flexural and Axial Loads*, Part of Ph.D.-thesis, Serie R, No. 233, Department of Structural Engineering, Technical University of Denmark, Lyngby, 91 pp.
- RILEM (1990a), 'Determination of Fracture Parameters ( $K_{Ic}$  and CTOD) of Plain Concrete Using Three-Point Bend Tests', Draft recommendation, TC89-FMT Fracture Mechanics of Concrete - Test Methods, *Materials and Structures*, RILEM, Vol. 23, pp. 457-460.
- RILEM (1990b), 'Size-Effect Method for Determining Fracture Energy and Process Zone Size of Concrete', Draft recommendation, TC89-FMT Fracture Mechanics of Concrete - Test Methods, *Materials and Structures*, RILEM, Vol. 23, pp. 461-465.
- Stang, H., Z. Li & S.P. Shah (1990), 'Pullout Problem: Stress versus Fracture Mechanical Approach', *Journal of Engineering Mechanics*, ASCE, Vol. 116, No. 10, pp. 2136-2150.
- Glavind, M. & H. Stang (1991), 'Evaluation of the Complete Stress - Strain Curve for High Strength Concrete', in *Fracture Processes in Concrete, Rock and Ceramics* (Eds. J.G.M. Van Mier, J.G. Rols & A. Bakker), Proceedings of the International RILEM/ESIS Conference, Vol. 1, pp. 749-759.
- Gopalaraman, V.S., S.P. Shah, G.B. Batson, M.E. Criswell, V. Ramakrishnan & M. Wecharatana (1991), 'Fracture Toughness of Fiber Reinforced Concrete', *ACI Materials Journal*, Vol. 88, pp. 339-353.
- Karhaloo, B.L. & P. Nallathambi (1991), 'Notched Beam Test: Mode I Fracture Toughness', in *Fracture Mechanics Test Methods for Concrete* (Eds. S.P. Shah & A. Carpinteri), RILEM Report 5, pp. 1-86.
- Shah, S.P. (1991), 'Do Fibers Increase the Tensile Strength of Cement-Based Matrixes?', *ACI Materials Journal*, Vol. 88, pp. 595-602.
- Traina, L.A. & S.A. Mansour (1991), 'Biaxial Strength and Deformational Behaviour of Plain and Steel Fiber Concrete', *ACI Materials Journal*, Vol. 88, pp. 354-362.
- Van Mier, J.G.M. & R.A. Vonk (1991), 'Fracture of Concrete Under Multiaxial Stress - Recent Developments', 53-MTC Multiaxial Testing of Concrete, Final Report, *Materials and Structures*, RILEM, Vol. 24, pp. 61-65.
- Aarre, T. (1992), *Tensile characteristics of FRG with special emphasis on its applicability in a continuous pavement*, Ph.D.-thesis, Serie R, No. 301, Department of Structural Engineering, Technical University of Denmark, Lyngby, 167 pp.
- Baabak, W., P.-C. Aïcin & G. Ballyvy (1992), 'On Predicting Modulus of Elasticity in High-Strength Concrete', *ACI Materials Journal*, Vol. 89, No. 5, pp. 517-520.
- Dahl, K.K.B. (1992), *Uniaxial Stress - Strain Curves for Normal and High Strength Concrete*, Serie R, No. 282, Department of Structural Engineering, Technical University of Denmark, Lyngby, 96 pp.
- Dahl, K.K.B. (1992a), *A Failure Criterion for Normal and High Strength Concrete*, Serie R, No. 286, Department of Structural Engineering, Technical University of Denmark, Lyngby, x + 115 pp.
- Dahl, K.K.B. (1992b), *A Constitutive Model for Normal and High Strength Concrete*, Serie R, No. 287, Department of Structural Engineering, Technical University of Denmark, Lyngby, x + 96 pp.
- Dahl, K.K.B. (1992c), *The Calibration and Use of a Triaxial Cell*, Serie R, No. 285, Department of Structural Engineering, Technical University of Denmark, Lyngby, x + 70 pp.
- Elices, M., G.V. Guinea & J. Planas (1992), 'Measurement of the Fracture Energy Using Three-Point Bend Tests: Part 3 - Influence of Cutting the P -  $\delta$  Tail', *Materials and Structures*, RILEM, Vol. 25, pp. 327-334.
- Ezeldin, A.S. & P.N. Balaguru (1992), 'Normal- and High-Strength Fiber-Reinforced Concrete under Compression', *Journal of Materials in Civil Engineering*, ASCE, Vol. 4, No. 4, pp. 415-429.

- Glavind, M. (1992), *Evaluation of the Compressive Behaviour of Fiber Reinforced High Strength Concrete*, Ph.D.-thesis, Serie R, No. 302, Department of Structural Engineering, Technical University of Denmark, Lyngby, 144 pp.
- Guinea, G.V., J. Planas & M. Elices (1992), 'Measurement of the Fracture Energy Using Three-Point Bend Tests: Part 1 - Influence of Experimental Procedures', *Materials and Structures*, RILEM, Vol. 25, pp. 212-218.
- Heshe, G. & C.V. Nielsen (1992a), *EU 264 - COMPRESIT, Subtask 1.6 - Behaviour in Tension*, NOVIT's Udviklingsfond, Aalborg, 27 pp.
- Heshe, G. & C.V. Nielsen (1992b), *EU 264 - COMPRESIT, Subtask 1.4 - Behaviour in Compression, Triaxial Stress State and Short Columns*, NOVIT's Udviklingsfond, Aalborg, 51 pp.
- Johnston, C.D. & A. Skarendahl (1992), 'Comparative Flexural Performance Evaluation of Steel Fibre-Reinforced Concretes According to ASTM C1018 Shows Importance of Fibre Parameters', *Materials and Structures*, RILEM, Vol. 25, pp. 191-200.
- Lahou, K., P.-C. Aitcin & O. Chaallal (1992), 'Behaviour of High-Strength Concrete Under Confined Stresses', *Cement & Concrete Composites*, Vol. 14, pp. 185-193.
- Li, V.C. (1992), 'Postcrack Sealing Relations for Fiber Reinforced Cementitious Composites', *Journal of Materials in Civil Engineering*, ASCE, Vol. 4, No. 1, pp. 41-57.
- Li, V.C. & T. Hashida (1992), *Ductile Fracture in Cementitious Materials?*, UMCEE Report No. 92-6, Department of Civil Engineering, University of Michigan, USA, 10 pp.
- Planas, J., M. Elices & G.V. Guinea (1992), 'Measurement of the Fracture Energy Using Three-Point Bend Tests: Part 2 - Influence of Bulk Energy Dissipation', *Materials and Structures*, RILEM, Vol. 25, pp. 305-312.
- Stang, H. (1992), 'Evaluation of Properties of Fiber Composite Materials', in *High Performance Fiber Reinforced Cement Composites* (Eds. H.W. Reinhardt & A.E. Naaman), Proceedings of the International RILEM/ACI Workshop, pp. 388-406.
- Duedahl, T. & M.S. Nielsen (1993), *Beregningsmodel til Bestemmelse af Spændings- og Deformationsforholdene for Bøjningspåvirkede CRC-Bjælker*, in Danish, M.Sc.-thesis, Department of Building Technology and Structural Engineering, Aalborg University, Aalborg, 109 pp.
- Giaccio, G., C. Rocco & R. Zerhino (1993), 'The Fracture Energy ( $G_f$ ) of High-Strength Concrete', *Materials and Structures*, RILEM, Vol. 26, pp. 381-386.

- Iyengar, K.T.S.R., B.K. Raghuprasad, T.S. Nagaraj & B. Patel (1993), 'Prediction of Load-Deflection Behaviour Using Fracture Energy  $G_f$ : A Comparative Study of Two Fracture Models for Concrete', *Engineering Fracture Mechanics*, Vol. 46, No. 1, pp. 27-33.
- Setunge, S., M.M. Attard & P.LeP. Darvall (1993), 'Ultimate Strength of Confined Very High-Strength Concretes', *ACI Structural Journal*, Vol. 90, pp. 632-641.

## Appendix 1

### Direct tensile tests, test method and $\sigma_B/\sigma_{cr}$ - $W$ relationships

This appendix contains a description of the test procedure together with experimental stress vs. crack width curves, that have been recorded from the tests reported in Section 2.3. The tensile bridging stresses are normalized with respect to the cracking stress.

#### A1.1 Test specimens and method

The specimens consist of small prisms with dimensions  $50 \times 50 \times 55$  mm, see figure 2.9 in Section 2.3.1. These prisms are saw-cut from compressit matrix beams with dimensions  $50 \times 50 \times 500$  mm, which are cast horizontally. From each beam approximately 8 prisms are obtained.

From each of the 8 compressit matrices listed in table 2.4, three beams are cast. The *curing conditions* are as follows:

- Cast in steel moulds on a vibratory table. Wrapped in wet towels.
- Demoulded the next day and wrapped in wet towels and plastic.
- Cured 4-5 days in a heating room at  $45^\circ$  C.
- Finally stored in laboratory at about  $20^\circ$  C until testing, i.e. for a period of about 5 months. During this period the prisms are saw-cut and prepared by sawing the notches with a diamond saw.

The *notches* have a depth of approximately 9.5 mm with a width of 3 mm. The notch depth is measured on each specimen before testing to obtain the correct cross-sectional area.

In order to ensure *rotational stiffness* between the specimen and the test machine, the prism is glued to a steel block on each end. The glue is a 2-component Schnellklebstoff X60 from Höttinger Baldwin Messtechnik in Darmstadt, Germany, which cures very fast. The adhesive joint attains 90 % of its strength in about 4 minutes, which is preferable in minimizing the time consumption. The surfaces of both the steel blocks and the specimens are *sandblasted* to enhance the adhesive bond.

Then the steel blocks are bolted to a prototype fixture, which again is tightly connected to the 100 kN Instron testing machine with standard fixtures, see figure A1.1 for the set-up.

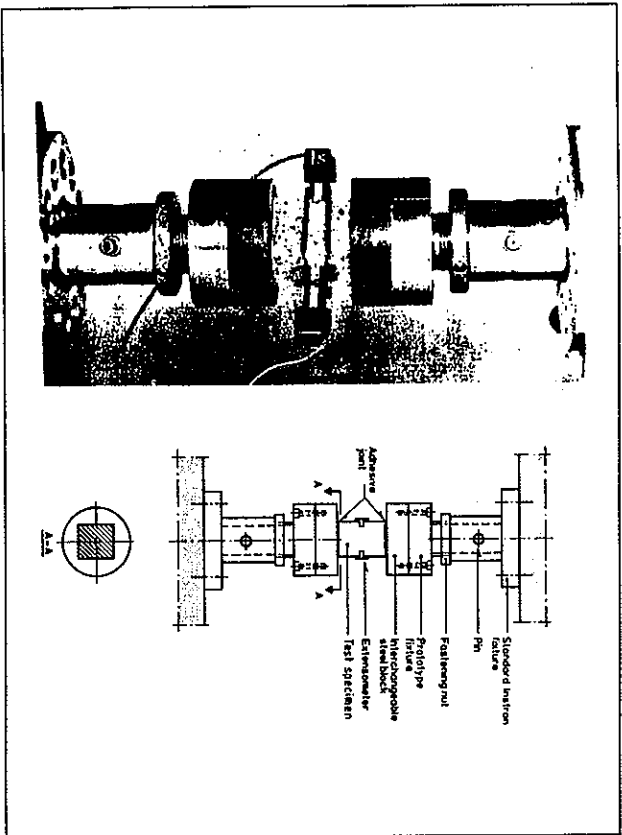


Figure A1.1: a) Photo of set-up; b) Schematic representation of set-up. Taken from Aarre (1992).

A total of 30 steel blocks are used in order to test multiple specimens before the blocks are cleaned. After each test the glue is burned off and the steel blocks are sandblasted before they are ready again. Each block has diameter 80 mm and thickness 25 mm and in order to fit the standard Instron fixture, it has 4 holes with diametrical distance 60 mm for 8 mm bolts.

Two Instron extensometers (type 2620-602) are placed on opposite sides of the specimen and it is the mean value of their strain measurements, that is supplied to the test machine as *feedback signal*. The test machine is designed to control the test under *constant extensometer signal rate*. The rate is preset manually (using the unit % per minute), but can be altered during the test, which is necessary to minimize the time consumption of each test.

For notched specimens a *measuring distance* of 12.5 mm is applied, while the unnotched prisms apply 25 mm. This give maximum strain values of 20 an 10 % respectively in the two

cases, because the *maximum displacement* of the extensometers is 2.5 mm. The purpose for using different measuring lengths is to ensure, that the final crack localizes within this length. For the notched specimens the final position of the crack is well-known, while the unnotched specimen cracks with equal probability anywhere along its length and therefore a longer measuring length is required.

Finally the *test procedure* is summarized below:

- The prism is glued to one of the steel blocks and fixed to the upper part of the test machine by means of 4 bolts.
- The other steel block is bolted to the lower part of the machine and covered with glue.
- Then the cross-head is moved upwards until the prism touches the steel block and a small compressive force is registered (less than 500 N). The glue cures for about 4 minutes, while the extensometers are mounted by means of rubber bands.
- The test is started by letting the extensometer strain increase linearly with time. The initial ramp rate of the control signal is preset to 0.02 % per minute.
- As cracks start to develop and the peak load is obtained the strain rate is increased manually from 0.02 % per minute in small steps in order to end up with 4 % per minute, when the strain is approximately 4 %.
- When the extensometers have reached their maximum value (2.5 mm), the test is terminated and the extensometers are removed, before the specimen is divided into two halves.

## A1.2 Recorded $\sigma_f/\sigma_{cr}$ - $w$ relationships

Each of the following 8 figures represents a compressive matrix and includes the test data obtained with that particular matrix. All the curves start at the normalized stress  $\sigma_f/\sigma_{cr} = 1$ , corresponding to the initiation of cracking.

The names utilized in the figures correspond to those in table 2.4, where UT is brief for uniaxial tension, followed by the aspect ratio of the steel fibres applied. The fibres are all straight Dramix steel fibres from the Belgian company Bekaert. Two different fibre qualities are applied and for the best quality 2 different fibre lengths are tested. In table A1.1, which is a copy of table 1.3 the fibre types are explained.



Fibre (OLP / Drammix)	Length (mm)	Diameter (mm)	As Recd. Ratio (H <sub>0</sub> /L <sub>0</sub> )	Tensile strength (MPa)	NOTE
OL 6/15 HC	6	0.15	40	2950	Brass-coated, high carbon.
OL 13/15 HC	13	0.15	87	2950	Ditto.
OL 12/40	12	0.40	30	1350	Low carbon.

Table A1.1: Drammix fibre types and properties. The fibres are loose and straight indicated by the designation OL.

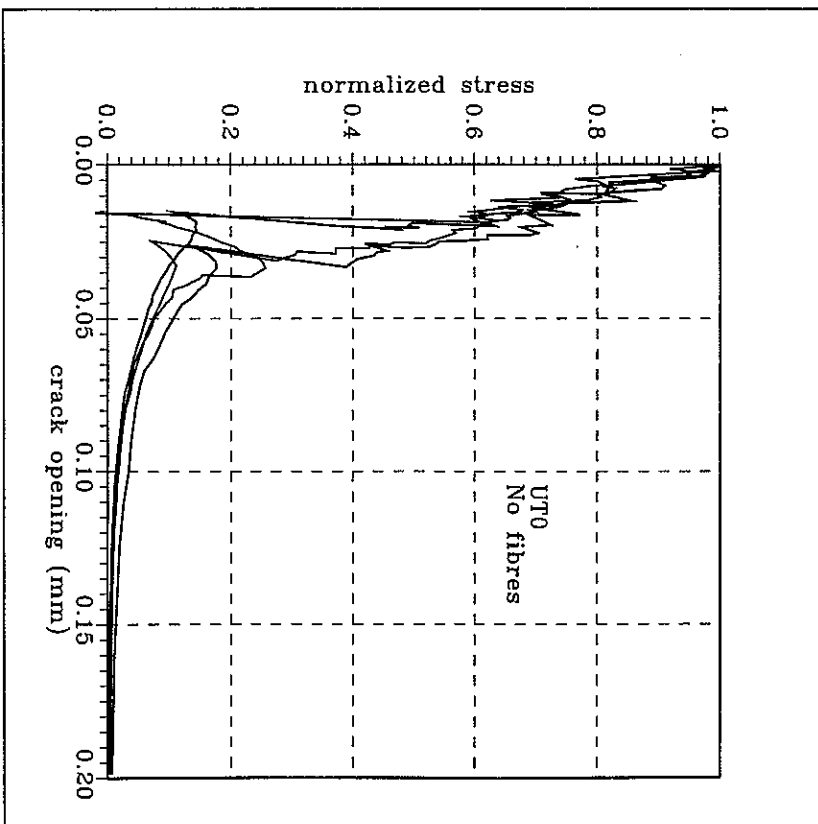


Figure A1.2: Experimental  $\sigma/\sigma_c$  -  $w$  curves for UTO without any steel fibres.

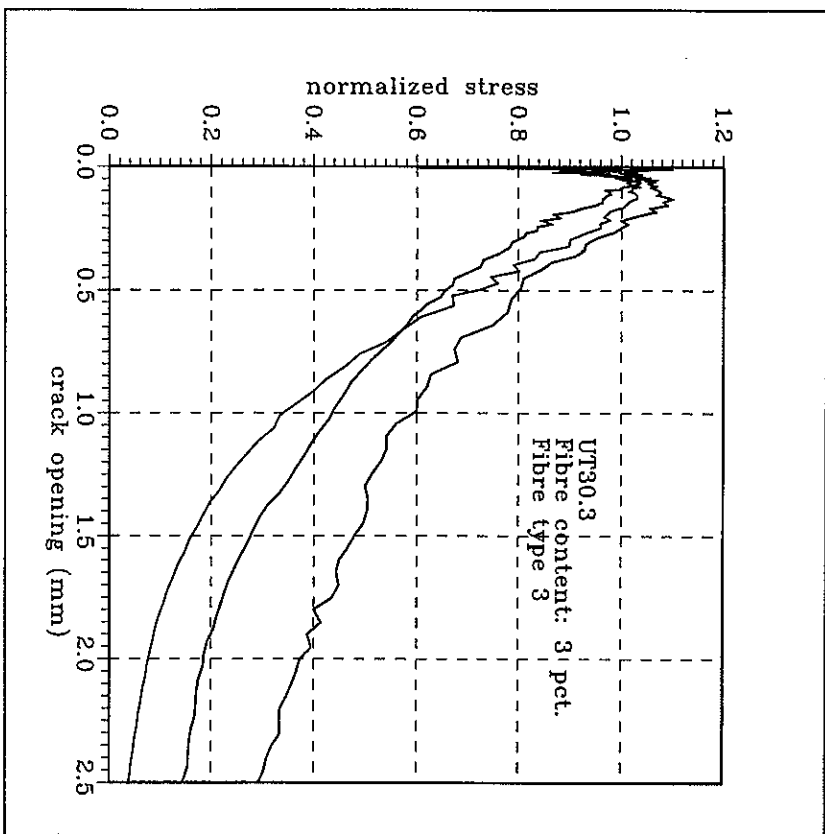


Figure A1.3: Experimental  $\sigma/\sigma_c$  -  $w$  curves for UT30 with 3 % fibres of type OL 12/40.

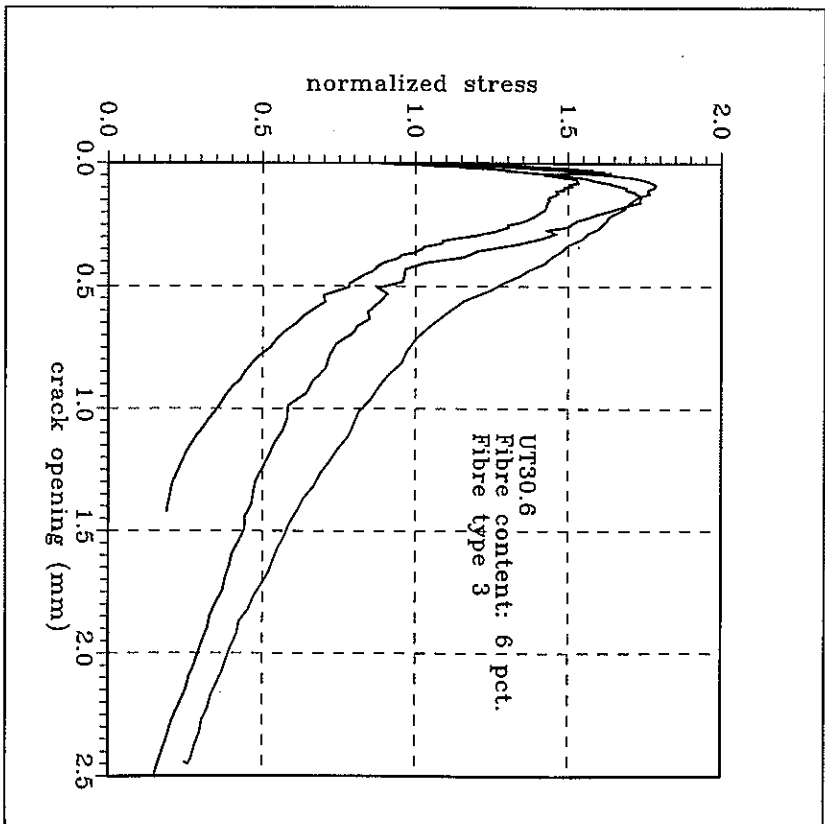


Figure A1.4: Experimental  $\sigma/\sigma_c$  -  $w$  curves for UT30 with 6 % fibres of type OL 12/40.

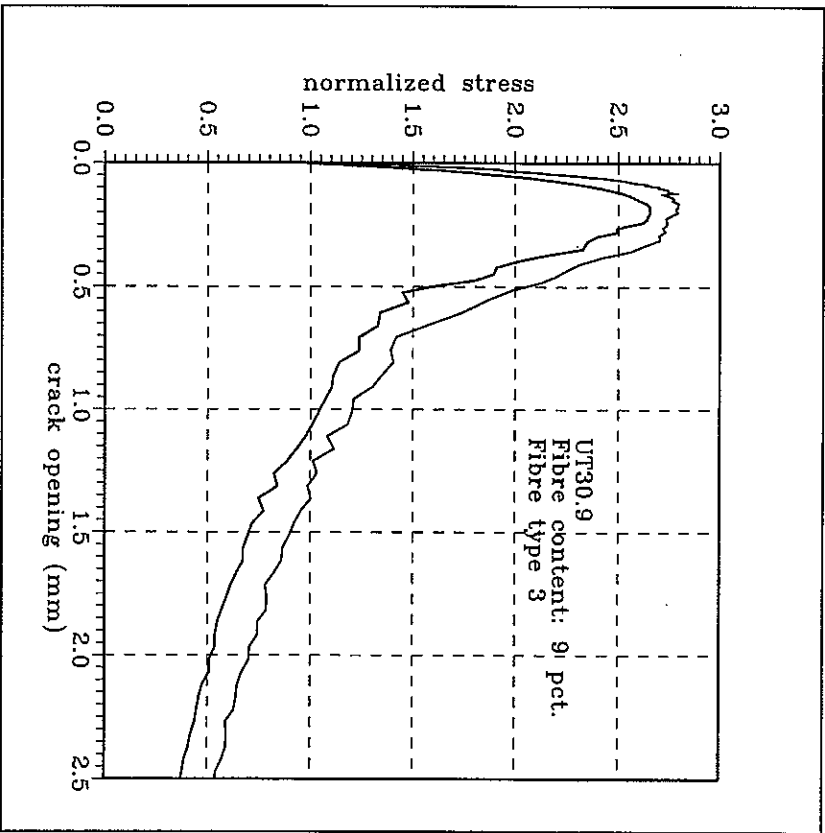


Figure A1.5: Experimental  $\sigma/\sigma_c$  - w curves for UT30 with 9 % fibres of type OL 12/40.

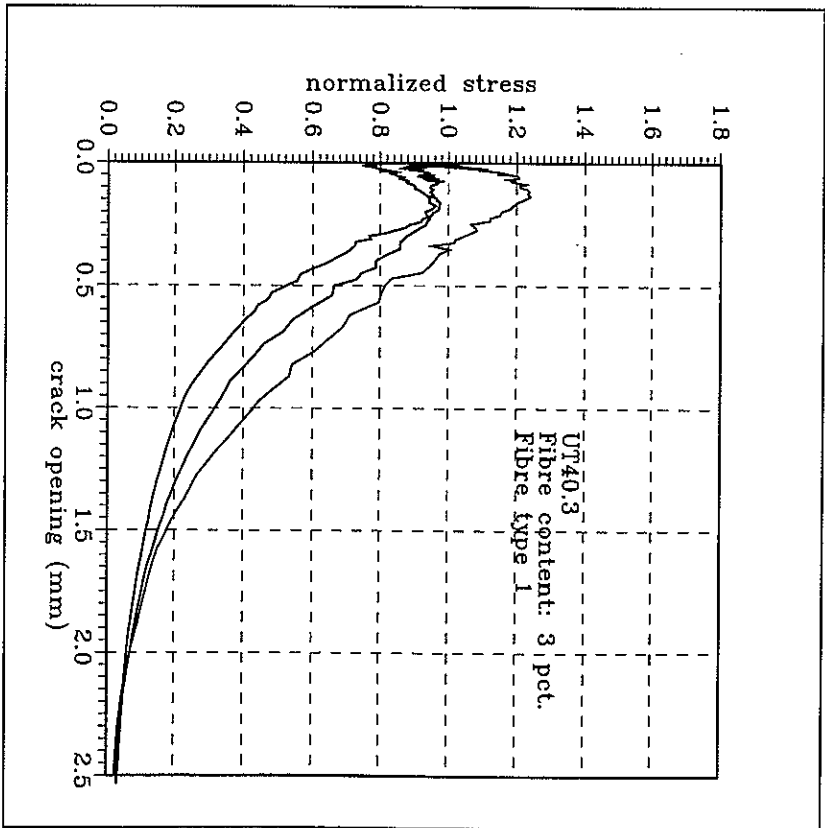


Figure A1.6: Experimental  $\sigma_f/\sigma_c$  - w curves for UT40 with 3 % fibres of type OL 6/1.5 HC.

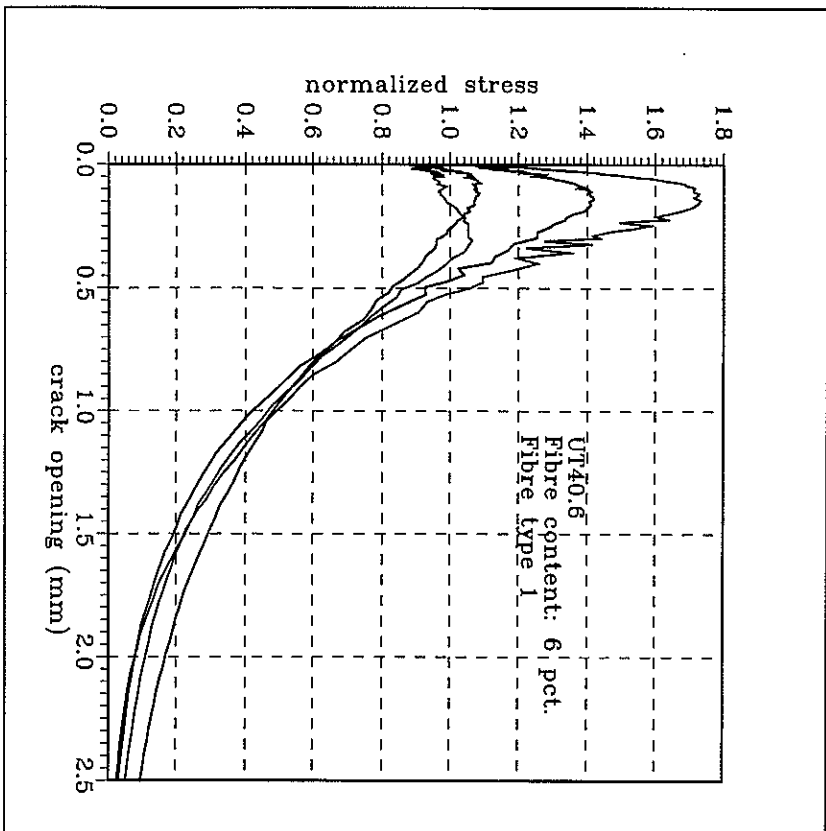


Figure A1.7: Experimental  $\sigma_f/\sigma_{cr}$  -  $w$  curves for UT40 with 6 % fibres of type QL 6/15 HC.

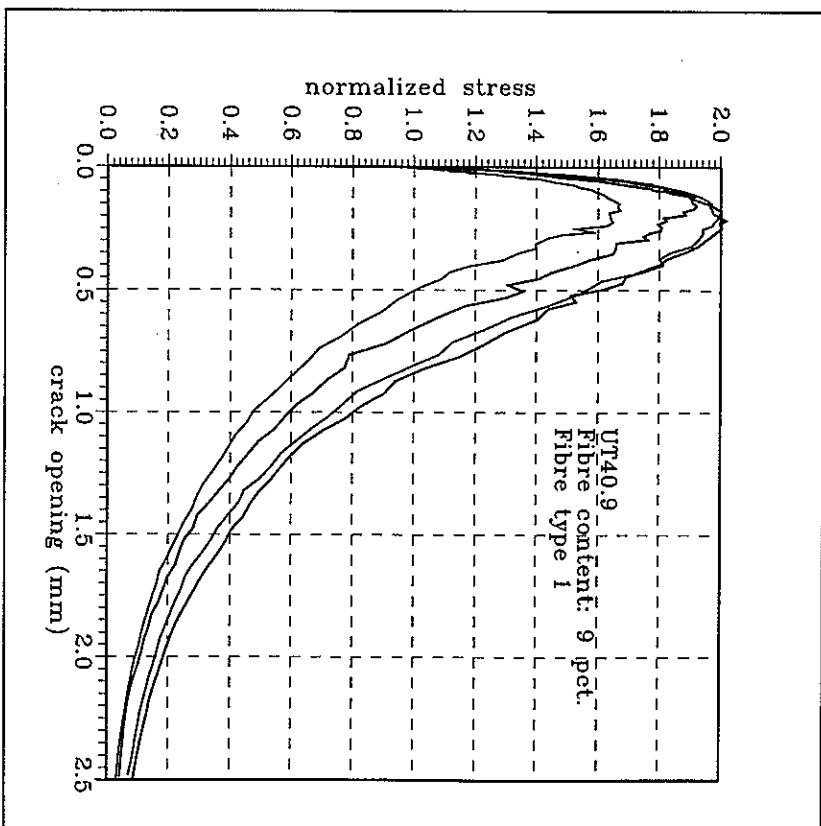


Figure A1.8: Experimental  $\sigma_f/\sigma_{cr}$  -  $w$  curves for UT40 with 9 % fibres of type OL 6/15 HC.

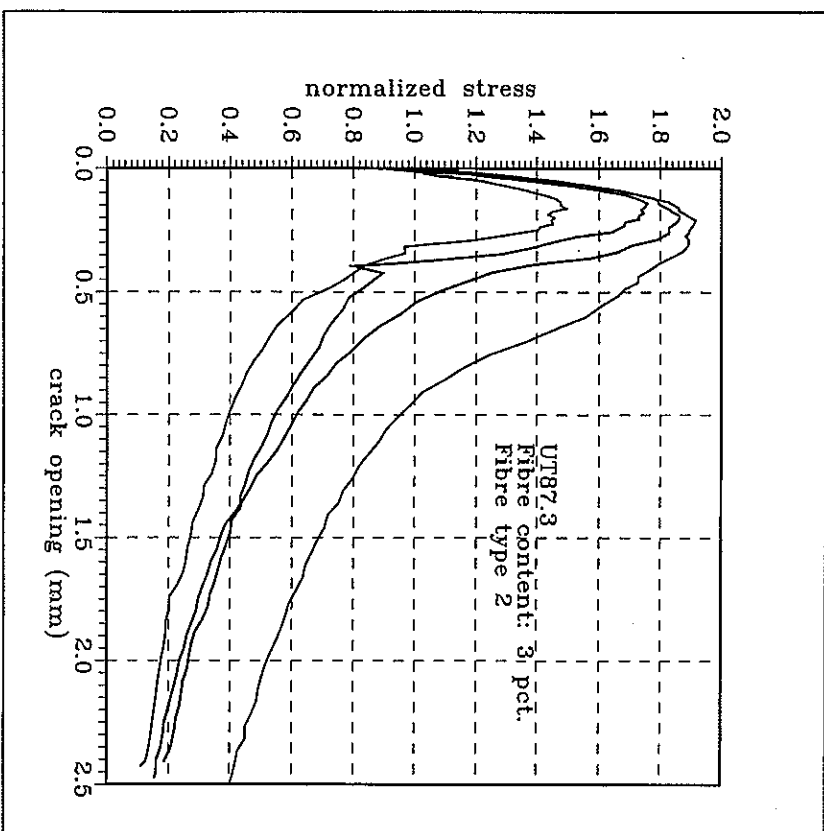


Figure A1.9: Experimental  $\sigma/\sigma_c - w$  curves for UT87 with 3 % fibres of type OL 13/15 HC.

## Appendix 2

### Uniaxial compressive tests, test method and stress - strain relationships

This appendix contains a description of the compressive tests on compress matrix together with a graphical representation of the stress - strain recordings reported in Section 3.2.

#### A2.1 Test specimens and method

The compressive tests are performed on  $\phi 45 \times 90$  mm cylinders under closed-loop control, which enables complete stress - strain curves, even though the stiffness of the test machine is relatively low, see e.g. Giavind & Stang (1991) and Dahl & Brincker (1989).

Three cylinders are cast from each of the 8 compress matrices listed in table 3.1. The curing conditions are as follows:

- Cast in steel moulds on a vibrating table. Wrapped in wet towels.
- Demoulded the next day and wrapped in wet towels.
- Cured 4-5 days in a heating room at 45° C.
- Finally stored in laboratory at about 20° C until testing, i.e. for a period of 1 to 2 months. During this period the cylinder end planes are ground accurately plane by use of a diamond grinding wheel.

The test setup is originally developed for standard cylinders ( $\phi 100 \times 200$  mm) and consists of a 1000 kN hydraulic jack controlled by a high-response servo valve. This servo valve is controlled by a MTS 458.20 MicroConsole and with a MTS 418.91 Profiler to supply the reference signal. The choice of small cylinder dimensions is due to the high compressive strengths to be expected ( $f_c > 150$  MPa). In order to fit the cylinders in the existing test setup a removable steel block is inserted between the existing load plate and the specimen.

The load frame consists of two hollow steel tubes with the upper cross-head fixed. The upper load plate has a spherical seat, allowing rotations in order to compensate for eventually non-parallel specimen ends. When load is applied, by the lower load plate moving upwards, the friction in the spherical bearing keeps the upper load plate from rotating. No intermediary layers are used between the cylinder and the load plates.

The longitudinal strains are measured by means of 2 LVDT's with 2.5 mm base and a sensitivity of approximately 0.5 V/mm, placed on opposite sides of the specimen around the load plates. The lateral strains are registered by means of a piano wire, wrapped around the mid-section of the cylinder and connected to a LVDT (HP 1000) with 25 mm base and a sensitivity of approximately 0.2 V/mm. The sensitivities of the LVDT's are of course checked in the actual configuration before the experiments are executed.

Furthermore each cylinder is equipped with two electrical resistance gages with the measuring length 18 mm to register the longitudinal strains of the middle third of the specimen.

The LVDT-signals are composed from the mean signal from the two longitudinal LVDT's and the lateral LVDT to make the feedback signal. The longitudinal transducers supply  $U_1$  and the transverse LVDT, connected to the piano wire, supplies the electrical voltage  $U_2$ . These two signals are added, using a programmable mV transmitter, corresponding to the following expression

$$U_f = U_1 + 1.56U_2$$

where  $U_f$  is the feedback signal. This composition of the feedback signal agrees very well with the suggestion in Dahl & Brincker (1989). In Glavind & Stang (1991) the composition is varied, i.e. the weight factor 1.56 is altered, but no significant effect is observed.

The MTS MicroConsole compares the feedback signal with the reference signal, provided by the MTS Profiler at a frequency of about 10 kHz. The reference signal increases linearly with time, defined by a signal rate and an end level. Several ramps can be executed subsequently, but in the present test programme only one ramp rate is used for the entire test. From pilot tests it is found that a ramp rate equal to 0.1 V per minute is appropriate. This results in an initial stress rate in the cylinder of about 0.4 MPa per second. The duration of each test is about 30 minutes, while the peak is reached in less than 10 minutes.

The test procedure is summarized below:

- The cylinder is placed on the lower load plate, which is moved slowly upwards in load control, until a small compressive load is registered (100 - 200 N).
- The LVDT's and the gages are mounted and connected to the datalogger.
- On the MTS MicroConsole the control mode is changed to closed-loop and the MTS Profiler is enabled. When the Profiler is started the test begins.
- The test proceeds past the peak load and it is stopped manually, when the load has dropped to less than one third of the peak load, or when the stress - strain curve gets almost horizontal.
- Before disconnecting the LVDT's the servo valve is switched to deformation control

by the MicroConsole and the test setup is ready for another specimen.

## A2.2 Recorded stress - strain curves

Each of the following 7 figures represents a mix of compressi matrix from table 3.1. Each figure contains 3 curves except for figure A2.4, where one test is unsuccessful. It is recalled that the compressi matrix without fibres is excluded, because the tests show unstable behaviour.

The curves are composed from electrical resistance gage signals, measuring over the middle-third of the cylinder until 75 % of peak, followed by the overall strains measured by means of 2 LVDT's.

The names utilized in the figures correspond to those in table 3.1, where UC is brief for uniaxial compression followed by the aspect ratio of the steel fibres. The fibres are all straight Dranix steel fibres. Two different fibre qualities are applied and for the best quality 2 different fibre lengths are tested. In table A1.1, which is a copy of table 1.3, the fibre types and geometries are summarized.

Fibre type Dranix	Length (mm)	Diameter (mm)	Aspect ratio L/d	Tensile strength (MPa)	Note
OL 6/15 HC	6	0.15	40	2950	Brass-coated, high carbon.
OL 13/15 HC	13	0.15	87	2950	Ditto.
OL 12/40	12	0.40	30	1350	Low carbon.

Table A2.1: Dranix fibre types and properties. The fibres are loose and straight indicated by the designation OL.

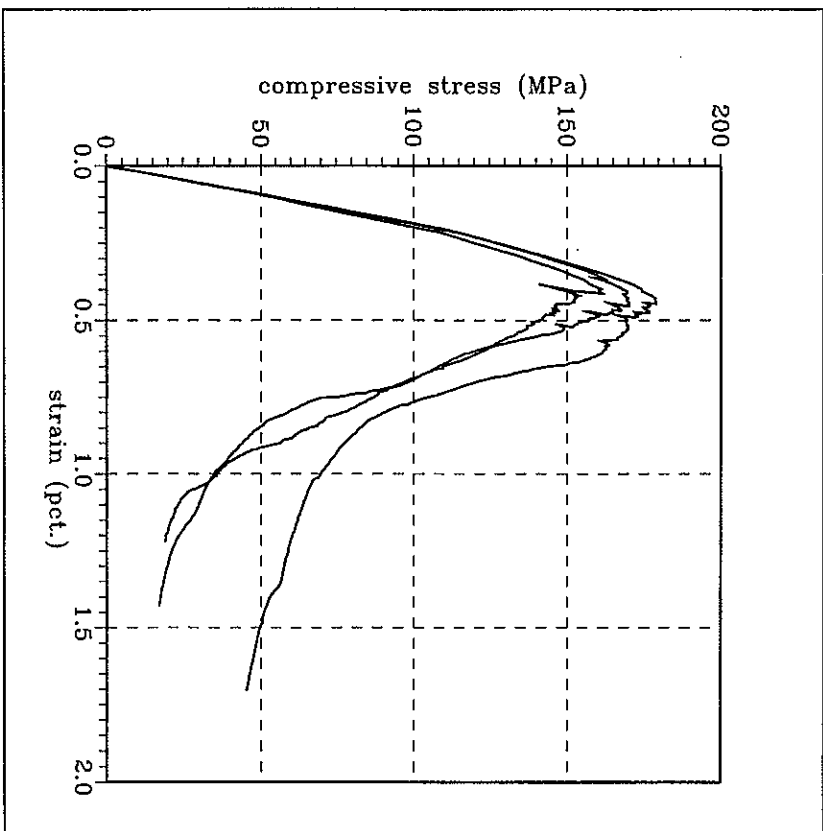


Figure A2.1: Stress - strain curves for UC30 with 3 % fibres of type OL 12/40.

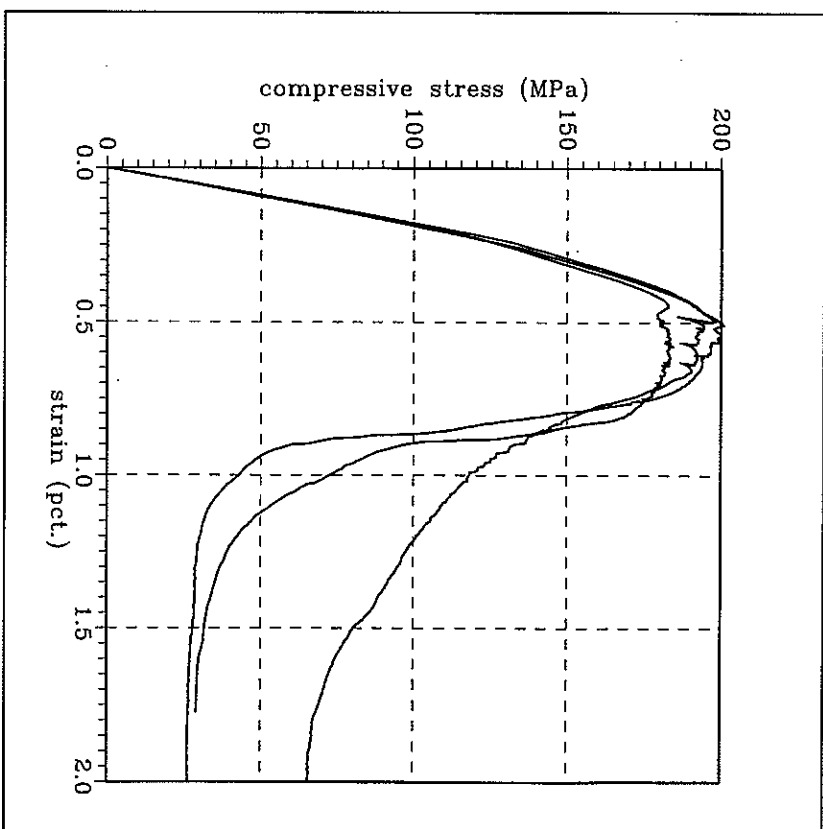


Figure A2.2: Stress - strain curves for UC30 with 6 % fibres of type OL 12/40.

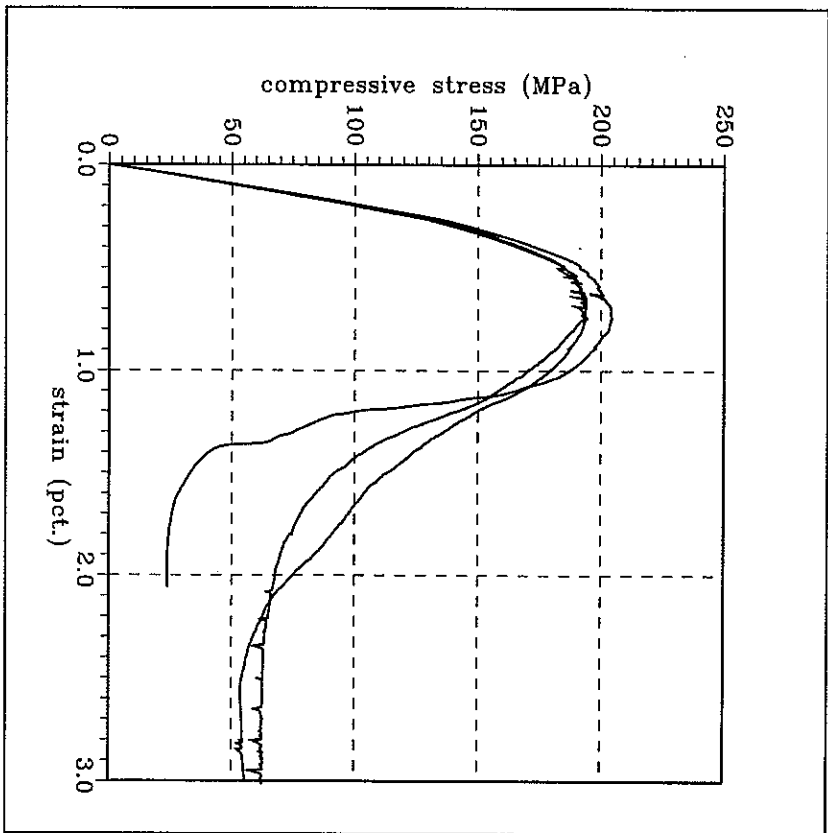


Figure A2.3: Stress - strain curves for UC30 with 9 % fibres of type OL 12/40.

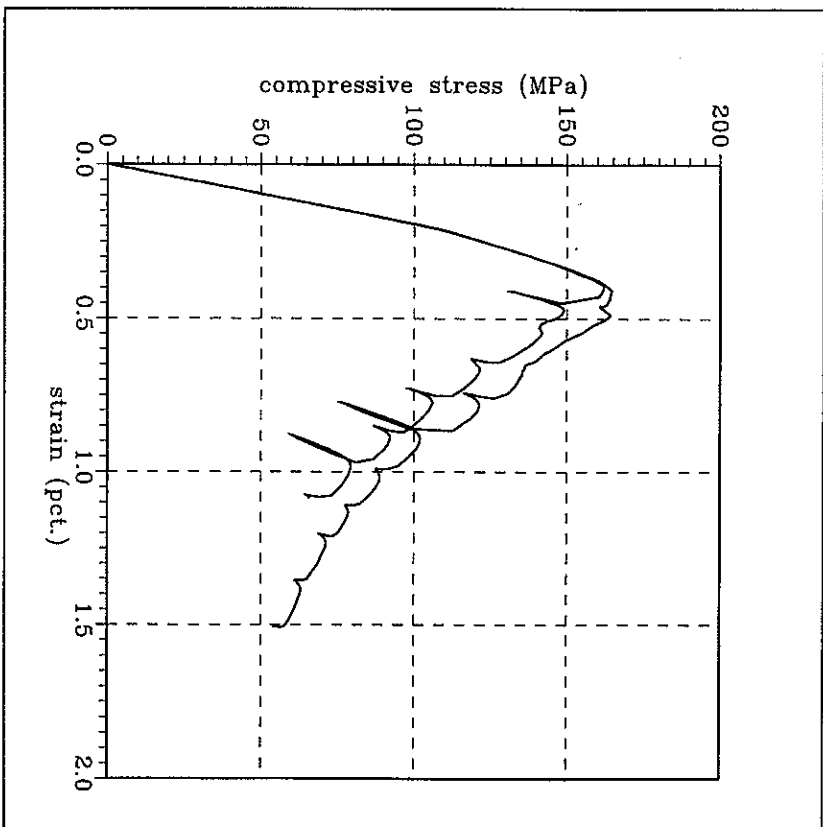


Figure A2.4: Stress - strain curves for UC40 with 3 % fibres of type OL 6/15.



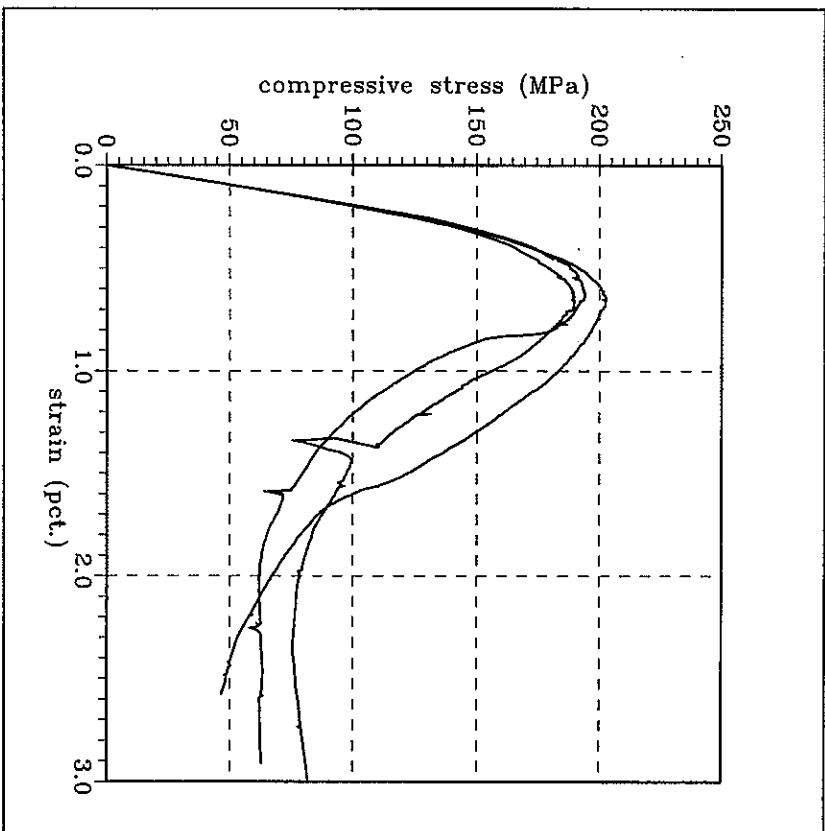


Figure A1.5: Stress - strain curves for UC40 with 6 % fibres of type OL 6/1.5 HC.

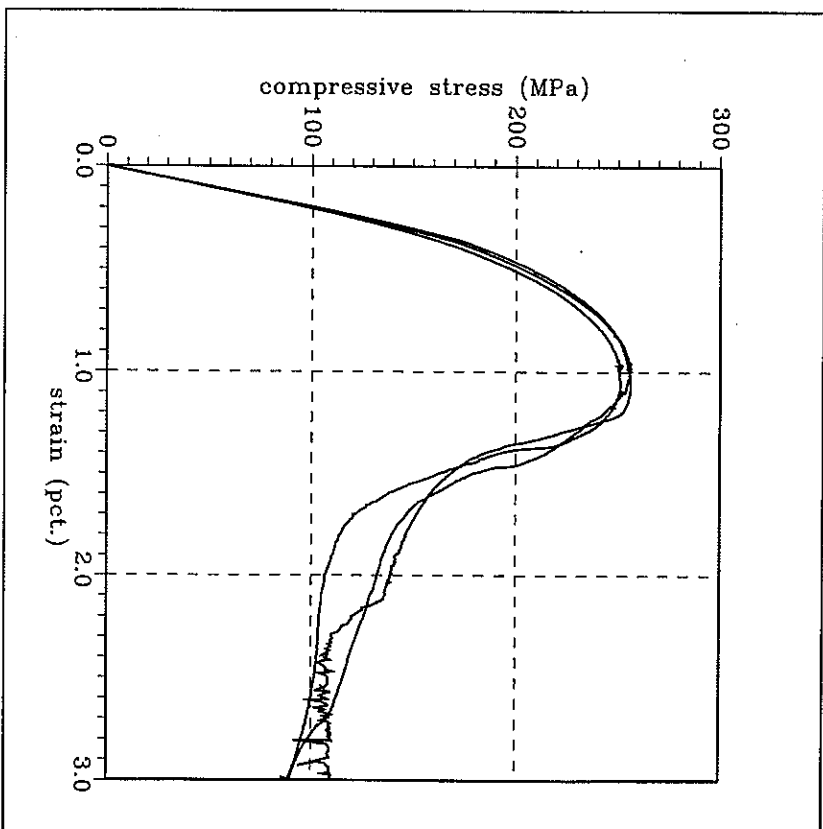


Figure A1.6: Stress - strain curves for UC40 with 9 % fibres of type OL 6/1.5 HC.

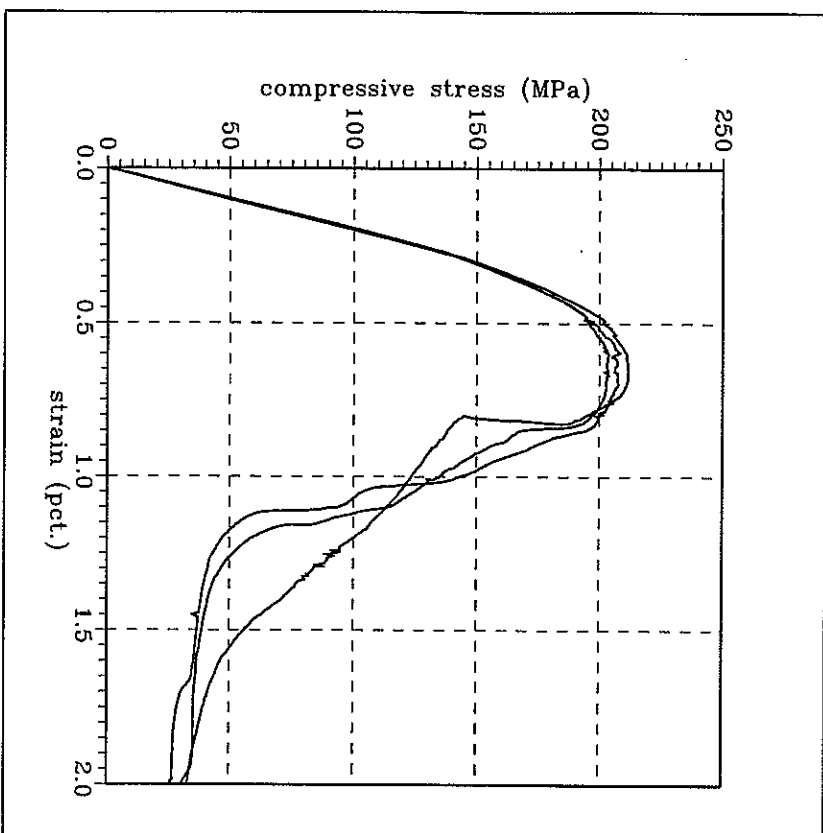


Figure A1.7: Stress - strain curves for UC87 with 3 % fibres of type OL 13/15 HC.

## Appendix 3

### Triaxial compressive tests

This appendix contains a description of the test procedure together with a description of the special test equipment, the so-called *triaxial cell*.

The equipment is developed by K.K.B. Dahl at the Department of Structural Engineering at Technical University of Denmark, see Dahl (1992c). The description in Dahl (1992c) includes documentation of both the calibration data and an explanation of the software necessary to control the tests.

#### A3.1 Triaxial cell and test method

In figure A3.1 the cross-section of the triaxial cell is shown together with a description of the various parts. The cell consists of three main parts:

- A *base unit*, that acts as the lower load plate for the concrete cylinder.
- A *barrel section* enclosing the oil pressure.
- A *piston* to apply the axial load from an external jack.

All parts are manufactured from high strength steel in order to sustain an internal oil pressure of maximum 140 MPa.

The *test procedure* includes the following steps:

- The concrete cylinder is placed on the base unit and covered with rubber membranes, which are tightly sealed at the upper and lower load plates.
- The barrel section is lowered down over the base unit by means of a crane and locked by steel clamps. The interface between the barrel and the base unit is sealed by means of a rubber o-ring and a brass ring.
- The cell is filled with hydraulic oil (about 3 litres). The hydraulic oil system is not described here, the reader is referred to Dahl (1992c). The oil is forced into the cell by means of air pressure (up to 6 bar).
- The oil-filled cell is now placed in the 10 MN hydraulic jack. For the present test

series only about one third of its capacity is occupied.

- The oil pressure is then raised to the specified level by means of an air-hydro pump. The maximum oil pressure is 140 MPa. Throughout the test series the stress rate is 0.3 MPa per second.

- Under constant oil pressure the vertical load is applied until failure, i.e. failures along the compressive meridian are observed. The external jack is load controlled using a stress rate of 0.3 MPa per second. During loading it is necessary to adjust the oil pressure because the volume of the test cylinder changes continuously.

- After a complete test the oil pressure is lowered and the oil is emptied from the cell back to the hydraulic system.

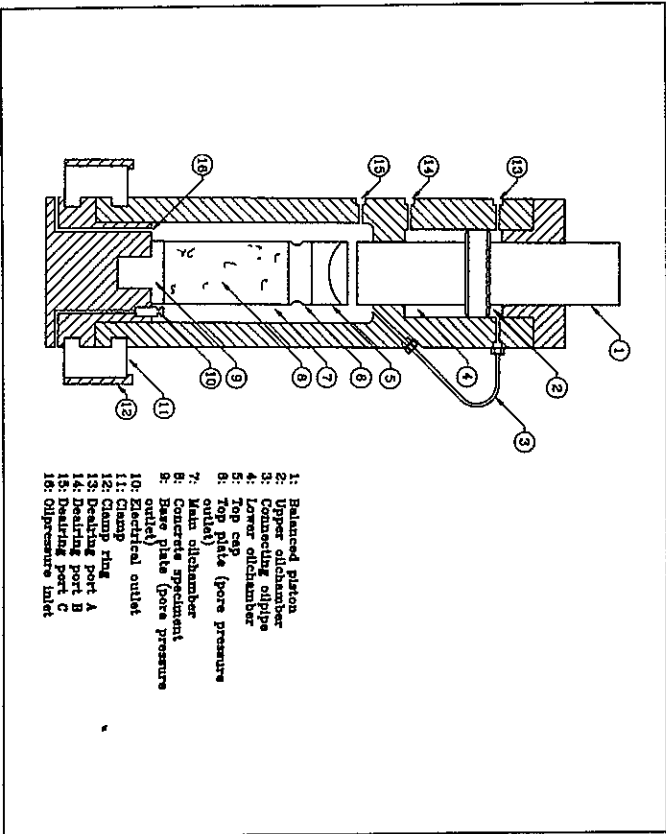


Figure A3.1: Schematic outline of triaxial cell. Taken from Dahl (1992c).

Throughout each test a *data logging* software programme called TRIAX, especially designed for the equipment, acquires the data from a datalogger. Values of the vertical load, the oil pressure and the strain values, measured by means of electrical resistance gages on the cylinders are stored. The data programme include the correct calibration factors and returns the values in physical units (N, MPa and microstrain).

The *oil pressure* is measured by means of a pressure transducer (HBM P3MA) with a maximum level of 200 MPa. Its sensitivity is 2 mV per V. K.K.B. Dahl reports a dependence of the piston friction and the oil pressure, where the friction increases with the oil pressure. This dependency is included in TRIAX.

The *electrical resistance gages* are especially designed in order to register strains up to 20%. It is known that confined concrete undergoes very large deformations and a so-called *post-yield* gage is developed at the Department of Structural Engineering, because the commercially available gages are very expensive. The gage factor of these post-yield gages is 2.16 and they have a measuring distance of 60 mm. No significant effect of the oil pressure normal to the face of these gages is found in Dahl (1992c).

The hydraulic system includes a safety blow-out valve, that ensures that the oil pressure does not exceed a specified level. If the pressure transducer register a higher value, the TRIAX programme cuts the air supply to the blow-out valve and the oil pressure is automatically lowered. The maximum allowable pressure is 140 MPa.

### A3.2 Preparation of test specimens

The test specimens consist of standard  $\phi 100 \times 200$  mm cylinders cast from compressit matrix with 6 % fibres. The fibres are Dramix steel fibres OL 12/40 with  $L_f/d_f = 30$ . Furthermore a few cylinders with plain compressit matrix are tested.

It is necessary to fit rubber membranes over the cylinder in order to avoid oil to enter the pores and cracks. If the cylinder surface contains holes the membranes are forced into these voids and puncture. Therefore it is essential that the cylinder surface is clean and smooth.

After casing the cylinders are *cured* according to the following:

- Wrapped in wet towels and demoulded after one day. Then wrapped in wet towels and plastic.
- Cured 4-5 days in a heating room at 45° C.
- Finally stored in laboratory at about 20° C until testing, i.e. for a period of 2-3

months. During this period the cylinders are prepared for triaxial testing.

The preparation of the cylinders consists of sandblasting in order to expose all voids near the surface. These voids are filled with a ready-mix compound called HUS-FIX, which contains cement, lime and very fine sand.

A total of 4 post-yield gages are mounted per cylinder, 2 vertical and 2 horizontal, mounted symmetrically about the center circumference.

The rubber membranes are manufactured by 1 mm thick oil resisting rubber, so-called NITRIL rubber. A sheet with dimensions 260 x 340 mm is glued together along its shortest side to form a tube. A steel cylinder with diameter 100 mm forms the template and the glue is so-called NEOTOL glue. One sheet of rubber per cylinder is not enough to ensure a tight membrane so 2 or 3 sheets are used for each test. For oil pressures below 50 MPa, 2 membranes are used and for pressures above 50 MPa, 3 membranes are used. Dahl (1992c) reports, that for pressures above 100 MPa the need is 4 membranes per test. In order to simplify the procedure each membrane is covered with *talcum powder* to minimize the friction during mounting. Furthermore it is important to ensure, that the glued overlaps are not placed on top of each other.

Around the top and the base plate, the membranes are tightened firmly by means of a heavy duty *torque clip*. The torque clip is rather narrow (about 6 mm) and it is fabricated by ASA, Sweden. Each clip lasts 2 to 3 tests before the threading starts to fail, because of the extremely hard tightening. At the top plate the electrical wires from the gages are guided out between the plate and the membranes. Grooves are cut in this plate to ensure, that the torque clip keeps the interface sealed. It should be noted, that the tightening of the torque clips together with the smoothness of the cylinder surface are the most important factors to ensure a successful test.

The reference cylinders without any oil pressure are also tested in the 10 MN jack through the empty triaxial cell. These tests include *intermediary layers* between the cylinder and the load plates, which is not used for the confined tests.

Unfortunately the tests did show, that the filling of the air voids on the cylinder surfaces was not sufficiently. In almost every test 2 or 3 gages did fail even before vertical loading started, because they are forced into the voids. Luckily the number of membranes prevents the oil to enter the cylinders. It is undoubted, that the dense compressi matrix produces a large number of small voids, which are fatal to the gages. Therefore it seems, that more experience is needed in preparation of the cylinders to avoid damaging the gages so that proper strain readings are possible.

SERIE R  
(Tidligere: Rapporter)

- R 298. JENSEN, RALPH BO: Modified Finite Element Method modelling Fracture Mechanical Failure in wooden beams. 1992.
- R 299. IBSSØ, JAN BEHRENDT & AGERSKOV, HENNING: Fatigue Life of Off-shore Steel Structures under Stochastic Loading. 1992.
- R 300. HANSEN, SVEND OLE: Reliability of Wind Loading on Low-Rise Buildings in a Group. 1992.
- R 301. AARRE, TINE: Tensile characteristics of FRC with special emphasis on its applicability in a continuous pavement. 1992.
- R 302. GLAVIND, METTE: Evaluation of the Compressive Behaviour of Fiber Reinforced High Strength Concrete. 1992.
- R 303. NIELSEN, LEIF OTTO: A C++ basis for computational mechanics software. 1993.
- R 304. Resuméoversigt 1992 - Summaries of Papers 1992.
- R 305. HANSEN, SØREN, STANG, HENRIK: Eksperimentelt bestemte mekaniske egenskaber for fiberbeton. 1993.
- R 306. NIELSEN, PER KASTRUP, ELGAARD JENSEN, HENRIK, SCHMIDT, CLAUD, NIELSEN, M.P.: Forskydning i armerede teglbælker. 1993.
- R 307. CHRISTOFFERSEN, JENS, JAGD, LARS, NIELSEN, M.P.: HOTCH-POTCH Pladelementet - Finite element til beregning af armerede betonplader. 1993.
- R 308. NIELSEN, LEIF OTTO: A C++ class library for FEM special purpose software. 1994.
- R 309. DULEVSKI, ENCHO M.: Global Structural Analysis of Steel Box Girder Bridges for Various Loads. 1994.
- R 310. Resuméoversigt 1993 - Summaries of Papers 1993.
- R 311. JIN-PING ZHANG: Strength of Cracked Concrete. Part 1 - Shear Strength of Conventional Reinforced Concrete Beams, Deep Beams, Corbels, and Prestressed Reinforced Concrete Beams without Shear Reinforcement. 1994.
- R 312. OLSEN, DAVID HOLKMANN: Fracture of Concrete A Test Series. 1994.
- R 313. OLSEN, DAVID HOLKMANN: Fracture of Concrete A Test Series Appendix I. 1994.
- R 314. DAHL, KAARE K.B.: Construction Joints in Normal and High Strength Concrete. 1994.
- R 315. KARLSHØJ, JAN: Principper og metoder for opstilling af datamodeller til byggetekniske anvendelser. 1994.
- R 316. HANSEN, THOMAS CORNELIUS: Fatigue and Crack Propagation. A new approach to predict crack propagation behavior. 1994.
- R 317. JAGD, LARS, CHRISTOFFERSEN, JENS, NIELSEN, M.P.: The HOTCH-POTCH Disk Element - Finite Element for Analysis of Reinforced Concrete Disks. 1994.
- R 318. JAGD, LARS, CHRISTOFFERSEN, JENS, NIELSEN, M.P.: The HOTCH-POTCH Disk Element - Finite Element for Analysis of Reinforced Concrete Shells. 1994.
- R 319. HANSEN, THOMAS CORNELIUS: Triaxial Tests with Concrete and Cement Paste. 1995.
- R 320. PETERSEN, R.I., AGERSKOV, H., MARTINEZ, L. LOPEZ, ASKEGAARD, V.: Fatigue Life of High-Strength Steel Plate Elements under Stochastic Loading. 1995.
- R 321. Resuméoversigt 1994 - Summaries of Papers 1994.
- R 322. IBSSØ, JAN BEHRENDT: Fatigue Life Prediction of Welded Joints Based on Fracture Mechanics and Crack Closure. 1995.

Hvis De ikke allerede modtager Afdelingens resuméoversigt ved udgivelsen, kan Afdelingen tilbyde at tilsende næste års resuméoversigt, når den udgives, dersom De udfylder og returnerer nedenstående kupon.

Returneres til

Afdelingen for Bærende Konstruktioner  
Danmarks Tekniske Universitet  
Bygning 118  
2800 Lyngby

Fremtidig tilsendelse af resuméoversigter udbedes af  
(bedes udfyldt med blokogstaver):

Silling og navn: .....

Adresse: .....

Postnr. og -distrikt: .....

The Department has pleasure in offering to send you a next year's list of summaries, free of charge. If you do not already receive it upon publication, kindly complete and return the coupon below.

To be returned to:

Department of Structural Engineering  
Technical University of Denmark  
Building 118  
DK-2800 Lyngby, Denmark.

The undersigned wishes to receive the Department's List of Summaries:  
(Please complete in block letters)

Title and name: .....

Address: .....

Postal No. and district: .....

County: .....